



HAL
open science

Analysis and Optimization of the Asian Mobile and Terrestrial Digital Television Systems

Ming Liu

► **To cite this version:**

Ming Liu. Analysis and Optimization of the Asian Mobile and Terrestrial Digital Television Systems. Electronics. INSA de Rennes, 2011. English. NNT : . tel-00662247

HAL Id: tel-00662247

<https://theses.hal.science/tel-00662247>

Submitted on 23 Jan 2012

HAL is a multi-disciplinary open access archive for the deposit and dissemination of scientific research documents, whether they are published or not. The documents may come from teaching and research institutions in France or abroad, or from public or private research centers.

L'archive ouverte pluridisciplinaire **HAL**, est destinée au dépôt et à la diffusion de documents scientifiques de niveau recherche, publiés ou non, émanant des établissements d'enseignement et de recherche français ou étrangers, des laboratoires publics ou privés.



N° d'ordre : D11-07



Thèse

présentée devant
l'INSTITUT NATIONAL DES SCIENCES APPLIQUÉES DE RENNES

pour obtenir le grade de

Docteur

spécialité : *Électronique*

Analysis and Optimization of the Asian Mobile and Terrestrial Digital Television Systems

par
LIU Ming

Soutenue le 30.03.2011 devant la commission d'examen

Composition du jury

Rapporteurs

Catherine Douillard Professeur à Télécom Bretagne
Jean-Marc Brossier Professeur à l'INPG

Examineurs

Pierre Duhamel Directeur de Recherches CNRS au LSS, SUPELEC
Guillaume Gelle Professeur à l'Université de Reims
Alain Untersee Ingénieur Teamcast
Jean-François Hélaré Professeur à l'INSA de Rennes
Matthieu Crussière Maître de Conférences à l'INSA de Rennes

*Institut d'Electronique et de Télécommunications de Rennes
Institut National des Sciences Appliquées de Rennes
Université Européenne de Bretagne*

To my Parents

To Xiao

Acknowledgements

It is my great pleasure to acknowledge the many people who made this thesis possible.

Foremost, I am heartily thankful to my supervisor, Prof. Jean-François H elard, for accepting me to pursue my Ph.D in IETR and for his invaluable guidance throughout the last three years. Thank you for helping me establish a clear direction of research and providing insightful advices. I would like also give my deepest gratitude to my co-advisor: Ma tre de Conf erences, Dr. Matthieu Crussiere. I quite enjoy the inspiring and stimulating discussions with you. Thank you for your always availability and your precious supports in my research and daily life. Thank you also for all the encouragement you gave me when I was frustrated.

I would like to express my sincere thanks to the members of my thesis defense committee, Prof. Catherine Douillard, Prof. Jean-Marc Brossier, Prof. Pierre Duhamel, Prof. Guillaume Gelle and Alain Untersee and for reading and evaluating my thesis. Their involvement and expert insights have greatly helped me to enrich my thesis.

I would like to thank my colleagues in the CPR team: Oudomsack Pierre Pasquero, Youssef Nasser, Ir ene Mahafeno, Lahatra Rakotondrainibe, Pierre Viland, Ali Maiga, Ayman Khalil, Karima Ragoubi and Yaset Oliva for the friendly working environment, and for the nice discussions. Thank you all for your hand-by-hand help when I was new here.

I thank my friends, Chen Jiaqi, Mu Pengcheng, Jing Guoqing, Sun Fan, Luo Yun, Zhou Fen, Guo Weiming, Xie Fuchun, Zhang Jiong, Wang Yu, R echo Jan, Driehaus Lena, Bai Cong, Chu Xingrong, Zhang Xiaoli, Peng Linning, Ji Hui, Zhang Jinglin, Zhang Shunying, Zhao Yu, Wang Hongquan, Yi Xiaohui, Zou Wenbin, Lu Weizhi for their kind help and all the fun we have during the past years.

Last but not least, I would like to express my heartfelt gratitude to my family, especially to my parents and my wife, for their infinite love and support.

Résumé étendu en français

Au cours des dernières décennies, la télévision (TV) en tant que système de diffusion a été un moyen particulièrement efficace pour informer les gens, les éduquer et les divertir. En 2009, le marché de la télévision à travers le monde représentait 268,9 milliards d'euros et 1.134.141 millions de téléviseurs. Dans un avenir proche, il est prévu que ce marché continue de grandir, d'une valeur totale estimée à 322,9 milliards d'euros en 2013. Cette forte prévision d'augmentation est liée à la demande des utilisateurs pour une plus grande variété de programmes et pour une qualité d'images améliorée. Il est également prévu que les systèmes de diffusion de la télévision évoluent afin de fournir de nouveaux services comme par exemple la réception sur terminal mobile, les programmes en trois dimensions (3-D), la vidéo sur demande (*video on demand*, *VoD* en anglais), etc. On comprend alors que les systèmes de diffusion analogiques traditionnels sont récemment arrivés en limite d'exploitation face à l'émergence de ces nouvelles demandes de services et de débits.

La télévision numérique, nouveau mode de diffusion de la télévision, permet au contraire d'offrir beaucoup plus de programmes et de déployer de nouveaux services. Grâce aux avancées considérables qu'ont récemment connu les techniques de traitement numérique du signal, il est aujourd'hui possible de profiter d'une meilleure qualité d'image et de son. La télévision numérique peut être acheminée par câble, satellite, voie hertzienne terrestre ou ADSL (*asymmetric digital subscriber line*). Parmi toutes ces alternatives, la diffusion de la télévision numérique terrestre (*digital television terrestrial broadcast*, DTTB en anglais) présente un grand intérêt en raison de son déploiement aisé sur de grandes zones de couverture, sa bonne qualité de service ainsi que sa possibilité d'adaptation aux scénarios de réception fixe et mobile. Aujourd'hui, on connaît quatre principales normes, à savoir la norme européenne « *Digital Video Broadcasting – Terrestrial* » (DVB-T) [1], la norme japonaise « *Integrated Services Digital Broadcasting – Terrestrial* » (ISDB-T) [2], la norme américaine « *Advanced Television Systems Committee* » (ATSC) [3], et la norme chinoise « *Digital Terrestrial/Television Multimedia Broadcasting* » (DTMB) [4].

La norme DTMB est l'une de celles qui a été développée le plus récemment. Ainsi, ses spécifications techniques adoptent des technologies parmi les plus récentes de l'état de l'art, comme par exemple les codes correcteurs d'erreurs de type LDPC (*Low Density Parity Check codes* en anglais) et la forme d'onde de transmission appelée TDS-OFDM (Time Domain Synchronous- Orthogonal Frequency Division Multiplexing) [5]. En par-

ticulier, le TDS-OFDM, également connu sous le nom de PRP-OFDM (*pseudo random postfix-OFDM* en anglais) ou KSP-OFDM (*known symbol padding-OFDM* en anglais), est une nouvelle forme de signal OFDM qui utilise pour intervalle de garde une séquence pseudo-aléatoire (*Pseudo Random Sequence*, PN en anglais), au lieu du préfixe cyclique (*cyclic prefix*, CP en anglais) classiquement utilisé dans la plupart des systèmes OFDM, alors appelés CP-OFDM. En plus de servir d'intervalle de garde, la séquence PN est également utilisée comme séquence d'apprentissage pour l'estimation de canal et la synchronisation. Par conséquent, aucune donnée pilote supplémentaire n'a besoin d'être insérée parmi le flux de symboles d'information ce qui va dans le sens d'une amélioration de l'efficacité de la transmission TDS-OFDM. En outre, comme chaque trame OFDM possède sa propre séquence d'apprentissage connue, la synchronisation des symboles TDS-OFDM est atteinte plus rapidement que celle des symboles CP-OFDM. Toutefois, le TDS-OFDM possède également ses difficultés techniques. Le problème majeur provient de l'interférence mutuelle inévitablement présente entre les échantillons de la séquence PN et ceux des symboles des trames OFDM. Ainsi, la séquence PN doit être retranchée du signal reçu avant la démodulation des symboles de données OFDM. Une estimation précise de la réponse impulsionnelle du canal (*Channel Impulse Response*, CIR en anglais) est alors nécessaire pour estimer la séquence PN reçue et pouvoir la retrancher précisément. Si l'estimation de canal est imprécise, des échantillons résiduels de la séquence PN seront présents au sein des symboles de données OFDM, ce qui aura pour conséquence de dégrader assez fortement les performances du système. C'est pourquoi, des méthodes d'estimation du canal particulièrement performantes sont nécessaires et essentielles pour les systèmes TDS-OFDM. Dans ce travail de thèse, nous avons donc cherché à proposer des techniques d'estimation de canal efficaces pour les systèmes TDS-OFDM. En outre, nous avons étudié en détail les spécifications du système DTMB et analysé les différences de conception et de performances de ce système avec le système européen DVB-T.

Nous résumons ici en français les éléments importants détaillés dans les chapitres du manuscrit de thèse.

Chapitre 1 : La diffusion de la télévision numérique

Afin de dresser le contexte général de cette thèse, ce chapitre donne un aperçu global des systèmes de diffusion de la télévision numérique, des standards et de leur déploiement à travers le monde.

Tout d'abord, un état des lieux du développement du marché de la télévision dans le monde est présenté en quelques chiffres clef. En 2009 notamment, on compte plus de 2 000 chaînes de télévision à travers le monde et plus de 3 milliards de téléspectateurs potentiels avec un temps d'audience quotidienne moyenne de 192 minutes. Il est incontestable que la télévision est l'une des sources les plus efficaces d'accès aux informations et de divertissement. Avec ce grand nombre de téléspectateurs, la télévision constitue un important vecteur de développement de marchés pour les équipementiers de l'électronique, et la transition vers la télévision numérique renforce naturellement cette tendance. En 2009, on recense environ 1 217 200 000 familles équipées avec au moins un téléviseur, avec une augmentation annuelle de 1% dans les dernières années. Le total des revenus du marché de la télévision à travers le monde en 2009 a été 268,9 milliards d'euros et devrait passer à 322,8 milliards d'euros en 2013.

En tant que pionnier de la recherche autour de la télévision numérique et de son déploiement, les États-Unis ont commencé la migration de leurs stations émettrices vers le système de diffusion numérique depuis le 13 juin 2009. Selon les recommandations faites par la commission européenne, la plupart des pays européens devront quant à eux avoir abandonné les systèmes analogiques pour la diffusion terrestre d'ici 2012. En fait, plusieurs pays tels que Autriche, Pays-Bas, Finlande, Norvège, Suède, Allemagne, Espagne, etc. ont déjà achevé leur transition vers la télévision numérique en Juin 2010. Cette transition est en cours dans d'autres pays européens, comme par exemple en France où plusieurs régions, à savoir l'Alsace, Basse Normandie, Pays de la Loire et Bretagne, ont arrêté la diffusion analogique au cours du premier semestre 2010. L'ensemble des stations émettrices françaises devraient avoir terminé leur basculement au numérique d'ici la fin de l'année 2011 [6]. Au Royaume-Uni, cinq des quinze régions avaient terminé la migration vers la télévision numérique en juin 2010 et le reste se terminera en 2012. En Chine, le gouvernement a décidé d'accélérer la transition nationale vers la télévision numérique en 2010 et prévoit de cesser la transmission de la télévision analogique en 2015.

La télévision numérique terrestre (TNT) est aujourd'hui le mode de réception le plus largement utilisé dans le monde. Il existe quatre normes distinctes associées à ce mode de diffusion dont l'état de déploiement est illustré sur la figure 1.

La norme **ATSC A/53** [3] développée par l'Advanced Television Standards Committee fut publiée en 1996 aux États-Unis. Cette norme utilise la transmission à porteuse unique avec modulation 8-VSB (*8-level vestigial sideband modulation* en anglais). Ce système, directement décliné du système traditionnel analogique, permet assez difficilement d'atteindre la charge utile de 19,4 Mbit/s requise pour une transmission de type HDTV dans une largeur de bande de 6 MHz. Cette norme est principalement conçue pour les réseaux multifréquences (*multi-frequency network*, MFN en anglais).

Le standard **DVB-T** fut développé par un consortium européen d'organisations publiques et privées – le Digital Video Broadcasting (DVB) [7] dans la fin des années 1990. Il utilise la modulation OFDM classique avec préfixe cyclique. Il peut fournir un débit flexible allant de 4,98 Mbit/s à 31,67 Mbit/s pour un canal TV de largeur 8 MHz afin de pouvoir répondre à des applications variées. Grâce à l'existence de l'intervalle de garde,

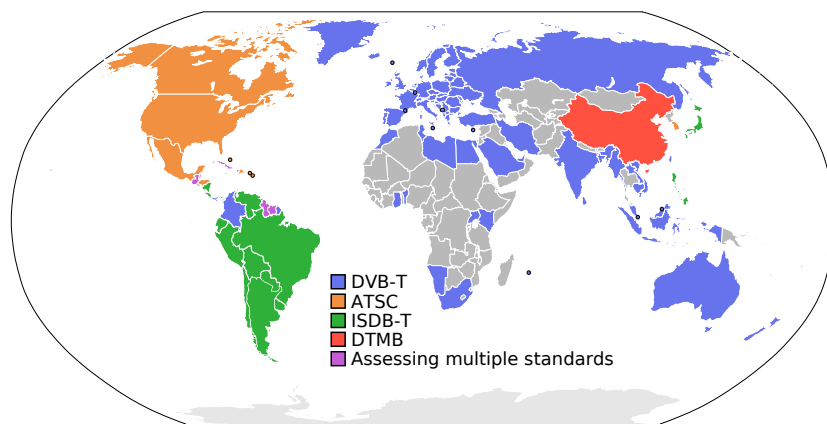


FIGURE 1 – DTTB normes dans le monde [7].

la norme DVB-T peut être déployée au sein d'un réseau mono-fréquence (*single frequency network*, SFN en anglais) correspondant à un réseau de transmission constitué d'émetteurs radio opérant sur une fréquence unique dans une région donnée.

La norme japonaise – **ISDB-T** est très similaire à la norme DVB-T. En particulier, elle présente une couche physique identique à celle du système européen si bien qu'un même récepteur frontal peut être utilisé. Cependant, ISDB-T se distingue par la découpe du signal en 13 segments fréquentiels permettant la diffusion vers divers types de récepteurs, d'une télévision fixe standard à un appareil mobile. Sur la base de ISDB-T, une norme améliorée nommée ISDB-T internationale, a également été développée pour les pays d'Amérique du Sud comme le Brésil, le Pérou, l'Argentine, le Chili, etc. La principale modification par rapport à l'original ISDB-T est l'introduction d'un code de compression vidéo plus avancé – H.264/MPEG-4 AVC. La norme ISDB-T et sa version améliorée ont été adoptées par le Japon lui-même et d'autres pays en Amérique du Sud.

Enfin, la norme **DTMB** a été publiée comme une norme nationale de la Chine en août 2006. Cette norme adopte des techniques récentes de l'état de l'art tels que la forme d'onde TDS-OFDM (Time Domain Synchrones-OFDM) et la technique avancée de codage de canal LDPC (low-density parity-check). La norme DTMB est conçue pour soutenir des scénarios de réception non seulement fixes, mais aussi portables et mobiles. Elle peut par exemple assurer la transmission de vidéos avec une qualité acceptable à une vitesse de 200 km/h correspondant à une réception à bord d'un train par exemple, et donc couvrir la majorité des scénarios pour la réception en mobilité. Enfin, la norme DTMB permet de fournir différents débits utiles allant de 4,813 Mbit/s à 32,486 Mbit/s. Cette norme a été adoptée par la Chine, Hongkong et Macao.

Chapitre 2 : Les techniques multiporteuses

Canal de propagation

Le terme « canal » fait référence au milieu physique dans lequel les signaux portant l'information sont propagés entre l'émetteur et le récepteur. Un modèle de canal important est le canal à trajets multiples. La propagation par trajets multiples est due aux différentes interactions, telles les réflexions et diffractions, de l'onde électromagnétique avec les obstacles présents dans le canal de propagation : sol, arbres, couches atmosphériques, bâtiments, etc. Le signal reçu est donc une somme de versions pondérées et retardées du signal transmis appelées échos. Le canal de propagation est souvent modélisé sous la forme d'un filtre pouvant être décrit par sa réponse impulsionnelle :

$$h(\tau, t) = \sum_{l=0}^{L-1} \gamma_l(t) \delta(\tau - \tau_l(t)), \quad (1)$$

avec L le nombre de trajets. Le $l^{\text{ème}}$ trajet est caractérisé par son retard de propagation $\tau_l(t)$ et son facteur d'atténuation $\gamma_l(t)$. Cette multitude de répliques de l'onde émise se traduit dans le domaine fréquentiel par une réponse du canal présentant de fortes atténuations pour certaines valeurs de fréquences définissant ainsi la sélectivité fréquentielle du canal dans une bande donnée. En passant dans le domaine dual par transformée de Fourier, la réponse du canal dans le domaine fréquentiel s'exprime donc :

$$\begin{aligned} H(t, f) &\triangleq \int_{-\infty}^{+\infty} h(\tau, t) e^{-j2\pi f\tau} d\tau \\ &= \int_{-\infty}^{+\infty} \sum_l \gamma_l(t) \delta(\tau - \tau_l(t)) e^{-j2\pi f\tau} d\tau \\ &= \sum_l \gamma_l(t) e^{-j2\pi f\tau_l(t)}. \end{aligned} \quad (2)$$

Si les paramètres du canal varient au cours du temps, le canal est qualifié de canal dynamique, sinon on parle de canal statique. Un modèle aléatoire de canal classique appelé WSSUS considère que la réponse impulsionnelle est *stationnaire au sens large (Wide-Sense Stationary, WSS)* et que les différents trajets sont *non corrélés (Uncorrelated Scattering, US)*. Les paramètres statistiques du canal WSSUS peuvent être caractérisés par la fonction d'autocorrélation du canal qui s'exprime :

$$\begin{aligned} \phi_h(\tau_1, \tau_2; t_1, t_2) &= \frac{1}{2} \mathbb{E} [h^*(\tau_1, t_1) h(\tau_2, t_2)] \\ &= \frac{1}{2} \mathbb{E} [h^*(\tau_1, t_1) h(\tau_2, t_1 + \Delta t)] = \phi_h(\tau_1; \Delta t) \delta(\tau_1 - \tau_2), \end{aligned} \quad (3)$$

où $\delta(\cdot)$ est la fonction delta de Dirac et $\Delta t = t_2 - t_1$.

Par ailleurs, l'autocorrélation de la fonction de transfert du canal WSSUS dans le plan temps-fréquence peut être définie par la « *spaced-time spaced-frequency correlation function* » :

$$\begin{aligned} \phi_H(\Delta f, \Delta t) &= \frac{1}{2} \mathbb{E} [H^*(f, t) H(f + \Delta f, t + \Delta t)] \\ &= \phi_t(\Delta t) \left(\sum_l \sigma_l^2 e^{-j2\pi \Delta f \tau_l} \right) = \phi_t(\Delta t) \phi_f(\Delta f), \end{aligned} \quad (4)$$

où,

$$\phi_f(\Delta f) \triangleq \sum_l \sigma_l^2 e^{-j2\pi\Delta f\tau_l}. \quad (5)$$

est la fonction de corrélation en fréquence, et $\phi_t(\Delta t)$ est la fonction de corrélation en temps. Précisément, avec le modèle de *Jakes* [8], cette dernière est donnée par :

$$\phi_t(\Delta t) = J_0(2\pi f_m \Delta t), \quad (6)$$

où $J_0(\cdot)$ est la fonction de Bessel de première espèce d'ordre zero et f_m est la fréquence Doppler maximale avec $f_m = v f_0 / c$ où f_0 est la fréquence porteuse, v la vitesse du mobile et c la célérité de la lumière.

Les dispersions temporelles du canal se caractérisent dans le domaine fréquentiel par une corrélation entre les différentes composantes spectrales. Pour décrire la dépendance entre les composantes fréquentielles, on définit la « *bande de cohérence du canal* » par [9, p.164], qui varie suivant le coefficient de corrélation considéré :

$$B_C \approx \frac{1}{50\tau_{rms}}, \quad \text{pour un pourcentage de corrélation égal à 90\%, et} \quad (7)$$

$$B_C \approx \frac{1}{5\tau_{rms}}, \quad \text{pour un pourcentage de corrélation égal à 50\%,} \quad (8)$$

où τ_{rms} est le retard RMS (*root mean square* en anglais). Si la bande passante du signal émis B est plus grande (respectivement plus faible) que B_C , le canal est dit « sélectif (respectivement non-sélectif) en fréquence » (*frequency selective* en anglais).

Le « *temps de cohérence* » T_C correspond quant à lui à la durée pendant laquelle la réponse impulsionnelle du canal peut être considérée comme constante. Une relation approximée peut être établie entre la fréquence Doppler maximale et le temps de cohérence [9, p.166] :

$$T_C \approx \frac{1}{f_m}, \quad \text{ou} \quad (9)$$

$$T_C \approx \frac{9}{16\pi f_m}, \quad \text{ou} \quad (10)$$

$$T_C = \sqrt{\frac{1}{f_m} \frac{9}{16\pi f_m}} = \frac{0.423}{f_m}. \quad (11)$$

Si la durée du signal est plus grande que T_C , le canal est dit « sélectif en temps » (*time selective* en anglais). Dans le cas contraire, il est non-sélectif en temps.

OFDM

L'OFDM est une technique de transmission particulièrement adaptée aux canaux multitrajets. Le principe de l'OFDM repose sur la transmission de plusieurs flux d'information multiplexés en fréquence sur une base de sous-porteuses orthogonales. Plus précisément, les données du flux à transmettre de débit élevé sont réparties sur N flux à bas débit transmis par les N sous-porteuses orthogonales. Les symboles transmis par chaque sous-porteuse ont donc une durée N fois plus grande que les symboles originaux. Ainsi, si le nombre de sous-porteuses est suffisamment grand, la durée des symboles devient bien

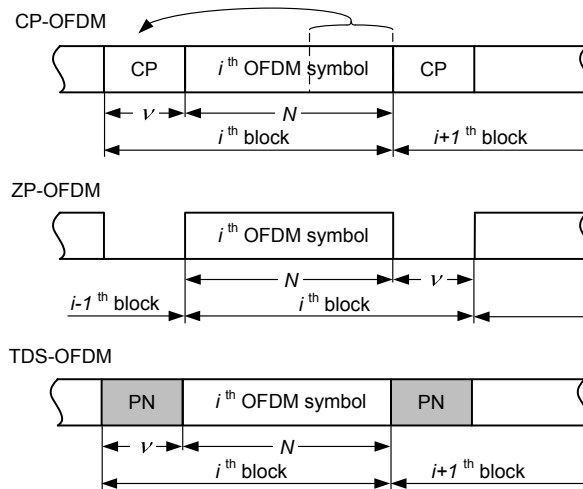


FIGURE 2 – Différents types d'intervalle de garde

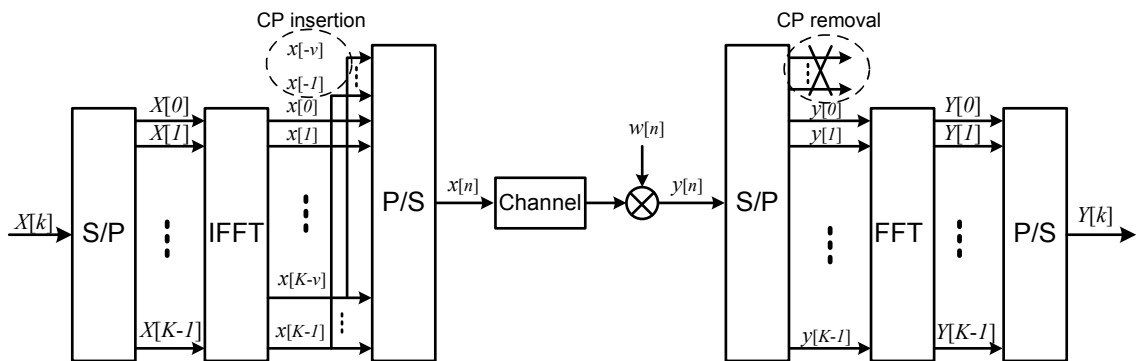


FIGURE 3 – Schéma de modulation/démodulation OFDM.

supérieure à l'étalement des retards de la réponse impulsionnelle du canal. Les effets d'interférence entre symboles (*intersymbol interference*, ISI en anglais) s'en retrouvent alors fortement minimisés. Dans le domaine fréquentiel, le canal sélectif en fréquence est divisé en N sous-canaux qui peuvent être vus comme localement non-sélectifs en fréquence. Aujourd'hui, l'OFDM est utilisé dans de nombreux standards tels que DAB, DVB-T, ADSL, WLAN, 3GPP LTE, WiMAX, UWB etc..

Pour éliminer l'effet de l'ISI résiduelle, un intervalle de garde peut être inséré en préfixe de chaque symbole OFDM. L'intervalle de garde peut être réalisé sous la forme d'une extension cyclique de la partie utile des symboles OFDM, ou en utilisant des symboles nuls ou encore par le biais d'une séquence déterministe connue. Ces différents choix conduisent à trois versions différentes de systèmes OFDM respectivement nommés CP-OFDM, ZP-OFDM et TDS-OFDM comme le décrit la figure 2.

CP-OFDM Le schéma de principe d'une transmission OFDM est présenté dans la figure 3. Les données à transmettre sont groupées par trames de N symboles complexes notées $X^{(i)} = [X^{(i)}[0], X^{(i)}[1], \dots, X^{(i)}[N-1]]^T$, où i représente l'indice de trame. Après Transformée de Fourier Discrète Inverse (*Inverse Fast Fourier Transform*, IFFT en an-

glais), on obtient les symboles OFDM dans le domaine temporel de même indice i :

$$\mathbf{x}^{(i)} = \mathbf{F}_N^{\mathcal{H}} \mathbf{X}^{(i)}, \quad (12)$$

où,

$$\mathbf{F}_N = \frac{1}{\sqrt{N}} \begin{bmatrix} 1 & 1 & \cdots & 1 \\ 1 & e^{-j\frac{2\pi}{N}} & \cdots & e^{-j\frac{2\pi(N-1)}{N}} \\ \vdots & \vdots & \ddots & \vdots \\ 1 & e^{-j\frac{2\pi(N-1)}{N}} & \cdots & e^{-j\frac{2\pi(N-1)^2}{N}} \end{bmatrix}_{N \times N} \quad (13)$$

est la matrice de Fourier de dimensions $N \times N$ avec $\mathbf{F}_N^{\mathcal{H}}$ la matrice hermitienne de la matrice \mathbf{F}_N . En dernier lieu, un préfixe cyclique obtenu par recopie des derniers échantillons du symbole $\mathbf{x}^{(i)}$ est inséré formant ainsi le $i^{\text{ème}}$ symbole OFDM muni de son intervalle de garde :

$$\mathbf{x}_{\text{cp}}^{(i)} = \mathbf{I}_{\text{cp}} \mathbf{x}^{(i)} = \mathbf{I}_{\text{cp}} \mathbf{F}_N^{\mathcal{H}} \mathbf{X}^{(i)}. \quad (14)$$

où

$$\mathbf{I}_{\text{cp}} = \begin{bmatrix} \mathbf{0}_{\nu \times (N-\nu)} & \mathbf{I}_{\nu} \\ \mathbf{I}_N & \end{bmatrix}, \quad (15)$$

est la matrice permettant de modéliser l'insertion du préfixe cyclique, avec $\mathbf{0}_{\nu \times (N-\nu)}$ la matrice de dimensions $\nu \times (N - \nu)$ dont tous les éléments sont à zéros, et avec \mathbf{I}_{ν} et \mathbf{I}_N respectivement les matrices unités de dimensions $\nu \times \nu$ et $N \times N$.

Du côté du récepteur, le $i^{\text{ème}}$ symbole reçu est constitué du produit de la matrice du canal par le $i^{\text{ème}}$ symbole transmis ainsi que d'une contribution en provenance du symbole précédent :

$$\mathbf{y}_{\text{cp}}^{(i)} = \mathbf{H}_{\text{ISI}} \mathbf{x}_{\text{cp}}^{(i)} + \mathbf{H}_{\text{IBI}} \mathbf{x}_{\text{cp}}^{(i-1)} + \mathbf{w}, \quad (16)$$

où \mathbf{w} est le vecteur de bruit additif blanc gaussien (*Additive Gaussian White Noise*, AWGN en anglais) de puissance σ_w^2 et $E\{\mathbf{w}\mathbf{w}^{\mathcal{H}}\} = \sigma_w^2 \mathbf{I}_N$. Par ailleurs, \mathbf{H}_{ISI} et \mathbf{H}_{IBI} sont des matrices de Toeplitz de dimensions $(N + \nu) \times (N + \nu)$:

$$\mathbf{H}_{\text{ISI}} = \begin{bmatrix} h_0 & 0 & \cdots & 0 \\ \vdots & \ddots & & \vdots \\ h_{L-1} & \ddots & \ddots & \vdots \\ 0 & \ddots & \ddots & \ddots \\ \vdots & \ddots & \ddots & \ddots & 0 \\ 0 & \cdots & 0 & h_{L-1} & \cdots & h_0 \end{bmatrix}_{(N+\nu) \times (N+\nu)}, \quad (17)$$

$$\mathbf{H}_{\text{IBI}} = \begin{bmatrix} 0 & \cdots & 0 & h_{L-1} & \cdots & h_1 \\ & & & \ddots & \ddots & \vdots \\ \vdots & & & & \ddots & h_{L-1} \\ \vdots & \ddots & & \ddots & \ddots & 0 \\ \vdots & \ddots & \ddots & \ddots & \ddots & \vdots \\ 0 & \cdots & \cdots & & & 0 \end{bmatrix}_{(N+\nu) \times (N+\nu)}, \quad (18)$$

Si le préfixe cyclique est suffisamment grand, c'est-à-dire de taille supérieure à l'étalement des retards du canal, il est possible d'éliminer les interférences en provenance du symbole OFDM précédemment. Le signal reçu après suppression du préfixe cyclique s'écrit alors :

$$\begin{aligned}
\mathbf{y}^{(i)} &= \mathbf{R}_{\text{cp}} \mathbf{y}_{\text{cp}}^{(i)} \\
&= \begin{bmatrix} & h_{L-1} & \cdots & h_0 & & \\ & & \ddots & & \ddots & \\ \mathbf{0}_{\nu-(L-1)} & & & & & \\ & & & & h_{L-1} & \cdots & h_0 \end{bmatrix}_{N \times (N+\nu)} \mathbf{x}_{\text{cp}}^{(i)} + \mathbf{w} \\
&= \underbrace{\begin{bmatrix} h_0 & 0 & \cdots & h_{L-1} & \cdots & h_1 \\ \vdots & \ddots & \ddots & & \ddots & \vdots \\ h_{L-1} & & \ddots & \ddots & & h_{L-1} \\ 0 & \ddots & & \ddots & \ddots & \\ \vdots & \ddots & \ddots & & \ddots & 0 \\ 0 & \cdots & 0 & h_{L-1} & \cdots & h_0 \end{bmatrix}}_{\mathbf{H}_{\text{circ}}} \mathbf{x}^{(i)} + \mathbf{w}. \tag{19}
\end{aligned}$$

où

$$\mathbf{R}_{\text{cp}} = [\mathbf{0}_{N \times \nu} \mid \mathbf{I}_N], \tag{20}$$

modélise le processus d'élimination du préfixe cyclique. La matrice de canal devient ainsi circulante et présente donc la propriété remarquable d'être diagonale dans la base de Fourier. Le signal reçu exprimé dans le domaine fréquentiel est donc décrit par :

$$\begin{aligned}
\mathbf{Y}^{(i)} &= \mathbf{F}_N \mathbf{y}^{(i)} = \mathbf{F}_N \mathbf{H}_{\text{circ}} \mathbf{F}_N^H \mathbf{X}^{(i)} + \mathbf{F}_N \mathbf{w} \\
&= \begin{bmatrix} H[0] & 0 & \cdots & \cdots & 0 \\ 0 & H[1] & \ddots & & \vdots \\ \vdots & \ddots & \ddots & \ddots & \vdots \\ \vdots & & \ddots & \ddots & 0 \\ 0 & \cdots & \cdots & 0 & H[N-1] \end{bmatrix} \mathbf{X}^{(i)} + \mathbf{W}, \\
&= \mathbf{H}_{\text{diag}} \mathbf{X}^{(i)} + \mathbf{W}, \tag{21}
\end{aligned}$$

avec $H[k] = \sum_{l=0}^{L-1} h_l e^{-j \frac{2\pi}{N} lk}$ le coefficient de la réponse fréquentielle du canal associé à la sous-porteuse k . Ainsi, la réponse fréquentielle du canal sur chaque sous-porteuse peut être considérée comme plate et le processus d'égalisation se réduit à une multiplication par un seul coefficient sur chaque sous-porteuse.

ZP-OFDM Comme le préfixe cyclique est une copie redondante des données utiles, son utilisation entraîne une dégradation de l'efficacité spectrale globale du système. Pour éviter cette perte, il a été proposé de remplacer le principe d'extension cyclique des symboles par une simple opération de zero-padding (ZP) [10]. Plus précisément, ν zéros sont ajoutés à la fin de chaque symbole OFDM. L'opération d'insertion de préfixe cyclique (15) est ainsi

remplacée par un processus ZP :

$$\mathbf{I}_{\text{zp}} = \begin{bmatrix} \mathbf{I}_N \\ \mathbf{0}_{N \times \nu} \end{bmatrix}. \quad (22)$$

Le signal ZP-OFDM s'écrit donc :

$$\mathbf{x}_{\text{zp}}^{(i)} = \mathbf{I}_{\text{zp}} \mathbf{x}^{(i)} = \mathbf{I}_{\text{zp}} \mathbf{F}_N^H \mathbf{X}^{(i)}. \quad (23)$$

Comme dans le cas CP-OFDM, le signal reçu s'exprime comme suit :

$$\mathbf{y}_{\text{zp}}^{(i)} = \mathbf{H}_{\text{ISI}} \mathbf{I}_{\text{zp}} \mathbf{x}^{(i)} + \mathbf{H}_{\text{IBI}} \mathbf{I}_{\text{zp}} \mathbf{x}^{(i-1)} + \mathbf{w}. \quad (24)$$

Contrairement au cas CP-OFDM, aucune cyclicité n'est présente au sein des symboles ZP-OFDM. Une méthode simple appelée *overlap-add* (OLA) peut alors être appliquée au signal ZP-OFDM afin de recréer la structure cyclique des signaux CP-OFDM avant l'application de la IFFT de réception. L'intérêt est de pouvoir ainsi profiter de la simplicité de l'opération d'égalisation à un coefficient présentée précédemment. L'opération OLA consiste en une recopie des échantillons contenus en fin de chaque symbole OFDM reçu en début de symbole comme le montre la figure 2. L'opération d'OLA peut être écrite par le biais de la matrice $N \times (N + \nu)$:

$$\mathbf{I}_{\text{OLA}} = \left[\mathbf{I}_N \mid \begin{array}{c} \mathbf{I}_\nu \\ \mathbf{0}_{(N-\nu) \times \nu} \end{array} \right]. \quad (25)$$

Le signal reçu après le processus d'OLA devient alors :

$$\begin{aligned} \mathbf{y}_{\text{OLA}}^{(i)} &= \mathbf{I}_{\text{OLA}} \mathbf{H}_{\text{ISI}} \mathbf{I}_{\text{zp}} \mathbf{x}^{(i)} + \mathbf{I}_{\text{OLA}} \mathbf{w} \\ &= \mathbf{H}_{\text{circ}} \mathbf{x}^{(i)} + \mathbf{w}', \end{aligned} \quad (26)$$

qui prend alors la même forme que dans le cas d'un signal CP-OFDM, avec $\mathbf{w}' = \mathbf{I}_{\text{OLA}} \mathbf{w}$ la composante de bruit obtenue après OLA. A puissance émise identique, on comprend alors que le rapport signal sur bruit obtenu pour chaque forme d'onde CP-OFDM et ZP-OFDM sera identique, puisque le gain en puissance utile dont profite la forme ZP-OFDM par rapport à la forme CP-OFDM est exactement compensé par l'augmentation du niveau de bruit due à l'opération d'OLA.

L'intérêt principal de la forme d'onde ZP-OFDM est en réalité liée au fait que l'opération de zero-padding, contrairement à l'opération d'extension cyclique, ne crée par d'ondulation sur la densité spectrale de puissance du signal émis puisqu'elle n'affecte pas l'orthogonalité entre les sous-porteuses. Ceci est un avantage non négligeable lorsque la densité spectrale de puissance est contrainte à l'émission par un masque de puissance très restrictif comme dans le cas des applications UWB.

TDS-OFDM De manière générale, l'utilisation d'un intervalle de garde a pour conséquence de dégrader le débit utile puisque qu'une portion de temps est dédiée à la transmission d'informations autres que les données utiles. Récemment, une structure alternative d'intervalle de garde a été proposée dans le but d'optimiser l'utilisation de la ressource spectrale. Dans cette nouvelle structure, l'intervalle de garde est composé d'une séquence

connue qui est réutilisée pour l'estimation de canal et la synchronisation (récupération de rythme, récupération de porteuse et de synchronisation de trame), afin de réduire le surcoût global de transmission. Cette solution est communément appelée TDS-OFDM [11], ou Pseudo Random Postfix-OFDM, PRP-OFDM [12] ou encore Known Symbol Padding-OFDM, KSP-OFDM [13]).

Le signal de TDS-OFDM peut s'écrire comme :

$$\mathbf{x}_{\text{TDS}}^{(i)} = \mathbf{x}_{\text{zp}}^{(i)} + \bar{\mathbf{c}}^{(i)} = \begin{bmatrix} \mathbf{x}^{(i)} \\ \mathbf{c}^{(i)} \end{bmatrix}. \quad (27)$$

où $\bar{\mathbf{c}}^{(i)} = [\mathbf{0}_N^T, \mathbf{c}^{(i)T}]^T$ avec $\mathbf{c}^{(i)} = [c_0^{(i)}, c_1^{(i)}, \dots, c_{\nu-1}^{(i)}]^T$ la séquence connue.

Le signal reçu s'écrit alors :

$$\mathbf{y}_{\text{TDS}}^{(i)} = \mathbf{H}_{\text{ISI}} \mathbf{x}_{\text{zp}}^{(i)} + \mathbf{H}_{\text{ISI}} \bar{\mathbf{c}}^{(i)} + \mathbf{H}_{\text{IBI}} \mathbf{x}_{\text{zp}}^{(i-1)} + \mathbf{H}_{\text{IBI}} \bar{\mathbf{c}}^{(i-1)} + \mathbf{w}. \quad (28)$$

On peut voir qu'il y a bien sûr apparition d'interférence mutuelle entre les données et la séquence connue au sein du signal reçu. En supposant que l'on dispose d'une estimation parfaite de la réponse du canal, on peut intégralement supprimer la contribution de la séquence PN au sein du flux d'échantillons reçus et ainsi transformer les symboles TDS-OFDM en symboles ZP-OFDM. Les processus décrits précédemment dans le cas du ZP-OFDM peuvent alors être directement mis en œuvre. Si le canal n'est pas parfaitement connu, des résidus de la séquence PN demeureront au sein du signal reçu et engendreront des interférences sur la partie utile des symboles OFDM. Ainsi, on comprend que le processus d'estimation de canal est une opération critique pour les systèmes TDS-OFDM et à laquelle il faut apporter un soin particulier. Ceci motive la suite des travaux présentés dans cette thèse et en particulier le fait de se concentrer sur l'élaboration d'algorithmes avancés d'estimation de canal pour les systèmes TDS-OFDM.

Chapitre 3 : Analyse et comparaison de DVB-T et DTMB

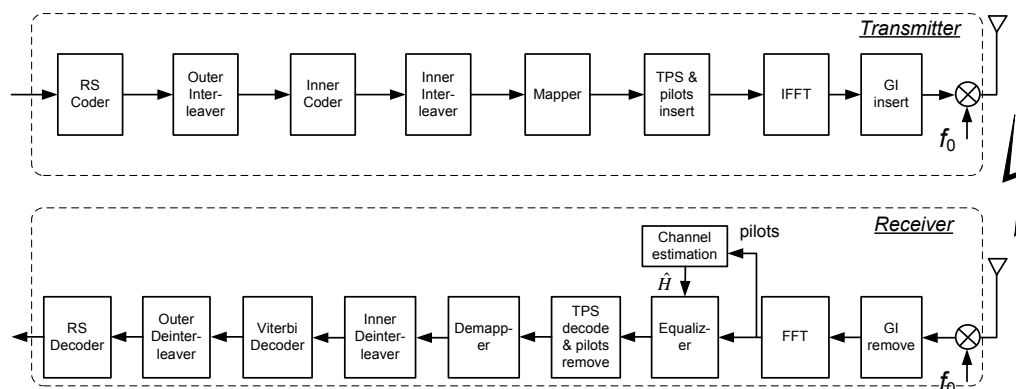


FIGURE 4 – Schéma du système DVB-T.

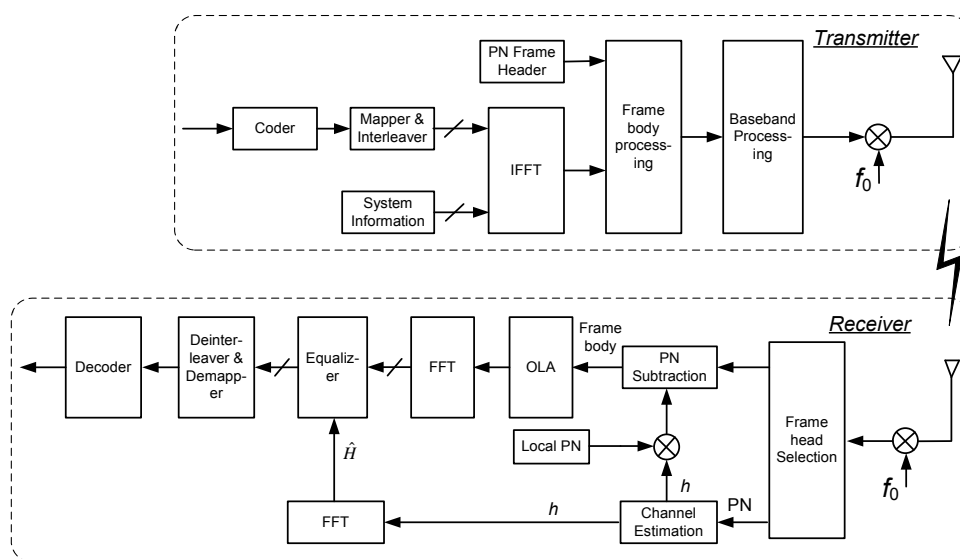


FIGURE 5 – Schéma du système DTMB.

Parmi toutes les normes de diffusion numérique existantes, DVB-T est sans nul doute la plus populaire. Cependant la norme DTMB attire aujourd'hui l'intérêt d'un grand nombre de chercheurs en raison des nouvelles techniques de traitement du signal qu'elle nécessite pour la mise au point de récepteurs performants. Avant d'aller plus loin sur ces aspects algorithmiques, il est intéressant dans un premier temps d'effectuer une analyse comparative entre les normes DVB-T et DTMB afin d'en cerner les avantages et limites respectifs.

Les schémas de principe des systèmes DVB-T et DTMB sont présentés sur les figures 4 et 5. La différence principale entre les deux systèmes tient aux opérations d'insertion et de retrait de l'intervalle de garde ainsi qu'à l'insertion des données d'apprentissage

TABLE 1 – Principaux paramètres de DVB-T et DTMB.

		DVB-T		DTMB	
		2K mode	8K mode	single carrier mode	multicarrier mode
Sample period		7/64 μ s		1/7.56 μ s	
OFDM symbol duration (T)		224 μ s	896 μ s	500 μ s	
Number of subcarriers		2 048	8 192	1	3 780
Number of active subcarriers		1 705	6 817	1	3 780
Subcarrier spacing (1/T)		4 464 Hz	1 116 Hz	–	2 kHz
Baseband bandwidth		7.61 MHz		7.56 MHz	
Guard Interval	Length	T/4, T/8, T/16, T/32		\approx T/6 (595 samples)	T/4 (420 samples), T/9 (945 samples)
	Duration	56 μ s, 28 μ s, 14 μ s, 7 μ s	224 μ s, 112 μ s, 56 μ s, 28 μ s	78.7 μ s	55.6 μ s, 125 μ s
	Power	non-boost		non-boost	boosted by 2
	Phase	–		constant in a superframe	changing or constant
Mapping		QPSK, 16QAM, 64QAM (optionally hierarchical)		4QAM-NR, 4QAM, 16QAM, 32QAM	4QAM, 16QAM, 64QAM
Interleaver	outer	convolutional interleaver		–	
	inner	bitwise + symbol interleaver		time domain	time & frequency domain
Channel coding	outer	Reed-Solomon (204, 188, t=8)		BCH (762, 752)	
	inner	convolutional code		LDPC (7493, 3048), (7493, 4572), (7493, 6096)	
	code rate	1/2, 2/3, 3/4, 5/6, 7/8		0.4 (7488, 3008), 0.6 (7488, 4512), 0.8 (7488, 6016)	

pour l'estimation de canal. Par ailleurs, certains paramètres importants des systèmes sont répertoriés dans le tableau 1 afin de faciliter l'analyse comparative.

Bande passante Les bandes passantes des deux systèmes sont très voisines et de l'ordre de 8 MHz, et ce afin de s'adapter aux canaux déjà utilisés pour la télévision analogique en Europe et en Chine. Le système DVB-T n'utilise pas de filtre de mise en forme particulier et assure la limitation de largeur de bande et la protection des canaux adjacents par l'extinction de 16,7 % sous-porteuses sur les bords du spectre. Le système DTMB quant à lui doit compter avec la présence de la séquence PN dont la densité spectrale de puissance occupe une bande plus large que le signal de données OFDM. Pour cette raison, la norme DTMB spécifie l'utilisation d'un filtre de mise en forme de type racine de cosinus surélevé (*square-root-raised-cosine* SRRC).

Afin de s'adapter à la largeur de bande de canal de télévision d'autres pays tels que les États-Unis, l'Australie et le Japon, DVB-T prévoit également des options supplémentaires de modification de la bande passante avec débits réduits dans la norme [1, Annexe E]. Ainsi la norme DVB-T présente une grande flexibilité d'application dans des pays différents.

TABLE 2 – Comparaison de l'efficacité d'exploitation de la puissance émise.

		DVB-T		DTMB
		2K mode	8K mode	multicarrier mode
FFT size		2 048	8 192	3 780
Number of active subcarriers		1 705	6 817	3 780
Number of data subcarrier		1 512	6 048	3 744
Guard Interval	Length	1/4, 1/8, 1/16, 1/32		1/4 (420 samples), 1/9 (945 samples)
	Power	non-boost		boosted by 2
Number of TPS		17	68	36
Number of pilots		176	701	–
Power efficiency factor		0.66 (GI=1/4), 0.73 (GI=1/8), 0.77 (GI=1/16), 0.79 (GI=1/32)		0.66 (GI=1/4), 0.81 (GI=1/9)

Concernant DTMB, 8 MHz est la bande passante unique qui a été spécifiée dans la norme. Cependant, des recherches récentes sont consacrées à la spécification de plus d'options pour couvrir les bandes 1.7, 6, 7, 8 et 10 MHz.

Paramètres concernant l'opération OFDM Pour le système DVB-T, on compte deux options, à savoir 2K ($2 \times 2^{10} = 2048$) et 8K ($8 \times 2^{10} = 8192$), pour la taille de la FFT réalisant la modulation OFDM. Le mode 2K est davantage approprié pour les faibles zones de couverture, mais peut offrir de meilleures performances de réception en mobilité. Le mode 8K présente une durée de l'intervalle de garde plus longue et un écart inter-porteuses plus étroit, ce qui indique une capacité à supporter le mode SFN sur une plus grande surface et va plutôt dans le sens d'une réception fixe. Ainsi, les modes 2K et 8K ont des caractéristiques complémentaires et peuvent être utilisés dans des scénarios différents. Pour le système DTMB, une FFT de taille 3780 points a été adoptée pour la modulation OFDM. Cette taille particulière a été choisie afin d'atteindre un bon compromis entre la réception mobile et la couverture SFN, mais aussi pour contourner les brevets bien établis pour les tailles de type $N = 2^p$.

Schéma de correction d'erreur Pour le système DVB-T, le schéma de codage de canal résulte d'une concaténation d'un code de Reed-Solomon RS (204, 118, $t = 8$) utilisé comme code externe, et d'un code convolutif de rendement 1/2 pouvant être poinçonné pour obtenir les rendements 2/3, 3/4, 5/6 et 7/8. Entre les deux codes, un entrelaceur convolutif avec un retard maximum de 2244 bytes est appliqué.

Pour le système DTMB, un code interne de type LDPC concaténé avec un code BCH (*Bose-Chaudhuri-Hocquenghem*) est adopté offrant trois options de rendement de codage, à savoir 0.4, 0.6 et 0.8. On peut remarquer qu'aucun entrelacement n'est prévu entre les deux codes. Par ailleurs, le code LDPC utilisé est une version raccourcie du code LDPC spécifié dans la norme DVB-S2. En conséquence, le système DTMB ne peut pas tirer pleinement partie du pouvoir de correction qu'il aurait été possible d'obtenir avec le code d'origine.

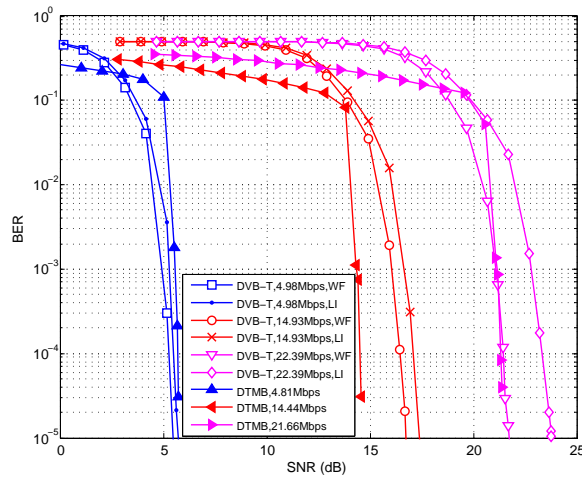


FIGURE 6 – Comparaison des performances TEB dans le canal P1, avec différentes modulations, taux de codage et méthodes d'estimation de canal.

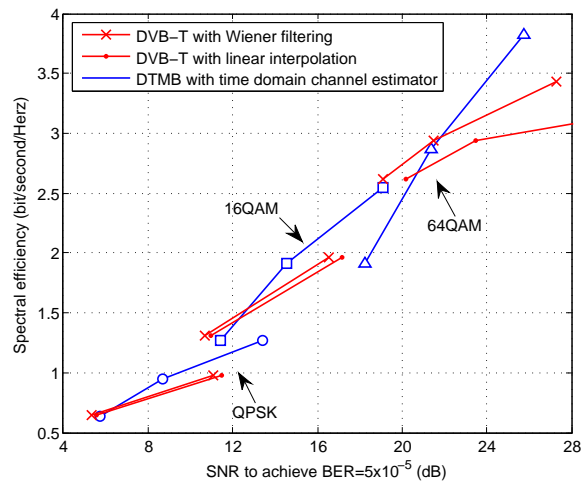


FIGURE 7 – Comparaison de l'efficacité spectrale dans le canal P1.

Évaluation des performances des systèmes

Efficacité d'exploitation de la puissance émise Chaque système doit allouer des ressources dédiées aux fonctions de synchronisation, d'estimation de canal et de signalisation. Il s'agit souvent de sous-porteuses réservées au sein du multiplex OFDM dont la puissance peut être augmentée par rapport aux sous-porteuses de données utiles afin de fiabiliser leur transmission. Dans le cas du système TDS-OFDM, ces données d'apprentissage sont en partie transmises au sein de l'intervalle de garde par le biais de la séquence PN. Dans tous les cas, la transmission de ces données se traduit par une utilisation d'une portion de la puissance d'émission qui n'est pas utilisée pour transmettre les données utiles. Pour évaluer cette perte, nous calculons « *le facteur d'efficacité d'exploitation de la puissance* » qui est défini par le taux de la puissance allouée aux sous-porteuses de don-

nées utiles sur la puissance totale consacrée à la transmission. Les résultats sont indiqués dans le tableau 2.

TEB Nous analysons ici les performances comparées des deux systèmes en termes de taux d'erreur binaire (TEB) pour différents modes de transmission et pour des conditions de canal différentes. Pour plus d'équité, les modes de transmission conduisant à des débits utiles similaires de chaque système sont choisis.

A titre d'exemple, la figure 6 présente les TEB obtenus dans le canal P1. De même, la figure 7 donne le SNR requis pour atteindre différentes efficacités spectrales pour un BER cible de 5×10^{-5} en utilisant des techniques classiques d'estimation de canal. On s'aperçoit que les performances des deux systèmes sont finalement assez proches malgré les différences notables de spécifications techniques.

Chapitre 4 : Estimation de canal basé sur la séquence PN

Nous étudions dans ce chapitre plusieurs techniques d'estimation de canal pour le système TDS-OFDM exclusivement basées sur l'exploitation de la séquence PN dans le domaine fréquentiel et temporel. L'intervalle de garde spécifié dans le standard DTMB est utilisé comme référence. Celui-ci est composé d'une séquence PN possédant un préfixe cyclique.

Estimation de canal dans le domaine fréquentiel

L'estimation de canal effectuée dans le domaine fréquentiel est basée sur l'application d'une transformée de Fourier rapide (FFT) sur la séquence PN. La présence du préfixe cyclique permet d'obtenir naturellement une matrice diagonale portant les coefficients fréquentiels du canal. L'estimation basée sur le critère des moindres carrés (LS) s'écrit alors simplement :

$$\bar{\mathbf{H}} = (\mathbf{P}_d^H \mathbf{P}_d)^{-1} \mathbf{P}_d^H \mathbf{D} = \mathbf{H} + (\mathbf{P}_d^H \mathbf{P}_d)^{-1} \mathbf{P}_d^H \mathbf{W}, \quad (29)$$

où \mathbf{D} , \mathbf{H} et \mathbf{W} sont respectivement les réponses fréquentielles de la séquence PN, la matrice diagonale des coefficients fréquentiels du canal, et le terme de bruit. L'estimateur dans le domaine fréquentiel est donc facile à appliquer avec une faible complexité de calcul.

Estimation de canal dans le domaine temporel

Dans le domaine temporel, les performances de l'estimation de canal vont essentiellement dépendre des bonnes propriétés de corrélation de la séquence PN. La fonction d'autocorrélation de la séquence PN s'écrit :

$$C_p[n] = \frac{1}{N_{\text{PN}}} p[n+m] \otimes p[m] = \begin{cases} 1 & n = 0 \\ -\frac{1}{N_{\text{PN}}} & 0 < n < N_{\text{PN}} \end{cases}. \quad (30)$$

La séquence PN reçue s'exprime comme :

$$\mathbf{d} = \mathbf{P}_{\text{circ}} \mathbf{h} + \mathbf{w}, \quad (31)$$

où $\mathbf{h} = [h[0], h[1], \dots, h[L-1], \dots, 0]^T$ et \mathbf{P}_{circ} est la matrice circulante de dimensions $N_{\text{PN}} \times N_{\text{PN}}$ avec la première ligne $[p[0], p[N_{\text{PN}}-1], p[N_{\text{PN}}-2], \dots, p[1]]$. Précisons que cette matrice est circulante grâce à la présence de l'extension cyclique en préfixe de la séquence PN.

Ainsi, l'estimateur dans le domaine temporel s'écrit :

$$\begin{aligned}
\bar{\mathbf{h}} &= \frac{1}{N_{\text{PN}}} \mathbf{P}_{\text{cor}} \mathbf{d} = \frac{1}{N_{\text{PN}}} \underbrace{\mathbf{P}_{\text{cor}} \mathbf{P}_{\text{circ}}}_{\mathbf{Q}} \mathbf{h} + \frac{1}{N_{\text{PN}}} \mathbf{P}_{\text{cor}} \mathbf{w} \\
&= \underbrace{\begin{bmatrix} 1 & -\frac{1}{N_{\text{PN}}} & -\frac{1}{N_{\text{PN}}} & \cdots & -\frac{1}{N_{\text{PN}}} \\ -\frac{1}{N_{\text{PN}}} & 1 & -\frac{1}{N_{\text{PN}}} & \cdots & -\frac{1}{N_{\text{PN}}} \\ -\frac{1}{N_{\text{PN}}} & -\frac{1}{N_{\text{PN}}} & 1 & \cdots & -\frac{1}{N_{\text{PN}}} \\ \vdots & \vdots & \vdots & \ddots & \vdots \\ -\frac{1}{N_{\text{PN}}} & -\frac{1}{N_{\text{PN}}} & -\frac{1}{N_{\text{PN}}} & \cdots & 1 \end{bmatrix}}_{\mathbf{Q}} \begin{bmatrix} h_0 \\ \vdots \\ h_{L-1} \\ \vdots \\ 0 \end{bmatrix} \\
&+ \frac{1}{N_{\text{PN}}} \begin{bmatrix} p[0] & p[1] & p[2] & \cdots & p[N_{\text{PN}} - 1] \\ p[N_{\text{PN}} - 1] & p[0] & p[1] & \cdots & p[N_{\text{PN}} - 2] \\ p[N_{\text{PN}} - 2] & p[N_{\text{PN}} - 1] & p[0] & \cdots & p[N_{\text{PN}} - 3] \\ \vdots & \vdots & \vdots & \ddots & \vdots \\ p[1] & p[2] & p[3] & \cdots & p[0] \end{bmatrix} \begin{bmatrix} w[0] \\ w[1] \\ w[2] \\ \vdots \\ w[N_{\text{PN}} - 1] \end{bmatrix} \quad (32)
\end{aligned}$$

où \mathbf{P}_{cor} est la matrice circulante de dimensions $N_{\text{PN}} \times N_{\text{PN}}$ dont la première ligne est $[p[0], p[1], \dots, p[N_{\text{PN}} - 1]]$. L'erreur quadratique moyenne (EQM) de cet estimateur est :

$$\begin{aligned}
\varepsilon_{\bar{\mathbf{h}}} &= \frac{1}{N_{\text{PN}}} \underbrace{\text{Tr} \left((\mathbf{Q} - \mathbf{I}_{N_{\text{PN}}}) \mathbf{\Lambda} (\mathbf{Q} - \mathbf{I}_{N_{\text{PN}}})^{\mathcal{H}} \right)}_{\text{interférences}} + \frac{\sigma_w^2}{N_{\text{PN}}^3} \underbrace{\text{Tr} \left(\mathbf{P}_{\text{cor}} \mathbf{P}_{\text{cor}}^{\mathcal{H}} \right)}_{\text{bruit}}, \quad (33)
\end{aligned}$$

où $\mathbf{\Lambda}$ est une matrice diagonale dont les L premiers éléments de la diagonale principale sont $[\alpha_0^2, \alpha_1^2, \dots, \alpha_{L-1}^2]$ et les autres éléments sont nuls. $\alpha_l^2 = \mathbb{E}[|h_l|^2]$ est la puissance moyenne du $l^{\text{ième}}$ trajet du canal. En comparant les expressions des EQM théoriques, on déduit que l'estimateur dans le domaine temporel surpasse l'estimateur dans le domaine fréquentiel comme le confirme les résultats présentés sur la figure 8. Cependant, on note la présence d'un plancher d'erreur à fort SNR pour l'estimateur temporel dû au terme d'interférence mis en évidence à l'équation 33.

Amélioration de l'algorithme d'estimation dans le domaine temporel

Afin d'améliorer la technique d'estimation dans le domaine temporel, nous proposons plusieurs améliorations visant à minimiser les effets de l'interférence. Une première approche vise à convertir la matrice de convolution de la séquence PN en une matrice identité de sorte à complètement annuler le terme d'interférence. Une seconde approche consiste à soustraire ce terme d'interférence en utilisant le résultat de l'estimation de canal.

Méthode 1 : Multiplication par la matrice inverse \mathbf{Q}^{-1} Comme la matrice \mathbf{Q} est connue et toujours de rang plein pour une m -séquence donnée, un nouvel estimateur est obtenu en effectuant une multiplication à gauche par \mathbf{Q}^{-1} dans l'expression de l'estimateur présenté dans (32) :

$$\hat{\mathbf{h}}_1 = \mathbf{Q}^{-1} \bar{\mathbf{h}} = \mathbf{h} + \frac{1}{N_{\text{PN}}} \mathbf{Q}^{-1} \mathbf{P}_{\text{cor}} \mathbf{w}. \quad (34)$$

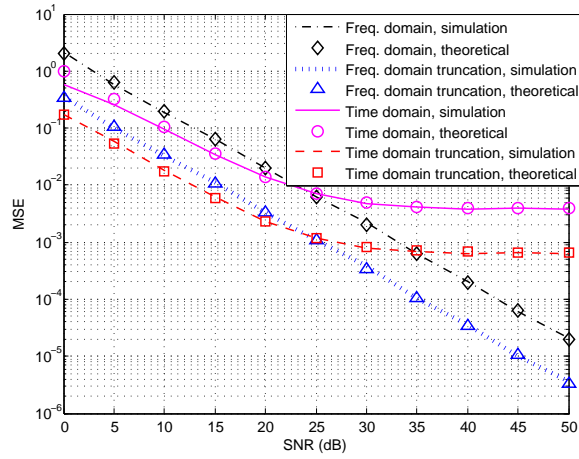


FIGURE 8 – Comparaison des performances des estimateurs dans les domaines temporel et fréquentiel. Les résultats sont obtenus avec 500 réalisations du canal TU-6.

Comme la matrice \mathbf{Q} est connue pour une m -séquence donnée, son inverse est facile à obtenir et peut être calculée par avance :

$$\mathbf{Q}^{-1} = \begin{bmatrix} \frac{2N_{\text{PN}}}{N_{\text{PN}}+1} & \frac{N_{\text{PN}}}{N_{\text{PN}}+1} & \frac{N_{\text{PN}}}{N_{\text{PN}}+1} & \cdots & \frac{N_{\text{PN}}}{N_{\text{PN}}+1} \\ \frac{N_{\text{PN}}}{N_{\text{PN}}+1} & \frac{2N_{\text{PN}}}{N_{\text{PN}}+1} & \frac{N_{\text{PN}}}{N_{\text{PN}}+1} & \cdots & \frac{N_{\text{PN}}}{N_{\text{PN}}+1} \\ \frac{N_{\text{PN}}}{N_{\text{PN}}+1} & \frac{N_{\text{PN}}}{N_{\text{PN}}+1} & \frac{2N_{\text{PN}}}{N_{\text{PN}}+1} & \cdots & \frac{N_{\text{PN}}}{N_{\text{PN}}+1} \\ \vdots & \vdots & \vdots & \ddots & \vdots \\ \frac{N_{\text{PN}}}{N_{\text{PN}}+1} & \frac{N_{\text{PN}}}{N_{\text{PN}}+1} & \frac{N_{\text{PN}}}{N_{\text{PN}}+1} & \cdots & \frac{2N_{\text{PN}}}{N_{\text{PN}}+1} \end{bmatrix} \quad (35)$$

L'EQM peut alors être calculée comme :

$$\varepsilon_{\hat{h}_1} = \frac{2\sigma_w^2}{N_{\text{PN}} + 1}. \quad (36)$$

Si l'estimation de la réponse impulsionnelle du canal est tronquée à la longueur réelle L , la matrice \mathbf{Q}^{-1} devient :

$$\bar{\mathbf{Q}}^{-1} = \begin{bmatrix} a & b & b & \cdots & b \\ b & a & b & \cdots & b \\ b & b & a & \cdots & b \\ \vdots & \vdots & \vdots & \ddots & \vdots \\ b & b & b & \cdots & a \end{bmatrix} \quad (37)$$

où

$$a = 1 + \frac{L-1}{N_{\text{PN}}^2 + 2N_{\text{PN}} - N_{\text{PN}}L - L + 1},$$

$$b = \frac{N_{\text{PN}}}{N_{\text{PN}}^2 + 2N_{\text{PN}} - N_{\text{PN}}L - L + 1}.$$

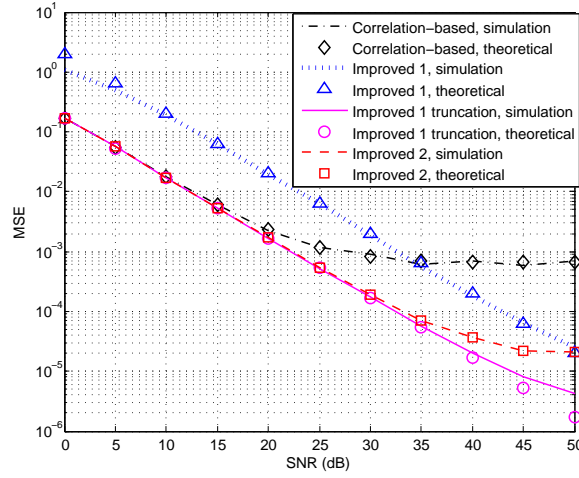


FIGURE 9 – Comparaison des performances des différents estimateurs dans le domaine temporel. Les résultats sont obtenus avec 500 réalisations de TU-6 canal.

L'EQM de l'estimation obtenue est alors améliorée :

$$\varepsilon_{\hat{h}_1} = \frac{N_{\text{PN}} - L + 2}{N_{\text{PN}}^2 + 2N_{\text{PN}} - N_{\text{PN}}L - L + 1} \sigma_w^2. \quad (38)$$

Méthode 2 : Soustraction de l'interférence Nous pouvons également soustraire les interférences introduites par la corrélation de la séquence PN en utilisant l'estimation du canal :

$$\hat{\mathbf{h}}_2 = \tilde{\mathbf{h}} - \bar{\mathbf{\Delta}} \tilde{\mathbf{h}}, \quad (39)$$

où $\tilde{\mathbf{h}}$ est le vecteur des estimés du canal de longueur L , $\bar{\mathbf{\Delta}}$ est une matrice de dimension $L \times L$ dont les éléments de la diagonale principale sont nuls et les autres éléments valent $-\frac{1}{N_{\text{PN}}}$. L'EQM de l'estimateur obtenu est :

$$\varepsilon_{\hat{h}_2} = \frac{(L-1)(L^2 - 3L + 3)}{N_{\text{PN}}^4 L} + \frac{1}{N_{\text{PN}}} \sigma_w^2 + \frac{(L-1)(2-L-N_{\text{PN}})}{N_{\text{PN}}^4} \sigma_w^2. \quad (40)$$

La méthode 1 et la méthode 2 peuvent abaisser le plancher d'erreur mis en évidence précédemment comme le montre la figure 9. La seconde méthode apparaît comme la plus efficace même à très fort SNR.

Dans la version complète du manuscrit, nous analysons également les effets de la dégradation des performances dans le cas de canaux à fortes dispersions temporelles. Plusieurs optimisations sont alors proposées pour améliorer les performances.

Chapitre 5 : Estimation de canal aidée par les données pour le système TDS-OFDM

Malgré les améliorations apportées dans le chapitre précédent, l'estimation de canal basée sur la séquence PN s'avère parfois peu fiable en particulier dans le cas de canaux fortement dispersifs en temps. Dans ce chapitre, on se propose d'élaborer une méthode d'estimation robuste et capable de supporter différents scénarios de transmission. Ayant déjà tiré pleinement partie de la séquence d'apprentissage PN, une amélioration supplémentaire des performances est recherchée par la mise en œuvre d'un processus dirigé par les décisions. En supposant que l'estimation basée sur la séquence PN est disponible en tant qu'estimation initiale, il est en effet possible de raffiner à l'aide d'un processus itératif les estimés de canal en exploitant le résultat des décisions prises sur les données utiles comme cela est classiquement fait dans les procédés de turbo-estimation. Dans la plupart des algorithmes de la littérature, le processus itératif inclut les fonctions de désentrelacement et de décodage de canal afin de fiabiliser au maximum les prises de décisions. Ceci est cependant très difficilement applicable au système TDS-OFDM du standard DTMB qui nous intéresse étant donné la très grande profondeur d'entrelacement et le type de code de canal choisi. On s'intéresse donc ici à appliquer les principes de l'estimation de canal turbo mais en exploitant directement les décisions prises en sortie du détecteur à sorties souples avant désentrelacement et décodage de canal. Un certain nombre de procédés de fiabilisation de ces décisions vont alors devoir être élaborés.

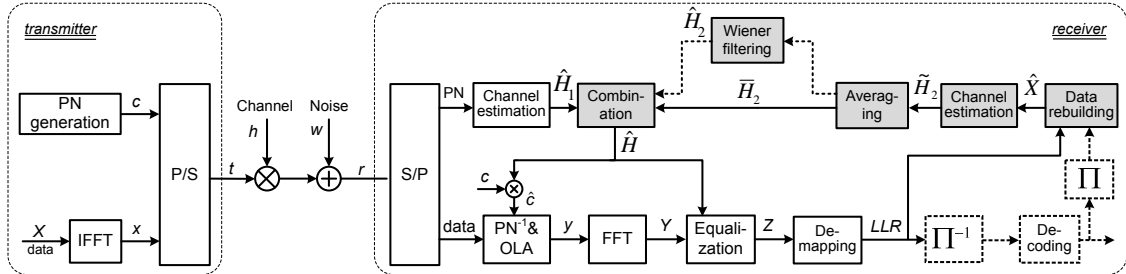


FIGURE 10 – Schéma fonctionnel du système TDS-OFDM. Les cases ombrées correspondent aux traitements utilisés pour la méthode proposée. Les blocs en pointillés correspondent aux traitements complémentaires nécessaires à l'estimation de canal Turbo.

Estimation instantanée de la réponse fréquentielle du canal

Comme le montre la figure 10 et comme expliqué précédemment, contrairement à un classique algorithme itératif d'estimation de canal turbo [14], la nouvelle méthode exclut le désentrelacement, le décodage de canal et l'entrelacement de la boucle de retour. En d'autres termes, les symboles de données estimés basés sur l'estimation de canal courante disponible sont reconstruits en utilisant directement les informations de sortie du *soft demapper*.

Sur la base des LLR (*Log Likelihood Ratios*), les probabilités d'un bit égal à 1 et 0 sont :

$$P(b[i, k, l] = 1 | Z[i, k]) = \frac{e^{\lambda_l[i, k]}}{1 + e^{\lambda_l[i, k]}}, \quad (41)$$

et

$$P(b[i, k, l] = 0 | Z[i, k]) = 1 - P(b[i, k, l] = 1 | Z[i, k]) = \frac{1}{1 + e^{\lambda_l[i, k]}}. \quad (42)$$

La probabilité que le symbole transmis $X[i, k]$ soit égal à un point de constellation spécifique α_j est calculée comme :

$$P(X[i, k] = \alpha_j | Z[i, k]) = \prod_{l=1}^{\log_2 \mu} P(b[i, k, l] = \kappa_l(\alpha_j) | Z[i, k]), \quad (43)$$

où Ψ est l'ensemble des points de la constellation, μ est l'ordre de modulation et $\kappa_l(\alpha_j) \in \{0, 1\}$ est la valeur du $l^{\text{ème}}$ bits de α_j . En utilisant ces probabilités comme des probabilités *a priori*, nous pouvons avoir les estimations des symboles de données comme suit :

$$\hat{X}[i, k] = \mathbb{E}[X[i, k] | Z[i, k]] = \sum_{\alpha_j \in \Psi} \alpha_j \cdot P(X[i, k] = \alpha_j | Z[i, k]). \quad (44)$$

Ces symboles estimés sont alors utilisés comme séquence d'apprentissage pour obtenir une nouvelle estimation de canal. Plus précisément, une estimation instantanée est obtenue pour chaque sous-porteuse :

$$\tilde{H}_2^{\text{LS}}[i, k] = \frac{\hat{X}[i, k]}{\mathbb{E}[|X[i, k]|^2 | Z[i, k]]} Y[i, k]. \quad (45)$$

Notons qu'en utilisant la puissance des données estimées $E_{\hat{X}}[i, k] = |\hat{X}[i, k]|^2$ pour remplacer le terme $\mathbb{E}[|X[i, k]|^2 | Z[i, k]]$, on obtient l'estimateur simplifié suivant :

$$\begin{aligned} \tilde{H}_2[i, k] &= \frac{1}{E_{\hat{X}}[i, k]} \hat{X}[i, k]^* Y[i, k] \\ &= \frac{\hat{X}[i, k]^* X[i, k]}{E_{\hat{X}}[i, k]} H[i, k] + \frac{1}{E_{\hat{X}}[i, k]} \hat{X}[i, k]^* W''[i, k], \end{aligned} \quad (46)$$

Raffinement de l'estimation de canal

Comme aucun processus de correction d'erreur n'est mis à contribution lors de la reconstruction des données, l'estimation du canal peut être fortement entachée d'erreurs. Quelques améliorations doivent alors être utilisées pour améliorer la qualité de l'estimation de canal instantanée.

Moving average en 1-D En utilisant le fait que la réponse fréquentielle de canal ne varie sensiblement pas au sein d'une bande de fréquence égale à la bande de cohérence du canal, le moyen le plus simple pour améliorer la qualité de l'estimation est de réaliser un moyennage mobile (*moving average* en anglais) [15] sur une largeur inférieure ou égale à la bande de cohérence. La figure 11 illustre ce procédé de moyennage où M est la taille de la fenêtre de moyennage. L'estimation moyenne pour la $k^{\text{ième}}$ sous-porteuse s'exprime

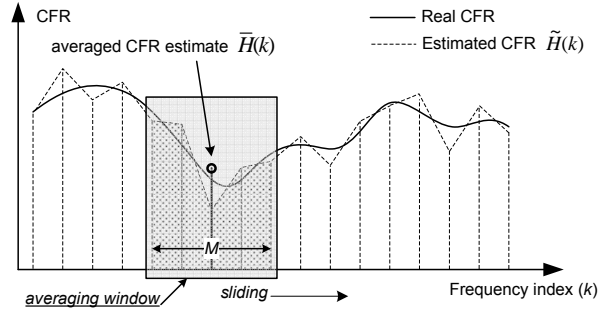


FIGURE 11 – Moving average en 1-D.

comme suit :

$$\begin{aligned}
 \bar{H}_2[k] &= \frac{1}{M} \sum_{m \in \Theta_k} \tilde{H}_2[m] \\
 &= \frac{H[k]}{M} \sum_{m \in \Theta_k} \frac{\hat{X}[m]^* X[m]}{E_{\hat{X}}[m]} + \frac{1}{M} \sum_{m \in \Theta_k} \frac{\hat{X}[m]^* W''[m]}{E_{\hat{X}}[m]} \\
 &\approx H[k] + \frac{1}{M} \sum_{m \in \Theta_k} \frac{\hat{X}[m]^* W''[m]}{E_{\hat{X}}[m]}, 0 \leq k \leq N-1,
 \end{aligned} \tag{47}$$

où $\Theta_k = \{k - \lfloor \frac{M-1}{2} \rfloor, k - \lfloor \frac{M-1}{2} \rfloor + 1, \dots, k + \lfloor \frac{M-1}{2} \rfloor\}$ est l'ensemble des indices de sous-porteuse dans la fenêtre de moyennage avec la $k^{\text{ième}}$ sous-porteuse placée au centre de cette fenêtre. L'EQM de l'estimation est alors :

$$\varepsilon_{\bar{H}_2, 1D} = \frac{1}{N} \sum_{k=0}^{N-1} \mathbb{E} \left\{ |H[k] - \bar{H}_2[k]|^2 \right\} = \frac{\sigma_{W''}^2}{M^2 N} \sum_{k=0}^{N-1} \sum_{m \in \Theta_k} \frac{1}{E_{\hat{X}}[m]}. \tag{48}$$

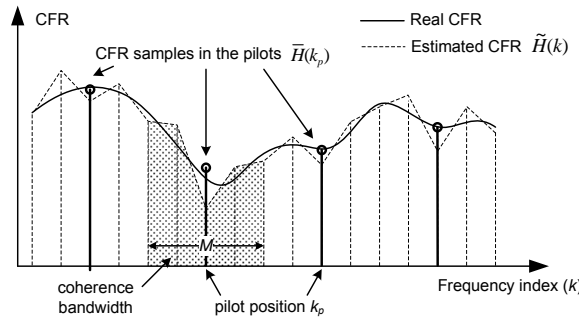


FIGURE 12 – Filtage de Wiener en 1-D.

Filtage de Wiener en 1-D Un second raffinement proposé et basé sur le filtrage de Wiener se compose de deux étapes : *moyennage* et *interpolation* comme représenté sur la figure 12.

Pour ce raffinement, un ensemble de sous-porteuses est d'abord choisi comme “pilotes virtuels”. Les coefficients de canal instantanés estimés dans l'environnement de chaque

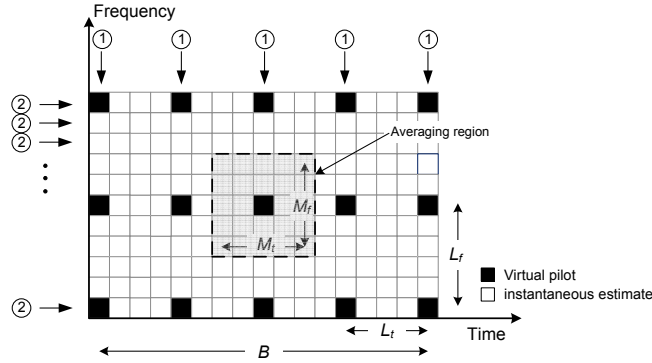


FIGURE 13 – Filtage de Wiener en 2-D.

pilote virtuel k_p sont moyennés afin d'obtenir une estimation plus précise notée $\bar{H}_2[k_p]$. En répétant le calcul de la moyenne pour tous les pilotes virtuels, nous pouvons obtenir des estimations plus fiables pour chaque pilote virtuel.

Ensuite, il suffit de procéder à un filtrage de Wiener pour obtenir l'estimation pour toutes les sous-porteuses :

$$\hat{H}_2[k] = \sum_{k_p \in \Xi} \omega_f[k, k_p] \bar{H}_2[k_p], \quad 0 \leq k \leq N - 1, \quad (49)$$

où les $\omega_f[k, k_p]$ sont les coefficients du filtre de Wiener.

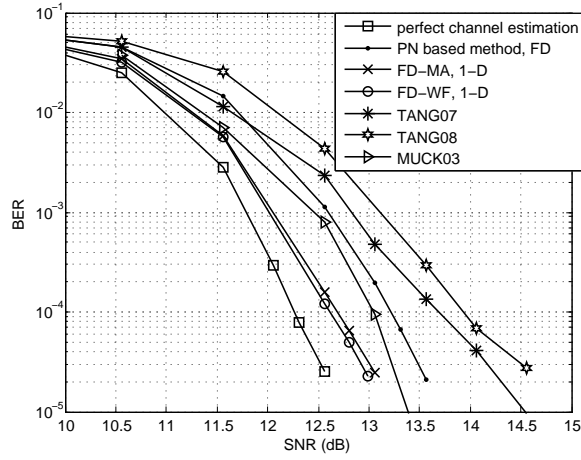
Moving average en 2-D Il est possible d'étendre le procédé de moyenne au domaine temporel, à savoir sur plusieurs symboles OFDM consécutifs. Ainsi, un plus grand nombre d'estimations de canal instantanées peuvent être impliquées dans le calcul de la moyenne mobile :

$$\begin{aligned} \bar{H}_2[i, k] &= \frac{1}{M_t M_f} \sum_{p, q \in \Theta_{i, k}} \tilde{H}_2[p, q] \\ &\approx H[i, k] + \frac{1}{M_t M_f} \sum_{p, q \in \Theta_{i, k}} \frac{\hat{X}[p, q]^* W''[p, q]}{E_{\hat{X}}[p, q]}, \end{aligned} \quad (50)$$

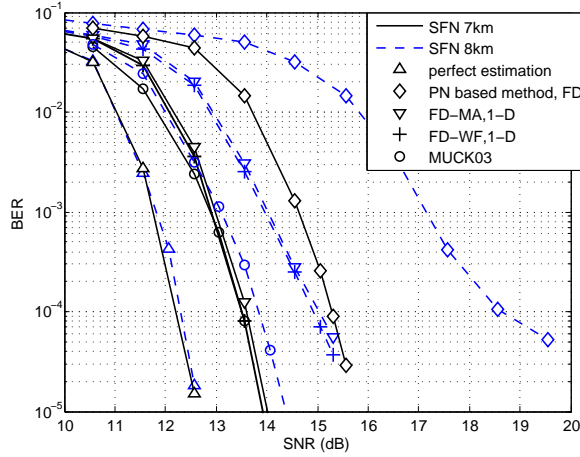
ce qui fournit finalement une estimation plus précise que dans le cas d'un moyennage restreint au seul domaine fréquentiel.

Filtage de Wiener en 2-D De la même manière que précédemment, il est possible d'effectuer un filtrage de Wiener 2-D sur B symboles OFDM comme représenté sur la figure 13. Le moyennage est effectué dans la région 2-D (zone ombrée) en se basant sur les pilotes virtuels. La profondeur du moyennage dans le domaine temporel est choisie en fonction du temps de cohérence du canal. L'interpolation est d'abord réalisée dans le domaine fréquentiel (①), puis dans le domaine temporel (②). Le résultat de l'interpolation est alors :

$$\hat{H}_2[i, k] = \underbrace{\sum_{i_p} \omega_t[i, k, i_p]}_{\text{domaine temporel}} \underbrace{\sum_{k_p} \omega_f[k, i_p, k_p]}_{\text{domaine fréquentiel}} \bar{H}_2[i_p, k_p], \quad (51)$$



(a) Canal TU-6.



(b) Canal SFN.

FIGURE 14 – TEB du système DTMB avec estimation de canal 1-D basée sur les données. 4QAM, $R = 0,8$. L'estimation basée sur la séquence PN est faite dans le domaine fréquentiel.

Combinaison dans le sens de l'EQM minimale

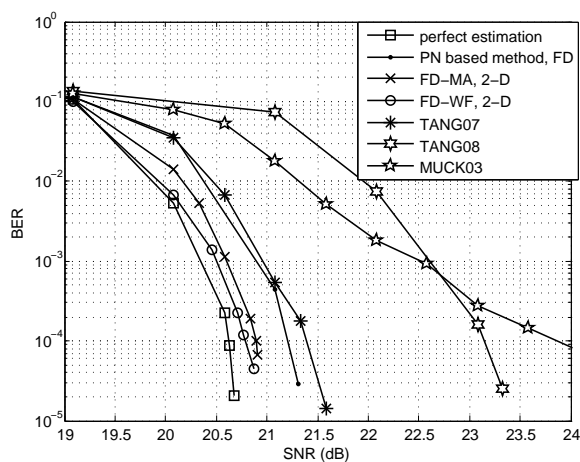
Lorsque les estimations basées sur la séquence PN et sur les prises de décisions sur les données sont obtenues, une combinaison linéaire est utilisée pour obtenir une estimation finale améliorée :

$$\hat{H} = \beta \hat{H}_1 + (1 - \beta) \hat{H}_2, \quad (52)$$

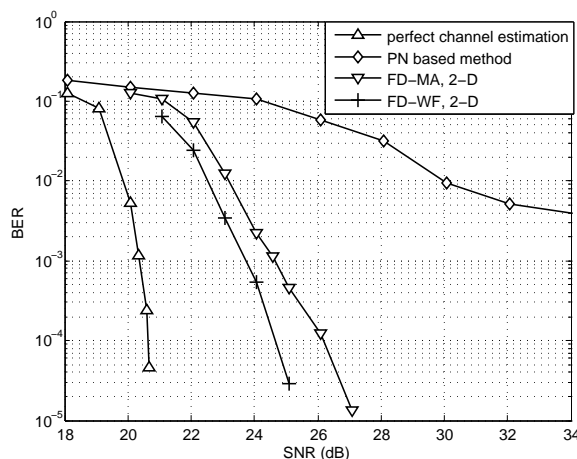
La valeur de pondération optimale permettant d'obtenir une EQM minimale est :

$$\beta_{opt} = \frac{\varepsilon_{\hat{H}_2}}{\varepsilon_{\hat{H}_1} + \varepsilon_{\hat{H}_2}}, \quad (53)$$

où $\varepsilon_{\hat{H}_1}$ est l'EQM de l'estimation basée sur la séquence PN et $\varepsilon_{\hat{H}_2}$ est l'EQM de l'estimation utilisant les données.



(a) Canal TU-6.



(b) Canal SFN.

FIGURE 15 – TEB du système DTMB avec estimation de canal 2-D. 64QAM $R=0,6$. $M_t = 2$, $M_f = 9$ pour canal TU-6, $M_t = 2$, $M_f = 3$ pour canal SFN.

Performances

Les figures 14 et 15 présentent le TEB du système DTMB utilisant les méthodes proposées pour l'estimation de canal. Les méthodes utilisant l'approche conjointe "PN/data aided" offrent des performances supérieures à celles des méthodes basées sur la séquence PN et des méthodes que l'on trouve dans la littérature. Les améliorations sont visibles pour toutes les tailles de constellations testées et pour tous les scénarios de transmission considérés. L'apport est le plus intéressant dans le cas des réseaux SFN pour lesquels le canal est particulièrement dispersif en temps. Ces résultats montrent l'intérêt des algorithmes développés dans ce travail de thèse.

Conclusions

Pour conclure, les travaux menés durant cette thèse ont principalement porté sur l'étude du système TDS-OFDM de la norme DTTB chinoise – DTMB. On peut résumer les apports des recherches effectuées selon les trois axes suivants :

1. Nous avons tout d'abord effectué l'analyse et la comparaison des deux normes de diffusion de la télévision numérique - DTMB et DVB-T en termes de spécification système, d'efficacité spectrale et énergétique, et de performances. Il est montré que les deux systèmes permettent d'atteindre des performances similaires et peuvent fournir des modes de transmission assez équivalents pour divers scénarios de réception. Finalement, les analyses et les comparaisons donnent une vue claire de ces deux systèmes.
2. Nous avons ensuite étudié les algorithmes d'estimation de canal basés sur la séquence PN. L'estimation de canal est l'une des fonctions clés impactant directement la qualité de la récupération des données pour les systèmes TDS-OFDM. Nous proposons donc plusieurs méthodes d'estimation de canal qui exploitent la séquence PN dans le domaine temporel ou dans le domaine fréquentiel. Différentes améliorations permettant d'améliorer les performances des estimateurs sont également élaborées, notamment dans le cas de canaux à fortes dispersions temporelles.
3. En dernier lieu, nous avons proposé un nouvel algorithme d'estimation de canal basée sur les décisions prises sur les données avec une complexité de calcul réduite contrairement aux approches classiques turbo. Précisément, nous proposons d'utiliser les symboles de données reconstruits comme séquence d'apprentissage virtuelle pour l'estimation de canal. Le décodeur LDPC et l'entrelaceur convolutif sont exclus de la boucle de rétroaction lors de la reconstruction des symboles de données afin de réduire la complexité de calcul ainsi que le délai de traitement. Plusieurs techniques de moyennage et de filtrage de Wiener à une ou deux dimensions sont utilisés pour atténuer les effets de la mauvaise fiabilité des décisions. Les résultats de simulation montrent que la nouvelle méthode d'estimation de canal peut améliorer significativement la précision de l'estimation obtenue à partir de la séquence PN, et, plus important, fournir une estimation de canal efficace à la fois dans le cas de constellations d'ordre élevé et pour les canaux difficiles de type SFN.

Contents

Acknowledgements	iii
Résumé étendu en français	v
Contents	xxxix
Glossary	xxxvii
Introduction	1
1 Digital Television Broadcast	7
1.1 Appealing Television Market	7
1.2 Digital TV Transition Trend	8
1.3 DTV Transmission	10
1.3.1 Transmission Methods	10
1.3.2 DTTB Standards	12
1.3.3 Mobile TV Broadcast Standards	15
1.3.4 Recent Progress	16
1.4 Conclusions	18
2 Background Material	19
2.1 Wireless Channel	19
2.1.1 Large- and Small-Scale Fading	20
2.1.2 Multipath Channel Model	22
2.1.2.1 Impulse and Frequency Responses of the Channel	22
2.1.2.2 Baseband Equivalent Model	24
2.1.2.3 Discrete Multipath Channel Model	26
2.1.3 Statistical Characteristics of Multipath Channel	27
2.1.3.1 Rayleigh Fading and Ricean Fading	27
2.1.3.2 Correlation Functions of Multipath Channel	28
2.1.4 Time and Frequency Coherence	32

2.1.4.1	Delay Spread and Coherence Bandwidth	32
2.1.4.2	Doppler Spread and Coherence Time	34
2.1.4.3	Time and Frequency Selectivity	34
2.1.5	Channel Models for Simulations	35
2.1.5.1	Fixed-Reception Channel Models	35
2.1.5.2	Time-Varying Channel Models	36
2.1.6	Generation Method	37
2.1.7	Single Frequency Network Channels	38
2.2	OFDM	40
2.2.1	CP-OFDM	41
2.2.2	ZP-OFDM	45
2.2.3	TDS-OFDM	47
2.2.4	Hybrid GI Structures	49
2.2.5	Intercarrier Interference due to CFO	50
2.3	Conclusion	53
3	Analysis and Comparison of DVB-T and DTMB Systems	55
3.1	System Specifications	55
3.1.1	Bandwidth	56
3.1.2	OFDM Parameters	57
3.1.3	Error Correction Scheme	60
3.2	System Performance Evaluation	62
3.2.1	Power Efficiency	62
3.2.2	BER Performance	64
3.2.2.1	Performance with Perfect Channel Estimation	66
3.2.2.2	Performance using Real Channel Estimation Techniques	69
3.2.2.3	Spectral Efficiency	71
3.3	Conclusion	73
4	PN Sequence based Channel Estimation for TDS-OFDM	75
4.1	A Brief Overview of the Channel Estimation in General OFDM Context	75
4.2	Overview of the channel estimation techniques in the PRP/KSP/TDS-OFDM context	77
4.2.1	PRP-OFDM	77
4.2.2	KSP-OFDM	78
4.2.3	TDS-OFDM	79
4.3	GI Structure in the DTMB System	80
4.4	Interference from Imperfect PN Removal	81
4.5	Frequency Domain PN-based Channel Estimation	85
4.6	Time Domain PN-based Channel Estimation	88
4.6.1	Correlation-based Estimator	88
4.6.2	Estimators with Reduced Error Floor	91
4.6.2.1	Method 1: Multiplying Inverse of Matrix	91
4.6.2.2	Method 1 with the Information of the Channel Length	93
4.6.2.3	Method 2: Subtracting Interference	94
4.7	Estimators in the Insufficient long CP Case	97
4.8	Complexity	100

4.9	Performance Evaluation and Analysis	102
4.9.1	Frequency Domain and Time Domain Estimators	102
4.9.2	Improved Time Domain Estimators	103
4.9.3	Improved Estimators in the Insufficient CP Case	107
4.10	Discussions about the PN-based Channel Estimation Strategies	109
4.10.1	Time or Frequency Domain Estimator?	109
4.10.2	Linear or Circular Cross-Correlation?	111
4.11	Conclusion	112
5	Data-aided Channel Estimation for TDS-OFDM	113
5.1	Introduction	113
5.2	General Presentation of the Proposed Method	115
5.3	Data-aided Instantaneous Channel Estimation	116
5.3.1	Received Signal	116
5.3.2	Soft Data Symbol Rebuilding	117
5.3.3	Instantaneous Channel Estimation	119
5.3.3.1	Simplified Estimator	120
5.4	Channel Estimation Refinements	121
5.4.1	1-D Approaches	122
5.4.1.1	1-D Moving Average	122
5.4.1.2	1-D Wiener filtering	123
5.4.2	2-D Approaches	125
5.4.2.1	2-D Moving Average	125
5.4.2.2	2-D Wiener Filtering	126
5.4.3	Pilot Pattern Selection	127
5.4.3.1	Pilot Spacing	127
5.4.3.2	Pilot Shape	128
5.5	MMSE Combination	129
5.6	Complexity Analysis	130
5.7	Simulation Results	132
5.7.1	Experiment Setups	132
5.7.2	1-D Methods	132
5.7.2.1	MSE	132
5.7.2.2	Impact of the Averaging Length	135
5.7.2.3	Pilot spacing in Wiener filtering	136
5.7.2.4	BER	138
5.7.2.5	1-D Methods with higher order constellations	143
5.7.2.6	Approximate Normalization	143
5.7.3	2-D Methods	144
5.7.3.1	Pilot Pattern Selection	144
5.7.3.2	MSE	145
5.7.3.3	BER	147
5.8	Conclusion	152
	Conclusions and Prospects	153
	A Derivation of (2.82)	157

B Analysis of the Estimation Error of the Frequency Estimator	159
C Norm of the Frequency Response of m-sequence	161
List of Figures	163
List of Tables	169
Bibliography	171

Acronyms and Abbreviations

4QAM-NR 4QAM-Nordstrom Robinson

16QAM 16-ary Quadrature Amplitude Modulation

64QAM 64-ary Quadrature Amplitude Modulation

256QAM 256-ary Quadrature Amplitude Modulation

AGC Automatic Gain Control

AWGN Additive White Gaussian Noise

BCH Bose-Chaudhuri-Hocquenghem multiple error correction binary block code

BER Bit Error Rate

CFO Carrier Frequency Offset

CFR Channel Frequency Response

CIR Channel Impulse Response

COST Committee on Science and Technology

CP Cyclic Prefix

CSI Channel State Information

DAB Digital Audio Broadcasting

DC Direct Current

DFT Discrete Fourier Transform

DQPSK Differential Quadrature Phase Shift Keying

DVB Digital Video Broadcasting

DVB-T Digital Video Broadcasting-Terrestrial

EBU European Broadcasting Union

ERP Equivalent Radiated Power

ETSI European Telecommunications Standards Institute

FCC Federal Communications Commission

FFT Fast Fourier Transform

- FIR** Finite Impulse Response
- FM** Frequency Modulation
- GI** Guard Interval
- GPS** Global Positioning System
- HAAT** Height Above Average Terrain
- ICI** InterCarrier Interference
- IDFT** Inverse Discrete Fourier Transform
- IFFT** Inverse Fast Fourier Transform
- IIR** Infinite Impulse Response
- ISI** Inter Symbol Interference
- ITU** International Telecommunication Union
- KSP-OFDM** Known Symbol Padding-Orthogonal Frequency Division Multiplexing
- LAN** Local Area Network
- LDPC** Low-Density Parity-Check
- LoS** Line-of-Sight
- LS** Least Squares
- MAP** Maximum A Posteriori
- MIMO** Multiple Input Multiple Output
- ML** Maximum Likelihood
- MMSE** Minimum Mean Squared Error
- MPEG** Moving Pictures Experts Group
- MSE** Mean Square Error
- OFDM** Orthogonal Frequency Division Multiplexing
- OLA** OverLap-and-Add
- PAPR** Peak to Average Power Ratio
- PDF** Probability Density Function
- PN** Pseudo Noise
- PRP-OFDM** Pseudo Random Postfix-Orthogonal Frequency Division Multiplexing
- PSAM** Pilot Symbol Assisted Modulation
- QAM** Quadrature Amplitude Modulation
- QPSK** Quaternary Phase Shift Keying
- RS** Reed-Solomon
- SFN** Single Frequency Network
- SIMO** Single Input Multiple Output
- SISO** Single Input Single Output
- SNR** Signal to Noise Ratio
- SRRC** Squared Root Raised Cosine

TDS-OFDM Time Domain Synchronous-Orthogonal Frequency Division Multiplexing

TV Television

US Uncorrelated Scattering

WLAN Wireless Local Area Network

WSS Wide Sense Stationary

ZF Zero Forcing

ZP Zero Padding

ZP-OFDM Zero Padded-Orthogonal Frequency Division Multiplexing

Context and Motivation

DURING the past several decades, the television (TV) broadcast has been the most effective medium to disseminate information, educate people and entertain the public around the world. By 2009, the worldwide TV market represents 268.9 billion EUR and 1,134,141 million TV households. It is predicted that the market will keep rising, to a total market value of 281.9 billion EUR in 2010 and 322.9 billion EUR in 2013. The power behind this growing market is the ever-increasing demands raised from the TV users. More diverse TV programs and consequently more TV channels are needed to meet the users' growing requirements. Improved video and sound qualities are also appealed by the users. People need mobile reception in their handheld devices anywhere to pick up the fast-paced world. There are also some emerging viewing requirements such as three dimensional (3D) TV, time shift viewing, video on demand (VoD), interactive TV and so on. However, the traditional analogue TV broadcast still uses dated cumbersome transmission techniques which are spectrum and power inefficient with limited capacity as well as limited video and sound quality.

As a part of the global progress towards information society, digital television (DTV) transition is an ongoing trend around the world. Major TV markets such as U.S., European countries, Japan and China have begun their DTV transition. By 2015, nearly 40 countries will stop the analogue TV broadcast and provide DTV services in their territories. In addition to providing dramatically improved video and sound qualities, DTV also enables TV stations to provide versatile programs and novel data services in a more flexible and efficient manner.

DTV can be delivered by coaxial cable, via satellite, through Internet connection or over-the-air (terrestrial broadcast). Among all approaches, the digital terrestrial TV broadcast (DTTB) attracts great interest due to its high flexibility to fixed and mobile receptions, large coverage, easy deployment and low-cost usability. Stimulated by the promising market potential, all major TV markets developed their own DTTB standards, namely the North America's ATSC standard, the European consortium based Digital Video Broadcasting-Terrestrial (DVB-T) standard, the Japanese Integrated Ser-

vices Digital Broadcasting-Terrestrial (ISDB-T) standard and the Chinese Digital Terrestrial/Television Multimedia Broadcasting (DTMB) standard.

Stimulated by the growing demand of the TV market, designing and improving DTTB standards have been always a hot research field. Researchers try to integrate the state-of-the-art signal processing techniques such as advanced video coding, capacity-approaching channel coding, Multiple-Input Multiple-Output (MIMO) transmission, efficient modulation schemes, and so on.

As the DTMB standard was developed recently, some state-of-the-art signal processing techniques including the low-density parity-check (LDPC) code and the Time Domain Synchronous-Orthogonal Frequency Division Multiplexing (TDS-OFDM) have been adopted in the standard. Especially, TDS-OFDM, also known as pseudo random postfix-OFDM (PRP-OFDM) and known symbol padding-OFDM (KSP-OFDM), is a new OFDM signal waveform and also a spectrum-efficient modulation scheme. It uses a known pseudo random (PN) sequence, instead of the classical cyclic prefix (CP), as the guard interval (GI). Besides serving as the GI, the PN sequence is also reused as the training sequence. Hence, no extra pilot is needed for channel estimation and synchronization. The overhead of the TDS-OFDM based system can thus be reduced. Moreover, as each OFDM block has its own training sequence, TDS-OFDM is expected to achieve faster synchronization.

However, TDS-OFDM also has some technical challenges. The major problem comes from the mutual interference between the PN sequence and OFDM data symbols. The PN sequence in the GI has to be first removed from the received signal before demodulating OFDM data symbols. An accurate channel impulse response (CIR) estimate is thus needed to predict the received PN sequence. Otherwise, there will be residual PN sequence in the OFDM data symbols introducing interference which consequently degrades the performance of the decoding. Therefore, finding efficient and reliable channel estimation methods is critical with TDS-OFDM. In this thesis, we will focus on this main challenge in TDS-OFDM through the study and the optimization of various new approaches to cope with this problem.

Project “*Mobile TV World*”

Launched in July 2006, “Mobile TV World” is a research project sponsored by the OSEO and the Regional Council of Brittany. Its major objective is to allow two small and medium enterprises (SME) from Brittany, namely TeamCast and Silicon Laboratories France, specialized in digital terrestrial and mobile TV to access new markets such as China and the U.S. The project is also expected to promote the research and development of the international mobile TV in Brittany region. As revealed in the name, this project concerns a number of digital terrestrial and mobile TV standards around the world as demonstrated in Figure 16.

The main activities of the project lie in the following aspects:

- identification and study of the technical standards for “Mobile TV” and “Digital Terrestrial TV” in Chinese and the U.S. markets;
- developing technological offerings for modulation and demodulation to meet the requirements of the Chinese and U.S. standards;
- carrying out exploratory research on the optimization of solutions and algorithms implemented in receivers; and

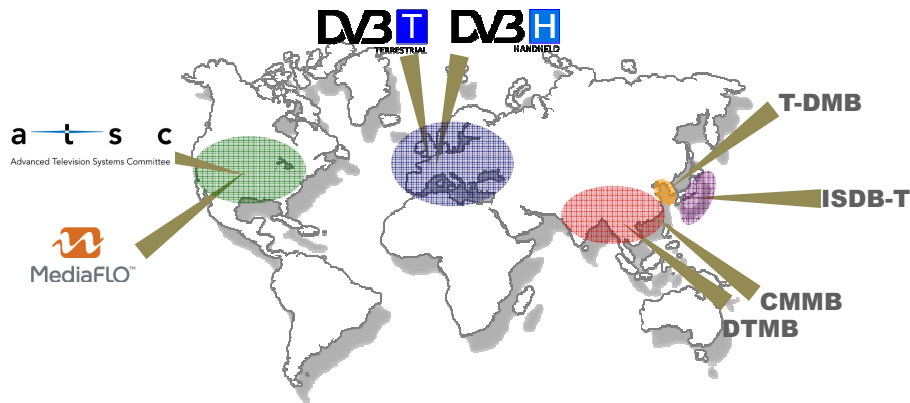


Figure 16: Research scope of the project “Mobile TV World”.

- contribution to multi-standard interoperability platforms.

The partners of this project consist of TeamCast and Silicon Laboratories France, Bretagne International and Broadcast Technology Innovation Consult (B.T.I.C.) and the Electronics and Telecommunications Institute of Rennes (IETR). Among them, Bretagne International and B.T.I.C are institutional organizations and the coordinators of the project. The two SMEs, TeamCast and Silicon Laboratories France, are specialized in the development of transmission and reception modules of digital terrestrial and mobile TV, respectively. IETR, an Academic Research Institution where the work of this thesis carried out, is in charge of the research on the optimization of reception algorithms and the multi-standard interoperability approach.

Thesis Organization and Contributions

In the past three years, we mainly concentrated on the Chinese DTTB standard—DTMB due to its promising technical prospect. We started our study from the system level analysis and evaluation of the DTMB system in terms of spectrum efficiency and overall bit error rate (BER) performance compared with the DVB-T system. It is shown in our analyses that, thanks to the TDS-OFDM waveform, DTMB enjoys higher spectrum efficiency than DVB-T. In order to show the BER performance of the two systems, we coded complete simulation chains based on MATLAB encapsulated C language for each system. Several channel models, including Rayleigh and Rician, stationary and time-varying ones, were also realized to test the performance in different channel conditions. Simulation results show that the performances of two systems are very close.

After that, we focused on the channel estimation problem in the TDS-OFDM based DTMB system. As previously mentioned, the channel estimation is the main challenge for TDS-OFDM. An accurate channel estimate is important not only to enable coherent detection but also to reduce the interference on OFDM data symbols.

We first investigated the classical training-based channel estimation using the PN sequence in the GI specified in the DTMB standard. We studied the channel estimation algorithms in either the frequency domain or the time domain. Through our analyses, the time domain estimator provides better performance than the frequency domain estimator, but suffers from an estimation error floor. Consequently, we proposed several

novel improved estimators which mitigate the error floor encountered by the time domain estimator. Furthermore, we analyzed the performance loss of the estimator due to long channel delay spread and proposed improved algorithms.

In order to achieve better channel estimation performance, we proposed several data-aided channel estimation algorithms. In contrast to the classical turbo channel estimation method, the proposed methods exclude the time-consuming (de-)interleaving and channel decoding from the feedback loop in order to reduce the computational complexity as well as the processing time delay. Simulation results show that the proposed methods can achieve a superior performance than the PN based channel estimation methods as well as the typical methods in the literatures especially in the harsh single frequency network channel cases.

The thesis is organized as follows:

In Chapter 1, we first introduce the general context of our research including the TV market of the world and the ongoing global DTV transition trends. Then we review the main digital terrestrial and mobile TV broadcast standards in terms of technical specifications and worldwide deployments. Finally, some underway DTV researches are covered.

In Chapter 2, we present background knowledge that will be used in the following chapters of this thesis. Concretely, we first introduce some wireless channel models considered in the thesis. Then we present the principle and several OFDM signal structures with different GIs and the corresponding demodulation methods.

In Chapter 3, we investigate the two main DTTB standards—DVB-T and DTMB in terms of system specifications including OFDM parameters, FEC block, etc., and system performance such as power efficiency, BER and spectral efficiency. In general, although there exist many differences in system specifications as well as channel estimation techniques, the overall performance of two systems is very close in the typical channel conditions. The two systems can provide equivalent working modes with various throughputs for different application scenarios.

In Chapter 4, we investigate the channel estimation methods exploring the PN sequence in the GI specified in DTMB. We propose to carry out the channel estimation in either frequency or time domain using the PN sequence, instead of the whole GI, as the training sequence. The frequency domain estimator is easy to implement with least complexity while the time domain estimator provides better performance but suffers from an estimation error floor. In order to mitigate the error floor in the time domain estimator, we propose several improved estimators which either turns the convolution matrix of PN sequence into a perfect identity matrix, or subtracting the interference using the CIR estimate. Furthermore, we analyze the performance loss of the estimator due to long CIR. Based on this analysis, we propose improved methods including the cyclicity compensation and the IBI removal process.

In Chapter 5, we propose novel iterative data-aided channel estimation algorithms. In contrast to the classical turbo channel estimation, the proposed algorithm does not include the decoding and interleaving processing when rebuilding the data symbols in order to reduce the computational complexity and the processing delay. Instantaneous data-aided channel estimates are obtained using the soft data symbols rebuilt from the output of the demapper instead of the decoder as in the classical Turbo channel estima-

tion. Several techniques including moving average and Wiener filtering in both 1-D and 2-D are proposed to refine the data-aided channel estimation. Comprehensive simulation results show that the proposed data-aided channel estimation algorithm provide superior performance over the PN-based methods as well as several typical methods in the literatures for different constellations and channel conditions.

Finally, we conclude this thesis and give some potential research directions in the future.

List of Publications

Journal Paper

- M. Liu, M. Crussière, and J.-F. Hélar, “A Novel Data-Aided Channel Estimation with Reduced Complexity for TDS-OFDM Systems,” submitted to *IEEE Transactions on Broadcasting*, under review.

International Conferences

- M. Liu, M. Crussière, J.-F. Hélar and O.P. Pasquero, “Analysis and Performance Comparison of DVB-T and DTMB Systems for Terrestrial Digital TV,” in *Proc. 11th IEEE Singapore International Conference on Communication Systems (ICCS 2008)*, pp.1399-1404, Guangzhou, China, Nov. 2008.
- M. Liu, M. Crussière, and J.-F. Hélar, “A Novel Iterative Data-aided Channel Estimation for Time Domain Synchronous-OFDM,” in *Proc. Fourth International Workshop on Signal Design and its Applications in Communications (IWSDA'09)*, pp.48-51, Fukuoka, Japan, Oct. 2009.
- M. Liu, M. Crussière, and J.-F. Hélar, “A Combined Time and Frequency Algorithm for Improved Channel Estimation in TDS-OFDM,” in *Proc. IEEE International Conference on Communications (ICC 2010)*, pp.1-6, Cape Town, South Africa, May 2010.
- M. Liu, M. Crussière, and J.-F. Hélar, “Enhanced Two-Dimensional Data-aided Channel Estimation for TDS-OFDM,” in *Proc. Fourth International Conference on Signal Processing and Communication Systems (ICSPCS'10)*, pp.1-6, Gold Coast, Australia, Dec. 2010.

Digital Television Broadcast

IN THIS CHAPTER, we present the digital television (DTV) broadcast which is the general background of this thesis from the market and the technical perspectives. The booming DTV market provides huge business opportunities which stimulates the progress of the DTV transmission technologies. Several DTV broadcast standards have been developed and many enhanced versions are under standardization. These are the motivation and stimulation of the researches carried out in this thesis.

1.1 Appealing Television Market

Since its first commercial deployment in 1930's, television (TV) broadcast has become the most popular and effective media to disseminate information due to some irreplaceable advantages, such as large coverage and low user cost. In 2009, there are more than 2 000 TV channels around the world and over 3 billion potential TV viewers with an averaging daily viewing time of 192 minutes [16]. TV becomes the most efficient household source of news, entertainment and sports. A major sport event, such as the European Football Championships and the Super Bowl, can attract tens of millions TV viewers. More impressively, the 2008 Beijing Olympic Games attracted as much as several billion TV viewers, approximately 70 percent of the world's population, around the world [17]. Meanwhile, some popular TV programs, such as the "Britain's Got Talent" in the United Kingdom and the "Chinese New Year's Eve Events" in China, gather a huge audience. TV makes the programs become hot topics of society. Obviously, TV broadcast has a massive influence over the world.

Mass audience presents tremendous business opportunities. The worldwide television market in 2009 represents 1 217.2 million households with at least one TV set, with an annual increase of 1% in the past years. According to the report of IDATE [18], the total revenue of the worldwide television market in 2009 was 268.9 billion EUR and is expected to increase to 322.8 billion EUR in 2013, as shown in Figure 1.1.

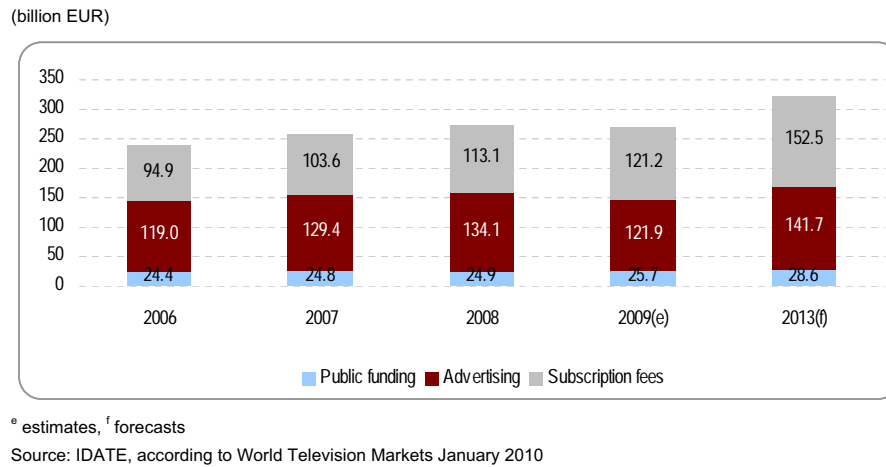


Figure 1.1: Worldwide TV market revenue 2006-2013 [18].

1.2 Digital TV Transition Trend

The underlying cause of the constant increase of the market data is the growing demands of the TV viewers. Nowadays, we are stepping to a new era of TV broadcasting. The high-definition (HD) display is becoming a common requirement as a direct consequence of the decrease of the prices of large screen TV sets. More and more programs are available to meet the diverse requirements of TV viewers. The traditional analogue broadcast TV cannot convey video with improved quality while the increasing number of TV channels runs out the limited analogue TV bands. More efficient transmission technique is thus needed to replace the analogue one. Benefiting from the development of the digital signal processing techniques, digital transmission enjoys the advantages of high capacity, reliability and spectrum-efficiency with low power-consumption. Therefore, the analogue switch off (ASO) and DTV transition become worldwide trend shown in Figure 1.2.

As a DTV research and deployment pioneer, the United States (U.S.) authorized additional broadcast channels dedicated to DTV broadcasting in order to promote the development of DTV in 1996. Before June 12, 2009, all broadcast stations in the U.S. were simultaneously transmitting both analogue and digital programs. Since June 13, 2009, all full-power TV stations have been transmitting in digital only.

Europe is the most successful DTV market. According to the recommendations made by the European Commission, most of European countries will end the analogue terrestrial television by 2012. In fact, by June 2010, several countries such as Switzerland, Netherlands, Finland, Norway, Sweden, Germany, Spain etc. have already completed their ASO. The DTV transition is in progress in other European countries. For example in France, several regions, namely Alsace, Lower Normandy, Pays de la Loire and Brittany, have stopped the analogue TV broadcast and turned to DTTB by June, 2010. All DTV transition is expected to be finished by the end of 2011 in France [6]. The ASO is also ongoing in the United Kingdom. Five out of all fifteen TV regions have completed the switch to DTV by June 2010 and the rest will finish by 2012 [20].

In China, the trail of DTV broadcast was first carried out during the end of 1990's. The parade of the China's 50th anniversary was broadcasted in live by a trail DTV system

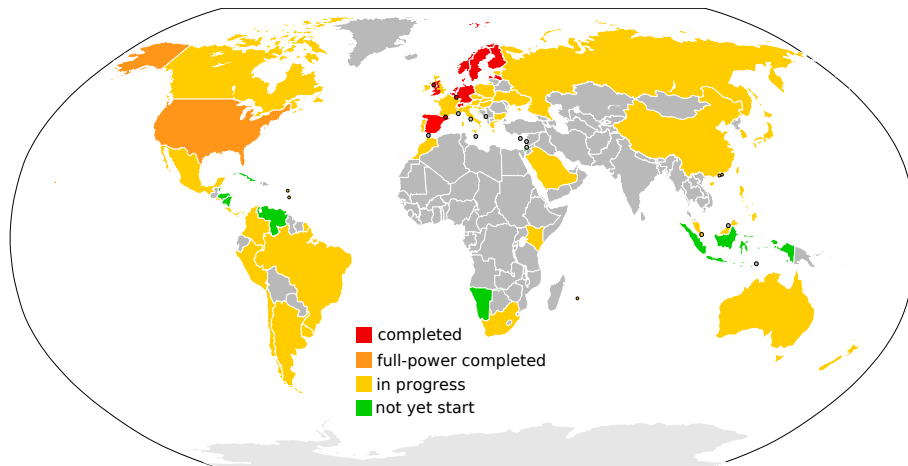


Figure 1.2: DTV transition progress in the world [19].

in 1999. The DTV transition in China began from the cable TV (CATV). A quarter of TV stations began to transmit DTV signal via CATV in 2005. 63.48 million, that is, more than 36% of all CATV households had switched to digital reception by the fourth quarter of 2009. Regarding the terrestrial TV broadcast, Chinese authority ratified its own terrestrial DTV standard in 2006 and started to carry it out in the domestic market in 2007. The Beijing Olympic Games was delivered by free-to-air DTV broadcast in 2008. The Chinese government decides to speed up the nationwide DTV transition in 2010 and plans to finish the ASO in 2015.

The ASO is scheduled in some other countries as well. Japan's ASO is planned for July 2011, Canada for August 2011, South Korea for the end of 2012, Australia for the end of 2013, India and Russia for 2015 [21]. Up to 2015, nearly 40 countries will finish the ASO and provide only DTV services.

DTV transition yields many advantages to our society. It not only provides consumers with high-quality TV programs and plentiful data services, but also benefits the broadcasters with its technological innovations. Figure 1.3 gives one example of the improved reception after DTV transition in Philadelphia, U.S. After DTV transition, the users of the American Broadcasting Company (ABC) are increased by over 2.5 million, mainly located in the coverage border. In the mean time, the transmitter power is dramatically reduced to about one tenth of that required by the analogue transmitter (7.56 kW ERP with digital system versus 74.1 kW ERP with analogue one), which means lower operation cost and, more importantly, less electromagnetic pollution to the ambient environment. Furthermore, thanks to the state-of-the-art digital signal processing techniques, one conventional 8 MHz TV channel can deliver up to six standard-definition TV (SDTV) programs (using the MPEG-2 video compression) or up to three high-definition TV (HDTV) programs (using the MPEG-4 AVC), which means that more virtual channels are available without additional spectrum bands. Some bands can thus be freed up and reallocated to other TV or wireless access services. It is commonly referred to as "digital dividend". Governments can make good use of the digital dividend to moderate the spectrum scarcity and stimulate the development of the new communication technologies. In Europe for instance, France, Sweden, Finland, Germany, Switzerland, and possibly United Kingdom

Station WPVI-TV • Analog Channel 6, DTV Channel 6 • Philadelphia, PA

Expected Operation on June 13: Granted Construction Permit

Digital CP (solid): 7.56 kW ERP at 332 m HAAT, Network: ABC
vs. Analog (dashed): 74.1 kW ERP at 332 m HAAT, Network: ABC

Market: Philadelphia, PA

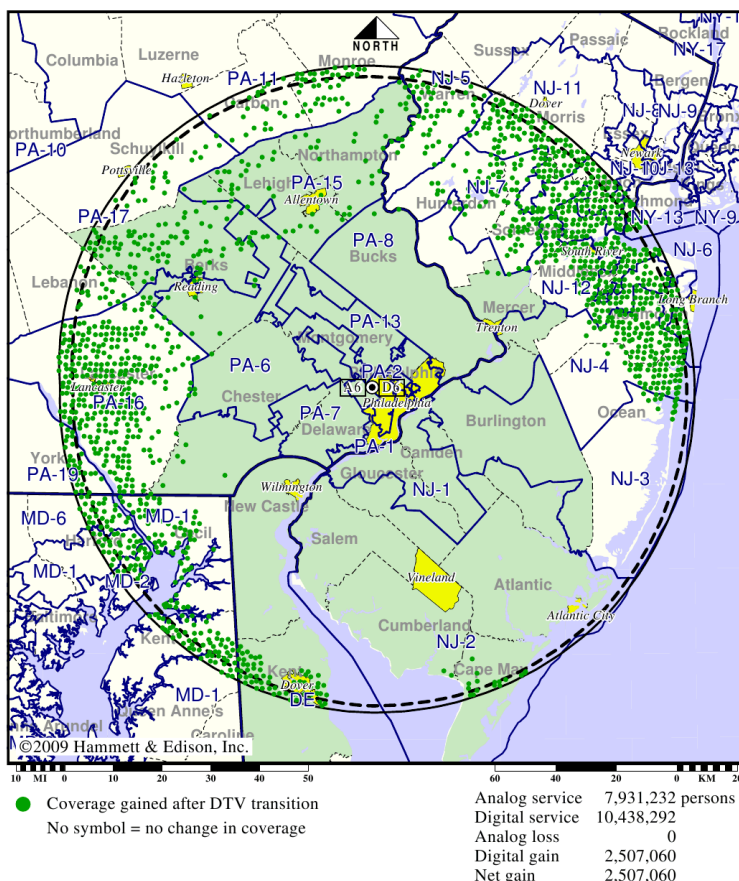


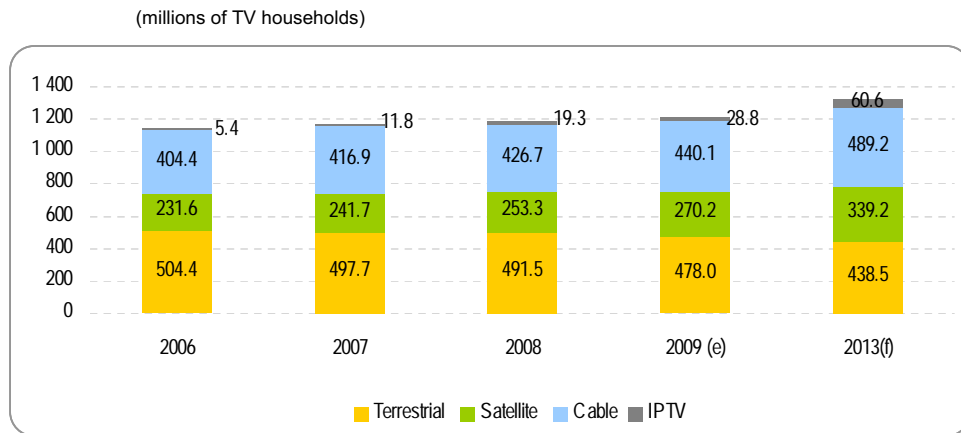
Figure 1.3: Coverage improvement after DTV transition in Philadelphia U.S. [22].

have already decided to use the 790-862 MHz band, which is released from broadcasting services, for Mobile Services [23].

1.3 DTV Transmission

1.3.1 Transmission Methods

In general, DTV services can be delivered via satellite, coaxial cable, Internet protocol TV (IPTV) and terrestrial broadcasting. The share of different transmission approaches is shown in Figure 1.4. Historically, terrestrial TV has been the most widely used reception mode in the world. It is normally used to broadcast free-to-air TV programs. In 2009, 478 million households, more than 39% of the world's total TV households, receive TV services from the terrestrial TV network on their primary TV sets. Moreover, it is also the preferred reception mode for the secondary household TV sets locating in kitchen



^e estimates, ^f forecasts

Source: IDATE, according to World Television Markets January 2010

Figure 1.4: Worldwide TV reception modes 2006-2013 [18].

or bedroom. Cable and satellite are the second and third place TV reception modes worldwide with more than 440 million and 270 million TV households, i.e., 36% and 22% market shares, respectively. They are also the preferred reception modes access to pay-TV. Compared to the previous three traditional reception modes, the emerging IPTV is adopted by 2.4% of TV households worldwide. However, it experiences a high growth with a five-fold increase between 2006 and 2009. It is more welcomed in the mature TV markets. The penetration rate of IPTV was 4.7% in Europe and 4.3% in North America in 2009. As for penetration rate, France is the leading national market worldwide with a penetration rate of 14.4% in 2009 [18].

From a technical point of view, each transmission approach has its advantages and disadvantages, and thus has its own appropriate application case.

The cable and IPTV-based transmission approaches are closed-circuit transmissions. Hence, they enjoy a better transmission environment and do not occupy the radio propagation spectrum. DTV services can be delivered to fixed locations where the infrastructure of communication networks covers. Therefore, it is suitable for the urban areas where users are geographically concentrated which can reduce the cost of mass infrastructure deployment.

The satellite-based transmission has vast coverage and does not rely on the communication infrastructure. Thus it is suitable for rural and sparsely populated areas. Yet, it needs specific reception devices, including a satellite dish and a set-top box for signal decoding and decryption, which are cumbersome for mobile receptions.

By contrast, the digital terrestrial television broadcast (DTTB) has more flexibility to indoor/outdoor, fixed/mobile receptions. Incorporating with advanced wireless transmission techniques, DTTB can provide satisfactory DTV services to a broad area with least requirements to the receiver. Hence, it attracts great interest from both industry and consumer in the past several years.

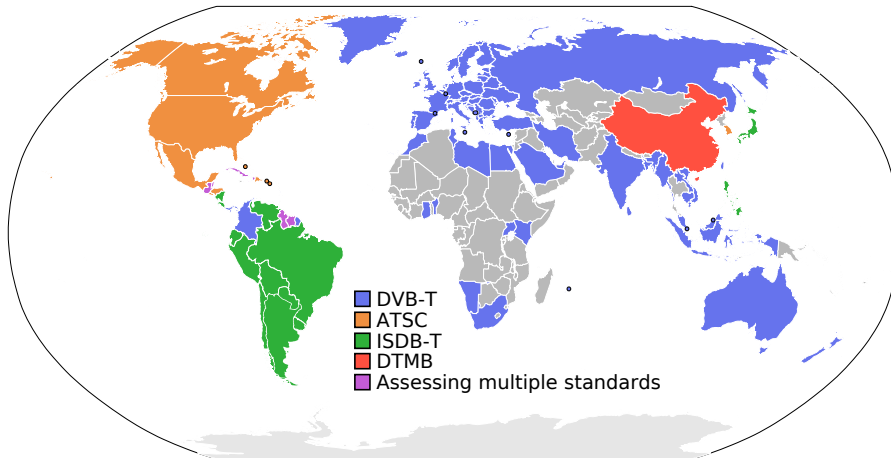


Figure 1.5: DTTB standards in the world (source from [7]).

1.3.2 DTTB Standards

Nowadays, there are mainly four DTTB standards in the world. The deployment status of these standards is shown in Figure 1.5.

The ATSC A/53 standard⁽¹⁾ It was developed by the Advanced Television Standards Committee and is the first published DTTB standard [3]. It was adopted by the Federal Communications Commission (FCC) in the U.S. in 1996. It evolves from the analogue National Television Standards Committee (NTSC) standard and uses single carrier transmission scheme with 8-level vestigial sideband modulation (8VSB). It can reliably deliver 19.4 Mbit/s payload in the traditional 6 MHz TV channel, which meets the transmission requirement of HDTV and ancillary data. As the development of ATSC was carried out during early 1990's, an era before smartphones and car entertainment systems, it was mainly designed for the single transmitter (multi-frequency network, MFN) implementation. As ATSC is optimized for a fixed reception with highly directional antennas in typical North American environments, it is not robust enough against Doppler shift and multipath propagation in mobile environments. ATSC is mainly used in North America and South Korea.

The DVB-T standard The Digital Video Broadcasting-Terrestrial (DVB-T) standard [1] is developed by an European consortium of public and private organizations – the Digital Video Broadcasting (DVB) Project [7]. It was first broadcast in the United Kingdom in 1998. Coded Orthogonal Frequency-Division Multiplexing (COFDM) is used as its basic transmission scheme. Compared with ATSC, DVB-T has much more adjustable parameters such as subcarrier number, channel coding rate, modulation and guard interval (GI) duration. It can thus provide a flexible net bit rate ranging from 4.98 Mbit/s to 31.67 Mbit/s for an 8 MHz TV channel in order to fit various applications. Besides, owing to the GI, DVB-T can easily cope with the multipath situations, even with high-

(1). It is called as **ATSC standard** when there is no ambiguity.

level (up to 0 dB) long delay echoes. It allows DVB-T to work in the single-frequency network (SFN), a distributed transmission mode using multiple synchronized on-channel transmitters to increase coverage and improve reception. In this sense, the deployment of DVB-T is more spectrum-efficient than ASTC. The flexibility and efficiency of DVB-T make it the most popular DTTB standard. By July 2009, DVB-T has been adopted in more than 35 countries and territories around the world, and more than 90 million DVB-T receivers have been sold.

The ISDB-T standard The Integrated Services Digital Broadcasting-Terrestrial (ISDB-T) standard [2] was developed by the Association of Radio Industries and Businesses (ARIB) of Japan. As indicated by its name, the ISDB-T was designed to support various types of multimedia services including TV and audio programs, text services, computer programs and even disaster warning messages. ISDB-T shares the same front-end receiver and channel coding components as DVB-T. Yet, it adopts the so-called Band Segmented Transmission (BST)-OFDM which divides each TV channel into 13 segments. Different services are able to use a portion of the channel bandwidth combining with different modulations and channel coding schemes in order to meet different requirements such as data rate and channel coding efficiency. ISDB-T can provide a data throughput ranging from 3.65 Mbit/s to 23.23 Mbit/s in one 5.57 MHz TV channel and from 280.85 kbit/s to 1787.28 kbit/s in one 428.6 kHz segmented band. Based on ISDB-T, Brazilian DTV research group developed an enhanced standard—“ISDB-T International” for South American countries such as Brazil, Peru, Argentina, Chile and so on. The main modification compared to the original ISDB-T is that an advanced video compression code, namely H.264/MPEG-4 AVC, is used to replace the original H.262/MPEG-2 Part 2 in ISDB-T. ISDB-T and its Brazilian version have been adopted by Japan itself and some other countries in South America.

The DTMB standard The Digital Terrestrial/Television Multimedia Broadcasting (DTMB) standard [4] was issued as a national standard of China in August 2006. The efforts to develop a DTTB standard were initiated in 1994 in China. After several years' research, a prototype DTV system was used to broadcast the celebration of China's 50th anniversary in 1999. In 2001, several proposals were submitted to answer the call for proposal for the Chinese DTTB standard. The aim is to design a new DTTB standard which should provide high bandwidth efficiency, larger coverage, low power-consumption SDTV/HDTV broadcast in fixed/mobile and indoor/outdoor receptions with independent intellectual property rights. After lab tests and field trials in 2003, three competing proposals, DMB-T (Digital Multimedia/TV Broadcasting-Terrestrial, a multicarrier solution from Tsinghua University), ADBT-T (Advanced Digital Television Broadcasting-Terrestrial, a single carrier solution from Shanghai Jiaotong University) and TiMi (Terrestrial Interactive Multiservice Infrastructure, another multicarrier solution from Academy of Broadcasting Science) started merging to form a hybrid but unified national standard. DTMB integrates some up-to-date signal processing techniques such as time domain synchronous-OFDM (TDS-OFDM) transmission scheme and low-density parity-check (LDPC) code. It is designed to support not only fixed but also mobile receptions. It can provide an acceptable video quality at a speed of 200 km/h, as high as train speed, which covers majority of the mobile reception scenarios. Like other OFDM based standards, DTMB

Table 1.1: Main Parameters of DTTB standards

Systems		ATSC	DVB-T	ISDB-T	DTMB
Source Coding	Video	MPEG-2 coded TV signals ISO/IEC 13818			Not specified
	Audio	ATSC Standard A/52 (Dolby AC-3)	MPEG-2 Layer II audio and Dolby AC-3	MPEG-2 AAC audio	
	Transport Stream	MPEG-2 TS transport stream			
Channel Coding	Inner	Rate 2/3 trellis code	Punctured convolutional codes with code rate 1/2, 2/3, 3/4, 5/6 and 7/8, generator polynomials $G_1 = 171_{OCT}$, $G_2 = 133_{OCT}$ constraint length = 7		LDPC(7493, 3048), (7493, 4572), (7493, 6096)
	Outer	R-S(207,187,t=10)	R-S(204,188,t=8)		BCH(762, 752)
Interleaver	Inner	12 to 1 trellis code interleaver	Bit-wise interleaver followed by symbol interleaver	Bit-wise interleaver, time and frequency interleaver	Convolutional interleaver with interleaving depth 170 or 510 OFDM symbols
	Outer	52-branch R-S block interleaver	12-branch R-S block interleaver		–
Transmission Scheme		single carrier	COFDM with 2k and 8k FFT size	BST-OFDM with 2k, 4k and 8k FFT size	TDS-OFDM with 3780 FFT size
Modulation		8-VSB	QPSK, 16QAM and 64QAM, with hierarchical and non-uniform modulation options for 16QAM and 64QAM	DQPSK, QPSK, 16QAM, 64QAM with hierarchical modulation	4QAM, 4QAM-NR, 16QAM and 64QAM
GI		–	1/32, 1/16, 1/8 and 1/4 OFDM symbol duration		945 (1/4), 595 ($\approx 1/7$) and 420 (1/9) symbols duration

can provide flexible net data rate ranging from 4.813 Mbit/s to 32.486 Mbit/s. After 2012, all TV sets sold in China should equip the DTMB receptors [24]. Since about 2/3 of China's overall 400 million TV households, mainly in rural area, will use the terrestrial DTV reception, DTMB draws great interests from industries. Besides mainland China, Hong Kong has also adopted the DTMB standard since 2007. By December 2009, Hong Kong had 1.06 million DTMB households, with a penetration rate up to 46%.

The main parameters of the DTTB standards are concluded in Table 1.1.

1.3.3 Mobile TV Broadcast Standards

With the rapid advance of the Third Generation (3G) cellular networks and other wireless access networks people are used to watching real-time TV programs or on-demand streaming videos on their portable devices whenever and wherever they want. However, the number of devices accessing TV programs is restricted by the bandwidth of the cellular or wireless access networks. In contrast, TV broadcast can efficiently deliver TV programs to unlimited number of receivers. On the other hand, the SDTV and HDTV programs delivered by the existing DTTB standards exceed the resolution of the screen of handheld devices while the power consumption required by the sophisticated decoding process of DTTB receivers is sometimes unaffordable for the battery-powered handheld devices. Hence, an emerging market segment of DTTB is efficiently and economically bringing DTV services to handheld devices. Many DTV broadcast standards dedicated to the handheld reception are proposed recently.

The DVB-H standard The DVB-Handheld (DVB-H) standard was published by the DVB project in November 2004. DVB-H evolved from the DVB-T standard with some additional features to meet the specific requirements of handsets such as mobile reception and power consumption. DVB-H can be used alongside mobile telephone networks. Its high-data-rate downstream channel can be used independently or as an enhancement of mobile telephone. DVB-H has officially been endorsed by the European Union as the “preferred technology for terrestrial mobile broadcasting” since March 2008. Mobile TV services based on DVB-H are now available in Europe, the U.S., South Africa and Asia [25].

The 1seg standard The 1seg services was started in Japan in 2006. The broadcaster can provide mobile TV and data services via the ISDB-T network, One segment, i.e. 1/13, of TV channel is allocated to the multimedia broadcast services for portable and handheld devices. The rest 12 segments can be flexibly used to transmit one HDTV program or three SDTV programs, or a medium definition TV program (occupying 8 segments) as well as a SDTV program. In other words, ISDB-T can transmit the same programs both in high and low definition within the same TV channel, which is an unique feature of ISDB-T. Brazil also launched a Mobile TV service at the beginning of 2008, based on the Brazilian version of ISDB-T.

The ATSC-M/H standard ATSC-M/H [26] is an enhanced version of ATSC A/53 by introducing additional channel coding mechanisms for mobile reception. Unlike ATSC A/53 being the exclusive DTTB standard in North American DTTB market, ATSC-M/H has a competitor—the Qualcomm’s MediaFLO [27] which transmits encrypted programs for handheld devices in the former UHF TV channel 55 (716-722 MHz). MediaFLO faces to the subscribed users while ATSC-M/H will mainly be used for the free-to-air broadcast. Services based on MediaFLO have been launched in some part of the U.S. and trialed in the U.K. and Germany.

The DMB standard The Digital Multimedia Broadcasting (DMB) standard [28] was developed by South Korea as the next generation digital technology to replace the FM radio. It sends multimedia programs including TV, radio and datacasting to mobile devices

via satellite (S-DMB) or terrestrial (T-DMB). It can support mobile TV reception with a speed up to 120 km/h. Based on DMB, South Korea started the world's first official mobile TV service in May 2005. In December 14, 2007, the International Telecommunication Union (ITU) formally approved T-DMB as a global mobile TV standard, along with three other standards—DVB-H, 1seg, and MediaFLO.

The CMMB standard The China Multimedia Mobile Broadcasting (CMMB) standard [29] was announced by the State Administration of Radio, Film, and Television (SARFT) of China in October 2006. It mainly uses high-power satellite broadcast to cover the whole country while terrestrial repeaters simultaneously send the same programs in the same channel to enhance the reception in the blind area of satellite signal. Mobile telephone networks are used as a return channel by CMMB so that users can make some interactive operations with their mobile TV. CMMB occupies 25 MHz bandwidth in the 2.6 GHz frequency band and provides 25 video and 30 radio channels as well as some additional data channels. The deployment of mobile TV broadcast in China started in earnest in 2007 for the broadcast of the Beijing Olympics in 2008. By the end of 2008, 118 cities had begun mobile TV broadcast and the CMMB network is planned to cover 337 cities in China by December 2010.

Although the mobile TV standards have some particular features to meet the requirements of handheld devices, in general, they have many similarities in both technical and market aspects with the existing DTTB standards. Many mobile TV standards are complements and extensions of the existing DTTB standards. For instance, the 1seg is a specific working mode of the ISDB-T standard. DVB-H and ATSC-M/H also have the backward compatibility to their terrestrial predecessors in order to share the existing terrestrial broadcast networks. Moreover, both mobile and terrestrial TV standards essentially aim to the same mobile TV market. Therefore, the terrestrial and mobile TV standards are commonly viewed as a whole.

1.3.4 Recent Progress

The DTTB standards kept evolving during the last few years. Many advanced signal processing techniques have been integrated in the new versions/generations of the DTTB standards to improve the efficiency as well as the capacity.

The DVB-T2 standard In June 2006, even before most countries began to launch their first generation DTV, the DVB project started research on the next generation terrestrial broadcasting standard, as known as Digital Video Broadcasting—Second Generation Terrestrial (DVB-T2) [30]. The new system is expected to provide a minimum 30% increase in payload than DVB-T under similar channel conditions. DVB-T2 has more parameter options in terms of channel coding rates, modulations, GI durations as well as FFT sizes, and thus has more flexibilities in choosing working modes. Concatenated LDPC and BCH codes are adopted to replace the classical convolutional and RS codes in DVB-T, providing superior error correction performance. The capacity of DVB-T2 is improved by means of adopting Multiple-Input Single-Output (MISO) technique, reducing the number of pilots and using larger part of the 8 MHz channel in the new 32K-FFT mode. As a result, in the United Kingdom's MFN case (using DVB-T with 64-QAM, 2K FFT mode, channel

coding rate $2/3$, GI $1/32$), using an equivalent mode in DVB-T2 (256-QAM, 32K FFT mode, channel coding rate $3/5$, GI $1/128$) will increase bit rate from 24.1 Mbit/s to 40.2 Mbit/s [31]. That is, over 66% gain in terms of bit rate is obtained using DVB-T2. The European Telecommunications Standards Institute (ETSI) finally adopted the DVB-T2 standard on September 9, 2009. The United Kingdom has assigned one multiplex (the slot corresponding to one analogue TV channel and supporting many digital broadcasting channels) to digital broadcasting using DVB-T2 in 2010. The Swedish Government granted two multiplexes to broadcast HDTV using DVB-T2 in June, 2010. In Spring 2010, Italy has finally assigned a national multiplex to Europa 7 HD which will use DVB-T2. Finland planned to launch DVB-T2 based broadcasting during 2011. South Africa, India and Sri-Lanka have also adopted DVB-T2 as the DTTB standard [7]. DVB-T2 trials in other countries such as Germany, Spain and Austria are underway as well.

The DVB-SH standard The DVB Satellite Services to Handhelds (DVB-SH) standard [32], a hybrid satellite/terrestrial mobile TV system, was published by the DVB Project in February 2007. DVB-SH uses satellite to achieve coverage of large regions or even a whole country. Terrestrial repeaters are used to improve service availability in areas where direct reception of the satellite signal is blocked. It thus works in frequencies below 3 GHz, typically S-Band frequencies around 2.2 GHz. Furthermore, it complements and improves the existing DVB-H physical layer standard by upgrading the FEC block and adopting 1.7 MHz bandwidth and 1k FFT options.

The DVB-NGH standard Moreover, to face the expected huge amount Rich-Media-content consumption in the short future, the DVB project launched a research program aiming at developing Next Generation Handheld (NGH) broadcast system—DVB-NGH [33]. The DVB Project issued a Call for Technologies in the last quarter of 2009 and received 33 responses. The standardization of DVB-NGH is expected to be finished in 2011. The first commercial NGH devices might become available in 2013.

Next generation Chinese standard In China, DTMB does not stop its evolution either. The presentation of Yang Z.X., a major inventor of the DTMB standard, in the 2010 China Digital Television Summit [24] indicates that the research on the second generation DTMB is ongoing. The main improvements lie in improving the spectrum efficiency; adopting multiple antennas to enhance the performance in SFN deployment; increasing available working modes; creating return channel based on mobile telephone network to enable interactive operations; and providing more signal bandwidth options including 1.7, 6, 7, 8 and 10 MHz to adapt to different services in different countries. A latest literature [34] reports some new features of the future Chinese DTTB standard including frame structure with flexibly padded TPFB sequence, multiservice support as well as the advanced channel coding and modulation schemes. Specifically, two coded modulation schemes were proposed: one is the LDPC code based scheme including QC-LDPC codes with a block length of 61440 bits and rates of $1/2$ and $2/3$, bitwise interleaving, constellation rotation with square QAMs and coordinate interleaving; the other scheme is the Bit Interleaved Coded Modulation with Iterative Demapping and Decoding (BICM-ID), including convolutional coded BICM with amplitude-phase-shift-keying (APSK) constellations, doping code and coordinate interleaving.

1.4 Conclusions

In this chapter, we have presented a global overview of the development of the world-wide DTV industry including the increasing TV market, the ongoing DTV transition in the world, several existing terrestrial and mobile DTV broadcast standards as well as the recent progress in the DTV research and industry. These give a brief background and a general context of following chapters.

IN THIS CHAPTER, we present some background knowledge that will be used in the following sections of this thesis. A first step to carry out the study of communication systems is to understand the communication channels in which the information will be conducted. We describe the channel models that are used in this thesis in the first part of this chapter. Some important properties of the channel are also given. The second part of this chapter is dedicated to the introduction of the basic knowledge of the OFDM system.

2.1 Wireless Channel

The term “channel” is referred to the medium in which the information-bearing signal passes from transmitter to receiver. An accurate channel model is extremely important for designing and evaluating communication systems. The classical additive white Gaussian noise (AWGN) channel is a fundamental channel model used in the research of communication techniques. It is a memoryless channel free of interference, dispersion and fading. The signal is only corrupted by the additive Gaussian-distributed random noise with constant spectral density. The main source of AWGN is the thermal noise at the receiver. As the Gaussian probability density function (PDF) has many conveniences with regard to mathematical derivations, the AWGN can be used as a starting point to study some basic problems in communication such as signal estimation and detection, channel capacity computation, channel coding design and so on.

Regarding radio-communications, if the signal is emitted by an isotropic antenna in a space free of absorbing or reflection, the signal energy decreases with the increase of distance according to an inverse-square law. This idealized *free-space* propagation model is used to describe the signal power attenuation due to the distance, which is referred to as *path loss* or *free space loss*. The real radio communication channel is however more complicated than the AWGN or free-space model.

As the signal travels in an open-air environment, it is easily affected by the ambience of transmission. For example, signal can be blocked or absorbed by obstructions causing a fluctuation of signal power; or it can also be reflected or diffracted by objects in the propagation path resulting in multiple copies of signal at the destination; or carrier frequency can vary due to the motion of the transmitter and/or receiver introducing Doppler

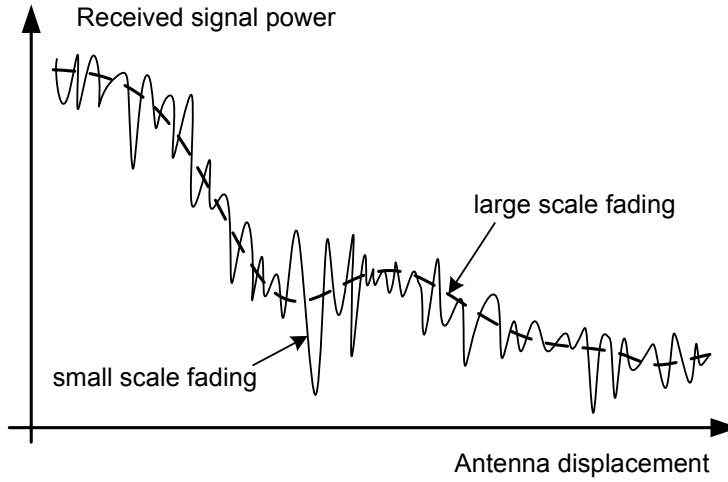


Figure 2.1: Large- and small-scale fading.

shift. In order to make the signal transmission reliable and to improve the performance of communication systems, radio channels should be modeled more precisely.

2.1.1 Large- and Small-Scale Fading

As depicted in Figure 2.1, the signal attenuation experienced in the mobile communication channel is a superimposition of two fading effects: *large-scale* fading and *small-scale* fading [35].

Large-scale fading

The large-scale fading demonstrates the average signal power attenuation (or path loss) due to the distance between the transmitter and receiver. It also takes into account the *shadowing* effect, a fact that the signal transmission is blocked or weakened by the prominent objects in the propagation path, such as hills, buildings and forests. Shadowing can result in a received power variation (6-10 dB) around the mean value. The overall path loss $L_p(d)$ can be expressed as a function of the distance d between transmitter and receiver as well as a random variation:

$$L_p(d) \text{ (dB)} = \underbrace{L_s(d_0) \text{ (dB)} + 10n \log_{10}\left(\frac{d}{d_0}\right)}_{\text{mean path loss}} + \underbrace{X_\sigma \text{ (dB)}}_{\text{lognormal variation}}, \quad (2.1)$$

where:

- $L_s(d_0)$ is a reference value in decibels describing the path loss at a distance d_0 from the transmitter. It is determined by either field measurements or theoretical calculation using the free-space propagation model;
- n is the exponent that is to describe the exponential attenuation of the path loss with respect to the distance. The value of n depends on the carrier frequency, antenna heights and propagation environments. For instance, in free space, $n = 2$; in urban streets where there exists a strong guided wave, n can be less than 2; in urban area

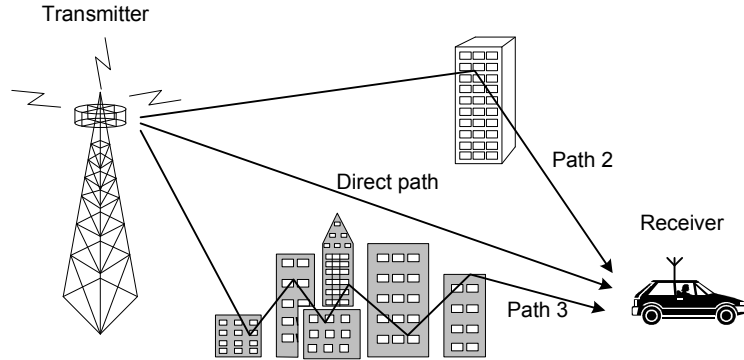


Figure 2.2: Multipath propagation.

cellular radio, n ranges from 2.7 to 3.5; while in obstructed environments, $n = 4 \sim 6$ [9];

- X_σ is a random variable with Gaussian distribution in decibels with zero mean and standard deviation σ (also in decibels). The value of X_σ is normally obtained by actual measurements. X_σ typically ranges from 6 to 10 dB.

As the large-scale fading model describes the variation of the received signal power as a function of the distance over large areas, it is useful in estimating the coverage of a wireless communication system. Since most of the receiving devices are equipped with an automatic gain control (AGC) circuit, the power variation of the received signal can easily be tracked and compensated. Consequently, the performance of a mobile communication system is substantially affected by the signal distortion and interference caused by the small-scale fading. Therefore, the channel models used in this thesis mainly concern the small-scale fading.

Small-scale fading

The small-scale fading refers to the dramatic changes in signal amplitude and phase which result from a small spacial displacement (as small as a half-wavelength) between the transmitter and receiver. The generation mechanism of small-scale fading can be recognized by two ways: time-spread of the signal and time-variation of the channel.

The time-spread of a received signal is caused by the existence of multiple signal propagation paths (referred to as *multipath propagation*) as depicted in Figure 2.2. Signal traveling through different paths experiences different propagation conditions and distances, and thus results in a bunch of signal replicas with different amplitudes, phases and arriving times. The superposition of several signal copies can lead to a dramatic fluctuation of the signal power on an order of 40 dB. Especially, the destructive superposition causes a serious signal power loss which makes the information retrieval at the receiver much difficult. Besides, the multipath propagation often lengthens the time required for the baseband signal to reach the receiver which causes signal smearing and overlapping in the boundaries of successive symbols. This phenomenon is known as intersymbol interference (ISI). The presence of ISI introduces errors in the symbol decision at the receiver. ISI becomes a barrier to achieve high data rate transmissions. Adaptive equalizer and powerful channel coding are also used to fight against ISI.

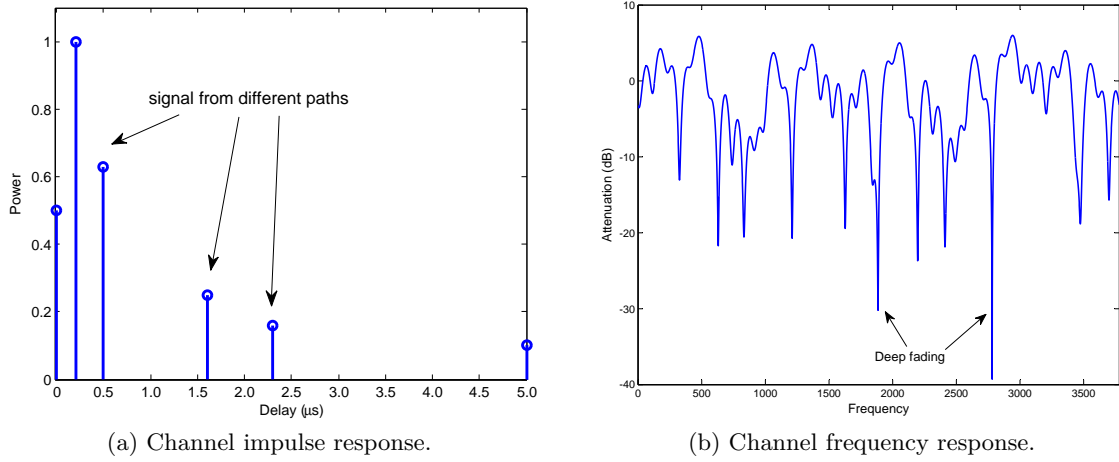


Figure 2.3: Responses of the TU-6 channel.

On the other hand, the time-variation of the channel arises from the changes of the propagation paths which can be caused by the relative motion of the transmitter and/or the receiver. The rate of change of the path determines the fading rapidity, namely the rate of change of the fading impairments. The relative motion between the transmitter and receiver causes a shift in the carrier frequency which is called the *Doppler frequency shift*. It is proportional to the velocity and the direction of motion of the receiver with respect to the direction of arrival of the received signal. More specifically, the Doppler frequency shift is computed by:

$$f_d = f_0 \frac{v}{c} \cos \theta = f_m \cos \theta, \quad (2.2)$$

where v is the velocity of the transmitter relative to the receiver, c is the speed of light, θ is the angle between the receiver's forward velocity and the line of sight from the transmitter to the receiver, and $f_m = v f_0 / c$ is the *maximum Doppler frequency shift* representing the case when the receiver is moving towards the transmitter. Moreover, even when the transmitter and receiver are stationary, the received signal may still vary due to the movement of ambient objects in the channel.

The channel variations impose the channel to be sounded and estimated frequently at a higher rate than that of the channel fluctuations, which is a heavy burden in terms of computational complexity and power consumption. Moreover, the Doppler effect causes a carrier frequency shift of the received signal, which consequently affects the signal demodulation and decoding.

2.1.2 Multipath Channel Model

2.1.2.1 Impulse and Frequency Responses of the Channel

The multipath propagation can be interpreted as a superposition phenomenon of time-domain signals with different arriving times. Thus, it is straightforward to describe the

multipath channel model in the time domain. The received signal $y(t)$ at a given time t is written as a linear combination of different versions of the original signal $x(t)$ through different propagation paths:

$$y(t) = \sum_l \alpha_l(t)x(t - \tau_l(t)), \quad (2.3)$$

where $\alpha_l(t)$ and $\tau_l(t)$ are respectively the attenuation and delay of the l^{th} propagation path at time t . They are determined by the distance that the signal covered in the l^{th} path as well as the nature of reflectors. As mentioned before, the values of $\alpha_l(t)$ and $\tau_l(t)$ can vary once the channel condition changes. The attenuation of each path is modeled as a *wide-sense-stationary* (WSS) stochastic process. Furthermore, different paths are assumed to be *uncorrelated scattering* (US), that is, the attenuation factors for different paths are statistically independent, i.e. $\mathbb{E}[\alpha_l^* \alpha_{l'}] = 0$ given $l \neq l'$. Since the channel is linear, it can be presented by the response $h(\tau, t)$ at time t to an impulse response transmitted at $t - \tau$. Given an input signal $x(t)$, the output signal passing a linear system characterized by $h(\tau, t)$ can be written as:

$$y(t) = \int_{-\infty}^{\infty} h(\tau, t)x(t - \tau)d\tau. \quad (2.4)$$

Comparing (2.3) and (2.4), it is easily obtained that the impulse response of the multipath fading channel (commonly referred to as the *channel impulse response*, CIR) is:

$$h(\tau, t) = \sum_l \alpha_l(t)\delta(\tau - \tau_l(t)), \quad (2.5)$$

where $\delta(\cdot)$ is the *unit impulse function* (or *Dirac delta function*). The CIR of the TU-6 channel is shown in Figure 2.3a as an example. The parameters of the TU-6 channel is listed in Table 2.2. It can be seen that a bunch of “fingers” spread in the time-delay domain. The height of each finger represents the amplitude of the signal component delivered by the corresponding path. Since (2.5) interprets the complicated radio propagation behavior into a concise linear form, it is extremely useful in the research of communication systems.

The characteristic of the channel can also be represented in the frequency domain by the *channel frequency response* (CFR). CFR can be obtained by applying Fourier transform to the CIR in the time-delay domain:

$$\begin{aligned} H(t, f) &\triangleq \int_{-\infty}^{+\infty} h(\tau, t)e^{-j2\pi f\tau} d\tau \\ &= \int_{-\infty}^{+\infty} \sum_l \alpha_l(t)\delta(\tau - \tau_l(t))e^{-j2\pi f\tau} d\tau \\ &= \sum_l \alpha_l(t)e^{-j2\pi f\tau_l(t)}. \end{aligned} \quad (2.6)$$

As an example, the frequency response of the TU-6 channel is given in Figure 2.3b. In addition, Figure 2.4a-d depict an example of the variation of the channel frequency response with respect to the velocity of the receiver. It can be seen that with the increase of the velocity, the channel varies more and more significantly.

CIR and CFR are basic tools to describe, study and exploit the behavior of the multipath fading channel.

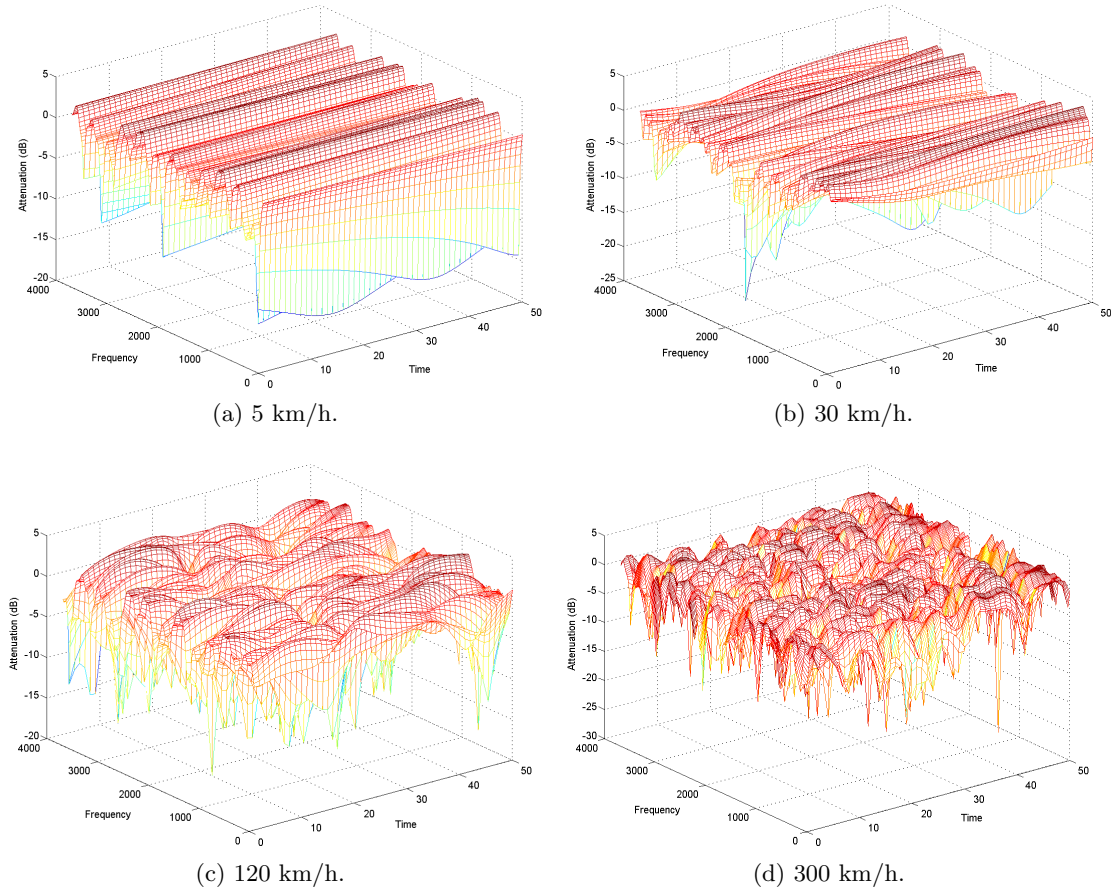


Figure 2.4: Channel frequency response of TU-6 channel with different velocities. Carrier frequency is 500 MHz. Channel bandwidth is 7.56 MHz. Each time slot represents $50\mu\text{s}$.

2.1.2.2 Baseband Equivalent Model

In typical wireless communication systems, most of the signal processing such as coding/decoding, modulation/demodulation, synchronization, equalization, etc. is actually carried out in *baseband*, that is, a frequency range from 0 Herz to a cut-off frequency. Then, the baseband signal is transformed to *passband* signal [36, p.150] by the *quadrature amplitude modulation* (QAM) [37, p.23]. The block diagram of the quadrature amplitude modulation and demodulation is shown in Figure 2.5. The passband signal is up-converted to the carrier frequency which is commonly at the radio frequency (RF) and finally transmitted via the antenna. Accordingly, at the receiver side, the received RF passband signal is transformed back to baseband signal and down-converted to baseband frequency. Thus, it is the RF passband signal which really experiences the wireless channel. Whereas, the frequency up-conversion and down-conversion is, in fact, nothing but a shift of carrier frequency, while the passband-baseband signal transformations at the transmitter and receiver are dual processes and can be viewed as “transparent” by the baseband signal

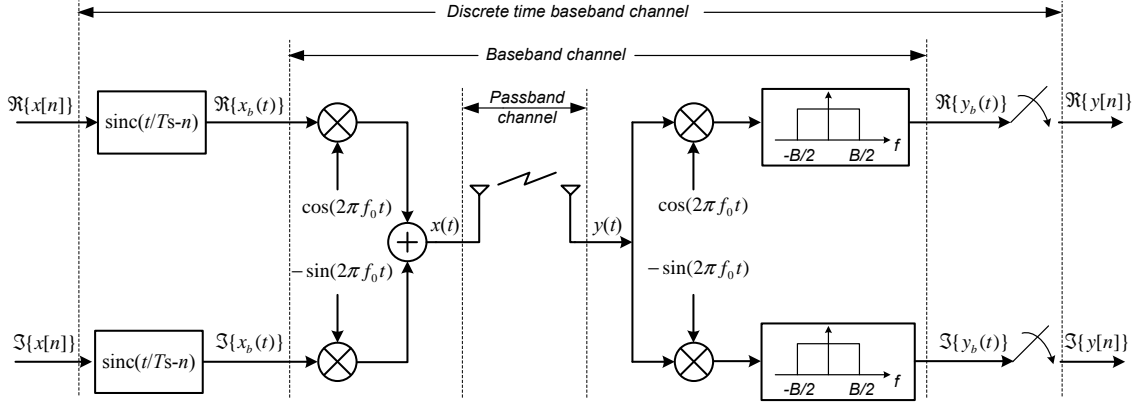


Figure 2.5: Quadrature amplitude modulation.

processing. Hence, it is more convenient to use a baseband equivalent representation of the channel in the study of communication systems.

Let's first recall the representation of the passband signal at the receiver side, which writes:

$$x(t) = \Re \left\{ x_b(t) e^{j2\pi f_0 t} \right\}, \quad (2.7)$$

where $\Re\{\cdot\}$ is the operation that takes the real part of a complex number, $x_b(t)$ is the baseband signal, and f_0 is the carrier frequency. Substituting (2.7) into (2.3), it gets:

$$\begin{aligned} y(t) &= \sum_l \alpha_l(t) \Re \left\{ x_b(t - \tau_l(t)) e^{j2\pi f_0 (t - \tau_l(t))} \right\} \\ &= \Re \left\{ \left[\sum_l \alpha_l(t) x_b(t - \tau_l(t)) e^{-j2\pi f_0 \tau_l(t)} \right] e^{j2\pi f_0 t} \right\}. \end{aligned} \quad (2.8)$$

Comparing (2.7) and (2.8), the portion in the square brackets in above equation represents the baseband equivalent signal received at the receiver side:

$$y_b(t) = \sum_l \alpha_l(t) x_b(t - \tau_l(t)) e^{-j2\pi f_0 \tau_l(t)}. \quad (2.9)$$

Denoting

$$\gamma_l(t) = \alpha_l(t) e^{-j2\pi f_0 \tau_l(t)} \quad (2.10)$$

as the baseband equivalent attenuation factor of the l^{th} path, a baseband equivalent CIR can be obtained in a similar form as (2.5):

$$h_b(\tau, t) = \sum_l \gamma_l(t) \delta(\tau - \tau_l(t)). \quad (2.11)$$

This expression demonstrates that the received baseband signal is the summation of the delayed replicas of the baseband signal. Moreover, from (2.10), it can be seen that a slightly change of path delay τ_l , as little as $1/4f_0$, can cause a significant change in phase ($\pi/2$). Or equivalently, a change of propagation distance of $c/4f_0$, namely a quarter of wavelength, can introduce $\pi/2$ phase shift. Moreover, given the Doppler frequency shift of f_d , the time required for a $\pi/2$ phase shift is $1/4f_d$, that is, a few milliseconds with

a Doppler frequency of tens of Herz in the common mobile reception case. Thus, this baseband equivalent channel model describes the characteristics of small-scale fadings. The according equivalent baseband CFR can be obtained via a similar Fourier transform as (2.6):

$$H_b(t, f) = \sum_l \gamma_l(t) e^{-j2\pi f \tau_l(t)}. \quad (2.12)$$

In the following chapters, we will use the baseband equivalent model but the subscript ‘ b ’ will be omitted for the sake of notation simplicity.

2.1.2.3 Discrete Multipath Channel Model

In above sections, the continuous time channel model is presented. Considering digital communication systems, it is more convenient to convert the continuous time channel model to a discrete time one. According to the sampling theorem [38, p.150], the baseband signal band-limited to $[-\frac{B}{2}, \frac{B}{2}]$ can be written as:

$$x_b(t) = \sum_n x[n] \text{sinc}\left(\frac{t - nT_s}{T_s}\right), \quad (2.13)$$

where $x[n]$ is the information-bearing discrete data symbol, T_s is the sampling period which fulfils $B = 1/T_s$. Substituting (2.13) to (2.9), it writes:

$$\begin{aligned} y_b(t) &= \sum_l \gamma_l(t) \sum_n x[n] \text{sinc}\left(\frac{t - \tau_l(t) - nT_s}{T_s}\right) \\ &= \sum_n x[n] \sum_l \gamma_l(t) \text{sinc}\left(\frac{t - \tau_l(t) - nT_s}{T_s}\right). \end{aligned} \quad (2.14)$$

Then, by sampling the received signal, i.e. $y[m] = y_b(mT_s)$, the received discrete time signal is given by:

$$y[m] = \sum_n x[n] \sum_l \gamma_l(mT_s) \text{sinc}\left(m - n - \frac{\tau_l(mT_s)}{T_s}\right). \quad (2.15)$$

Let $p = m - n$. The above equation turns:

$$y[m] = \sum_p x[m-p] \sum_l \gamma_l(mT_s) \text{sinc}\left(p - \frac{\tau_l(mT_s)}{T_s}\right). \quad (2.16)$$

As shown in Figure 2.6, the channel can be modeled as an L^{th} order channel filter in discrete-time domain [37]. The filter order L is determined by the maximum delay that channel memory effect is non-trivial. The received signal is expressed as:

$$y[m] = \sum_{i=0}^{L-1} h_i[m] x[m-i], \quad (2.17)$$

where

$$h_i[m] = \sum_l \gamma_l(mT_s) \text{sinc}\left(i - \frac{\tau_l(mT_s)}{T_s}\right), \quad (2.18)$$

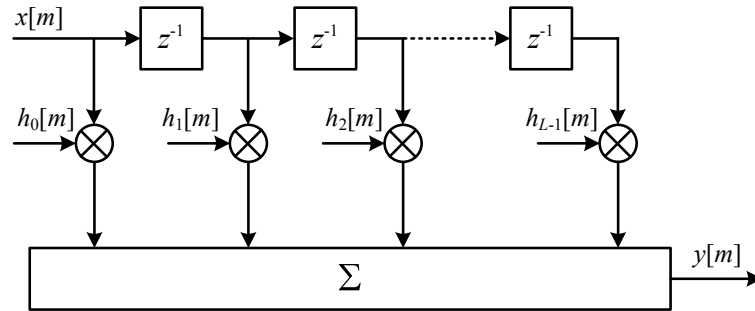


Figure 2.6: Symbol-spaced tapped delay line channel model.

is the i^{th} complex-valued channel filter tap at time m . It can be seen from (2.18) that the discrete channel model is a sampled version of the continuous time channel model with a sampling period T_s . As the $h_i[m]$'s are the summation of samples of WSS random process, it itself is a WSS process for any given i [37, 39]. Meanwhile, the sampling nature of the discrete channel model implies that the channel should be band-limited to $[-\frac{B}{2}, \frac{B}{2}]$, the same as the baseband signal. Since a band-limited stochastic process does not fulfill the US condition, strictly speaking, different paths of the discrete channel model are correlated. This can be verified in (2.18) that the $h_i[m]$ consists of the contributions from all channel paths (γ_l 's), especially from those with delays close to iT_s . It may lead to inaccurate performance evaluation of the wireless systems sensitive to the channel correlation properties [40]. However, in most of the studies [37, 41], $h_i[m]$ is still assumed independent of $h_{i'}[m']$ for all $i \neq i'$ and all m, m' .

Analogous to (2.11), the discrete channel model can be written as:

$$h[l, n] = \sum_i h_i[n] \delta[l - i], \quad (2.19)$$

where $\delta[l - i]$ is the *discrete-time unit impulse function* [42, p.30], $\delta[l - i] = 1$ when $l = i$ and 0 otherwise. The corresponding CFR can be obtained via a K -point discrete Fourier transform (DFT):

$$H[k, n] \triangleq \sum_{l=0}^{K-1} h[l, n] e^{-j \frac{2\pi}{K} kl}. \quad (2.20)$$

2.1.3 Statistical Characteristics of Multipath Channel

2.1.3.1 Rayleigh Fading and Ricean Fading

In a rich multipath environment, the superposition of a large number of scattered signal copies can be modeled as a zero-mean complex-valued Gaussian process by applying the central-limited theorem [36, p. 59]. The envelope (magnitude) of the received signal at any time is *Rayleigh-distributed* [36, p. 44] with the PDF:

$$p(r) = \frac{r}{\sigma^2} \exp\left(-\frac{r^2}{2\sigma^2}\right), \quad r \geq 0, \quad (2.21)$$

where r is the envelope amplitude of the received signal, and $2\sigma^2$ is the mean power of the multipath signal. The Rayleigh process models the fading channels without strong *line-of-sight* (LoS) signal component. Thus, the Rayleigh faded signal component is sometimes

called the *random* or *diffuse* component. Experiments show that the Rayleigh fading model can appropriately describe the channel conditions even when the number of multipath signal components is modest.

When there exist strong non-fading components, such as LoS paths, the channel can no longer be modeled as zero-mean. A direct-current (DC) component should be added to the Gaussian-distributed multipath components, resulting in a *Rice-distributed* [36, p. 46] signal envelope. The channel with LoS path is thus referred to as a *Ricean fading* channel. The PDF of the amplitude of Ricean random variable is:

$$p(r) = \frac{r}{\sigma^2} \exp\left(-\frac{r^2 + s^2}{2\sigma^2}\right) I_0\left(\frac{rs}{\sigma^2}\right), \quad r \geq 0, \quad (2.22)$$

where s is the peak amplitude of the dominant non-fading component and $I_0(\cdot)$ is the modified zeroth-order *Bessel* function of the first kind [36, p. 43]. The *Ricean factor* K presents the ratio of dominant signal component power and the variance of the multipath signal and is computed as:

$$K = 10 \log_{10} \left(\frac{s^2}{2\sigma^2} \right) (dB). \quad (2.23)$$

When the power of the dominant component diminishes ($s \rightarrow 0$), the Ricean PDF converges to the Rayleigh PDF.

The Rayleigh fading and Ricean fading are suitable to model the flat fading channels which will be presented in following sections. They are also used to describe the stochastic behavior of multipath taps. In fact, each “isolate” multipath tap is an aggregate of a large number of statistically independent reflected and scattered “micro paths” with roughly the same time delay. With the central limit theorem, the channel taps can be modeled as circularly symmetric complex Gaussian random variables [37]. Consequently the magnitude of each tap follows the Rayleigh distribution when there is no dominant micro path, otherwise it follows Ricean distribution.

2.1.3.2 Correlation Functions of Multipath Channel

When the surrounding of the channel does not change within a significantly long time compared to the signal duration, the parameters $\gamma_l(t)$, $\tau_l(t)$ in (2.5) can be viewed as fixed within that timescale and the time variable t can be removed from the expressions of these parameters. In this case, the channel is referred to as a *static channel*.

Whereas, when the channel condition changes or the transmitter and receiver are in motion, the parameters of the channel are changing as well. As each channel path contains a large number of reflected and scattered signal copies, it is proper to describe the channel parameters as random variables. According to Bello’s model [43], for each delay τ , the channel response $h(\tau, t)$ is modeled as a *wide-sense-stationary* (WSS) stochastic process. The autocorrelation function of $h(\tau, t)$ writes:

$$\begin{aligned} \phi_h(\tau_1, \tau_2; t_1, t_2) &= \frac{1}{2} \mathbb{E} [h^*(\tau_1, t_1) h(\tau_2, t_2)] \\ &= \frac{1}{2} \mathbb{E} [h^*(\tau_1, t_1) h(\tau_2, t_1 + \Delta t)] = \phi_h(\tau_1, \tau_2; \Delta t), \end{aligned} \quad (2.24)$$

where $\Delta t = t_2 - t_1$. Typically, the fading situations of the propagation paths with different delays are independent. Thus, the random process $h(\tau_1, t)$ and $h(\tau_2, t)$ are uncorrelated

for $\tau_1 \neq \tau_2$. This is usually called *uncorrelated scattering* (US). Incorporating with the WSS assumption, this channel model is referred to as *wide-sense-stationary uncorrelated scattering* (WSSUS) channel [43]. The autocorrelation function of WSSUS CIR is thus:

$$\phi_h(\tau_1, \tau_2; t_1, t_2) = \frac{1}{2} \mathbb{E} [h^*(\tau_1, t_1)h(\tau_2, t_1 + \Delta t)] = \phi_h(\tau_1; \Delta t)\delta(\tau_1 - \tau_2), \quad (2.25)$$

where $\phi_h(\tau_1; \Delta t)$ is the delay cross-power spectral density [43]. The Fourier transform of $\phi_h(\tau_1; \Delta t)$ with respect to the time difference Δt yields the so-called *scattering function* [43]:

$$S(\tau, f_d) = \int_{-\infty}^{\infty} \phi_h(\tau_1; \Delta t)e^{-j2\pi f_d \Delta t} d(\Delta t), \quad (2.26)$$

where f_d is the Doppler frequency. Integrating the scattering function $S(\tau, f_d)$ over the Doppler frequency yields the *delay power spectrum* (or *multipath intensity profile*) [36]:

$$\rho(\tau) = \int_{-\infty}^{\infty} S(\tau, f_d) df_d, \quad (2.27)$$

which coincides with the delay cross-power spectral density $\phi_h(\tau_1; \Delta t)$ when Δt is equal to 0. The delay power spectrum function represents the average power of the channel as a function of delay τ . It is useful to determine the significant paths as well as the *maximum delay spread* τ_{max} which represents the maximum delay that the multipath channel spreads [35].

The CFR $H(t, f)$ presents the variations of the channel in time-frequency plan. For each fixed time t' , $H(t', f)$ gives the change of the channel with respect to different frequencies f , and vice versa. The time-frequency correlation of the channel response is very important for understanding the channel variation behavior. Similar to the impulse response, $H(t, f)$ is also modeled as WSS random process. The autocorrelation function of $H(t, f)$ writes:

$$\phi_H(\Delta t, \Delta f) = \frac{1}{2} \mathbb{E} [H^*(t, f)H(t + \Delta t, f + \Delta f)]. \quad (2.28)$$

It is called the *spaced-frequency spaced-time autocorrelation function*. In many channel models [1, 44], the multipath is assumed to be crowded around a bunch of fixed delays. Similar as in [45], it is also assumed that the attenuation of each path has the same correlation function $\phi_t(\Delta t)$ in time domain:

$$\phi_{\gamma_l} \triangleq \frac{1}{2} \mathbb{E} [\gamma_l^*(t)\gamma_l(t + \Delta t)] = \sigma_l^2 \phi_t(\Delta t), \quad \forall l, \quad (2.29)$$

where σ_l^2 is the average power of the l^{th} path. Substituting (2.12) into (2.28) and taking into account (2.29), it gets:

$$\begin{aligned} \phi_H(\Delta t, \Delta f) &= \sum_l \frac{1}{2} \mathbb{E} [\gamma_l^*(t)\gamma_l(t + \Delta t)] e^{-j2\pi \Delta f \tau_l} \\ &= \phi_t(\Delta t) \left(\sum_l \sigma_l^2 e^{-j2\pi \Delta f \tau_l} \right). \end{aligned} \quad (2.30)$$

Define the correlation function in the frequency domain:

$$\phi_f(\Delta f) \triangleq \sum_l \sigma_l^2 e^{-j2\pi \Delta f \tau_l}. \quad (2.31)$$

Hence,

$$\phi_H(\Delta t, \Delta f) = \phi_t(\Delta t)\phi_f(\Delta f). \quad (2.32)$$

That is, the spaced-frequency spaced-time autocorrelation function $\phi_H(\Delta t, \Delta f)$ can be written as a product of the *spaced-time correlation function* $\phi_t(\Delta t)$ and the *spaced-frequency correlation function* $\phi_f(\Delta f)$. It should be noted here that the spaced-frequency correlation function can also be obtained from the Fourier transform of the delay power spectrum with respect to the delay τ :

$$\phi_f(\Delta f) = \int_{-\infty}^{\infty} \rho(\tau) e^{-j2\pi\tau\Delta f} d\tau. \quad (2.33)$$

The time-domain correlation describes the time-varying behavior of the channel and thus mainly depends on the changes of the channel conditions, particularly the relative motion speed of the transmitter and receiver. A widely used model characterizing the time-varying channel is the *Jakes' model* [8], in which the autocorrelation function is given as:

$$\phi_t(\Delta t) = J_0(2\pi f_m \Delta t), \quad (2.34)$$

where $J_0(\cdot)$ is the zeroth-order *Bessel* function of the first kind and f_m is the maximum Doppler frequency shift. An example of spaced-time correlation function is shown in Figure 2.7a. The Fourier transform of the spaced-time correlation function yields the so-called *Doppler power spectrum*. According to the Jakes' model, it writes [46, p.265]:

$$S_D(f_d) = \begin{cases} \frac{1}{\pi f_m \sqrt{1-(f_d/f_m)^2}}, & |f_d| \leq f_m \\ 0 & \text{otherwise.} \end{cases} \quad (2.35)$$

The Doppler power spectrum gives the average power of the channel output as a function of the Doppler frequency f_d . As in a typical multipath environment, the received signal comes from different paths and the associated Doppler shifts are generally different from each other. Thus, the composite effect of the paths with different Doppler shifts is the signal spectral broadening rather than a shift. This spectral dispersion is shown in Figure 2.7b. Doppler power spectrum can also be obtained by integrating the scattering function $S(\tau, f_d)$ over the delay τ ,

$$S_D(f_d) = \int_{-\infty}^{\infty} S(\tau, f_d) d\tau. \quad (2.36)$$

The frequency-domain correlation depends on the multipath delay spread, as shown in (2.31). In the extreme case, when the channel has no delay spread, i.e. the CIR is an unite impulse function, the CFR will be a constant value for all frequencies and the correlation will be always 1. Whereas, when the CIR spreads in time domain, the correlation changes for different frequencies. Thus, the frequency-domain correlation function $\phi_f(\Delta f)$ differs with different types of power delay profiles of the channel.

Exponentially Decaying Power Delay Profile As mentioned before, the signal power exponentially attenuates with respect to the propagation distance and thus with respect to the delay. Hence, it is reasonable to model the multipath power delay profile

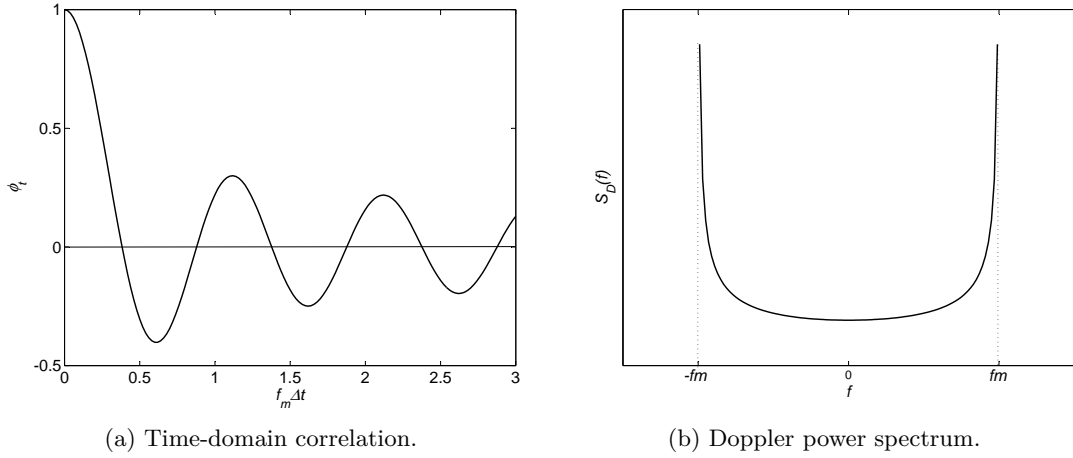


Figure 2.7: OFDM signal waveform.

being exponentially decaying as a function of delay τ . More specifically, the average power of the l^{th} path is [47]:

$$\sigma_l^2 = \frac{1}{\tau_{rms}} e^{-\frac{\tau_l}{\tau_{rms}}}, \quad (2.37)$$

where τ_{rms} is the root mean square (rms) delay spread which is the square root of the second central moment of the power delay profile and is defined as:

$$\tau_{rms} = \sqrt{\overline{\tau^2} - (\bar{\tau})^2}, \quad (2.38)$$

where

$$\bar{\tau} = \frac{\sum_l |\gamma_l|^2 \tau_l}{\sum_l |\gamma_l|^2} \quad (2.39)$$

$$\overline{\tau^2} = \frac{\sum_l |\gamma_l|^2 \tau_l^2}{\sum_l |\gamma_l|^2}. \quad (2.40)$$

Taking (2.37) into (2.31), we can get

$$r_f(\Delta f) = \sum_l \frac{1}{\tau_{rms}} e^{-\frac{\tau_l}{\tau_{rms}}} e^{-j2\pi\Delta f\tau_l}. \quad (2.41)$$

When the number of paths increase to infinity, the sum in (2.41) can be approximated by an integral:

$$\begin{aligned} r_f(\Delta f) &= \int_0^{+\infty} \frac{1}{\tau_{rms}} e^{-(j2\pi\Delta f\frac{1}{\tau_{rms}})\tau} d\tau \\ &= \frac{1}{1 + j2\pi\Delta f\tau_{rms}}. \end{aligned} \quad (2.42)$$

Uniform Power Delay Profile The “worst case” of the multipath channel considered in the literature is the one with *uniform power delay profile*. In other words, the average power of all paths are the same within a period of delay:

$$\sigma_l^2 = \frac{1}{\tau_{max}}, \quad 0 \leq \tau \leq \tau_{max}, \quad (2.43)$$

where τ_{max} is the *maximum delay spread* which represents the maximum delay that the multipath channel can achieve. That means the signal power does not further attenuate for the components with longer propagation distance. A data symbol will apparently introduce more ISI to the following symbol in such a channel condition. Assuming there are infinite paths, and substituting (2.43) into (2.31), we can get

$$\begin{aligned} r_f(\Delta f) &= \lim_{l \rightarrow \infty} \sum_l \frac{1}{\tau_{max}} e^{-j2\pi\Delta f\tau_l} \\ &= \int_0^{\tau_{max}} \frac{1}{\tau_{max}} e^{-j2\pi\Delta f\tau} d\tau \\ &= \frac{1 - e^{-j2\pi\Delta f\tau_{max}}}{j2\pi\Delta f\tau_{max}} \\ &= e^{-j\pi\Delta f\tau_{max}} \frac{\sin(\pi\Delta f\tau_{max})}{\pi\Delta f\tau_{max}} \\ &= \text{sinc}(\Delta f\tau_{max}) e^{-j\pi\Delta f\tau_{max}}, \end{aligned} \quad (2.44)$$

where $\text{sinc}(x) = \frac{\sin(\pi x)}{\pi x}$ is the *normalized sinc function*.

The relationship among the channel correlation functions and power density functions is shown in Figure 2.8. The channel correlation function (2.42) and (2.44) are useful for the algorithms exploiting the channel correlation properties. As we will show later, the correlation functions will be used in the Wiener filtering based channel estimation techniques.

2.1.4 Time and Frequency Coherence

From above discussion, one can know the correlation of received signals that are spaced Δf in frequency or Δt in time from (2.31) and (2.34), respectively. However, in the designing of the communication systems, it is also useful to know the range of the time/frequency in which the channel is non-varying. There come the concepts of *coherence bandwidth* and *coherence time*.

2.1.4.1 Delay Spread and Coherence Bandwidth

The coherence bandwidth B_C is a statistical range of frequencies over which the channel response holds approximately the same gain and linear phase for all spectral components. That is to say, the frequency attenuations within the coherence bandwidth have strong potential similarities, and the signal in this range can be viewed as exhibiting the same fading. Hence, coherence bandwidth is useful in designing the system as well as the channel estimation mechanism.

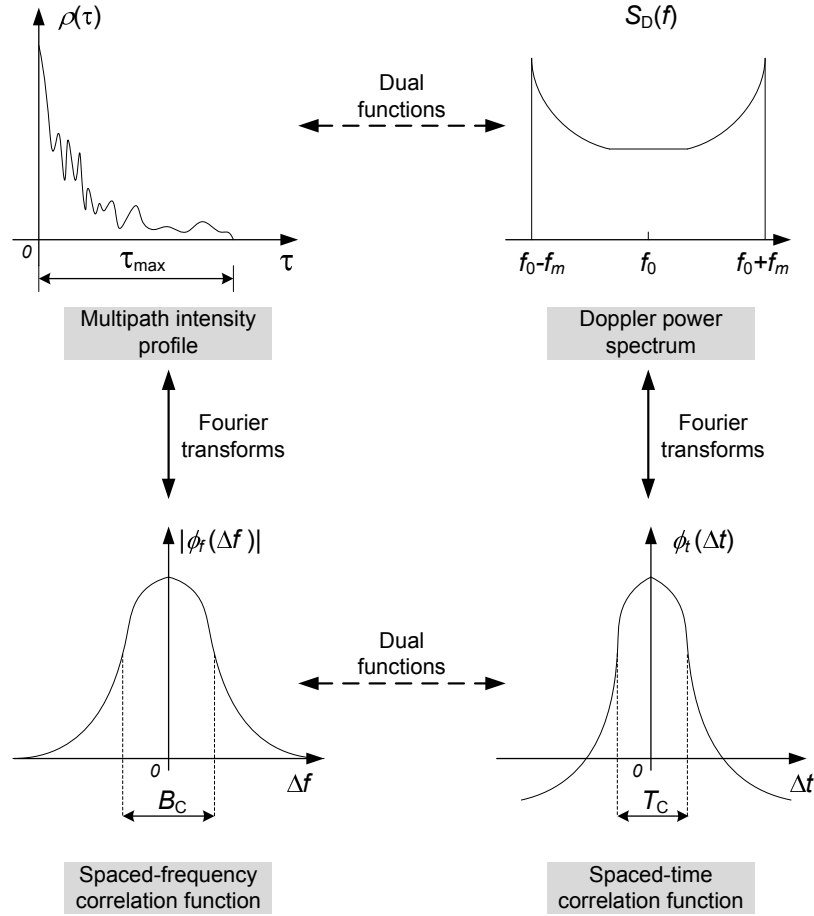


Figure 2.8: Relationship among the channel correlation functions and power density functions.

As mentioned before, the frequency correlation of the channel is directly linked to the delay spread. Thus, a straightforward (but maybe not so accurate) estimate of coherence bandwidth is the reciprocal of the maximum delay spread:

$$B_C \approx \frac{1}{\tau_{max}}. \quad (2.45)$$

Apparently, τ_{max} is a coarse indicator of the time-dispersion behavior of the channel because it only represents the maximum length of the channel spreading. While channels with the same τ_{max} can exhibit different power delay profiles which will produce quite different frequency correlations as demonstrated in (2.42) and (2.44). A more meaningful measurement of the channel delay spread is the rms delay spread which already takes into account the delay profile in its definition given by (2.38). The exact relationship between coherence bandwidth and rms delay spread, however, does not really exist. Several approximate relationships based on measurements have been presented. When the coherence bandwidth is defined as the frequency range over which the channel frequency

response has a correlation function of at least 0.9, the coherence bandwidth is [48]:

$$B_C \approx \frac{1}{50\tau_{rms}}. \quad (2.46)$$

While, if the correlation function is relaxed to above 0.5, the coherence bandwidth is approximately [9, p.164]:

$$B_C \approx \frac{1}{5\tau_{rms}}. \quad (2.47)$$

Equations (2.46) and (2.47) are the most used approximations of the coherence bandwidth, although there are other measurements and expressions such as those given by [35, Eq.(11) and (12)].

2.1.4.2 Doppler Spread and Coherence Time

Similar to the coherence bandwidth, the coherence time T_C is defined as the time duration within which the channel response is basically unchanged. Intuitively, the channel consistence in time depends on the rate of the variation of the channel conditions, more specifically the speed of the relative motion between the transmitter and receiver. Hence, an approximated relationship can be established between the maximum Doppler frequency and the coherence time:

$$T_C \approx \frac{1}{f_m}. \quad (2.48)$$

A more precise description of coherence time is defined as the time over which the time correlation function is above 0.5, which leads [49]:

$$T_C \approx \frac{9}{16\pi f_m}. \quad (2.49)$$

A popular rule of thumb to determine the coherence time is the geometric mean of (2.48) and (2.49), which yields [9, p.166]:

$$T_C = \sqrt{\frac{9}{16\pi f_m^2}} = \frac{0.423}{f_m}. \quad (2.50)$$

2.1.4.3 Time and Frequency Selectivity

Comparing the signal occupation with the channel coherence in time and frequency, one can understand the characteristics of the fading that signal experiences. More precisely, in the frequency domain, if the signal bandwidth is smaller than the coherence bandwidth, the channel affects all signal frequency components in the same manner. This type of channel fading is referred to as *flat fading*. One example is the red signal shown in Figure 2.9. On the contrary, if the signal bandwidth is larger than the coherence bandwidth, the signal is not affected equally by the channel. Some frequency components suffer destructive channel effects while others experience better channel conditions. This type of fading is termed as *frequency-selective fading*. The blue signal in Figure 2.9 undergoes frequency selective fading.

Analogously, in the time domain, if the signal symbol duration is longer than the coherence time, the channel varies significantly within a symbol duration. This type of

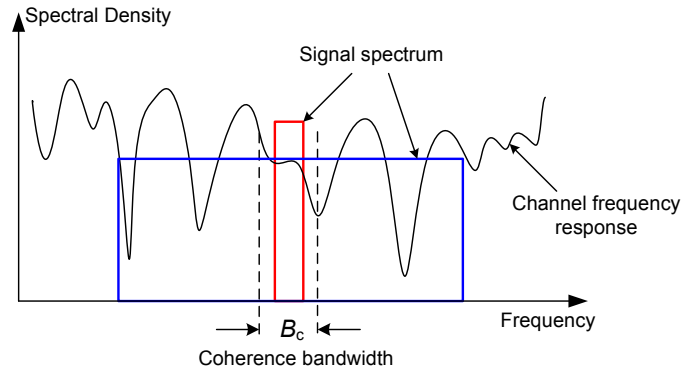


Figure 2.9: Flat fading and frequency-selective fading.

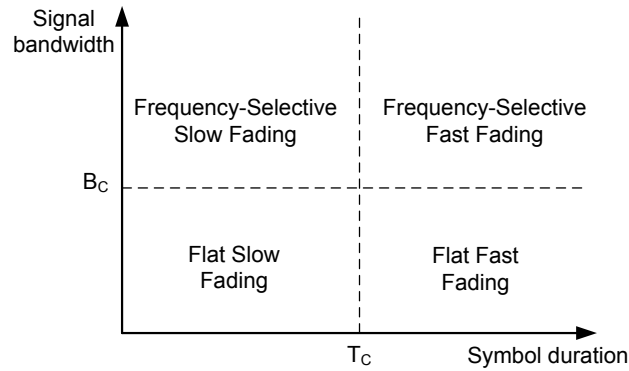


Figure 2.10: Relationship of signal frequency/time selectivity and coherence bandwidth/time.

fading is called *fast fading*. If the signal symbol duration is shorter than the coherence time, the channel changes at a rate slower than the signal symbol rate. This type of fading is named as *slow fading*. Thus, combining the frequency selectivity/non-selectivity and the fast/slow fading behaviors in time, the channel can be classified into four categories. Figure 2.10 presents the relationship between selectivities and coherences.

2.1.5 Channel Models for Simulations

2.1.5.1 Fixed-Reception Channel Models

The DVB-T standard specifies two static channel models, namely P1 and F1, that characterize the portable and fixed reception cases, respectively.

In the portable reception scenario, there is no LoS signal. The P1 channel is thus characterized as a Rayleigh fading. More concretely, given the input signal $x(t)$, after passing the channel, the output signal $y(t)$ is written as:

$$y(t) = \frac{1}{\sqrt{\sum_{l=1}^L \rho_l^2}} \sum_{l=1}^L \rho_l e^{-j\theta_l} x(t - \tau_l) \quad (2.51)$$

where τ_l , θ_l and ρ_l are the relative delay, phase shift and attenuation of the l^{th} path. The corresponding values of the parameters of specified by the P1 channel model in the DVB-T standard are deterministic as listed in Table 2.1.

Table 2.1: Parameters of the P1 and F1 channels

Path index l	Attenuation ρ	Relative Delay τ (μs)	Phase Shift θ (rad)
1	0.057 662	1.003 019	4.855 121
2	0.176 809	5.422 091	3.419 109
3	0.407 163	0.518 650	5.864 470
4	0.303 585	2.751 772	2.215 894
5	0.258 782	0.602 895	3.758 058
6	0.061 831	1.016 585	5.430 202
7	0.150 340	0.143 556	3.952 093
8	0.051 534	0.153 832	1.093 586
9	0.185 074	3.324 866	5.775 198
10	0.400 967	1.935 570	0.154 459
11	0.295 723	0.429 948	5.928 383
12	0.350 825	3.228 872	3.053 023
13	0.262 909	0.848 831	0.628 578
14	0.225 894	0.073 883	2.128 544
15	0.170 996	0.203 952	1.099 463
16	0.149 723	0.194 207	3.462 951
17	0.240 140	0.924 450	3.664 773
18	0.116 587	1.381 320	2.833 799
19	0.221 155	0.640 512	3.334 290
20	0.259 730	1.368 671	0.393 889

While in the fixed reception scenario, the received signal often contains a dominant signal component (LoS). This channel model is called F1 channel. The amplitude of each path is therefore characterized by a Rician distribution. The signal passing Rician channel can be written in a similar way as (2.51):

$$y(t) = \frac{1}{\sqrt{\sum_{l=1}^L \rho_l^2}} \left(\rho_0 x(t) + \sum_{l=1}^L \rho_l e^{-j\theta_l} x(t - \tau_l) \right) \quad (2.52)$$

where ρ_0 is the LoS component whose value is computed by the Rician K -factor as given in (2.23).

2.1.5.2 Time-Varying Channel Models

The COST207 working group specified a series of channel models based on the WSSUS assumption. Among them, the Typical Urban-six paths (TU-6) model is a statistical channel model that describes the typical propagation environments in cities and suburbs areas. For the sake of hardware designing and software simulation, the channel model is described in a discrete form with L paths as shown in Table 2.2 [44]. The TU-6 channel model is widely used to evaluate the performance of a wireless communication system in a time-varying frequency-selective fading propagation environment.

Another channel model specified by the COST207 group is the Hilly Terrain (HT) channel. The maximum time delay of the HT channel is very long (17.2 μs) due to the hilly propagation situation. The detail of the HT channel is depicted in Table 2.3.

Table 2.2: Power Delay Profile of the TU-6 Channel Model

Path	Delay (μs)	Power (dB)	Power (linear)
0	0	-3	0.5
1	0.2	0	1
2	0.5	-5	0.63
3	1.6	-6	0.25
4	2.3	-8	0.16
5	5.0	-10	0.1

Table 2.3: Power Delay Profile of the Hilly Terrain (HT) Channel Model

Path	Delay (μs)	Power (dB)	Power (linear)
0	0	0	1
1	0.2	-2	0.63
2	0.4	-4	0.4
3	0.6	-7	0.2
4	15.0	-6	0.25
5	17.2	-12	0.06

Note that, for a statistical channel model, the powers given in the power delay profiles are actually *average* path powers. The gain for each path is a random process whose statistical characteristics follow some distributions specified in the channel models. For each realization of the channel, we have to generate the channel coefficients according to the specifications of the channel model. For example, a typical method to generate channel coefficients according to COST207 is given in [46, p.284].

2.1.6 Generation Method

In simulations, it is convenient to use the discrete channel model as given in Section 2.1.2.3. It requires that the delays of the paths coincide with the sampling intervals of the system. Therefore, we have to generate the filter taps of the discrete channel model from the power delay profiles.

The channel generation is depicted in Figure 2.11. We assume that the power delay profiles are discrete samples of a “real” CIR with a sampling rate the same as the system. This assumption enables us to reconstruct the real CIR via interpolation. We use sinc function to make the interpolation. The shape of the sinc function is determined by the sampling rate of the system. For the complexity consideration, we limit the interpolation length to 10 samples. Then, we can get the channel gains at the sampling intervals by sampling the interpolated CIR with a rate of the system. Since the channel is causal, we only select the channel gains whose delays are greater than 0. This yields the sample-spaced CIR as shown by the red curve in Figure 2.11.

Note that, due to the interpolation, the sample-spaced CIR is slightly (half interpolation length) longer than the maximum delay specified by the power delay profile. For instance, the TU-6 channel has a maximum delay of 5 μs which corresponds to $\lceil \frac{5}{1/7.56} \rceil = 38$ samples in the DTMB system. Given an interpolation length of 10 samples, the sample-spaced CIR is 43 samples.

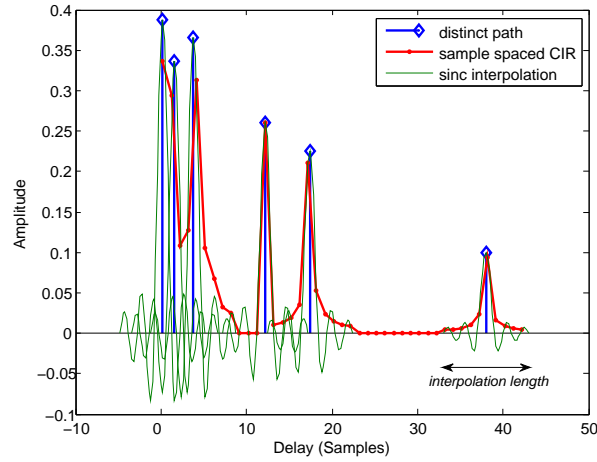


Figure 2.11: Sample spaced CIR generation by interpolation.

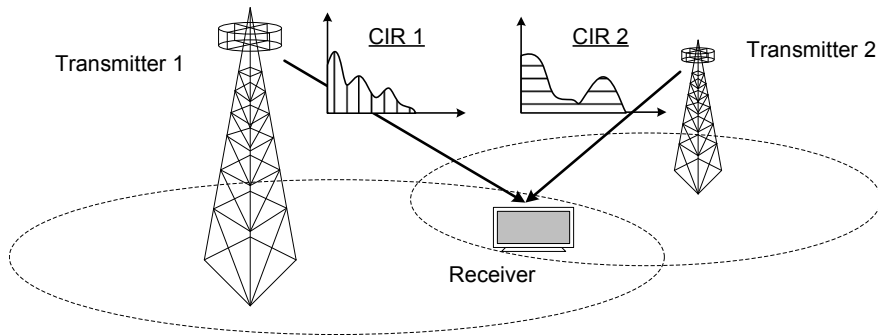


Figure 2.12: SFN broadcasting.

2.1.7 Single Frequency Network Channels

Single Frequency Network (SFN) is a network of transmitting stations which simultaneously transmit the same signal over the same frequency channel. As the signal is transmitted to different areas using the same channel, SFN is a means to extend the transmission coverage without additional frequency resources. It provides higher spectrum efficiency, better coverage, less power consumption, and higher reliability. SFN is particularly interesting for broadcasting. Several European countries have already deployed SFNs in operations of DTTB. SFN can be used for other radio communication systems, such as WLAN networks as well.

In the meantime, SFN is considered as a severe channel condition. The broadcasting areas of different transmitters are overlapped to each other in some regions. In the overlapped areas, the signal transmitted from a farther transmitter is considered as an artificial echo with strong power and long time delay. This leads to a channel with extremely long time delay spread in the time domain, and strong selectivity in the frequency domain. Therefore, the systems using SFN should use long GI to prevent the ISI and, more importantly, adopt robust channel estimation techniques which are effective in highly frequency-selective channels.

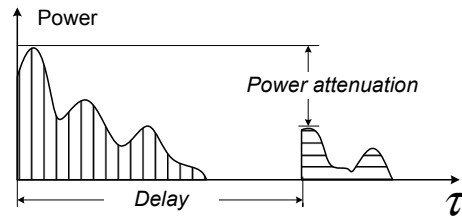


Figure 2.13: Equivalent CIR of the SFN channel.

An example of the SFN broadcasting with two transmitters is depicted in Figure 2.12. Same signal is sent from two different transmitters at the same time on the same carrier frequency (TV broadcasting channel). The signal from these two transmitters experiences independent fadings. The equivalent CIR of the SFN channel is the combination of the CIRs of two independent TU-6 channels as shown in Figure 2.13. The difference of two propagation distances causes time delay and power attenuation on the second CIR. For instance, when the difference is 7 km, the corresponding propagation time difference is $7000/(3 \times 10^8) = 23.33 \mu s$.

2.2 OFDM

Researchers never stop developing communication systems with higher data rates. Besides bandwidth, power and noise, the available data rate of the systems is also limited by ISI – an interfering phenomenon that the consecutive signal symbols spread and overlap. ISI is caused by the channel memory effects such as the dispersion of signal arrival time with the multipath channel, or the parasitic capacitance and inductance in the signal wireline. The presence of ISI will blur the distinction of successive symbols. Especially when ISI affects a large portion of the symbol, it introduces ambiguity in the symbol decision and thus reduces the performance of the receiver. Therefore, in order to limit the effect of ISI, the duration of the symbol should be designed significantly long compared to the maximum time delay of the channel impulse response, which implies that the applicable symbol rate is limited by the memory of the time-dispersive channel. Possible solution to reduce ISI includes enlarging the data symbol duration and inserting a guard interval. However, these methods degrade the system efficiency. In addition, many techniques such as receiver equalization, transmitter pre-equalization and diversity reception can be employed to mitigate the effect of ISI so that the data can be transmitted with a symbol period comparable to, or even smaller than the channel's memory. Yet, these techniques have high computational complexity and more efficient high data rate transmission scheme is needed. ISI is thus a great challenge for the traditional single carrier transmission scheme.

A possible solution is the multicarrier transmission which employs a number of separated subbands to transmit several low-speed data streams in parallel. A high-speed data stream is divided into a bunch of low-speed ones. The symbol duration is so long that the influence of ISI can either be tolerated or easily corrected. The data transmission in each band is thus reliable even in presence of ISI. As the overall data rate of a multicarrier system is the summation of the individual data rates in each band, such a system can achieve a high data rate in multipath channels. Classical multicarrier transmission requires that all the subbands are separated and spaced in the frequency domain in order to prevent mutual interference between subbands. This frequency-division arrangement of subbands needs filter bank and reduces the spectrum efficiency.

Orthogonal frequency-division multiplexing (OFDM) is thus invented to achieve high data rate transmissions with improved spectrum efficiency. It permits the overlap of individual subbands while maintaining the independency of the information transmitted in them. The invention of OFDM techniques dates back to the late 1950s and early 1960s for the military high-frequency radio. In 1970, Weinstein and Ebert proposed the frequency-division multiplexing (FDM) using the fast Fourier transform (FFT) and guard interval (GI) which is, in fact, what we call OFDM nowadays [50]. The use of FFT greatly reduces the complexity of implementation. In 1985, Cimini [51] demonstrated the use of OFDM for mobile communications. Since 1990s, with the rapid development of electronics, OFDM is adopted by many communication standards such as the asymmetric digital subscriber loop (ADSL, in which OFDM is usually called *Discrete Multitone*, DMT) [52], DVB/DAB standards [1, 53], IEEE 802.11a wireless local area network (WLAN) [54], IEEE 802.16 wireless metropolitan area networks (WiMAX) [55], the 3GPP Long Term Evolution (LTE) air interface E-UTRAN [56] and so on. It is also promising candidate for the future communication standards including the wireless personal area network (PAN) ultra-

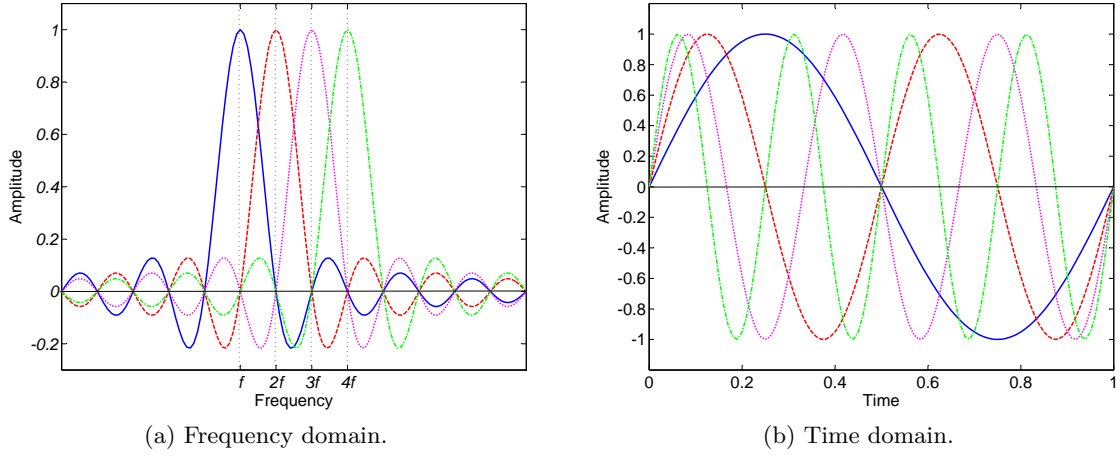


Figure 2.14: OFDM signal waveform.

wideband (UWB) IEEE 802.15.3a [57], mobile broadband wireless access (MBWA) IEEE 802.20 [58] and power line communications (PLC) [59].

The wide interest in OFDM is due to its significant advantages over traditional transmission schemes. The main advantages that OFDM offers include:

- robustness against ISI and frequency-selective fading caused by multipath channels;
- simple equalizer structure;
- high spectral efficiency;
- efficient implementation using FFT;
- robustness against narrow band interference;
- flexible spectrum allocation.

On the other hand, OFDM has some limitations such as:

- sensitivity to the carrier frequency offset (CFO);
- sensitivity to time and frequency synchronization error;
- high peak-to-average-power ratio (PAPR), requiring high linearity transmitter, which reduces the power efficiency.

In the following sections of this chapter, the OFDM signal will be formulated. Several OFDM formations will also be presented.

2.2.1 CP-OFDM

OFDM uses a bunch of orthogonal subcarriers to transmit data symbols in parallel. The OFDM carrier waveform is shown in the frequency and time domains in Figure 2.14a and 2.14b, respectively. In the time domain, the OFDM signal can be seen as a superposition of a number of sinusoidal signals with different periods. While in the frequency domain it can be viewed as a group of sinc function waveforms which are well placed so that the main peak of each sinc waveform is located at the nulls of all other waveforms to prevent intercarrier interference (ICI).

A typical block diagram of OFDM modulation is given in Figure 2.15. The serial data stream $X[k]$ is first converted to N parallel low-speed streams. The parallel data symbols are transmitted blockwise. Each data block contains N data symbols. The transmitted symbol duration is hence lengthened N times, namely $T = NT_s$, where T_s is the original data symbol duration. T is actually the “useful part” of an OFDM duration that is used for data transmission, i.e., the part excluding GI. The extension of the symbol duration means the data symbols are more robust to ISI.

The i^{th} transmission block is denoted as an $N \times 1$ column vector $\mathbf{X}^{(i)} = [X^{(i)}[0], X^{(i)}[1], \dots, X^{(i)}[N-1]]^T$, where $X^{(i)}[k] = X[k + iN]$, $0 \leq k \leq N-1$. The frequency-domain data symbols are then modulated to different subcarriers via an N -point inverse discrete Fourier transform (IDFT). The i^{th} time-domain data block $\mathbf{x}^{(i)}$ is:

$$\mathbf{x}^{(i)} = \mathbf{F}_N^H \mathbf{X}^{(i)}, \quad (2.53)$$

where

$$\mathbf{F}_N = \frac{1}{\sqrt{N}} \begin{bmatrix} 1 & 1 & \dots & 1 \\ 1 & e^{-j\frac{2\pi}{N}} & \dots & e^{-j\frac{2\pi(N-1)}{N}} \\ \vdots & \vdots & \ddots & \vdots \\ 1 & e^{-j\frac{2\pi(N-1)}{N}} & \dots & e^{-j\frac{2\pi(N-1)^2}{N}} \end{bmatrix}_{N \times N} \quad (2.54)$$

is the $N \times N$ unitary matrix corresponding to the discrete Fourier transform (DFT) operation.⁽¹⁾ \mathbf{F}_N^H is the *Hermitian transpose* of \mathbf{F}_N which represents the IDFT operation. As \mathbf{F}_N is an unitary matrix, we have $\mathbf{F}_N^{-1} = \mathbf{F}_N^H$. The subcarrier spacing is selected as the reciprocal of the data block duration, i.e. $\Delta f = \frac{1}{T}$.

In classical OFDM systems, a cyclic prefix (CP) composed of the last ν samples of a data block is inserted before each data block to prevent interblock interference (IBI) between successive data blocks. CP is selected longer than the length of channel dispersion. The CP insertion operation can be expressed as an $(N + \nu) \times N$ matrix:

$$\mathbf{I}_{\text{cp}} = \left[\begin{array}{c|c} \mathbf{0}_{\nu \times (N-\nu)} & \mathbf{I}_{\nu} \\ \hline & \mathbf{I}_N \end{array} \right], \quad (2.55)$$

where $\mathbf{0}_{\nu \times (N-\nu)}$ is a $\nu \times (N - \nu)$ matrix in which all elements are zero, \mathbf{I}_{ν} and \mathbf{I}_N are $\nu \times \nu$ and $N \times N$ identity matrices, respectively. The data block and its CP form an OFDM symbol:

$$\mathbf{x}_{\text{cp}}^{(i)} = \mathbf{I}_{\text{cp}} \mathbf{x}^{(i)} = \mathbf{I}_{\text{cp}} \mathbf{F}_N^H \mathbf{X}^{(i)}. \quad (2.56)$$

The transmitted signal then passes through a multipath channel modeled as a FIR filter of order L . At the received side, supposing the system is perfectly synchronized in time and frequency, the received signal is affected by the multipath channel and AWGN:

$$y^{(i)}[n] = \sum_{l=0}^{L-1} h_l x_{\text{cp}}^{(i)}[n-l] + w[n], \quad (2.57)$$

where $w[n]$ is the AWGN. Organize the received signal in vector form:

$$\mathbf{y}_{\text{cp}}^{(i)} = \mathbf{H}_{\text{ISI}} \mathbf{x}_{\text{cp}}^{(i)} + \mathbf{H}_{\text{IBI}} \mathbf{x}_{\text{cp}}^{(i-1)} + \mathbf{w}, \quad (2.58)$$

(1). Note that a scale factor $\frac{1}{\sqrt{N}}$ is used so that the Fourier transform matrix \mathbf{F}_N is unitary. The signal power after the FFT/IFFT operation is therefore **unchanged**.

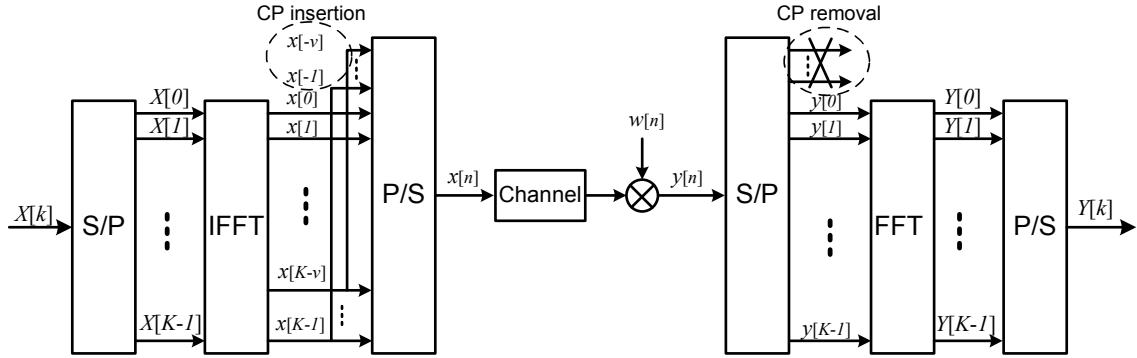


Figure 2.15: Block diagram of OFDM modulation and demodulation.

where \mathbf{w} is the vector of AWGN with noise power σ_w^2 and $E\{\mathbf{w}\mathbf{w}^H\} = \sigma_w^2 \mathbf{I}_N$, while \mathbf{H}_{ISI} and \mathbf{H}_{IBI} are $(N + \nu) \times (N + \nu)$ *Toeplitz* matrix:

$$\mathbf{H}_{\text{ISI}} = \begin{bmatrix} h_0 & 0 & \cdots & 0 \\ \vdots & \ddots & \ddots & \vdots \\ h_{L-1} & & \ddots & \vdots \\ 0 & \ddots & \ddots & \ddots \\ \vdots & \ddots & \ddots & \ddots \\ 0 & \cdots & 0 & h_{L-1} & \cdots & h_0 \end{bmatrix}_{(N+\nu) \times (N+\nu)}, \quad (2.59)$$

$$\mathbf{H}_{\text{IBI}} = \begin{bmatrix} 0 & \cdots & 0 & h_{L-1} & \cdots & h_1 \\ \vdots & & & \ddots & \ddots & \vdots \\ \vdots & & & & \ddots & h_{L-1} \\ \vdots & \ddots & \ddots & \ddots & \ddots & 0 \\ \vdots & \ddots & \ddots & \ddots & \ddots & \vdots \\ 0 & \cdots & \cdots & & & 0 \end{bmatrix}_{(N+\nu) \times (N+\nu)}, \quad (2.60)$$

which represent the interference between the symbols within the i^{th} OFDM block and the interference between two successive OFDM blocks, respectively. Discarding CP at the receiver not only eliminates the IBI, but also converts the linear channel convolution into a circular one, which facilitates the diagonalization of the channel matrix, and enables one-tap equalization. More specifically, the CP removal operation is carried out by left multiplying matrix:

$$\mathbf{R}_{\text{cp}} = [\mathbf{0}_{N \times \nu} \mid \mathbf{I}_N], \quad (2.61)$$

which, in fact, removes the first ν row of $\mathbf{y}_{\text{cp}}^{(i)}$. After discarding CP and assuming $\nu > L$, the received signal becomes:

$$\begin{aligned} \mathbf{y}^{(i)} &= \mathbf{R}_{\text{cp}} \mathbf{y}_{\text{cp}}^{(i)} \\ &= \begin{bmatrix} & h_{L-1} & \cdots & h_0 & & \\ & & \ddots & & \ddots & \\ \mathbf{0}_{\nu-(L-1)} & & & & & \\ & & & & h_{L-1} & \cdots & h_0 \end{bmatrix}_{N \times (N+\nu)} \mathbf{x}_{\text{cp}}^{(i)} + \mathbf{w}. \end{aligned} \quad (2.62)$$

After some simple manipulations, the above equation becomes:

$$\mathbf{y}^{(i)} = \begin{bmatrix} h_0 & 0 & \cdots & h_{L-1} & \cdots & h_1 \\ \vdots & \ddots & \ddots & & \ddots & \vdots \\ h_{L-1} & & \ddots & \ddots & & h_{L-1} \\ 0 & \ddots & & \ddots & \ddots & \\ \vdots & \ddots & \ddots & & \ddots & 0 \\ 0 & \cdots & 0 & h_{L-1} & \cdots & h_0 \end{bmatrix}_{N \times N} \mathbf{x}^{(i)} + \mathbf{w}. \quad (2.63)$$

It can be found that the channel convolution matrix becomes a circulant matrix. The property of circulant matrix tells us that it is diagonalized by the DFT and IDFT operations. It yields:

$$\begin{aligned} \mathbf{Y}^{(i)} &= \mathbf{F}_N \mathbf{y}^{(i)} = \mathbf{F}_N \underbrace{\begin{bmatrix} h_0 & 0 & \cdots & h_{L-1} & \cdots & h_1 \\ \vdots & \ddots & \ddots & & \ddots & \vdots \\ h_{L-1} & & \ddots & \ddots & & h_{L-1} \\ 0 & \ddots & & \ddots & \ddots & \vdots \\ \vdots & \ddots & \ddots & & \ddots & 0 \\ 0 & \cdots & 0 & h_{L-1} & \cdots & h_0 \end{bmatrix}}_{\mathbf{H}_{\text{circ}}} \mathbf{F}_N^H \mathbf{X}^{(i)} + \mathbf{F}_N \mathbf{w} \\ &= \begin{bmatrix} H[0] & 0 & \cdots & \cdots & 0 \\ 0 & H[1] & \ddots & & \vdots \\ \vdots & \ddots & \ddots & \ddots & \vdots \\ \vdots & & \ddots & \ddots & 0 \\ 0 & \cdots & \cdots & 0 & H[N-1] \end{bmatrix} \mathbf{X}^{(i)} + \mathbf{W}, \\ &= \mathbf{H}_{\text{diag}} \mathbf{X}^{(i)} + \mathbf{W}, \end{aligned} \quad (2.64)$$

where $\mathbf{W} = \mathbf{F}_N \mathbf{w}$ is the DFT of the AWGN, and \mathbf{H}_{diag} is a diagonal matrix whose k^{th} element of the main diagonal $H[k] = \sum_{l=0}^{L-1} h_l e^{-j \frac{2\pi}{N} lk}$ is the channel frequency attenuation for the k^{th} subcarrier. It can be seen from (2.64) that the time-domain convolution of the channel and the signal (shown in (2.58)) is turned into a frequency-domain point-wise product of their Fourier transforms as depicted in Figure 2.16. In other words, the

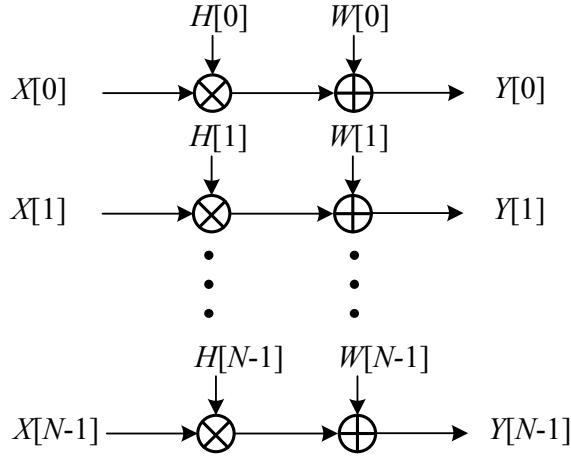


Figure 2.16: Ideal OFDM transmission model.

OFDM transmission divides the wideband frequency-selective channel into a set of parallel narrow-band flat-fading channels. The signal symbols are transmitted in parallel, and the multipath channel effect is merely a multiplicative complex-valued attenuation or amplification. Hence, it is not necessary to use a cumbersome FIR-filter-based equalizer [60]. Instead, the received signal can be equalized by a simple one-tap equalizer \mathbf{G} in frequency domain:

$$\mathbf{Z}^{(i)} = \mathbf{G}\mathbf{Y}^{(i)}. \quad (2.65)$$

The equalizer \mathbf{G} can be either *Zero Forcing* (ZF) equalizer [41, p.35]:

$$\mathbf{G}_{\text{ZF}} = \mathbf{H}_{\text{diag}}^{-1} = \begin{bmatrix} H[0]^{-1} & \dots & \dots & 0 \\ \vdots & H[1]^{-1} & & \vdots \\ \vdots & & \ddots & \vdots \\ 0 & \dots & \dots & H[N-1]^{-1} \end{bmatrix}, \quad (2.66)$$

or *Minimum Mean Square Error* (MMSE) equalizer [41, p.36]:

$$\mathbf{G}_{\text{MMSE}} = \mathbf{H}_{\text{diag}}^{\mathcal{H}} \left(\mathbf{H}_{\text{diag}} \mathbf{H}_{\text{diag}}^{\mathcal{H}} + \sigma^2 \mathbf{I}_N \right)^{-1} = \begin{bmatrix} \frac{H[0]^*}{|H[0]|^2 + \sigma^2} & \dots & \dots & 0 \\ \vdots & \frac{H[1]^*}{|H[1]|^2 + \sigma^2} & & \vdots \\ \vdots & & \ddots & \vdots \\ 0 & \dots & \dots & \frac{H[N-1]^*}{|H[N-1]|^2 + \sigma^2} \end{bmatrix}, \quad (2.67)$$

The feature of reduced-complexity equalization is the main advantage of OFDM. Note that, since the signal in the GI wastes a portion of the transmission power, only $\frac{N}{N+\nu}$ of the transmission power is used in the OFDM data symbols in the CP-OFDM. In other words, the CP-OFDM system suffers from a power efficiency loss with a factor of $\frac{N}{N+\nu}$.

2.2.2 ZP-OFDM

To avoid the power efficiency loss of CP-OFDM, it has been proposed to replace nonzero CP by zero-padding (ZP) in [10]. Specifically, ν zero-valued symbols are appended

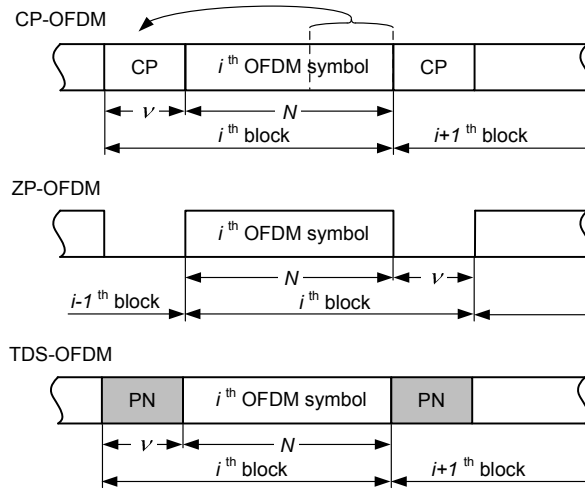


Figure 2.17: Different types of GI.

at the end of the IFFT-modulated data block. The CP insertion operation in (2.55) is thus replaced by a ZP process:

$$\mathbf{I}_{zp} = \begin{bmatrix} \mathbf{I}_N \\ \mathbf{0}_{N \times \nu} \end{bmatrix}. \quad (2.68)$$

The ZP-OFDM signal is thus:

$$\mathbf{x}_{zp}^{(i)} = \mathbf{I}_{zp} \mathbf{x}^{(i)} = \mathbf{I}_{zp} \mathbf{F}_N^H \mathbf{X}^{(i)}. \quad (2.69)$$

Similar to (2.58), the received signal can be written as:

$$\mathbf{y}_{zp}^{(i)} = \mathbf{H}_{ISI} \mathbf{I}_{zp} \mathbf{x}^{(i)} + \mathbf{H}_{IBI} \mathbf{I}_{zp} \mathbf{x}^{(i-1)} + \mathbf{w}. \quad (2.70)$$

When $\nu > L$, the second term in the above equation vanishes, i.e. ZP cancels the IBI contribution. Since the ZP-OFDM signal does not have the cyclic data structure, if we process the ZP-OFDM with a length of N samples, as we do in the CP-OFDM case, there will be intercarrier interference (ICI) between the data symbols in different subcarriers. Hence, some additional processing should be made to the ZP-OFDM signal in order to maintain orthogonality between subcarriers.

A first solution is to equalize the ZP-OFDM signal within a greater length of received symbols. More specifically, the linear convolution of the transmitted data block and the channel is turned into point-wise product of their $(N + \nu)$ -point DFTs [38, p.586]. It means that the ZP-OFDM signal can be equalized by the simple one-tap equalizers (2.66) and (2.67) with a larger DFT size, i.e. $(N + \nu)$. The $(N + \nu)$ -length equalized data can easily be converted into the N -length frequency symbol via an $(N + \nu)$ -length IFFT, truncating the last ν samples and finally a ν -length FFT. This yields the fast symbol recovery algorithms proposed in [10]. The increased DFT size also provides redundancy which guarantees the ZF recovery of the ZP-OFDM signal in the presence of channel zeros in some (at most ν) subcarriers [10]. It is recognized as a major advantage of ZP-OFDM over the classical CP-OFDM.

The second solution is the so-called overlap-and-add (OLA) method. As shown in Figure 2.18, the signal (composed of noise and the signal tail resulting from the multipath

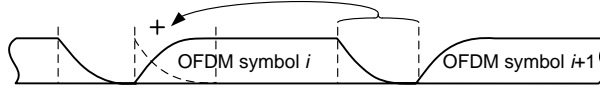


Figure 2.18: Overlap-and-add process to equalize ZP-OFDM signal.

channel) in the ZP part is added to the beginning part of the OFDM data symbols. OLA constructs the cyclic data structure in the received ZP-OFDM signal and thus enables the simple one-tap equalization within N -length as in the CP-OFDM case. The advantage of the OLA solution is that it avoids the $(N + \nu)$ -point IFFT/FFT operations while obtaining a simple one-tap equalizer for each subcarrier. However, it does not have the immunity to the channel nulls. OLA process is expressed as the $N \times (N + \nu)$ matrix:

$$\mathbf{I}_{\text{OLA}} = \left[\mathbf{I}_N \left| \begin{array}{c} \mathbf{I}_\nu \\ \mathbf{0}_{(N-\nu) \times \nu} \end{array} \right. \right]. \quad (2.71)$$

The received signal after OLA process becomes:

$$\begin{aligned} \mathbf{y}_{\text{OLA}}^{(i)} &= \mathbf{I}_{\text{OLA}} \mathbf{H}_{\text{ISI}} \mathbf{I}_{\text{zp}} \mathbf{x}^{(i)} + \mathbf{I}_{\text{OLA}} \mathbf{w} \\ &= \mathbf{H}_{\text{circ}} \mathbf{x}^{(i)} + \mathbf{w}', \end{aligned} \quad (2.72)$$

where \mathbf{H}_{circ} is the same circulant matrix as in (2.64). That is, the OLA process creates the circular convolution of channel and transmitted signal. Therefore, the simple one-tap equalization (2.66) and (2.67) can be used for ZP-OFDM. $\mathbf{w}' = \mathbf{I}_{\text{OLA}} \mathbf{w}$ is the noise component after OLA. Note that the noise in the GI is added in the OFDM data part in the OLA process, which means that the noise is slightly *colored* and its power is accordingly *boosted* with an equivalent noise power $\sigma_{w'}^2 = \frac{\nu + N}{N} \sigma_w^2$. Taking into account the noise augmentation in ZP-OFDM and the power efficiency loss in CP-OFDM, it yields that ZP-OFDM with OLA and CP-OFDM have the same performance in term of the signal to interference and noise ratio (SINR) [61].

In general, CP- and ZP-OFDM have some features in common in terms of bandwidth efficiency, equalization complexity and SINR. While, on the other hand, ZP-OFDM has its own advantages over CP-OFDM. For example, ZP-OFDM spends less power than CP-OFDM to achieve the same receiving SINR. Moreover, CP creates cyclic data structure which leads to ripples in the average power spectral density (PSD) [62]. The ripples means extra power backoff (as much as 1.5 dB) at the transmitter. Since the ZP-OFDM does not have the cyclic data structure, it has a more smooth PSD in the useful bandwidth. Therefore, ZP-OFDM is the preferred transmission scheme for the applications in which the maximum transmission power is strictly limited, such as the multiband-OFDM-based UWB system [62].

2.2.3 TDS-OFDM

As the GI occupies a portion of transmission time and thus decreases the useful bit rate of the system, some alternative approaches are proposed to improve the transmission efficiency. An OFDM system that does not use GI is proposed in [63]. The IBI due to the multipath channel is mitigated by using ISI cancellation such as the one proposed in [64]. However, the performance of the non-GI transmission method significantly degrades in

hash channel conditions. In [65, 66], instead of using one CP for each OFDM symbol, a number of OFDM symbols are grouped together as a frame and protected by one single CP for the frame so that the global overhead is reduced. Presented in [67] for CP-OFDM and in [68] for ZP-OFDM, it is proposed to adaptively adjust the length of the GI according to the length of channel. All these propositions are committed to optimizing the system throughput by carefully selecting the length of the GI.

Recently, it is proposed to replace the CP or ZP by a known sequence which is reused for channel estimation and synchronization (including timing recovery, carrier recovery and frame synchronization) so that the overall transmission overhead is reduced. This idea was first reported in [69, 70] then discussed in [71, 72, 73, 74, 75] in the context of single carrier communications. This method uses a known, constant sequence as GI for all data blocks. As training sequences before and after a specific data block are identical, the first sequence can be viewed as a ‘‘CP’’ of the following transmission block which consists of the data block and the second training sequence. Therefore, the low-complex frequency-domain equalization can be carried out in the transmission block.

The same idea was also applied in the OFDM context. The new OFDM signal waveform is referred to as Time Domain Synchronous-OFDM (TDS-OFDM) [11, 5] or Pseudo Random Postfix-OFDM (PRP-OFDM) [12] or Known Symbol Padding-OFDM (KSP-OFDM) [13] depending on different designs of the known sequence in the GI. As this thesis is dedicated to propose improved algorithm for the DTMB system, we will call this OFDM signal waveform as TDS-OFDM in our discussion.

The TDS-OFDM signal can be viewed as filling the null gap between time-domain ZP-OFDM symbols with ν -length known sequence $\mathbf{c}^{(i)} = [c_0^{(i)}, c_1^{(i)}, \dots, c_{\nu-1}^{(i)}]^T$. Denoting $\bar{\mathbf{c}}^{(i)} = [\mathbf{0}_N^T, \mathbf{c}^{(i)T}]^T$, it writes:

$$\mathbf{x}_{\text{TDS}}^{(i)} = \mathbf{x}_{\text{zp}}^{(i)} + \bar{\mathbf{c}}^{(i)} = \begin{bmatrix} \mathbf{x}^{(i)} \\ \mathbf{c}^{(i)} \end{bmatrix}. \quad (2.73)$$

The received TDS-OFDM signal is:

$$\mathbf{y}_{\text{TDS}}^{(i)} = \mathbf{H}_{\text{ISI}}\mathbf{x}_{\text{zp}}^{(i)} + \mathbf{H}_{\text{ISI}}\bar{\mathbf{c}}^{(i)} + \mathbf{H}_{\text{IBI}}\mathbf{x}_{\text{zp}}^{(i-1)} + \mathbf{H}_{\text{IBI}}\bar{\mathbf{c}}^{(i-1)} + \mathbf{w}. \quad (2.74)$$

The first and second terms in above equation are the channel-distorted TDS-OFDM signal, while the third and fourth terms are the IBI contribution from the previous OFDM block. Obviously, there is mutual interference between data and known sequence: the first term contains the interference from the data to the known sequence, while the fourth term represents the interference on the data from the known sequence of the previous OFDM block. As the known sequence is used as training sequence to make synchronization and channel estimation, this mutual interference makes difficulties in synchronization/channel estimation as well as data recovery. When GI is longer than channel, the third term vanishes. With perfect knowledge of the channel, the contribution of the known sequence, including the second and fourth term in (2.74), can be totally subtracted from the received signal. The TDS-OFDM is then converted into a ZP-OFDM signal after the removal of known sequence. Therefore, the following equalization and data recovery processings are the same as those used for ZP-OFDM signal.

An other interesting observation is that if the known sequence is constant for all OFDM symbols, i.e. $\mathbf{c}^{(i-1)} = \mathbf{c}^{(i)}$, the channel convolution is again turned into a circular

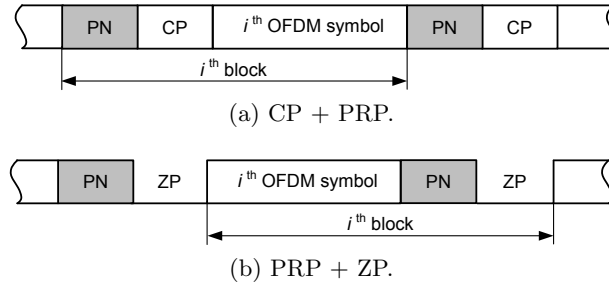


Figure 2.19: Some variants of the GI formation.

one within the data of $N + \nu$ -length [41, 70, 71, 13, 76]:

$$\mathbf{y}_{\text{TDS}}^{(i)} = \mathbf{H}_{\text{circ}} \mathbf{x}_{\text{TDS}}^{(i)} + \mathbf{w}. \quad (2.75)$$

Equalization can thus be carried out over the whole OFDM symbol (including data and known sequence) [76].

If the known sequence is transmitted in the same power level as the data, the TDS-OFDM also has a power efficient loss factor $\frac{N}{N+\nu}$ similar to CP-OFDM due to the power spent in the GI. In addition, if the OLA process is used to equalize the TDS-OFDM, the resulting noise is augmented by $\frac{N+\nu}{N}$ times. At a first glance, the TDS-OFDM suffers from both power efficiency loss and noise augmentation and will probably have worse performance than the other two systems. However, since TDS-OFDM reuses the known sequence as training sequence for channel estimation and synchronization, it economizes the cost of the pilot subcarriers which are commonly reserved for channel estimation and synchronization in CP- and ZP-OFDM. Hence, TDS-OFDM may offer an improved spectrum efficiency and consequently better transmission efficiency. Besides, as each TDS-OFDM block has its own training sequence, the TDS-OFDM can achieve faster channel tracking than CP- and ZP-OFDM, in which the channel estimation is usually carried out over several OFDM symbols. The TDS-OFDM based modulation has been officially adopted by the Chinese DTTB standard – DTMB.

2.2.4 Hybrid GI Structures

Besides the above three major types, there are also some other variants of the GI formation to meet specific needs. They can be recognized as the combinations of the three major GI types.

The first type is the combination of CP and known sequence. It is proposed to insert a PN sequence before each OFDM symbol, i.e. before CP, to achieve a faster and better channel estimation [77, 78]. The data structure is illustrated in Figure 2.19a. At the receiver side, the channel estimation can be made using either time domain correlation [77, 78] or frequency domain division of the transmitted and received known sequences [77]. The channel estimation using time domain training sequence outperforms the frequency domain pilot-based method in low SNR cases. Moreover, it is convenient to use the time domain training sequence for synchronization. However, the limitation of this scheme is also obvious: as the training sequence is not protected by any GI, the channel estimation is vulnerable to ISI. The performance degrades as the channel length increases.

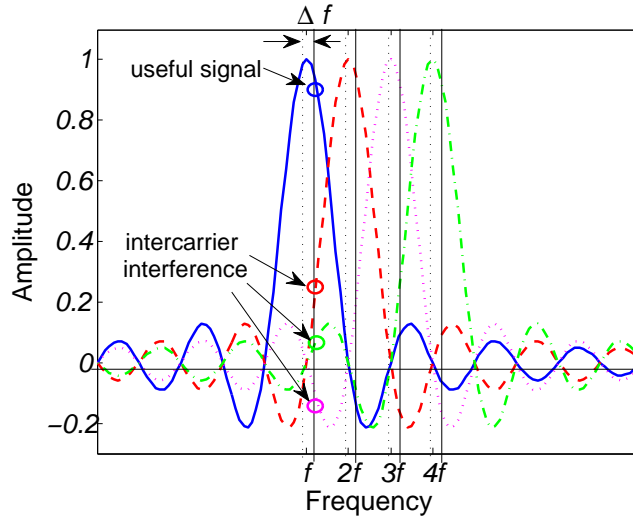


Figure 2.20: Intercarrier interference when there is a frequency shift.

A second alternative is to combine known sequence and ZP [79, 80]. As depicted in Figure 2.19b, some null samples are appended after the postfix to prevent the ISI to the following OFDM symbol. The whole postfix including the known sequence and null samples is used to make channel estimation. This hybrid GI scheme takes the advantage of channel estimation accuracy of PRP-OFDM and the advantage of ISI prevention of ZP-OFDM. It should be noticed that as there is no GI to protect the known sequence, the channel estimation is affected by the ISI coming from OFDM data symbol. Hence, estimation technique with better interference cancellation capability should be used to achieve satisfactory estimation results, for example, the time domain correlator-bank based approach or the decision-directed least square approach [80].

2.2.5 Intercarrier Interference due to CFO

The orthogonality between subcarriers guarantees the parallel transmission of data. However, CFO will destroy the orthogonality and introduce ICI to the OFDM symbols. CFO mainly comes from two sources: residual frequency difference between transmitter and receiver oscillators and Doppler frequency shift due to the motion of the transmitter and/or receiver. As shown in Figure 2.20, when there exists a frequency shift Δf , the useful data in a specific subcarrier is affected by the interference from other subcarriers. We analyze the impact of ICI due to CFO in this section.

The transmitted OFDM data symbol is:

$$x[n] = \frac{1}{\sqrt{N}} \sum_{k=0}^{N-1} X[k] e^{j \frac{2\pi}{N} kn}, \quad 0 \leq n \leq N-1, \quad (2.76)$$

After channel, it becomes:

$$y[n] = \sum_{l=0}^{L-1} h_l[n] x[n-l]_N + w[n], \quad 0 \leq n \leq N-1, \quad (2.77)$$

where $[\cdot]_N$ is the modular N operation. After FFT, the frequency domain received signal is:

$$\begin{aligned}
Y[m] &= \frac{1}{\sqrt{N}} \sum_{n=0}^{N-1} y[n] e^{-j\frac{2\pi}{N}mn} \\
&= \frac{1}{N} \sum_{n=0}^{N-1} \sum_{l=0}^{L-1} h_l[n] \sum_{k=0}^{N-1} X[k] e^{j\frac{2\pi}{N}k(n-l)} e^{-j\frac{2\pi}{N}mn} + \frac{1}{\sqrt{N}} \sum_{n=0}^{N-1} w[n] e^{-j\frac{2\pi}{N}mn} \\
&= \frac{1}{N} \sum_{n=0}^{N-1} \sum_{l=0}^{L-1} h_l[n] \sum_{k=0}^{N-1} X[k] e^{-j\frac{2\pi}{N}n(m-k)} e^{-j\frac{2\pi}{N}kl} + \frac{1}{\sqrt{N}} \sum_{n=0}^{N-1} w[n] e^{-j\frac{2\pi}{N}mn} \\
&= X[m] \frac{1}{N} \sum_{n=0}^{N-1} \sum_{l=0}^{L-1} h_l[n] e^{-j\frac{2\pi}{N}ml} + \frac{1}{N} \sum_{n=0}^{N-1} \sum_{l=0}^{L-1} h_l[n] \sum_{\substack{k=0 \\ k \neq m}}^{N-1} X[k] e^{-j\frac{2\pi}{N}n(m-k)} e^{-j\frac{2\pi}{N}kl} \\
&+ \frac{1}{\sqrt{N}} \sum_{n=0}^{N-1} w[n] e^{-j\frac{2\pi}{N}mn} \\
&= \alpha[m]X[m] + \xi[m] + W[m].
\end{aligned} \tag{2.78}$$

The first term is the desired signal $X[m]$ affected by a multiplicative distortion $\alpha[m]$. More precisely, recall that

$$H[k, n] = \sum_{l=0}^{L-1} h_l[n] e^{-j\frac{2\pi}{N}kl}, \tag{2.79}$$

we get:

$$\begin{aligned}
\alpha[m] &= \frac{1}{N} \sum_{n=0}^{N-1} \sum_{l=0}^{L-1} h_l[n] e^{-j\frac{2\pi}{N}ml} \\
&= \frac{1}{N} \sum_{n=0}^{N-1} H[m, n] \\
&= \bar{H}[m],
\end{aligned} \tag{2.80}$$

where $\bar{H}[m] = \frac{1}{N} \sum_{n=0}^{N-1} H[m, n]$ is the average CFR within the duration of N data samples for the m^{th} subcarrier. The second term in (2.78) is the ICI term which is composed of the contribution from all subcarriers except the m^{th} one:

$$\begin{aligned}
\xi[m] &= \frac{1}{N} \sum_{n=0}^{N-1} \sum_{l=0}^{L-1} h_l[n] \sum_{\substack{k=0 \\ k \neq m}}^{N-1} X[k] e^{-j\frac{2\pi}{N}n(m-k)} e^{-j\frac{2\pi}{N}kl} \\
&= \sum_{\substack{k=0 \\ k \neq m}}^{N-1} X[k] \frac{1}{N} \sum_{n=0}^{N-1} \sum_{l=0}^{L-1} h_l[n] e^{-j\frac{2\pi}{N}kl} e^{-j\frac{2\pi}{N}n(m-k)} \\
&= \sum_{\substack{k=0 \\ k \neq m}}^{N-1} X[k] \frac{1}{N} \sum_{n=0}^{N-1} H[k, n] e^{-j\frac{2\pi}{N}n(m-k)} \\
&= \sum_{\substack{k=0 \\ k \neq m}}^{N-1} X[k] H_{m,k},
\end{aligned} \tag{2.81}$$

where $H_{m,k} = \frac{1}{N} \sum_{n=0}^{N-1} H[k, n] e^{-j \frac{2\pi}{N} n(m-k)}$ is the off-diagonal component in the channel matrix. Note that, $m - k$ is the frequency difference of the transmit and receive signals. It means that $H_{m,k}$ is the frequency response arisen from a frequency shift of $m - k$ for the m^{th} subcarrier. Since ICI is an aggregate of a large number of independent signal, i.e. $X[k]$'s, the distribution of $\xi[m]$ converges to a Gaussian law as the number of subcarriers increases according to the central limit theorem [81]. Hence, $\xi[m]$ is modeled as a Gaussian random variable with zero mean.

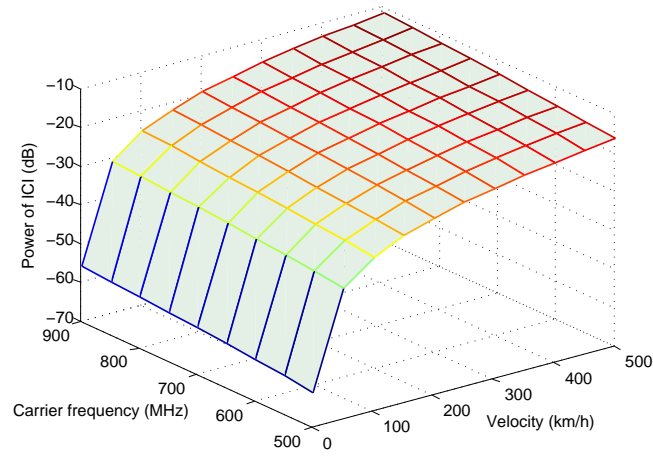
To evaluate the impact of the motion of the receiver on the receiving signal, we analyze the ICI resulting from the Doppler frequency shift. Given that the signal is random sequence and independent of channel, and also the signal power is normalized to unite, i.e. $\mathbb{E}[|X[k]|^2] = 1$, the power of ICI for the m^{th} subcarrier is computed as:

$$\begin{aligned} P_{\text{ICI}}(m) &= \mathbb{E}[|\xi[m]|^2] = \sum_{\substack{k=0 \\ k \neq m}}^{N-1} \mathbb{E}[|X[k]H_{m,k}|^2] = \sum_{\substack{k=0 \\ k \neq m}}^{N-1} \mathbb{E}[|H_{m,k}|^2] \\ &= \frac{N-1}{N} + \frac{2}{N^2} \sum_{\substack{k=0 \\ k \neq m}}^{N-1} \sum_{d=1}^{N-1} \left[(N-d) J_0(2\pi f_m d T_s) \cos\left(\frac{2\pi}{N} d(m-k)\right) \right] \end{aligned} \quad (2.82)$$

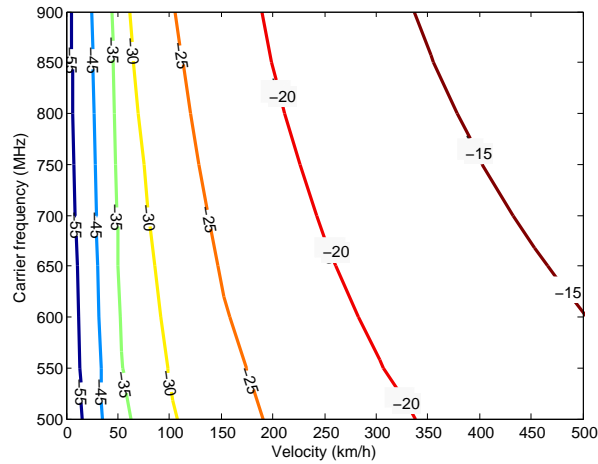
where $J_0(\cdot)$ is the zeroth-order *Bessel* function of the first kind, f_m is the maximum Doppler frequency shift and T_s is the baseband symbol duration. Detailed derivation of the last step is shown in Appendix A. Therefore, the overall ICI power can be computed by averaging over all subcarriers:

$$\begin{aligned} \sigma_{\text{ICI}}^2 &= \frac{1}{N} \sum_{m=0}^{N-1} P_{\text{ICI}}(m) \\ &= \frac{N-1}{N} + \frac{2}{N^3} \sum_{d=1}^{N-1} \left[(N-d) J_0(2\pi f_m d T_s) \sum_{m=0}^{N-1} \sum_{\substack{k=0 \\ k \neq m}}^{N-1} \cos\left(\frac{2\pi}{N} d(m-k)\right) \right] \\ &= \frac{N-1}{N} + \frac{4}{N^3} \sum_{d=1}^{N-1} \left[(N-d) J_0(2\pi f_m d T_s) \sum_{q=1}^{N-1} \cos\left(\frac{2\pi}{N} dq\right) \right]. \end{aligned} \quad (2.83)$$

Using the above expression, we can estimate the influence of ICI. For example, Figure 2.21 presents the ICI power with typical velocity and carrier frequency ranges of the DTMB system. We can have an important observation from these results. The ICI power of the DTMB system due to the Doppler frequency is less than -25 dB with a velocity as high as 100 to 200 km/h. This indicates that ICI is a less significant factor compared to noise at a SNR level of 25 dB which covers the SNR requirements of most application scenarios. It means that the impact of the channel variations within one OFDM symbol is not significant for the DTMB system in common velocity and carrier frequency ranges. This enables us to assume that the channel is *quasi-static*, i.e. constant within one OFDM symbol but changing from one to another, in our following studies.



(a)



(b)

Figure 2.21: ICI resulting from the Doppler frequency in DTMB with $T_s = 1/7.56\mu s$, $N = 3780$.

2.3 Conclusion

This chapter mainly concerns some background knowledge that is used in the research of this thesis. The wireless communication channel has been first described from different perspective. Specifically, we have briefly introduced the multipath channel models as well as some important statistical characteristics which will be extensively used in our further studies on the channel estimation techniques. After that, the basic concept of the OFDM transmission scheme has been introduced and formulated. Several different OFDM waveforms have been presented. Among them, we will carry out detailed study on TDS-OFDM, especially channel estimation techniques associated to it.

Analysis and Comparison of DVB-T and DTMB Systems

AMONG all the existing DTTB standards, DVB-T is the most popular one. It was one of the DTTB pioneers that started business operation in the late 1990's and has been adopted by more than 35 countries and territories around the world. More than 90 million DVB-T receivers have been sold. Meanwhile, DTMB draws great interests from both industries and researchers because of the enormous TV market in China and the novel required signal processing techniques to decode the received signal. Therefore, it is interesting for us to carry out investigations to see the advantages and the limitations of each standard, which is the aim of this chapter.

3.1 System Specifications

The block diagrams of the DVB-T and DTMB systems are presented in Figure 3.1 and Figure 3.2. The general structures of the two systems are similar to each other. The main difference between them is the traditional CP insertion and removal in the DVB-T system, which are replaced by the PN sequence insertion and removal in the DTMB system. The use of the PN sequence as GI is the key feature of DTMB. Besides, there are many differences in the technical details which will be revealed in the following sections.

Some important system parameters are listed in Table 3.1. Note that the parameters of the DVB-T system are for the 8 MHz TV channels. Concerning the DTMB standard, it consists of single carrier and multicarrier transmissions which are originated from two former technical proposals to the Chinese DTTB standard: the single-carrier ADBT-T and the multi-carrier DMB-T, respectively. The standard does not require any specifications to be dedicated to single or multicarrier mode, and the modulation and GI configuration are suppose to be independent of the transmission mode. Nonetheless, there are still some preferred combinations for each mode due to the history of the development. For instance, the 595-length GI is commonly adopted by the single carrier transmission mode [82], and the 64QAM modulation is generally used by the multicarrier mode [83]. Therefore, we list the parameters separately for each mode. Here, we would like to highlight some remarks on different parameter selections of the two systems.

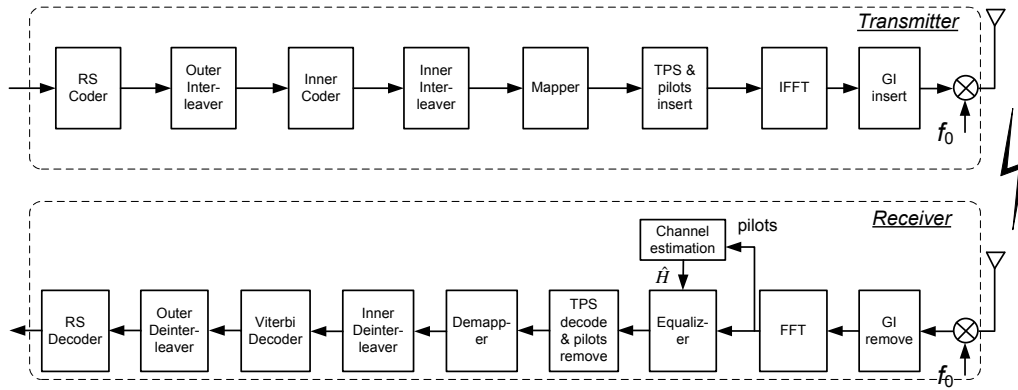


Figure 3.1: Block diagram of the DVB-T system.

3.1.1 Bandwidth

The baseband signal bandwidths of the two systems are close to each other. They are originally designed slightly less than 8 MHz in order to fully exploit the spectrum of the European and Chinese analogue TV channels while reducing the possible cross-talk to the adjacent channels. As OFDM has very good out-of-band attenuation property, the DVB-T system does not adopt any baseband pulse shaping filter. Instead, it “shuts down” about 16.7% subcarriers located in the edges of the spectrum to limit the signal bandwidth and protect adjacent channels. On the other hand, the DTMB system inserts the time domain PN sequence which has a wider signal bandwidth than the OFDM data symbol. Thus, the DTMB system adopts the squared root raised cosine (SRRC) filter with a roll-off factor of $\alpha = 0.05$ to shape the baseband signal. Note that the $\alpha = 0.05$ roll-off factor is very rigorous for the engineering implementation. It determines the maximum signal bandwidth should be less than $8/(1 + 0.05) = 7.62$ MHz which is close to DVB-T.

In order to adapt to the TV channel bandwidths in some other countries such as U.S., Australia and Japan, DVB-T also provides some other bandwidth options with reduced net bit rates in the standard [1, Annex E]. This makes DVB-T having a high flexibility to the implementation in different countries. It can be an important reason that makes DVB-T the most popular DTTB standard in the world. Concerning DTMB, 8 MHz is the only bandwidth that has been specified in the standard. However, we noticed that 6 MHz bandwidth has also been proposed recently for the comparing test campaigns carried out in Cuba and South America [24, 84]. The OFDM symbol duration is changed from $500 \mu\text{s}$ to $666.67 \mu\text{s}$, resulting in a subcarrier spacing changing from 2 kHz to 1.5 kHz. Given the subcarrier number of 3780, the baseband signal bandwidth is $3780 \times 1.5 \text{ kHz} = 5.67$ MHz. It also needs a SRRC filter with a roll-off factor of $\alpha = 0.05$ to fit the 6 MHz analogue TV channel. The comparison of the useful bit rates in 6 MHz and 8 MHz channels is given in [84] and reprinted in Table 3.2. Besides, as indicated in the presentation of Yang Z.X. [24], more options of signal bandwidth including 1.7, 6, 7, 8 and 10 MHz will be integrated in an enhanced version of the DTMB standard in order to adapt to different services in different countries.

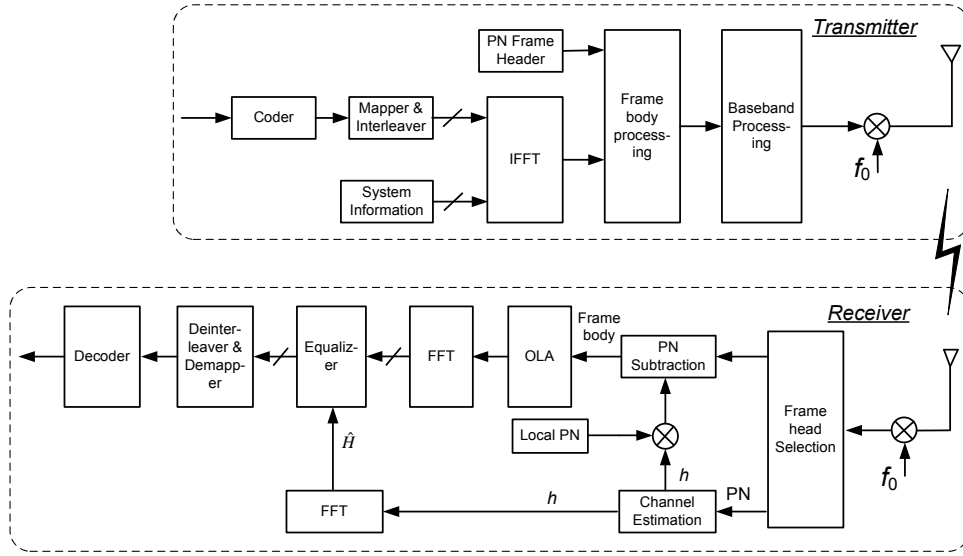


Figure 3.2: Block diagram of the DTMB system.

3.1.2 OFDM Parameters

There are two options, i.e. 2K ($2 \times 2^{10} = 2048$) and 8K ($8 \times 2^{10} = 8192$), for the size of the FFT for the OFDM modulation in DVB-T. The FFT size is intentionally selected as a power of two so that efficient FFT operations such as the Cooley-Tukey algorithm and some other improved methods [85] can be used. It can be seen from Table 3.1 that the 2K mode DVB-T system has a shorter OFDM symbol duration ($224 \mu\text{s}$) and a wider subcarrier spacing (4464 Hz). Shorter symbol duration means a shorter GI that is used to fight against ISI given the same efficiency loss (i.e. the same ratio of GI over data symbol), while the wider subcarrier spacing suggests that the OFDM modulation is more robust to the Doppler frequency shift due to the mobile reception. So the 2K mode is suitable only for small-coverage SFNs but can provide better mobile reception performance. On the contrary, the 8K mode has a longer GI duration but a narrower subcarrier spacing, which indicates a capability of supporting large-area SFNs with fixed reception. The 2K and 8K modes have complementary characteristics and can be used in different scenarios.

In DTMB, however, a 3780-point FFT is adopted for the OFDM modulation. The real reason of the selection of this FFT size is hard to guess. However, based on our studies and analyses, we find some plausible explanations.

First of all, the FFT size should be different than the conventional choices (power of two) to avoid the well-established patents. The FFT block is the central element of any OFDM based system. Conventionally, the FFT algorithms with a size of power of two have been well studied in the literatures [85], and more importantly, have been issued as patents [86]. Considering the potential hundreds of millions of sales, patent royalties would be a sky-high number if the inventor does not hold the intellectual property. The huge expense on patent will prevent the industrialization and popularization of the standard. Therefore, the intellectual property was seen as a key requirement for the proposals at the first beginning of the standardization. This may be an important motivation of using the 3780-point FFT in DTMB.

Table 3.1: Main Parameters of the DVB-T and DTMB Systems.

		DVB-T		DTMB	
		2K mode	8K mode	single carrier mode	multicarrier mode
Sample period		7/64 μ s		1/7.56 μ s	
Useful part of OFDM symbol duration (T)		224 μ s	896 μ s	500 μ s	
Number of subcarriers		2 048	8 192	1	3 780
Number of active subcarriers		1 705	6 817	1	3 780
Subcarrier spacing (1/T)		4 464 Hz	1 116 Hz	–	2 kHz
Baseband bandwidth		7.61 MHz		7.56 MHz	
Guard Interval	Length	T/4, T/8, T/16, T/32		\approx T/6 (595 samples)	T/4 (420 samples), T/9 (945 samples)
	Duration	56 μ s, 28 μ s, 14 μ s, 7 μ s	224 μ s, 112 μ s, 56 μ s, 28 μ s	78.7 μ s	55.6 μ s, 125 μ s
	Power	non-boost		non-boost	boosted by 2
	Phase	–		constant in a superframe	changing or constant
Mapping		QPSK, 16QAM, 64QAM (optionally hierarchical)		4QAM-NR, QPSK, 16QAM, 32QAM	QPSK, 16QAM, 64QAM
Interleaver	outer	convolutional interleaver		–	
	inner	bitwise + symbol interleaver		time domain	time & frequency domain
Channel coding	outer	Reed-Solomon (204, 188, t=8)		BCH (762, 752)	
	inner	convolutional code		LDPC (7493, 3048), (7493, 4572), (7493, 6096)	
	code rate	1/2, 2/3, 3/4, 5/6, 7/8		0.4 (7488, 3008), 0.6 (7488, 4512), 0.8 (7488, 6016)	

Secondly, an FFT size around 4K (4×2^{10}) is a good trade-off between the resistance to the long channel delay spread and the adaptability to high speed reception. It allows for a doubling of the transmitter distance in SFNs compared to the 2K mode and, is less susceptible to the Doppler shifts compared to the 8K mode in the case of mobile reception. It provides a compromise between the 2K and 8K modes and offers more flexibility for the network planning. Since the very beginning of the standardization, DTMB has been considered as a standard not only for the terrestrial DTV broadcast, but also for the emerging handheld DTV transmission. The support to the mobile reception was naturally taken into account in the system design. This could be another important reason that the FFT size of the DTMB system is selected around 4K.

Table 3.2: Comparison of the Net Bit Rates in 6 MHz and 8 MHz Channels [84].

Modulation	Code Rate	Guard Interval			
		GI = 1/9		GI = 1/4	
		8 MHz	6 MHz	8 MHz	6 MHz
QPSK	0.4	5.414	4.061	4.813	3.610
	0.6	8.122	6.092	7.219	5.414
	0.8	10.829	8.122	9.626	7.219
16QAM	0.4	10.829	8.122	9.626	7.220
	0.6	16.243	12.281	14.438	10.829
	0.8	21.658	16.244	19.251	14.438
64QAM	0.4	16.243	12.281	14.438	10.829
	0.6	24.365	18.274	21.658	16.244
	0.8	32.486	24.365	28.877	21.658

Thirdly, it may be due to the restriction of the signal bandwidth. The duration of OFDM data symbol is set to $500 \mu s$ which helps to generate a Super Frame with fixed duration of 125 ms.⁽¹⁾ Every eight Super Frames form a Minute Frame which has a duration exactly equal to one minute. This facilitates the time checking with a timing system such as the Global Positioning System (GPS). The $500 \mu s$ OFDM data symbol produces a subcarrier spacing of $1/(500 \mu s) = 2$ kHz. Recall that the maximum signal bandwidth under the constraint of the SRRC filter should be less than 7.62 MHz. The maximum FFT size is accordingly less than $7.62 \text{ MHz}/2 \text{ kHz} = 3810$. Thus, the FFT size of 3780 may be a good option that fits the bandwidth constraint and can be easily factorized.

If the 3780-point FFT is implemented using a 4096-point FFT and interpolation algorithm, the hardware cost increases according to the required precision of the interpolation. Moreover, if the 4096-point FFT is used, it would work at a symbol rate different from the system symbol rate. This will increase the complexity of the hardware implementation. Therefore, it is better to use a dedicated 3780-point FFT processor for the OFDM modulation in the DTMB system. In [87], the 3780-point FFT is realized by decomposing 3780 into $9 \times 7 \times 3 \times 5 \times 4$, and using Winograd Fourier transform algorithm (WFTA) for computing the 7, 9, 3, 5, 4-point DFTs. The processing latency of the 3780-point FFT is approximately 1.97 times greater than that of a radix-4 4096-point FFT, while the required buffer is about 1.33 times greater than that needed by the 4096-point FFT. In general, the hardware cost of a 3780-point FFT is close to the traditional 4096-point FFT. There are also some other methods which can process non-power-of-two FFT operation such as the one given in [88], which provides more flexibilities to the OFDM implementation.

(1). One Super Frame contains different numbers of OFDM symbols (including data and GI) according to different GI lengths. When the GI length is 420, every 225 OFDM symbols form a Super Frame ($225 \times (420 + 3780) \times 1/(7.56 \mu s) = 125 \text{ ms}$). When the GI length is 595, every 216 OFDM symbols form a Super Frame ($216 \times (595 + 3780) \times 1/(7.56 \mu s) = 125 \text{ ms}$). When the GI length is 945, every 200 OFDM symbols form a Super Frame ($200 \times (945 + 3780) \times 1/(7.56 \mu s) = 125 \text{ ms}$).

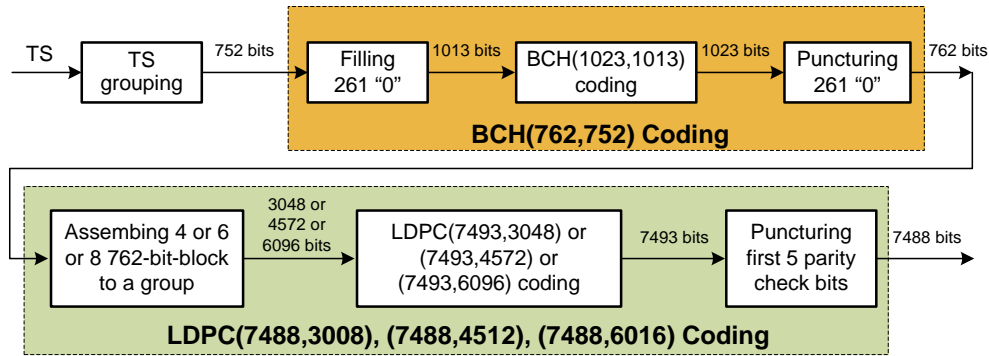


Figure 3.3: Block diagram of the encoder of channel coding in DTMB.

3.1.3 Error Correction Scheme

In DVB-T, the channel coding scheme consists of Reed-Solomon RS (204, 118, $t=8$) code (outer code) and punctured convolutional code with code rate $1/2$, $2/3$, $3/4$, $5/6$ and $7/8$ (inner code). Both bitwise and symbol interleavings are performed to avoid long sequences of severely corrupted bits feeding to the inner decoder of receiver. The bitwise and symbol interleavings are performed within one OFDM block. Between outer and inner coding, a convolutional interleaver with a maximum delay of 2244 bytes is adopted. It indicates that the errors at the output of inner decoder is spread over several OFDM blocks, which can effectively improve the error correction ability in presence burst errors.

In DTMB, concatenated Bose, Ray-Chaudhuri and Hocquenghem (BCH) code and LDPC code is adopted as channel coding scheme providing three options of code rates, i.e. $R=0.4$, $R=0.6$ and $R=0.8$. The detailed structure of the forward error correction (FEC) block in DTMB is given in Figure 3.3. The randomized transport stream (TS) of the video is first segmented into groups. Each group contains 752 bits of information. Then, 261 zeros are padded before each 752-bit group to form a 1013-bit data block. The data block is coded by BCH(1023, 1013) code. The first 261 bits of the 1023-length codewords are removed to form the 762-bit codewords. The padding and removing 261 bits as well as the BCH(1023, 1013) form the BCH(762, 752) code which serves as the outer code of the FEC block. Consequently, four or six or eight 762-bit codewords are concatenated together to form the 3048 or 4572 or 6096-bit data block according to different code rates. The data block is then fed into the LDPC encoder to generate a 7493-bit codeword. Finally, the first five parity check bits are punctured to reduce the codeword length to 7488 which is twice as much as the data subcarriers specified in DTMB.

Table 3.3: LDPC Codes Performance [89].

Code Rate	Block Length (bits)	Information Bits	Bit Energy to Noise Density Ratio (E_b/N_0)	Performance away from the Shannon Limit
≈ 0.4	7488	3008	2.1 dB	2.3 dB
≈ 0.6	7488	4512	2.3 dB	1.6 dB
≈ 0.8	7488	6016	3.3 dB	1.2 dB

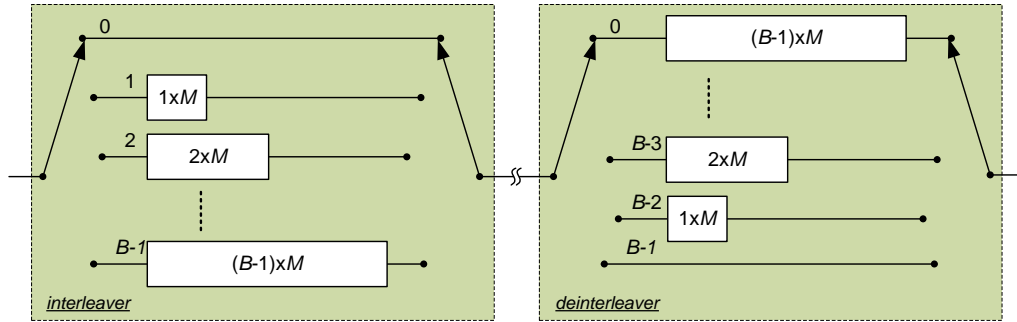


Figure 3.4: Structure of the convolutional interleaver.

The use of the state-of-the-art LDPC codes is the most significant characteristic of the DTMB system. LDPC codes have excellent error correction capability. The performance of some LDPC codes approaches the Shannon limit [90]. We know that the decoding of LDPC codes suffers from the cycles in Tanner Graph of the code [91]. Cycles are more likely to appear when the code has a short block length. Thus, the LDPC codes with longer codewords will achieve better performance. For example, the LDPC codes in DVB-S2 may have either 64800 bits (normal) or 16200 bits (short) in an error correction block, and provide performance only 0.7 dB to 1.2 dB away from the Shannon limit [92]. However, we note that the block length of the LDPC codes used in DTMB is short compared to those in DVB-S2. The performance of the LDPC codes in DTMB is given in [89] and is reprinted in Table 3.3. It can be found that, due to the limitation of the relatively short codeword length, the performance of the LDPC codes in DTMB is slightly worse than those in DVB-S2, especially in the low code rate case. In contrast, the BCH(762, 752) code can only correct one-bit errors which is much weaker than the RS code used in DVB-T. Its effect can only be seen in a very low BER level. Yet, there is no interleaver between the BCH and LDPC codes. Therefore, the error correction in DTMB mainly relies on the LDPC codes.

A convolutional interleaver is adopted in DTMB to assist the LDPC codes. Its structure, as shown in Figure 3.4, is the similar to the outer interleaver in DVB-T. There are two options of the interleaving depths, i.e. $M = 240$ and $M = 720$, which is much greater than in DVB-T. Both modes have the same interleaving branches $B = 54$. This interleaver scrambles *modulated data symbols* over a large number of OFDM blocks to obtain a high diversity gain. For instance, the overall delay of this time interleaving and deinterleaving is $B \times (B - 1) \times M$ samples which corresponds to 170 and 510 OFDM symbols for the two modes, respectively. The frequency domain interleaving only exists in the multicarrier mode. It maps time domain interleaved symbols to 3780 subcarriers in a scrambling order.

The extremely long interleaver and the powerful LDPC codes will offer major efforts of error correction in DTMB. The overall performance of the FEC block of the DTMB system will be evaluated in detail through simulations in the following sections.

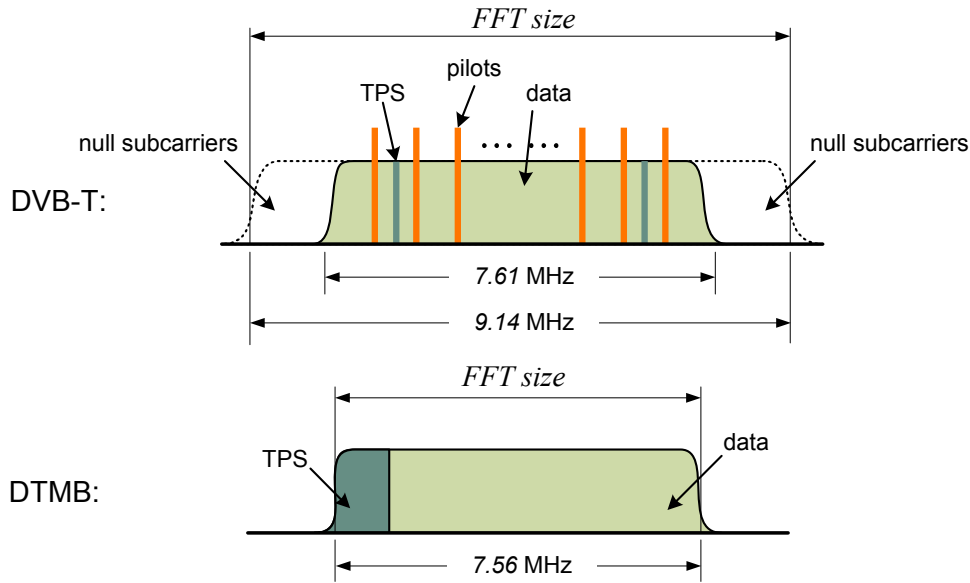


Figure 3.5: Frequency signal structures of DVB-T and DTMB in a 8 MHz channel.

3.2 System Performance Evaluation

3.2.1 Power Efficiency

An important way to compare the efficiency of different systems is to see the overhead spent for assisting transmission. As shown in Figure 3.5, in DVB-T, some subcarriers at side parts, referred to as null subcarriers, are not used for data transmission in order to limit the signal spectrum within a 8 MHz analogue TV channel. Only the central 83.3% subcarriers, namely 1705 for 2K mode and 6817 for 8K mode, are actually “active” for data transmission. Specifically, about 88.7% active subcarriers, i.e. 1512 for 2K mode and 6048 for 8K mode, are used to transmit useful data information. They are usually called as data subcarriers. The rest active subcarriers are allocated to the necessary information to assist the transmission including pilots and Transmission Parameter Signalling (TPS). In order to aid channel estimation and synchronization, continual and scattered pilots are inserted in frequency domain OFDM symbols, occupying more than 10% active subcarriers, that is, 176 for 2K mode and 701 for 8K mode. There are about 1% active subcarriers, i.e. 17 for 2K mode and 68 for 8K mode, allocated to TPS which relates to the transmission parameters, e.g. channel coding and modulation. The transmission of pilots and TPS however degrades the efficiency of spectrum utilization and results in a useful data rate loss.

In DTMB, as there is a SRRC filter to shape the baseband signal, all the 3780 subcarriers are active for information transmission. In addition, the synchronization and channel estimation are carried out by using PN sequences. Hence, there is less spectrum efficiency loss due to pilots. The only spectrum efficiency degradation comes from the 36 symbols of system information in each OFDM block. These symbols take about 1% subcarriers, which is equivalent to the cost of TPS in DVB-T. Eventually, the spectrum utilization of DTMB is about 10% higher than that of DVB-T.

Table 3.4: Power Efficiency Comparison.

		DVB-T		DTMB
		2K mode	8K mode	multicarrier mode
FFT size		2 048	8 192	3 780
Number of active subcarriers		1 705	6 817	3 780
Number of data subcarrier		1 512	6 048	3 744
Guard Interval	Length	1/4, 1/8, 1/16, 1/32		1/4 (420 samples), 1/9 (945 samples)
	Power	non-boost		boosted by 2
Number of TPS		17	68	36
Number of pilots		176	701	–
Power efficiency factor		0.66 (GI=1/4), 0.73 (GI=1/8), 0.77 (GI=1/16), 0.79 (GI=1/32)		0.66 (GI=1/4), 0.81 (GI=1/9)

GI is also an expense of transmission power and useful data rate. In DVB-T, CP is a duplicate of data part with the same power. However, in DTMB, GI is boosted⁽²⁾ to obtain better channel estimation and synchronization performance. The boosted PN sequence spends more power than the non-boosted CP given the same GI length.

In order to evaluate the transmission costs in the two systems, all factors mentioned above should be taken into account. An evaluation of power efficiency can be obtained by calculating the ratio of the power allocated to the data subcarriers over all power spent in the transmission:

$$\gamma = \frac{P_{data}}{P_{all}}. \quad (3.1)$$

Specifically, in DVB-T, this power efficiency factor can be computed by

$$\gamma_{DVB-T} = \frac{N_{data}}{N_{data} + N_{TPS} + N_{pilot} \times \eta_{pilot}} \times \frac{1}{1 + \nu}, \quad (3.2)$$

where N_{data} , N_{TPS} , N_{pilot} represent the number of data, TPS and pilot subcarriers, respectively. $\eta_{pilot} = 16/9$ is the power boost factor for pilot subcarriers. ν stands for the fraction of GI over OFDM data part. In DTMB, a similar expression can be written as:

$$\gamma_{DTMB} = \frac{N_{data}}{N_{data} + N_{TPS}} \times \frac{1}{1 + \nu \times \eta_{GI}}, \quad (3.3)$$

where η_{GI} is the boost factor for GI. It should be noticed that this power efficiency factor presents the power allocated to data subcarriers and is independent of mapping and coding schemes. Or, in other words, it is a measurement of the transmission overhead in terms of power, showing the efficiency of the system data structure.

Parameters and the resulting power efficiency factors of each system are presented in Table 3.4. With GI = 1/4 case, although DTMB has a higher spectrum utilization ratio

(2). The power of GI is boosted in the 1/4 and 1/9 cases, while it remains the same in the 1/6 case.

Table 3.5: Simulation Parameters and useful bitrates with GI =1/4.

System	Modulation	Code Rate		Bitrate (Mbps)	
		without outer code	with outer code	without outer code	with outer code
DVB-T	QPSK	1/2	0.46	5.4	4.98
	16QAM	3/4	0.69	16.2	14.93
	64QAM	3/4	0.69	24.3	22.39
DTMB	QPSK	≈ 0.4	≈ 0.4	4.88	4.81
	16QAM	≈ 0.6	≈ 0.6	14.63	14.44
	64QAM	≈ 0.6	≈ 0.6	21.96	21.66

of 10%, DTMB and DVB-T have approximately the same power efficiency factors. This is mainly due to the fact that the boosted PN sequence takes a large portion of the power of the transmitted signal, decreasing the overall power efficiency. However, this problem is less significant in the GI = 1/9 mode of DTMB. The power efficiency factor in that case is 0.81, which is not only significantly higher than the equivalent GI = 1/8 mode in DVB-T, but is even slightly higher than in the case of the minimum GI of 1/32. Besides increasing the spectrum utilization, PN sequence makes it possible to achieve a faster channel acquisition in DTMB. This feature is expected to make DTMB more robust in high mobility scenarios.

In general, power efficiency factors demonstrate that DTMB has equivalent power efficiency as DVB-T in long GI (1/4) case, while DTMB with a short GI (1/9) has a better power efficiency compared with all cases in DVB-T.

3.2.2 BER Performance

In this section, we analyze the bit error rate (BER) performance of the two systems in AWGN, Ricean (F1) and Rayleigh (P1) channels. The length of GI is set to 1/4 which is the only common option in both systems. From the previous section, this GI length leads to similar power efficiency factors. That is to say, the same portion of signal power is allocated to the data transmission. As shown in Table 3.5, we selected three pairs of working modes from each system, representing low, medium and high throughput applications, respectively. The two working modes in each pair provide approximately the same useful bitrates and can thus deliver the same amount of programs and services. Comparisons are carried out among these working modes to show the performance of each system in different application scenarios. In DVB-T, the 2K mode is adopted for the OFDM modulation and the Viterbi algorithm is used in the inner decoder. In DTMB, the interleaving depth is chosen as 240. The LDPC decoder adopts the message-passing algorithm. The maximum iteration times of decoding algorithm is set to be 50 which is a good trade-off between error correcting performance and time consuming.

All the simulation results are presented in terms of BER versus average signal-to-noise-ratio (SNR) which is defined by the average time domain signal power over noise power. Assuming the data with unite power, the average SNR can be computed as:

$$\text{SNR}_{\text{av}} = \frac{P_{\text{signal}}}{P_{\text{noise}}} = \frac{(\eta_{\text{GI}} \times \nu + 1)/(\nu + 1)}{\sigma_n^2}, \quad (3.4)$$

where η_{GI} is the boost factor, ν stands for the fraction of GI over data part and σ_n^2 is the noise power. For DTMB where $\eta_{\text{GI}} = 2$, the average SNR changes with different GI lengths, while for DVB-T where GI has the same power as data part, the average SNR does not change with different GI lengths.

Furthermore, when GI is long enough to prevent ISI, the system is well synchronized and the channel estimation is perfect, the BER performance is determined by the actual SNR in the data subcarriers which is called as carrier-to-noise-ratio (C/N). Therefore, it is interesting to derive the relationship between the average SNR and the C/N. In DVB-T, GI has the same power as data part. Assuming that the frequency domain data symbols have unite power, the C/N is:

$$C/N = \frac{1}{\sigma_n^2}. \quad (3.5)$$

After OFDM modulation, each N_{data} frequency domain data symbols generate N_{FFT} time domain samples. The average time domain signal power can be computed as:

$$P_{\text{signal}} = \frac{N_{\text{data}} + N_{\text{TPS}} + N_{\text{pilot}} \times \eta_{\text{pilot}}}{N_{\text{FFT}}}. \quad (3.6)$$

Using the definition of average SNR, it yields:

$$\begin{aligned} \text{SNR}_{\text{av}} &= \frac{N_{\text{data}} + N_{\text{TPS}} + N_{\text{pilot}} \times \eta_{\text{pilot}}}{N_{\text{FFT}} \sigma_n^2} \\ &= \frac{N_{\text{data}} + N_{\text{TPS}} + N_{\text{pilot}} \times \eta_{\text{pilot}}}{N_{\text{FFT}}} \times C/N. \end{aligned} \quad (3.7)$$

Rewriting in decibel form, it turns:

$$\begin{aligned} \text{SNR}_{\text{av}}(\text{dB}) &= 10 \log_{10} \frac{N_{\text{data}} + N_{\text{TPS}} + N_{\text{pilot}} \times \eta_{\text{pilot}}}{N_{\text{FFT}}} + C/N(\text{dB}) \\ &= \chi_{\text{DVB-T}} + C/N(\text{dB}). \end{aligned} \quad (3.8)$$

Taking the parameters of DVB-T, the $\chi_{\text{DVB-T}} = -0.46$ dB and is not affected by the GI length. Therefore, the BER performance of DVB-T is the same for different GI lengths.

In DTMB, GI is boosted by a factor of two. Again, assuming the frequency domain data symbols having unite power, C/N is:

$$C/N = \frac{1}{\sigma_{\text{OLA}}^2}, \quad (3.9)$$

where $\sigma_{\text{OLA}}^2 = (1 + \nu)\sigma_n^2$ is equivalent noise power after OLA. Taking the definition of average SNR (3.4) into account, it yields the relationship between average SNR and C/N in data:

$$\text{SNR}_{\text{av}} = \frac{\eta_{\text{GI}} \times \nu + 1}{(1 + \nu)\sigma_n^2} = \frac{\eta_{\text{GI}} \times \nu + 1}{\sigma_{\text{OLA}}^2} = (\eta_{\text{GI}} \times \nu + 1) \times C/N. \quad (3.10)$$

Write the above equation in decibel:

$$\begin{aligned} \text{SNR}_{\text{av}}(\text{dB}) &= 10 \log_{10}(\eta_{\text{GI}} \times \nu + 1) + C/N(\text{dB}) \\ &= \chi_{\text{DTMB}}(\text{dB}) + C/N(\text{dB}). \end{aligned} \quad (3.11)$$

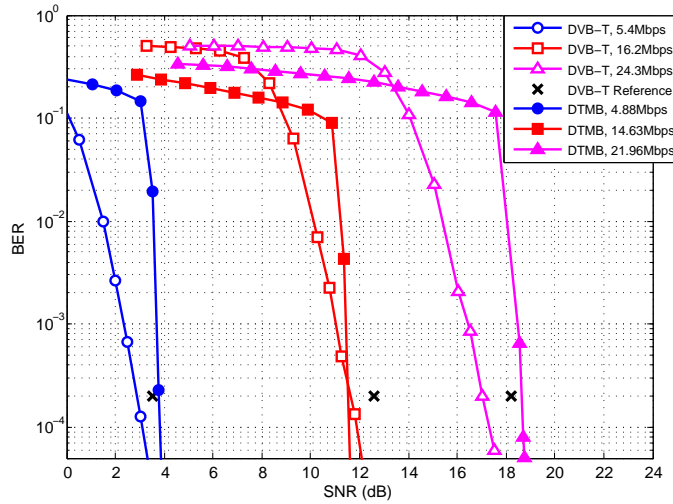


Figure 3.6: BER comparison of DVB-T and DTMB without outer codes in AWGN channel, $GI = 1/4$.

Taking the parameters of DTMB, the $\chi_{DTMB} = 1.76$ dB when $GI=1/4$ and $\chi_{DTMB} = 0.87$ dB when $GI=1/9$. Since we present the results in terms of average SNR while the BER performance is determined by C/N , a larger GI will result in a worse BER performance given the same average SNRs. Note that, the above equation also indicates that we can obtain the BER performance with $GI=1/9$ by shifting the curves with $GI=1/4$ to left side $1.76 - 0.87 = 0.89$ dB.

The average SNR will be used to evaluate the performance throughout this thesis. In the following sections, we will use the term SNR instead of average SNR for the presentation convenience.

3.2.2.1 Performance with Perfect Channel Estimation

In this subsection, we evaluate the BER performance of the two systems using the perfect channel estimation which excludes the influence of the channel estimator and achieves the best performance in the given channel conditions. In fact, this comparison demonstrates the global efficiency of the two systems including the efficiency of data structure and the efficiency of error correction block. The comparisons are carried out in both AWGN channel and multipath channels.

Figure 3.6 gives the results in AWGN channel without taking into account the outer code. In DVB-T, for quasi-error-free (QEF) reception, the projected post-RS BER is less than 10^{-11} , requiring a post-Viterbi BER of less than 2×10^{-4} . Therefore, we investigate the required SNR to achieve $BER = 2 \times 10^{-4}$ after inner decoder. C/N references given by [1] are also printed as cross in the figure. Note that, according to the analysis in previous part, the references given in C/N should be shifted 0.46 dB to the left to get the corresponding references in SNR. After this shift, it can be observed that simulation results are very close to the references, proving the correctness of our simulations. The BER performance of DTMB without outer code is also shown in the same figure. It can be seen that in terms of SNR, the two systems have almost the same performance in

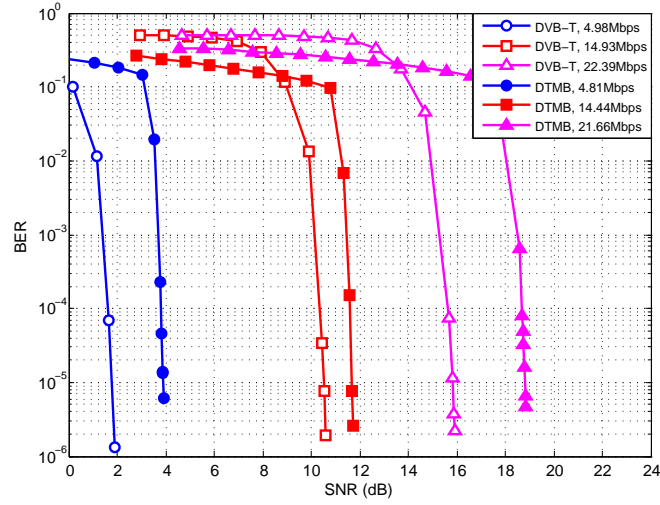


Figure 3.7: BER comparison of DVB-T and DTMB with outer codes in AWGN channel, $GI = 1/4$.

medium data rate case, while in the low and high data rate situations, DVB-T is better when BER equals to 2×10^{-4} .

Figure 3.7 shows the simulation results of both systems with outer code. Profiting from the RS(204, 118) code with eight bytes error correction capability and the interleaving between inner and outer codes, the performance of DVB-T is notably improved, exhibiting a sharp flop. However, the BCH(762, 752) code of the DTMB system can only correct one bit error and does not exhibit any effect at BER level of 10^{-4} . No significantly improvement can be observed when the outer code is taken into account for DTMB. The BER is measured at the output of outer decoder of each system. The performance is evaluated by the required SNR to achieve a BER level of 5×10^{-5} . From Figure 3.7, DVB-T is 2.0 dB, 1.1 dB and 2.6 dB better than DTMB in three applications. Comparing Figure 3.6 and Figure 3.7, we can see different philosophies for the two systems. In DVB-T, the task of error correction is shared by inner and outer channel codings. So each of them should be sufficiently effective and the interleaving between them is important. On the other hand, in DTMB, the duty of error correcting is mainly fulfilled by the LDPC codes. The LDPC codes have such a superior performance that the effect of the BCH code can only be seen in a very low BER level. We can understand why there is no interleaving between inner and outer codes in DTMB. Hence, it is more reasonable to compare the two systems with full error correcting ability.

Simulation results shown in Figure 3.8 and Figure 3.9 are obtained in two typical multipath broadcasting channels when including inner code, outer code and interleaving of each system. All simulations are carried out under the assumption of perfect channel estimation and synchronization. Since there exists the LoS component in the F1 channel, similar conclusions can be drawn as in the AWGN channel case. DVB-T is 1.7 dB, 0.6 dB and 2.2 dB better than DTMB in F1 channel in low, medium and high throughput cases, respectively. Since the P1 channel contains more, deeper frequency domain fades, the performances of the two system accordingly change. DVB-T still performs better in the low and high throughput cases. Whereas, the differences between the performances

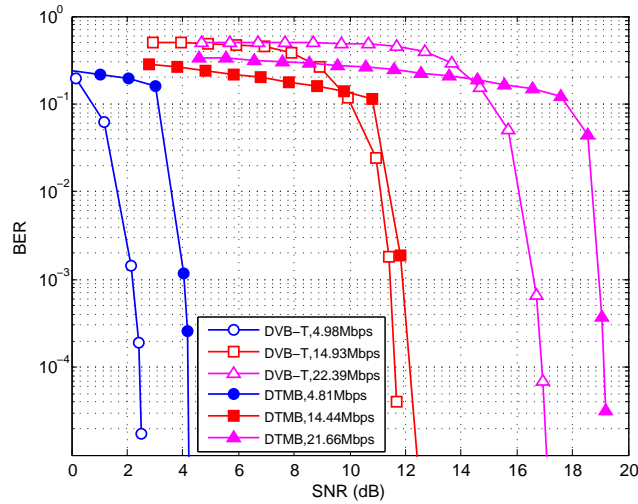


Figure 3.8: BER comparison of DVB-T and DTMB in F1 channel with outer codes, $GI = 1/4$.

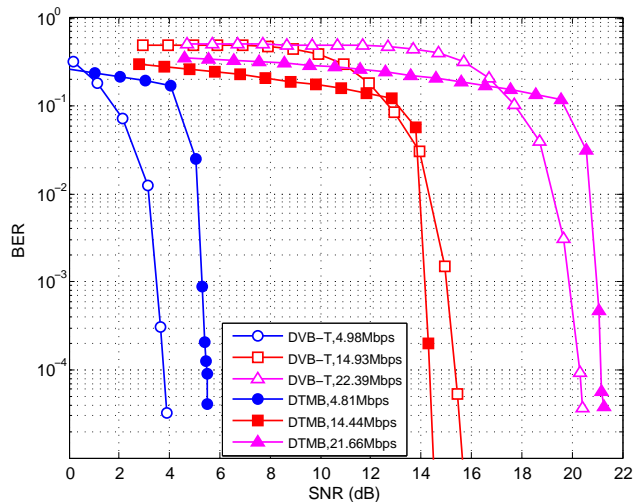


Figure 3.9: BER comparison of DVB-T and DTMB in P1 channel with outer codes, $GI = 1/4$.

of the two systems are less than those in F1 channel. Concerning the medium throughput case, DTMB acquires 1.0 dB gain over DVB-T in P1 channel.

One may be surprised by the fact that the convolutional-code-based error correction scheme outperforms the state-of-the-art LDPC code-based one. In fact, the results presented here are the overall performance of each system which is not only determined by the error correction ability of the coding scheme but also contains the influence of the transmission overhead (including pilots, GI , etc.) as well as the power allocation strategy. For instance, the power of GI is boosted by a factor of two in DTMB to guarantee reliable synchronization and channel estimation. However, the benefit brought by this power boost cannot be reflected in the simulation with perfect synchronization and channel estimation. In the meantime, the power boost in GI will consume some additional

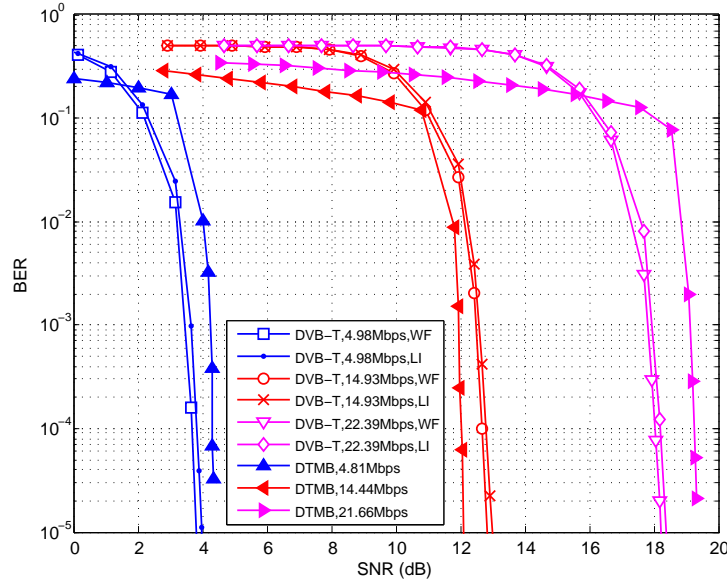


Figure 3.10: BER performance comparison in F1 channel, with different modulations, code rates and channel estimation methods.

energy which consequently degrades the BER performance. This leads to the result that DTMB seems to be less efficient than DVB-T. In the following section, we will take the real channel estimation techniques into account to perform a more global comparison.

3.2.2.2 Performance using Real Channel Estimation Techniques

DVB-T and DTMB have different channel estimation schemes, namely frequency domain pilot-assisted channel estimation in DVB-T and time domain PN sequence based channel estimation in DTMB. The efficiency, performance and adaptability of the two schemes are different. Hence, it is interesting to investigate the system performance taking into account the influence of the channel estimation accuracy.

As revealed in Section 4.1, 4.2 and 5.1, there are numerous channel estimation techniques in the literatures with diverse performance-complexity-adaptability trade-offs. Again, for the sake of fairness in the comparison, we adopt the most classical yet widely applicable methods for each system. More concretely, for DVB-T, the channel estimation is performed (OFDM) block-by-block. In each OFDM block, CFR is estimated for all pilots including continual and scattered ones. Then, the CFR estimates for pilots are interpolated to obtain the channel estimate over all subcarriers. Both linear interpolation and Wiener filtering techniques are used to process the interpolation. On the other hand, we use the time domain PN-correlation-based estimation method which will be presented in Chapter 4 for DTMB. The estimation is also carried out in a block-by-block manner. The performance is obtained with the assumption of perfect synchronization in each system.

Figure 3.10, Figure 3.11 and Figure 3.12 present the BER performance of the DVB-T and DTMB systems in F1, P1 and TU-6 channels, respectively. Comparing with the results of F1, P1 channel with perfect channel estimation, it can be found that the degradation due to the channel estimation error is more significant in DVB-T. For instance,

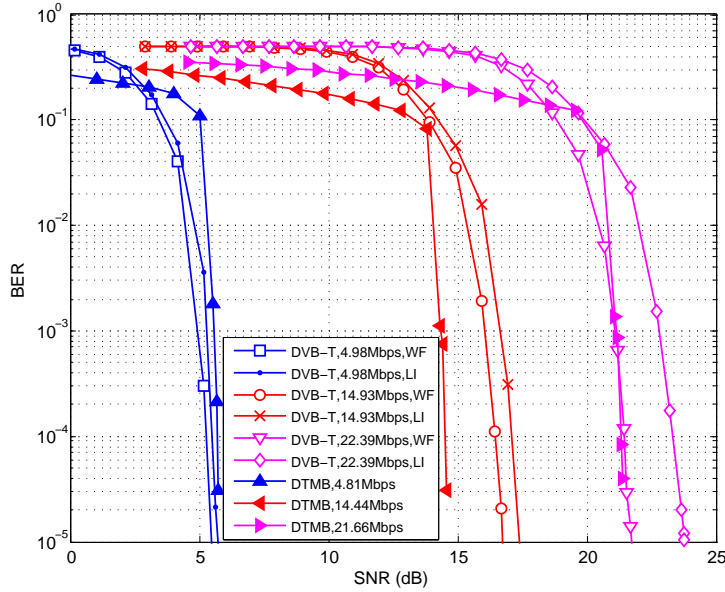


Figure 3.11: BER performance comparison in P1 channel, with different modulations, code rates and channel estimation methods.

the BER degradation is over 1.3 dB in low throughput case and is over 1.1 dB in high throughput case in F1 channel. In P1 channel, the degradations are more significant: 1.7 dB, 1.8 dB and 3.1 dB in low, medium and high throughput case, respectively, when the linear interpolation technique is used. This is because the P1 channel contains deep fades. If pilots locate in the deep fading subbands, the resulting CFR estimates are highly affected by the noise. The channel estimation becomes less reliable.

On the other hand, the degradation due to the imperfect channel estimation is relatively small in DTMB. For example, the degradations are 0.2 to 0.6 dB in F1 channel and 0.1 to 0.2 dB in P1 channel. It indicates that the time domain correlation-based channel estimation in DTMB is more reliable than the frequency domain pilot-assisted estimation in DVB-T, which is partially ascribed to the power boost of GI. Hence, the differences between the two systems in low and high throughput cases decrease. Especially in P1 channel, the two systems achieve the approximately the same performance in low throughput case, while DTMB outperforms DVB-T with linear interpolation in high throughput case. Similar results can be seen in the TU-6 channel as well. Note that the linear interpolation technique cannot provide effective channel estimation for high throughput application, while DTMB works normally in all cases.

The simulation results suggest that the corresponding working modes of each system can provide similar performance in typical channel conditions. DVB-T slightly outperforms DTMB in good channel conditions such as F1 channel, while DTMB is more reliable thanks to the more effective channel estimator in a more severe channel condition such as P1 channel.

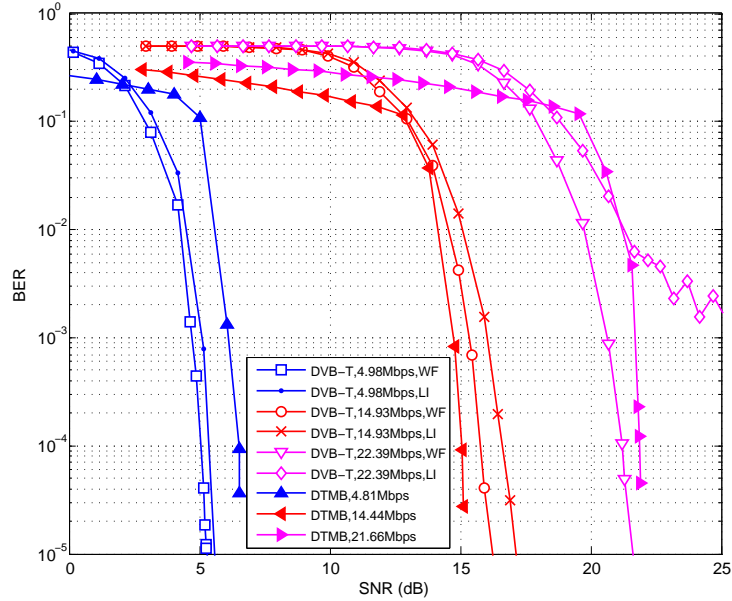


Figure 3.12: BER performance comparison in TU-6 channel with a velocity of 30km/h, with different modulations, code rates and channel estimation methods.

3.2.2.3 Spectral Efficiency

In the previous sections, we present the comparisons of several working modes of the DVB-T and DTMB systems. However, the net data rates of the working modes of each comparing pair are not exactly the same. In addition, the baseband signal bandwidths are slightly different, as well. More precise comparisons can be carried out in terms of spectral efficiencies for the two systems. The spectral efficiency is a measure of how efficiently the physical layer protocol of a system utilizes the frequency spectrum. It is computed by the net bitrate (bit/s) divided by the bandwidth (Hz) of the baseband signal.

Figure 3.13, Figure 3.14 and Figure 3.15 present the spectral efficiency verses required SNR to achieve a BER level of 5×10^{-5} using real channel estimation techniques. These figures demonstrate how efficiently (in terms of required SNR) each system transmits useful information.

For DTMB, we perform a comprehensive study. All the combinations of constellations and coding rates are simulated in the three typical broadcasting channels. In general, spectral efficiencies of the two systems are very close. We can have some interesting observations. In DTMB, there are some working modes having the same net data rate, for example QPSK with $R=0.8$ code and 16QAM with $R=0.4$ code, as well as 16QAM with $R=0.6$ code and 64QAM with $R=0.4$ code. However, the robustness of these working modes is different. In a good channel condition, such as F1 channel, it is better to choose a lower order constellation with a higher code rate. For instance, as shown in Figure 3.13, QPSK with $R=0.8$ code performs better than 16QAM with $R=0.4$ code. The same situation can be observed in the comparison of 16QAM with $R=0.6$ code and 64QAM with $R=0.4$ code. This can be explained by the fact that a weaker code (i.e. with higher code rate) can effectively correct errors in a good channel condition. Whereas, in severe channel conditions, such as P1 channel, the performance of the code with higher rate

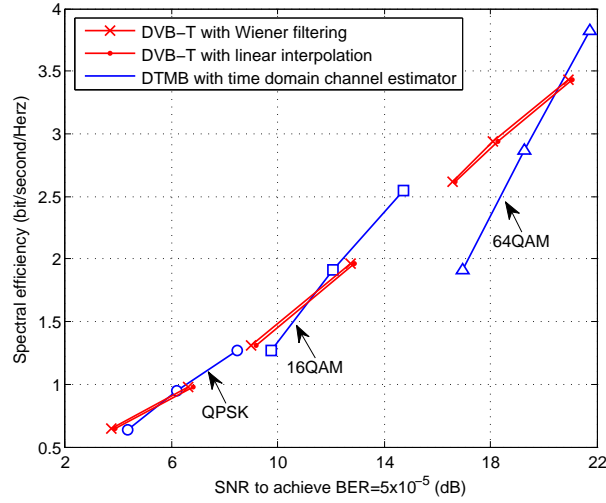


Figure 3.13: Spectral efficiency comparison in F1 (Ricean) channel, $GI = 1/4$.

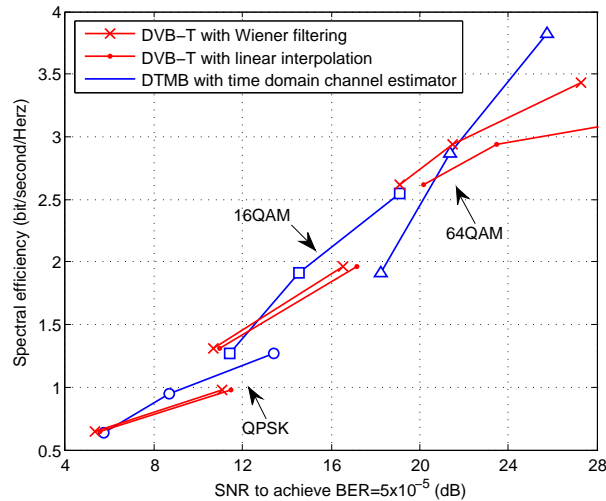


Figure 3.14: Spectral efficiency comparison in P1 (Rayleigh) channel, $GI = 1/4$.

degrades more significantly. This can be observed by comparing the curves in Figure 3.13 and Figure 3.14. In this case, the working modes with higher order constellation and lower code rate may be more effective. For example, the working mode of 16QAM with $R=0.4$ code outperforms the one of QPSK with $R=0.8$ code. These observations may be introductive when selecting suitable working modes for given channel conditions.

Finally, we investigate the efficiencies of the two systems when shorter GIs are adopted. The results are given in Figure 3.16, Figure 3.17 and Figure 3.18. As explained in the power efficiency analysis in Section 3.2.1, more power is allocated to the useful data part in DTMB when GI is shorter. Thus, DTMB performs more robustly than DVB-T with a shorter GI. The simulation results show that DTMB outperforms DVB-T in most cases given similar spectral efficiencies. However, we should note that the differences between the two systems are very small. In general, the efficiencies of the two systems are equivalent.

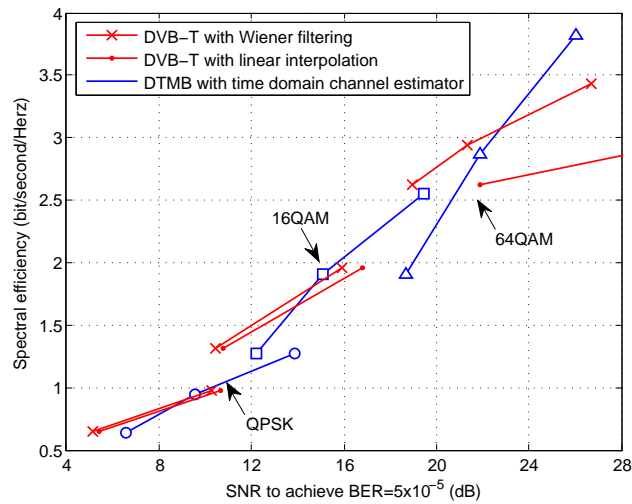


Figure 3.15: Spectral efficiency comparison in TU-6 channel, $GI = 1/4$.

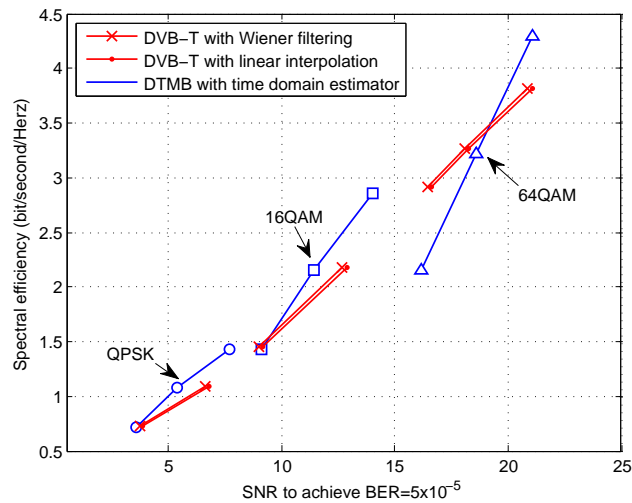


Figure 3.16: Spectral efficiency comparison in F1 (Ricean) channel with $GI = 1/8$ in DVB-T and $GI = 1/9$ in DTMB.

3.3 Conclusion

In this chapter, we have investigated the two main DTTB standards—DVB-T and DTMB in terms of system specifications including OFDM parameters design, FEC block, etc. and system performance such as power efficiency, BER and spectral efficiency. In general, although there exist many differences in system specifications as well as channel estimation techniques, the overall performance of two systems is very close in typical channel conditions. The two systems can provide equivalent working modes with various throughputs for different application scenarios. As DVB-T has more code rates, modulation schemes, subcarrier number and bandwidth options, it can provide more working mode combinations than DTMB. However, DTMB has a much concise data structure and

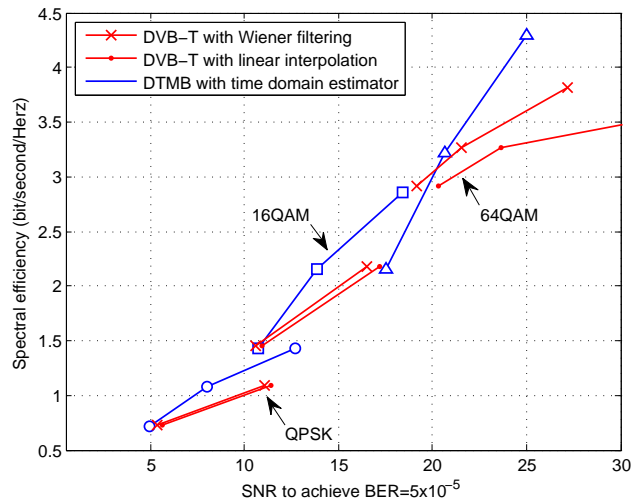


Figure 3.17: Spectral efficiency comparison in P1 (Rayleigh) channel with $GI = 1/8$ in DVB-T and $GI = 1/9$ in DTMB.

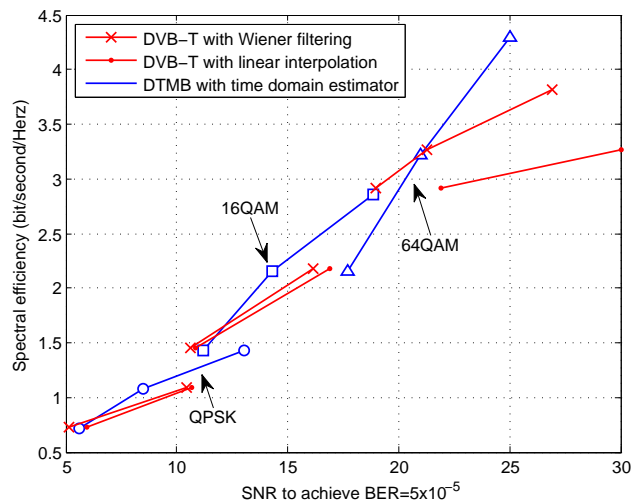


Figure 3.18: Spectral efficiency comparison in TU-6 channel with a velocity of 30km/h. $GI = 1/8$ in DVB-T and $GI = 1/9$ in DTMB.

a higher spectral utilization efficiency. More bandwidth options are also proposed for an enhanced version of DTMB to provide more flexibility.

PN Sequence based Channel Estimation for TDS-OFDM

AS PRESENTED PREVIOUSLY, the TDS-OFDM signal can be converted to ZP-OFDM by removing the known sequence in GI. However, the quality of the GI removal depends on the accuracy of channel estimation. A straightforward way to estimate channel is to use the known PN sequence in GI of the TDS-OFDM signal. In this chapter, we present several PN-sequence-based channel estimation techniques for TDS-OFDM.

4.1 A Brief Overview of the Channel Estimation in General OFDM Context

In wireless communications, besides the additive noise, the received signal is also distorted by the channel fades which affects the amplitude, frequency and phase of the signal. This makes the signal detection unreliable at the receiver side. Some precaution or correction methods should be used to fight against the channel distortions. Differential modulations, such as differential phase-shift keying (DPSK) etc., carry and recover the useful information by the differential relationships between consecutive data symbols, and thus avoid the need of channel information for demodulation at the receiver side. However, such modulation schemes result in low useful data rate. A 3-4 dB loss of SNR is classically committed. Coherent modulations are more efficient but need to compensate the channel distortions on the received signal and track the channel variations. This arises the channel estimation problem.

Generally speaking, channel estimation techniques for the OFDM based systems can be grouped into three main categories: *training-based*, *blind* and *semi-blind* estimations.

Training-based channel estimation As the name implies, the training-based channel estimation is performed by using some predefined training sequences which are periodically inserted into data symbols in the transmitter and are known beforehand by the receiver [93, 94, 95, 96, 45, 97, 98, 39].⁽¹⁾ With the knowledge of the transmitted training sequence and the observation of the sequence after transmission, it is easy for the receiver to analyze the channel effect confronted by the transmitted signal. More specifically, in

(1). The training sequence is also known as *pilot* or *reference signal*. The method that uses pilots to track the channel condition is also referred to as pilot-symbol-assisted-modulation (PSAM) [99, 100].

the OFDM system context, some subcarriers are reserved as pilots which bears known sequences. The CFR is first estimated on these discrete positions. Then, some interpolation techniques, such as linear interpolator [101], Wiener filtering [95, 96], FFT-based interpolation [102, 103] and other techniques [104], are used to compute the CFR over all frequencies. Some researches on the selection of optimal pilot pattern were also conducted in [105, 106, 107, 108, 109]. Many techniques such as singular value decomposition (SVD) and frequency domain filter were proposed to improve the pilot-assisted channel estimation method [93, 94]. An additional time domain filtering was proposed in [110] to further reduce the noise. The correlation properties of CFR over time and frequency were exploited to form a robust MMSE channel estimator in [45]. In order to estimate the time varying channel, linear interpolation of partial channel information was proposed in [108] in a MIMO-OFDM context. Algorithm in [111] proposed a specific time domain pilot signal in cooperation with the FFT operation to track the channel variations at a low computational complexity cost.

As the receiver has perfect knowledge of the reference sequence, the training-based techniques provide reliable and low-complexity channel estimation. It is widely used in many modern communication systems such as WLAN, DVB-T etc. The limitation of the training-based scheme is that the bandwidth efficiency is somehow compromised by the transmission of pilots. In fact, designer should consider the worst case in the application scenario which spends more resources than what is necessary. This implies that the system operates inefficiently in a common situation. Take the DVB-T system as an example. One subcarrier out of twelve is allocated as pilot for channel estimation in each OFDM symbol in order to handle highly frequency-selective channel situation. The transmission efficiency of the system is thus under-exploited.

Blind channel estimation Blind channel estimation schemes (see [112] and reference therein) do not rely on any pre-known signal to probe the channel conditions. Instead, they exploit the inherent characteristics of the signal, e.g. the cyclostationarity induced by the insertion of CP [113, 114, 115] or oversampling [116], the presence of virtual subcarriers [117] etc. The blind channel estimation is attractive for some applications where bandwidth is scarce because it can economize the resources that are originally allocated to pilots. However, the drawback of the blind estimation scheme is also obvious. As the second or higher-order statistics are commonly needed, the blind estimation scheme is computationally intensive. Meanwhile, it requires to accumulate a large amount of data symbols to achieve a reliable estimation. The resulting processing time delay and storage are considerably high. Moreover, some of the blind estimation techniques suffer from the lack of robustness [118]. These facts prevent the implementation of the blind channel estimation scheme on real time systems.

Semi-blind channel estimation When the blind methods are used in conjunction with some training data, it yields the so-called semi-blind algorithms [119, 114, 118, 120] (and the references therein) which exploit the positive aspects of both techniques. This scheme relies on the fact that most communication systems employ pilot symbols for the purpose of synchronization. This *a priori* knowledge of pilots is helpful to avoid the possible pitfalls of blind techniques especially those with a lack of consistency. On the other hand, with the assistance of data symbols, the semi-blind methods improve the

accuracy of the initial channel estimation obtained from pilot symbols at the beginning of a channel estimation cycle [114]. Combining the information from different sources, the semi-blind techniques can achieve a performance superior to that of training-based and blind techniques separately. Furthermore, as the unknown data symbols are also involved in the semi-blind estimation, it allows estimating a longer channel delay spread. It could be interesting for the applications in mountainous areas or the SFN broadcasting which has artificial echoes with extremely long delays. On the other hand, the use of semi-blind techniques can adapt a system to higher channel-variation situations. More specifically, channel is assumed to be static or slowly varying in some applications. The training sequence is sparse in time direction. The system is incapable in face of fast channel variations. The semi-blind method is a supplementary means to the already existing pilots so that the systems can track the channel variations between two pilot-assisted channel estimations. It enables the system to work in a higher mobility scenario. In general, the semi-blind estimation method can enhance the channel estimation of an existing system without any modification and hence with no penalty in terms of bandwidth efficiency.

4.2 Overview of the channel estimation techniques in the PRP/KSP/TDS-OFDM context

The usage of PN as GI is “double-edged sword”. On one hand, it improves the spectrum efficiency by economizing the cost of transmitting redundant data in CP and the pilots in data symbols; on the other hand, the channel memory effect introduces mutual interference between PN sequence and OFDM data symbols. That is to say, the interference from data symbols degrades the performance of PN sequence based channel estimation, and consequently the channel estimation error causes imperfect PN sequence removal and further increases the difficulty when recovering data symbols. The channel estimation is thus the key point in the transmissions where known sequences are used as GI. A number of researches have been carried out on the challenging channel estimation issue. Due to the differences among the known sequences of PRP-/KSP-/TDS-OFDM, we will separately overview the channel estimation techniques for each case.

4.2.1 PRP-OFDM

A semi-blind channel estimation technique were first proposed in [12] for PRP-OFDM. The conventional CP is replaced by a known vector weighted by a pseudo random scalar. The pseudo random scalar is selected to meet the requirements of peak-to-average-ratio (PAPR), in-band flatness and out-of-band radiation [121]. Based on the fact that data symbols are random while the known sequence is deterministic, the channel can be simply estimated by the first-order statistics, i.e. the expectation, of the received signal. The interference introduced by data symbols is suppressed by the expectation operation. It is proved that the first-order statistics based estimator outperforms second-order statistics based and subspace-based ones in slowly time-varying channel [122]. The method is validated based on the assumption that the channel is static or slowly varying. This limits the range of mobility that it can adapt to [123]. Another disadvantage is that this method needs to accumulate a number of OFDM symbols (e.g. 72 OFDM symbols in the example given in [12]) for a reliable estimation. The resulting processing delay and storage are high.

The estimation algorithm was extended to the variant-channel case based on a Moving Average (MA) CIR model in the context of MIMO in [124] and [125]. Another generic Wiener filtering based time-variant CIR estimation approach is demonstrated in [126]. The channel variation is tracked using more sophisticated estimation techniques, namely Kalman filtering or Wiener filtering, instead of the simple expectation calculation process in static channels. In the meantime, the computational complexity accordingly increases. In contrast to the first-order-statistics based interference cancellation approach, an iterative interference suppression and CIR estimation scheme was proposed in [127]. The output information from the soft-output decoder is employed to estimate the interference introduced by OFDM data symbols on the training sequence. By iteratively removing the interference from the known sequence, the estimation performance is progressively improved. However, the annoying BER error floor still appears in high SNR region due to the residual interference.

4.2.2 KSP-OFDM

A series of channel estimation methods were proposed in [13] in a general KSP transmission case: an ML estimator with Gaussian assumption on the data being proposed for static channels; while two other techniques with the help of the basis expansion model (BEM) being proposed for doubly selective channels. These three methods exploit all the received data symbols containing contributions from the training sequence and blindly filter out the contribution of the unknown surrounding data symbols. However, it assumes that the autocorrelation matrix of the disturbance (including contributions from the noise, data symbols and channel) is known (or already estimated from the received data symbols) before the channel estimation. Performance indicates that even if the autocorrelation matrix is perfectly known, the estimation MSE shows an error floor at high SNR. It means that there is still some residual disturbance affecting the channel estimation.

In [128, 129], the training sequence is placed not only in GI but also on some OFDM subcarriers. To reduce the influence of data symbols on the channel estimation results, a linear transform is applied to the time-domain samples so that the observations are separated into a subset containing data symbols and a subset independent of data symbols. Therefore, an estimator is obtained using the observations only from the latter subset to avoid the influence of data symbols on the final estimation. Although performing better than the estimator proposed in [13], it still shows an error floor at high SNR due to the residual interference from data symbols.

A possible solution to avoid the influence of data symbols is to use *only* the training sequence located in frequency-domain pilot subcarriers for channel estimation [130]. The training sequence in GI is discarded because it is contaminated by the data symbols. The orthogonality between subcarriers prevents the interference from data symbols so that the estimation error is also avoided. This method is somehow similar to the classical pilot-symbol-assisted estimation method in CP-OFDM context. However, the convenience of the circular data structure brought by CP does not retain, while the loss of spectrum efficiency due to the frequency-domain pilots is still committed. These facts make this scheme less efficient.

Other methods to mitigate the interference in an iterative (turbo) manner were proposed in [131] and [132]. Decoded data symbols are used to update the channel estimate in a joint data-aided/decision-directed estimation algorithm in [131]. While in [132] the

expectation-maximization (EM) algorithm, an iterative algorithm that converges to the ML estimate, is used to achieve better performance. The main disadvantage of these methods lies in the huge complexity demanded by the computation of the autocorrelation matrix as well as the matrix inversion.

4.2.3 TDS-OFDM

In the past few years, there have been many literatures [133, 134, 135, 136, 137, 138, 5, 76, 139, 140, 141, 142, 143, 144] dedicated to the channel estimation problem in the TDS-OFDM context, more specifically in the DTMB system case.

A first idea is to estimate the CIR via a time domain correlation between the received PN sequence and the perfect one [133, 134, 135, 136]. These methods exploit the strong noise suppression ability in the PN correlation operation so that it can provide a rough channel estimate in presence of moderate ISI. However, the method is not robust enough when facing a strong ISI. Later, this PN-correlation-based method was enhanced by performing correlations in several different observation windows so that it can cope with different channel lengths [138]. The potential limitation of this method is that the PN sequence used in the estimation contains ISI in face of long channel delay spreads. This inevitably results in an estimation error floor. A latest work [143] was dedicated to fixing this problem. Only the ISI-free part of the PN sequence is used in the estimation. When the channel length is so long that the ISI-free part in one GI is not sufficient for estimation (i.e. comparatively shorter than the channel length), the ISI-free parts of the PN sequences in two consecutive OFDM symbols are combined together to form a complete PN sequence. Then the correlation is carried out between this new PN sequence and the perfect one to obtain the CIR. The basis of the estimation using combined PN sequence is that the channel responses are identical within two OFDM symbols. It limits the applicable velocity range of this method. A notable degradation can be observed with a moderate Doppler frequency (10 Hz comparing to the subcarrier spacing of 2 kHz) as shown in [143]. Another method proposed in [139, 145] involved a decision feedback loop in the PN-correlation-based estimation. The hard-decided data symbols of the previous OFDM symbol are used to eliminate the ISI from the PN sequence. The accuracy of the hard-decision affects the performance of the method.

An other idea is to (iteratively) remove ISI from the PN sequence before making (or updating) the channel estimation. A first approach [137] adopted the iterative version of the echo cancellation method in the CP-OFDM systems with insufficient length of CP [64]. However, the complexity brought by repeatedly FFT-IFFT conversions is considerably high. The hard decision used to determine the data symbols has potential risk of damaging the estimation, especially in high constellation cases and in channels with deep frequency fades. It appears a high floor of symbol error rate. It was proposed in [76] to carry out the channel estimation using the PN sequence and its tail spread in the beginning part of each OFDM data symbol. By iteratively removing the data symbol, the channel estimation can progressively be improved. However, the estimation results suffer an error floor even at low SNR due to the existence of ISI in the PN sequence.

An extension of [76] was presented in [142]. In order to remove the mutual interference between the PN sequence and OFDM data symbols, it proposes an estimation scheme that alternately removes the interference of PN on OFDM data symbols when making the demodulation and decision, and consequently removes the interference of OFDM data

symbols on PN sequence when making the channel estimation. In addition, a so-called partial decision is also used to reduce the error detection of data symbols. The received data symbols that fall into a predefined decision region are hard decided. The rest data symbols are left as they were. An other method adopting decision feedback with partial decision is found in [141]. The use of partial decision can avoid error decisions of the data symbols. The methods in [142, 141] thus outperform the classical hard-decision one in [137]. The idea of partial decision is also used in the selection of virtual pilots in [140, 146, 144]. It was proposed in [140] to use the partially decided data symbols as the virtual pilot to estimate the channel response in frequency domain. The FFT-based interpolation is used to obtain the channel estimation over all subcarriers. This method was then extended to transmit diversity case in [146]. This idea has the risk that the available virtual pilot may not be sufficient and well located to estimate the channel. For example, it may be lack of virtual pilots in the subbands that the channel is deeply faded. In the meantime, the random location of the virtual pilots cannot guarantee the sampling of the channel response fulfilling the sampling theorem. It was suggested in [144] to involve the NR code in the partial decision feedback loop to improve the quality of the virtual pilots. However, the use of this scheme is limited only in the case where the NR code is adopted.

There are also some works [147, 148] dedicated to simplifying the channel estimation method with some modifications to the original TDS-OFDM signal structure. In [147], authors proposed to use a dual PN padding method in which GI is composed of concatenation of two identical PN sequences. The channel estimation can be carried out without iteration so that the computational complexity is reduced. However, an inherent loss of spectrum efficiency is also committed due to the extended GI length. A latest modification can be found in [148]. Authors proposed to replace the classical PN sequence by a so-called time-domain padded frequency-binary (TPFB) sequences. Since the TPFB sequence is binary sequence (composed of '+1' and '-1') in frequency domain, the complex-value divisions in the traditional frequency domain LS estimation turns to a series of sign flips which simplifies the computational complexity. In the meantime, the flat frequency response of the TPFB sequence leads to a more accurate channel estimation [75]. The disadvantage of the TPFB sequence is that it has a higher peak to average power to average ratio (PAPR) compared to the PN sequences. Only some selected TPFB sequences can be used to avoid high PAPR.

In general, the classical way of making channel estimation is to exploit the known sequence (generally PN sequence) in GI. The PN-based estimation is either used independently or in combination with other data-aided techniques. Anyway, the PN-based channel estimation is a fundamental technique in the PRP/KSP/TDS-OFDM context. In this chapter, we will study several PN-based channel estimation techniques according to the specification of the DTMB standard.

4.3 GI Structure in the DTMB System

The design of the PN-based estimation method greatly depends on the composition of GI. Therefore, it is necessary to discuss the GI structure first. In the DTMB system, the ν -length GI consists of an N_{PN} -length maximum length sequence (m-sequence) as well

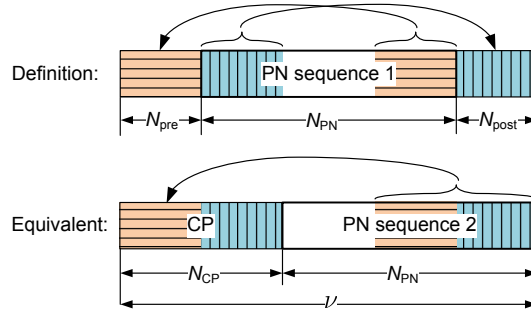


Figure 4.1: Structure of the GI.

as its pre- and post- circular extensions [4]. Since any circular shift of an m-sequence is itself an m-sequence [149], GI can also be treated as another N_{PN} -length m-sequence, denoted as $p[n]$, with an N_{CP} -length CP as shown in Figure 4.1. The length of each part is presented in Table 4.1.

Table 4.1: Composition of the GI specified in DTMB.

Length (samples)	GI Length	
	420	945
N_{PN}	255	511
N_{pre}	83	217
N_{post}	82	217
N_{CP}	165	434

Based on the observation that the delays of most of the channel models [1, 83, 44] are short compared to the equivalent CP duration, a straightforward way is to use the PN sequence, instead of the whole GI, to make channel estimation. When the CIR is shorter than this CP, the circular convolution between the CIR and the PN sequence holds. After removing CP, the received PN sequence $d[n]$ is written as:

$$\begin{aligned}
 d[n] &= p[n] \otimes h[n] + w[n] \\
 &= \sum_{l=0}^{L-1} h_l \cdot p[n-l]_{N_{\text{PN}}} + w[n], \quad 0 \leq n < N_{\text{PN}},
 \end{aligned} \tag{4.1}$$

where \otimes denotes the circular convolution and $(\cdot)_{N_{\text{PN}}}$ denotes modular N_{PN} operation. The circular convolution will facilitate the following estimation process. However, there are also some limitations, as the length of the training sequence determines the maximum length of CIR that can be estimated using the sequence. Using part of GI as training sequence decreases the range of the CIR that can be estimated. Another disadvantage is that if the CIR is longer than CP, the estimation suffers from the interference from the previous OFDM data symbols.

4.4 Interference from Imperfect PN Removal

Before presenting the proposed channel estimation method, it is worthwhile to expose the underlying harm that the unreliable channel estimate will bring to the OFDM data

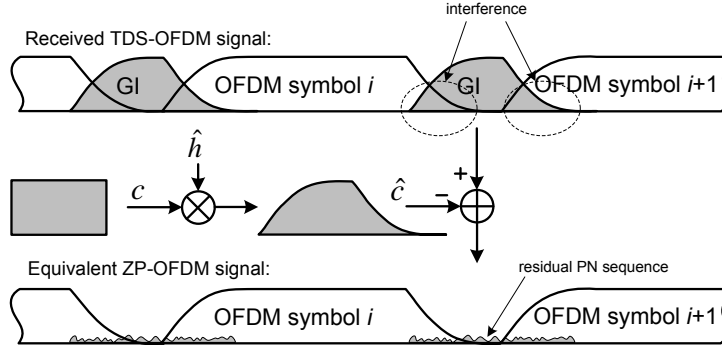


Figure 4.2: PN removal of the TDS-OFDM signal.

symbols in terms of mean power of the interference. Recall that the i^{th} OFDM data block:

$$x^{(i)}[n] = \frac{1}{\sqrt{N}} \sum_{k=0}^{N-1} X^{(i)}[k] e^{j \frac{2\pi}{N} nk}, \quad 0 \leq n \leq N-1. \quad (4.2)$$

After padding the ν -length PN sequence $\{c^{(i)}[n]\}_{n=0}^{\nu-1}$ before the OFDM symbol $x^{(i)}[n]$, it forms the i^{th} transmission block:

$$t^{(i)}[n] = \begin{cases} c^{(i)}[n] & -\nu \leq n < 0 \\ x^{(i)}[n] & 0 \leq n \leq N-1. \end{cases} \quad (4.3)$$

Suppose that the channel can be modeled as the tapped-delay-line as given in (2.17). Furthermore, the channel is assumed to be quasi-static, i.e. $h_l[n]$'s are constant within one OFDM symbol duration and can be denoted as $h_l^{(i)}$ for the i^{th} OFDM symbol. Thus, the received signal is written as:

$$y^{(i)}[n] = \sum_{l=0}^{L-1} h_l^{(i)} t^{(i)}[n-l] + w[n]. \quad (4.4)$$

Taking (4.3) into account, (4.4) can be expressed as:

$$y^{(i)}[n] = \begin{cases} \sum_{l=0}^{n+\nu} h_l^{(i)} c^{(i)}[n-l] + \sum_{l=\nu+1}^{L-1} h_l^{(i)} x^{(i-1)}[n-l]_N + w[n] & -\nu \leq n < -\nu + L - 1 \\ \sum_{l=0}^{L-1} h_l^{(i)} c^{(i)}[n-l] + w[n] & -\nu + L - 1 \leq n < 0 \\ \sum_{l=0}^n h_l^{(i)} x^{(i)}[n-l] + \sum_{l=\nu+1}^{L-1} h_l^{(i)} c^{(i)}[n-l] + w[n] & 0 \leq n < L - 1 \\ \sum_{l=0}^{L-1} h_l^{(i)} x^{(i)}[n-l] + w[n] & L - 1 \leq n < N \end{cases} \quad (4.5)$$

where $[n]_N$ is the residue of n modulo N . It can be seen from (4.5) and Figure 4.2 that there are some mutual interference between OFDM data symbols and PN sequence due to the channel memory effect. In order to recover the data symbols, it is necessary to remove the PN sequence from the received signal first. Since the PN sequence $c^{(i)}[n]$ is

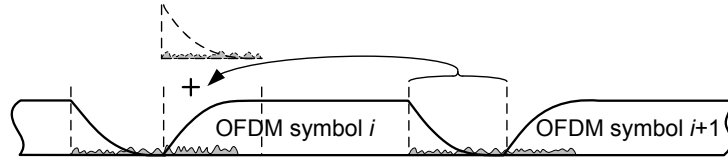


Figure 4.3: OLA.

perfectly known by the receiver, the received distorted PN sequence can be estimated by making linear convolution of PN sequence $c^{(i)}[n]$ and the estimated CIR \hat{h} :

$$\hat{c}^{(i)}[n] = \sum_{l=0}^{L-1} \hat{h}_l^{(i)} c^{(i)}[n-l], \quad -\nu \leq n < L-1. \quad (4.6)$$

The PN sequence is removed from the received signal by subtracting the estimated PN sequence

$$\begin{aligned} \bar{y}^{(i)}[n] &= y^{(i)}[n] - \hat{c}^{(i)}[n] \\ &= \begin{cases} \sum_{l=0}^{n+\nu} \Delta h_l^{(i)} c^{(i)}[n-l] + \sum_{l=l'+1}^{L-1} h_l^{(i)} x^{(i-1)}[n-l]_N + w[n] & -\nu \leq n < -\nu + L - 1 \\ \sum_{l=0}^{L-1} \Delta h_l^{(i)} c^{(i)}[n-l] + w[n] & -\nu + L - 1 \leq n < 0 \\ \sum_{l=0}^n h_l^{(i)} x^{(i)}[n-l] + \sum_{l=l'+1}^{L-1} \Delta h_l^{(i)} c^{(i)}[n-l] + w[n] & 0 \leq n < L - 1 \\ \sum_{l=0}^{L-1} h_l^{(i)} x^{(i)}[n-l] + w[n] & L - 1 \leq n < N \end{cases} \end{aligned} \quad (4.7)$$

where $\Delta h_l^{(i)} = h_l^{(i)} - \hat{h}_l^{(i)}$ is the estimation error of the l^{th} channel tap. If the CIR is perfectly estimated, the PN sequence and its tail can be completely removed from the received signal. Otherwise, there will be some residual contribution of the PN sequence in the received signal as shown in Figure 4.2.

Suppose that the length of GI exceeds that of CIR, there is no IBI between two adjacent OFDM symbols. After removing the PN sequence, OLA is performed by adding the following GI to the beginning part of the OFDM symbol as shown in Figure 4.3. It can be found that the OLA process not only boosts the AWGN but also brings the residual PN sequence to the OFDM data symbols from the next GI. More precisely, the OLA process is written as:

$$r^{(i)}[n] = \bar{y}^{(i)}[n] + \bar{y}^{(i+1)}[n-\nu], \quad 0 \leq n < L-1. \quad (4.8)$$

Considering (4.7), the received signal after removing GI is written as:

$$\begin{aligned} r^{(i)}[n] &= \sum_{l=0}^{L-1} h_l^{(i)} x^{(i)}[n-l]_N + w'[n] + \xi[n] \\ &= x^{(i)}[n] \otimes h^{(i)}[n] + w'[n] + \xi[n], \quad 0 \leq n < N, \end{aligned} \quad (4.9)$$

where \otimes denotes the circular convolution, $w'(n)$ is the noise after OLA, and $\xi[n]$ is the contribution of the residual PN sequence in the received signal. More specifically, take

(4.7) and (4.8), and suppose the PN sequences are identical for all OFDM blocks, the residual PN sequence in the received signal can be written as:

$$\xi[n] = \sum_{l=0}^{L-1} \Delta h_l c[n-l]_\nu, \quad 0 \leq n < \nu. \quad (4.10)$$

The interference for the k^{th} subcarrier is thus:

$$\begin{aligned} I[k] &= \frac{1}{\sqrt{N}} \sum_{n=0}^{N-1} \xi[n] e^{-j \frac{2\pi}{N} nk} \\ &= \frac{1}{\sqrt{N}} \sum_{l=0}^{L-1} \Delta h_l \sum_{n=0}^{\nu-1} c[n-l]_\nu e^{-j \frac{2\pi}{N} nk}. \end{aligned} \quad (4.11)$$

Denote $c[n-l]_\nu$ by $c_l[n]$, representing a circular shift of l bits of sequence $c[n]$ towards right side. Using the US assumption, i.e. $\mathbb{E}[h_l^* h_{l'}] = \sigma_l^2 \delta[l-l']$, the power of the interference is:

$$\begin{aligned} \sigma_I^2[k] &= \mathbb{E}[I^*[k] I[k]] \\ &= \frac{1}{N} \sum_{l=0}^{L-1} \sigma_{\Delta h_l}^2 \sum_{n_1, n_2=0}^{\nu-1} c_l^*[n_1] c_l[n_2] e^{-j \frac{2\pi}{N} (n_2 - n_1) k} \end{aligned}$$

where $\sigma_{\Delta h_l}^2 = \mathbb{E}[|\Delta h_l|^2]$ is the variance of the estimation error of the l^{th} channel tap. Substituting n_1, n_2 by $q = n_2 - n_1$ and $n = n_1$, it yields:

$$\sigma_I^2[k] = \frac{1}{N} \sum_{l=0}^{L-1} \sigma_{\Delta h_l}^2 \left[\sum_{n=0}^{\nu-1} |c[n]|^2 + \sum_{q=1}^{\nu-1} 2 \cos\left(\frac{2\pi}{N} kq\right) \sum_{n=0}^{\nu-1-q} c_l^*[n] c_l[n+q] \right], \quad (4.12)$$

In the above equation, the part in the brackets is only determined by the PN sequence and is constant for a given sequence. Thus the power of the interference is determined by the length of CIR L and the MSE of CIR estimation. Hence, the worse the channel estimation, the more interference will be introduced to the OFDM data symbols, which motivates us to propose additional processings to improve the channel estimation results.

From (4.12), it can be found that the distribution of the interference depends on the index of subcarrier k . Intuitively, the interference can not be modeled as white noise. Figure 4.4 gives an example of the interference power distribution which is obtained when SNR=10 dB in the TU-6 channel. The interference power for each subcarrier is averaged over 200 realizations of the channel. Figure 4.4a presents the interference when the frequency domain PN-based channel estimation method is adopted. It can be found that the interference due to the residual PN sequence concentrates in low and high frequencies, which indicates that the power spectral density of the interference is not uniform. This is resulted from the error boost in the DC component of the frequency domain estimator. On the other hand, the time domain estimation method does not result in an error boost in DC. The interference due to the imperfect PN removal does not concentrate in the low frequency region.

More precise normality test is carried out by investigating the *kurtosis* [150, 151] of the interference. The kurtosis is defined by:

$$ku = \frac{\mu_4}{\sigma^4}, \quad (4.13)$$

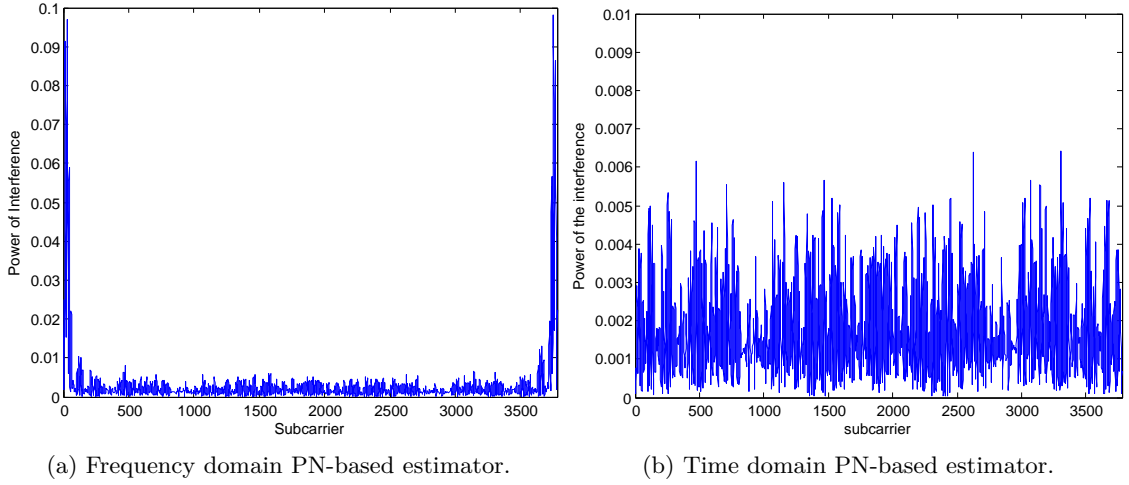


Figure 4.4: Distribution of the interference resulted from the residual PN sequence when SNR = 10 dB in the TU-6 channel.

Table 4.2: Kurtosis values of the interference caused by the imperfect PN removal.

Estimation Method		SNR=0dB	SNR=10dB	SNR=20dB	SNR=30dB
Time domain estimator	TU-6 channel	4.54	4.65	4.54	5.99
	SFN channel	4.60	6.57	6.80	6.43
Frequency domain estimator	TU-6 channel	23.49	24.09	25.85	25.36
	SFN channel	33.43	25.61	23.54	28.61

where μ_4 is the fourth moment about the mean and σ is the standard deviation of the interference. For a Gaussian distribution, the kurtosis is equal to 3. While, higher kurtosis means more of the variance is resulted from the infrequent extreme deviations. Therefore, it is sufficient to claim that a signal does not follow the Gaussian distribution if its kurtosis is not equal to 3. Table 4.2 presents the kurtosis values of the interference power in conditions. Each kurtosis value is computed using 1.5×10^6 samples of the interference. Not surprisingly, when the frequency domain estimator is used, the kurtosis in all cases are much greater than 3, which means the interference does not follow the Gaussian distribution. Concerning the time domain estimator, the kurtosis values are also higher than 3, which indicates that the distribution of the interference can not be modeled by a Gaussian variable.

4.5 Frequency Domain PN-based Channel Estimation

From the convolution theorem, the circular convolution is turned to element-wise product by an N_{PN} -length FFT operation:

$$\mathbf{D} = \mathbf{P}_d \mathbf{H} + \mathbf{W}, \quad (4.14)$$

where the $\mathbf{D} = [D[0], D[1], \dots, D[N_{\text{PN}} - 1]]^T$ and $\mathbf{W} = [W[0], W[1], \dots, W[N_{\text{PN}} - 1]]^T$ are the vector form of N_{PN} -point FFT of received PN sequence and AWGN, respectively. $D[k] = \frac{1}{\sqrt{N_{\text{PN}}}} \sum_{n=0}^{N_{\text{PN}}-1} d[n] e^{-j \frac{2\pi}{N_{\text{PN}}} nk}$, $W[k] = \frac{1}{\sqrt{N_{\text{PN}}}} \sum_{n=0}^{N_{\text{PN}}-1} w[n] e^{-j \frac{2\pi}{N_{\text{PN}}} nk}$, \mathbf{P}_d is a diagonal matrix whose k^{th} element of the main diagonal is $P[k] = \frac{1}{\sqrt{N_{\text{PN}}}} \sum_{n=0}^{N_{\text{PN}}-1} p[n] e^{-j \frac{2\pi}{N_{\text{PN}}} nk}$. \mathbf{W} is still AWGN and the variance is the same as the time domain AWGN, namely $\sigma_W^2 = \sigma_w^2$. $\mathbf{H} = [H[0], H[1], \dots, H[N_{\text{PN}} - 1]]^T$ is the vector form of CFR and $H[k] = \sum_{l=0}^{L-1} h_l e^{-j \frac{2\pi}{N_{\text{PN}}} lk}$. The least square (LS) estimation [152] is performed:

$$\bar{\mathbf{H}} = (\mathbf{P}_d^H \mathbf{P}_d)^{-1} \mathbf{P}_d^H \mathbf{D} = \mathbf{H} + \underbrace{(\mathbf{P}_d^H \mathbf{P}_d)^{-1} \mathbf{P}_d^H \mathbf{W}}_{\boldsymbol{\xi}_{\bar{\mathbf{H}}}}. \quad (4.15)$$

From (4.15), it can be found that the training sequence should be selected such that its frequency response does not contain zero, or very small value. Otherwise, the noise component will be boosted. The estimate $\bar{\mathbf{H}}$ is unbiased. The MSE of the estimated CFR $\bar{\mathbf{H}}$ is:

$$\begin{aligned} \varepsilon_{\bar{\mathbf{H}}} &= \frac{1}{N_{\text{PN}}} \text{Tr} \left(\mathbb{E} [\boldsymbol{\xi}_{\bar{\mathbf{H}}} \boldsymbol{\xi}_{\bar{\mathbf{H}}}^H] \right) \\ &= \frac{1}{N_{\text{PN}}} \text{Tr} \left(\mathbb{E} [(\mathbf{P}_d^H \mathbf{P}_d)^{-1} \mathbf{P}_d^H \mathbf{W} \mathbf{W}^H \mathbf{P}_d (\mathbf{P}_d^H \mathbf{P}_d)^{-1}] \right) \\ &= \frac{\sigma_W^2}{N_{\text{PN}}} \text{Tr} \left((\mathbf{P}_d^H \mathbf{P}_d)^{-1} \right) \\ &= \frac{\sigma_W^2}{N_{\text{PN}}} \sum_{k=0}^{N_{\text{PN}}-1} \frac{1}{|P[k]|^2} \\ &= \frac{2N_{\text{PN}} \sigma_W^2}{N_{\text{PN}} + 1}, \end{aligned} \quad (4.16)$$

where $\text{Tr}(\cdot)$ is the trace operation. The last equation uses the results computed in Appendix C. It can be seen that the MSE of the PN-based channel estimation is inversely proportional to the SNR of the received PN sequence.

The CIR estimate $\bar{\mathbf{h}}$ is obtained by applying an N_{PN} -point IFFT (i.e. $\frac{1}{\sqrt{N_{\text{PN}}}} \mathbf{F}_{N_{\text{PN}}}^H$)⁽²⁾ to $\bar{\mathbf{H}}$.

$$\bar{\mathbf{h}} = \frac{1}{\sqrt{N_{\text{PN}}}} \mathbf{F}_{N_{\text{PN}}}^H \bar{\mathbf{H}} = \mathbf{h} + \underbrace{\frac{1}{\sqrt{N_{\text{PN}}}} \mathbf{F}_{N_{\text{PN}}}^H \boldsymbol{\xi}_{\bar{\mathbf{H}}}}_{\boldsymbol{\xi}_{\bar{\mathbf{h}}}}, \quad (4.17)$$

where $\mathbf{F}_{N_{\text{PN}}}$ is an $N_{\text{PN}} \times N_{\text{PN}}$ FFT matrix as shown in (2.54). $\mathbf{h} = [h_0, h_1, \dots, h_{L-1}, 0, \dots, 0]^T$ is the vector that contains the true CIR in the first L elements. The MSE of the

(2). According to the definition of the CFR (2.20), a scale factor $\frac{1}{\sqrt{N_{\text{PN}}}}$ should be multiplied to the IFFT matrix $\mathbf{F}_{N_{\text{PN}}}^H$.

estimate \bar{h} is:

$$\begin{aligned}
\varepsilon_{\bar{h}} &= \frac{1}{N_{\text{PN}}} \text{Tr} \left(\mathbb{E}[\boldsymbol{\xi}_{\bar{h}} \boldsymbol{\xi}_{\bar{h}}^{\mathcal{H}}] \right) \\
&= \frac{1}{N_{\text{PN}}} \mathbb{E} \left[\text{Tr}(\boldsymbol{\xi}_{\bar{h}} \boldsymbol{\xi}_{\bar{h}}^{\mathcal{H}}) \right] && (\because \mathbb{E}[\text{Tr}(\cdot)] = \text{Tr}(\mathbb{E}[\cdot])) \\
&= \frac{1}{N_{\text{PN}}} \mathbb{E} \left[\text{Tr}(\boldsymbol{\xi}_{\bar{h}}^{\mathcal{H}} \boldsymbol{\xi}_{\bar{h}}) \right] && (\because \text{Tr}(\mathbf{AB}) = \text{Tr}(\mathbf{BA})) \\
&= \frac{1}{N_{\text{PN}}^2} \mathbb{E} \left[\text{Tr}(\boldsymbol{\xi}_{\bar{H}}^{\mathcal{H}} \mathbf{F}_{N_{\text{PN}}} \mathbf{F}_{N_{\text{PN}}}^{\mathcal{H}} \boldsymbol{\xi}_{\bar{H}}) \right] && (\because \text{Tr}(c\mathbf{A}) = c \cdot \text{Tr}(\mathbf{A})) \\
&= \frac{1}{N_{\text{PN}}^2} \mathbb{E} \left[\text{Tr}(\boldsymbol{\xi}_{\bar{H}}^{\mathcal{H}} \boldsymbol{\xi}_{\bar{H}}) \right] && (\because \mathbf{F}_{N_{\text{PN}}} \mathbf{F}_{N_{\text{PN}}}^{\mathcal{H}} = \mathbf{I}_{N_{\text{PN}}}) \\
&= \frac{1}{N_{\text{PN}}^2} \text{Tr} \left(\mathbb{E}[\boldsymbol{\xi}_{\bar{H}} \boldsymbol{\xi}_{\bar{H}}^{\mathcal{H}}] \right) \\
&= \frac{1}{N_{\text{PN}}} \varepsilon_{\bar{H}} \\
&= \frac{2\sigma_W^2}{N_{\text{PN}} + 1}.
\end{aligned} \tag{4.18}$$

Moreover, when the length of the PN is large, the estimation error is approximately a Gaussian random variable according to the central limit theorem. That is $\xi_{\bar{h}} \sim \mathcal{N}(0, \varepsilon_{\bar{h}})$.

Equation (4.17) gives an N_{PN} -length CIR estimate. In fact, only the first L samples of \bar{h} contain useful components of the CIR estimate, while the latter $(N_{\text{PN}} - L)$ samples contain only noise. If the CIR length is known, the \bar{h} can be truncated to L -length so that only the useful part of the estimate is kept:

$$\hat{\mathbf{h}} = \mathbf{I}_{L \times N_{\text{PN}}} \bar{\mathbf{h}} = \mathbf{h} + \underbrace{\mathbf{I}_{L \times N_{\text{PN}}} \boldsymbol{\xi}_{\bar{h}}}_{\boldsymbol{\xi}_{\hat{h}}}, \tag{4.19}$$

where $\mathbf{I}_{L \times N_{\text{PN}}}$ is an $L \times N_{\text{PN}}$ matrix whose left $L \times L$ submatrix is an identity matrix. The length of CIR can either be estimated using the statistical characteristics of the channel [153], or be simply determined by the distance between the first and last significant channel paths in \bar{h} . Considering that the noise is white in both time and frequency domains, the average noise power over N_{PN} samples is reduced with a ratio of $\frac{L}{N_{\text{PN}}}$.

Consequently, the N -length CFR estimation $\hat{\mathbf{H}}$ is obtained by padding $N - L$ zeros to $\hat{\mathbf{h}}$ and then applying an N -point FFT (i.e. $\sqrt{N}\mathbf{F}_N$):

$$\hat{\mathbf{H}} = \sqrt{N}\mathbf{F}_N \mathbf{I}_{N \times L} \hat{\mathbf{h}} = \mathbf{H} + \underbrace{\sqrt{N}\mathbf{F}_N \mathbf{I}_{N \times L} \boldsymbol{\xi}_{\hat{h}}}_{\boldsymbol{\xi}_{\hat{H}}}, \tag{4.20}$$

where $\mathbf{I}_{N \times L}$ is the $N \times L$ matrix whose upper $L \times L$ submatrix is an identity matrix. It pads $N - L$ zeros to the L -length $\hat{\mathbf{h}}$. \mathbf{F}_N is the $N \times N$ FFT matrix as defined in (2.54).

It can be easily found that the CFR estimate \hat{H} is unbiased. The corresponding MSE is thus:

$$\begin{aligned} \varepsilon_{\hat{H}} &= \frac{1}{N} \text{Tr} \left(\mathbb{E} [\boldsymbol{\xi}_{\hat{H}} \boldsymbol{\xi}_{\hat{H}}^H] \right) \\ &= \frac{1}{N} \mathbb{E} \left[\text{Tr} \left(N \boldsymbol{\xi}_h^H \mathbf{I}_{L \times N_{\text{PN}}}^T \mathbf{I}_{N \times L}^T \mathbf{F}_N^H \mathbf{F}_N \mathbf{I}_{N \times L} \mathbf{I}_{L \times N_{\text{PN}}} \boldsymbol{\xi}_h \right) \right] \\ &= \mathbb{E} \left[\text{Tr} \left(\boldsymbol{\xi}_h^H \mathbf{I}_{L/N_{\text{PN}}} \boldsymbol{\xi}_h \right) \right] \\ &= \mathbb{E} \left[\text{Tr} \left(\bar{\boldsymbol{\xi}}_h^H \bar{\boldsymbol{\xi}}_h \right) \right] \\ &= L \varepsilon_{\bar{h}} \end{aligned} \tag{4.21}$$

$$= \frac{2L\sigma_W^2}{N_{\text{PN}} + 1}, \tag{4.22}$$

where $\mathbf{I}_{L/N_{\text{PN}}}$ is an $N_{\text{PN}} \times N_{\text{PN}}$ matrix whose first L elements of the main diagonal are 1's, rest elements are all 0's. $\bar{\boldsymbol{\xi}}_h$ is an L -length vector whose elements are the first L elements of $\boldsymbol{\xi}_h$. (4.21) also indicates the noise suppression effect of the truncation process. Compared to the result in (4.16), the MSE of estimate (4.20) is reduced with a ratio of $\frac{L}{N_{\text{PN}}}$.

With the method presented in this section, the channel estimation is made based on the knowledge of the frequency response of the PN sequence. It is a generic estimator that can adapt to the case using any training sequence (not necessarily PN) as long as its frequency response does not contain zeros.

4.6 Time Domain PN-based Channel Estimation

4.6.1 Correlation-based Estimator

Besides the frequency domain estimation method presented in the last section, the channel estimation can also be carried out in the time domain. The time domain method mainly exploits the normalized autocorrelation property of the PN sequence [149]:

$$C_p[n] = \frac{1}{N_{\text{PN}}} p[n+m] \otimes p[m] = \begin{cases} 1 & n = 0 \\ -\frac{1}{N_{\text{PN}}} & 0 < n < N_{\text{PN}} \end{cases}, \tag{4.23}$$

where \otimes denotes the circular correlation. The correlation result is shown in Figure 4.5.

When the PN is sufficiently long, i.e. $-\frac{1}{N_{\text{PN}}} \approx 0$, the normalized autocorrelation function C_p is approximately discrete-time unit impulse function. The CIR can be extracted from the received PN sequence using this impulse function. The circular cross-correlation between the received PN sequence and the local generated one is performed as:

$$\begin{aligned} R[n] &= p[n+m] \otimes d[m] \\ &= p[n+m] \otimes [p[m] \otimes h[m]] + p[n+m] \otimes w[m] \\ &= [p[n+m] \otimes p[m]] \otimes h[m] + p[n+m] \otimes w[m]. \end{aligned} \tag{4.24}$$

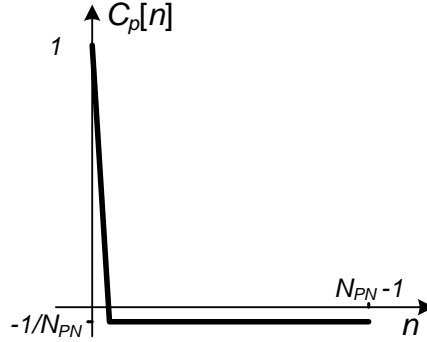


Figure 4.5: Circular correlation result of the m-sequence.

A straightforward time domain channel estimator is chosen as:

$$\begin{aligned} \bar{h}[n] &= \frac{1}{N_{\text{PN}}} R[n] = C_p[n] \otimes h[m] + \frac{1}{N_{\text{PN}}} p[n+m] \otimes w[m] \\ &= h[n] - \underbrace{\frac{1}{N_{\text{PN}}} \sum_{\substack{m=0 \\ m \neq n}}^{L-1} h[m]}_{\text{self interference}} + \underbrace{\frac{1}{N_{\text{PN}}} \sum_{q=0}^{N_{\text{PN}}-1} p[q] w[q+n]}_{\text{noise}}, 0 \leq n < N_{\text{PN}}. \end{aligned} \quad (4.25)$$

The CIR estimate suffers from the interference caused by the imperfect orthogonality between PN sequences as well as the noise. The estimator is asymptotically unbiased as $N_{\text{PN}} \rightarrow \infty$.

Rewrite the received PN sequence (4.1) in vector form:

$$\mathbf{d} = \mathbf{H}_{\text{circ}} \mathbf{p} + \mathbf{w} = \mathbf{P}_{\text{circ}} \mathbf{h} + \mathbf{w}, \quad (4.26)$$

where

$$\begin{aligned} \mathbf{p} &= [p[0], p[1], \dots, p[N_{\text{PN}} - 1]]^T, \\ \mathbf{d} &= [d[0], d[1], \dots, d[N_{\text{PN}} - 1]]^T, \\ \mathbf{w} &= [w[0], w[1], \dots, w[N_{\text{PN}} - 1]]^T \quad \text{and} \\ \mathbf{h} &= [h[0], h[1], \dots, h[L-1], \dots, 0]^T \end{aligned}$$

are the vector form of PN sequence, received PN sequence, AWGN, and CIR, respectively. \mathbf{H}_{circ} and \mathbf{P}_{circ} are the $N_{\text{PN}} \times N_{\text{PN}}$ circulant matrices with first row $[h_0, 0 \dots 0, h_{L-1}, \dots, h_1]$ and $[p[0], p[N_{\text{PN}} - 1], p[N_{\text{PN}} - 2], \dots, p[1]]$, respectively. The last equality uses the com-

mutativity of the convolution. The estimator in (4.25) is written as:

$$\begin{aligned}
\bar{\mathbf{h}} &= \frac{1}{N_{\text{PN}}} \mathbf{P}_{\text{cor}} \mathbf{d} = \frac{1}{N_{\text{PN}}} \underbrace{\mathbf{P}_{\text{cor}} \mathbf{P}_{\text{circ}}}_{\mathbf{Q}} \mathbf{h} + \frac{1}{N_{\text{PN}}} \mathbf{P}_{\text{cor}} \mathbf{w} \\
&= \underbrace{\begin{bmatrix} 1 & -\frac{1}{N_{\text{PN}}} & -\frac{1}{N_{\text{PN}}} & \cdots & -\frac{1}{N_{\text{PN}}} \\ -\frac{1}{N_{\text{PN}}} & 1 & -\frac{1}{N_{\text{PN}}} & \cdots & -\frac{1}{N_{\text{PN}}} \\ -\frac{1}{N_{\text{PN}}} & -\frac{1}{N_{\text{PN}}} & 1 & \cdots & -\frac{1}{N_{\text{PN}}} \\ \vdots & \vdots & \vdots & \ddots & \vdots \\ -\frac{1}{N_{\text{PN}}} & -\frac{1}{N_{\text{PN}}} & -\frac{1}{N_{\text{PN}}} & \cdots & 1 \end{bmatrix}}_{\mathbf{Q}} \begin{bmatrix} h_0 \\ \vdots \\ h_{L-1} \\ \vdots \\ 0 \end{bmatrix} \\
&\quad + \frac{1}{N_{\text{PN}}} \begin{bmatrix} p[0] & p[1] & p[2] & \cdots & p[N_{\text{PN}} - 1] \\ p[N_{\text{PN}} - 1] & p[0] & p[1] & \cdots & p[N_{\text{PN}} - 2] \\ p[N_{\text{PN}} - 2] & p[N_{\text{PN}} - 1] & p[0] & \cdots & p[N_{\text{PN}} - 3] \\ \vdots & \vdots & \vdots & \ddots & \vdots \\ p[1] & p[2] & p[3] & \cdots & p[0] \end{bmatrix} \begin{bmatrix} w[0] \\ w[1] \\ w[2] \\ \vdots \\ w[N_{\text{PN}} - 1] \end{bmatrix} \quad (4.27)
\end{aligned}$$

where \mathbf{P}_{cor} is an $N_{\text{PN}} \times N_{\text{PN}}$ circulant matrix with the first row $[p[0], p[1], \dots, p[N_{\text{PN}} - 1]]$. It performs the circular correlation operation. Denote $\mathbf{Q} \triangleq \frac{1}{N_{\text{PN}}} \mathbf{P}_{\text{cor}} \mathbf{P}_{\text{circ}}$. The estimation error $\boldsymbol{\xi}_{\bar{\mathbf{h}}} = \bar{\mathbf{h}} - \mathbf{h} = (\mathbf{Q} - \mathbf{I}_{N_{\text{PN}}}) \mathbf{h} + \frac{1}{N_{\text{PN}}} \mathbf{P}_{\text{cor}} \mathbf{w}$.

Suppose that the channel taps are uncorrelated. The MSE of the estimate is:

$$\begin{aligned}
\varepsilon_{\bar{\mathbf{h}}} &= \frac{1}{N_{\text{PN}}} \text{Tr} \left(\mathbb{E}[\boldsymbol{\xi}_{\bar{\mathbf{h}}} \boldsymbol{\xi}_{\bar{\mathbf{h}}}^{\mathcal{H}}] \right) \\
&= \frac{1}{N_{\text{PN}}} \text{Tr} \left(\mathbb{E}[(\mathbf{Q} - \mathbf{I}_{N_{\text{PN}}}) \mathbf{h} \mathbf{h}^{\mathcal{H}} (\mathbf{Q} - \mathbf{I}_{N_{\text{PN}}})^{\mathcal{H}}] \right) + \frac{1}{N_{\text{PN}}^3} \text{Tr} \left(\mathbb{E}[\mathbf{P}_{\text{cor}} \mathbf{w} \mathbf{w}^{\mathcal{H}} \mathbf{P}_{\text{cor}}^{\mathcal{H}}] \right) \\
&= \underbrace{\frac{1}{N_{\text{PN}}} \text{Tr} \left((\mathbf{Q} - \mathbf{I}_{N_{\text{PN}}}) \boldsymbol{\Lambda} (\mathbf{Q} - \mathbf{I}_{N_{\text{PN}}})^{\mathcal{H}} \right)}_{\text{self interference}} + \underbrace{\frac{\sigma_w^2}{N_{\text{PN}}^3} \text{Tr} \left(\mathbf{P}_{\text{cor}} \mathbf{P}_{\text{cor}}^{\mathcal{H}} \right)}_{\text{noise}}, \quad (4.28)
\end{aligned}$$

where $\boldsymbol{\Lambda}$ is a diagonal matrix whose first L elements of the main diagonal is $[\alpha_0^2, \alpha_1^2, \dots, \alpha_{L-1}^2]$, and the rest elements are all 0's. $\alpha_l^2 = \mathbb{E}[|h_l|^2]$ is the average power of the l^{th} channel tap. The power of the channel is normalized such that $\sum_{l=0}^{L-1} \alpha_l^2 = 1$.

The estimation error is composed of two parts: the interference resulting from the correlation of PN sequences and the noise. It can be found that the interference comes from the contributions of the off-diagonal elements in \mathbf{Q} . The interference vanishes if

$\mathbf{Q} = \mathbf{I}_{N_{\text{PN}}}$. More concretely, the interference is computed:

$$\begin{aligned}
& (\mathbf{Q} - \mathbf{I}_{N_{\text{PN}}}) \mathbf{\Lambda} (\mathbf{Q} - \mathbf{I}_{N_{\text{PN}}})^{\mathcal{H}} \\
= & \begin{bmatrix} \frac{1}{N_{\text{PN}}^2} (1 - \alpha_0^2) & \frac{1}{N_{\text{PN}}^2} (1 - \alpha_1^2 - \alpha_0^2) & \cdots & \frac{1}{N_{\text{PN}}^2} (1 - \alpha_{L-1}^2 - \alpha_0^2) & \cdots & \\ \frac{1}{N_{\text{PN}}^2} (1 - \alpha_0^2 - \alpha_1^2) & \frac{1}{N_{\text{PN}}^2} (1 - \alpha_1^2) & \cdots & \frac{1}{N_{\text{PN}}^2} (1 - \alpha_{L-1}^2 - \alpha_1^2) & & \\ \vdots & \vdots & \ddots & \vdots & & \\ \frac{1}{N_{\text{PN}}^2} (1 - \alpha_0^2 - \alpha_{L-1}^2) & \frac{1}{N_{\text{PN}}^2} (1 - \alpha_1^2 - \alpha_{L-1}^2) & \cdots & \frac{1}{N_{\text{PN}}^2} (1 - \alpha_{L-1}^2) & & \\ & & & & \frac{1}{N_{\text{PN}}^2} & \\ \vdots & \vdots & & \vdots & & \ddots \\ & & & & & \frac{1}{N_{\text{PN}}^2} \end{bmatrix}.
\end{aligned} \tag{4.29}$$

Therefore, the MSE of the estimator is finally:

$$\varepsilon_{\bar{h}} = \frac{N_{\text{PN}} - 1}{N_{\text{PN}}^3} + \frac{1}{N_{\text{PN}}} \sigma_w^2. \tag{4.30}$$

The second term in the expression of the MSE is proportional to the noise variance. That is to say, it decreases as the SNR increasing, while the first term is only determined by the length of the PN sequence and irrespective of the SNR level. In other words, it produces an estimation error floor with an MSE level of $(N_{\text{PN}} - 1)/N_{\text{PN}}^3$. For example, the error floor appears at 1.53×10^{-5} and 3.82×10^{-6} given the 255-length and 511-length PN sequences, respectively. It gives the best estimation result that the correlation-based estimator can achieve. In addition, the error floor appears when $(N_{\text{PN}} - 1)/N_{\text{PN}}^3 > 1/N_{\text{PN}} \sigma_w^2$, i.e. $\text{SNR}(\text{dB}) > 10 \log_{10} (N_{\text{PN}}^2 / (N_{\text{PN}} - 1))$, that is, 24.1 dB and 27.1 dB, given the 255-length and 511-length PN sequences, respectively.

4.6.2 Estimators with Reduced Error Floor

Due to the imperfect correlation property of the PN sequence, the correlation-based estimator proposed in the last section suffers from an estimation error floor at high SNR. Here we propose some new methods to eliminate or reduce the estimation error floor.

4.6.2.1 Method 1: Multiplying Inverse of Matrix

From the analysis in the last section, the estimation error floor comes from the fact that \mathbf{Q} is not a perfect identity matrix. Therefore, we propose to perform a linear transformation $\mathbf{\Omega}$ such that $\mathbf{\Omega} \mathbf{Q} = \mathbf{I}_{N_{\text{PN}}}$. Since \mathbf{Q} is known and always full rank for a given m -sequence, $\mathbf{\Omega} = \mathbf{Q}^{-1}$. A new estimator is obtained by left multiplying \mathbf{Q}^{-1} to the correlation-based estimator (4.27):

$$\hat{\mathbf{h}}_1 = \mathbf{Q}^{-1} \bar{\mathbf{h}} = \mathbf{h} + \frac{1}{N_{\text{PN}}} \mathbf{Q}^{-1} \mathbf{P}_{\text{cor}} \mathbf{w}. \tag{4.31}$$

The new estimator is unbiased. The estimation error is $\xi_{\hat{h}_1} = \frac{1}{N_{\text{PN}}}\mathbf{Q}^{-1}\mathbf{P}_{\text{cor}}\mathbf{w}$. The MSE of the estimator is:

$$\begin{aligned}\varepsilon_{\hat{h}_1} &= \frac{1}{N_{\text{PN}}}\text{Tr}\left(\mathbb{E}[\xi_{\hat{h}_1}\xi_{\hat{h}_1}^{\mathcal{H}}]\right) \\ &= \frac{1}{N_{\text{PN}}^3}\text{Tr}\left(\mathbb{E}\left[\mathbf{Q}^{-1}\mathbf{P}_{\text{cor}}\mathbf{w}\mathbf{w}^{\mathcal{H}}\mathbf{P}_{\text{cor}}^{\mathcal{H}}(\mathbf{Q}^{-1})^{\mathcal{H}}\right]\right) \\ &= \frac{\sigma_w^2}{N_{\text{PN}}^3}\text{Tr}\left(\mathbf{Q}^{-1}\mathbf{P}_{\text{cor}}\mathbf{P}_{\text{cor}}^{\mathcal{H}}(\mathbf{Q}^{-1})^{\mathcal{H}}\right).\end{aligned}\quad (4.32)$$

Considering that

$$\mathbf{Q}^{-1} = \left(\frac{1}{N_{\text{PN}}}\mathbf{P}_{\text{cor}}\mathbf{P}_{\text{circ}}\right)^{-1} = N_{\text{PN}}\mathbf{P}_{\text{circ}}^{-1}\mathbf{P}_{\text{cor}}^{-1}$$

and

$$(\mathbf{Q}^{-1})^{\mathcal{H}} = N_{\text{PN}}(\mathbf{P}_{\text{cor}}^{-1})^{\mathcal{H}}(\mathbf{P}_{\text{circ}}^{-1})^{\mathcal{H}}$$

it yields:

$$\begin{aligned}&\mathbf{Q}^{-1}\mathbf{P}_{\text{cor}}\mathbf{P}_{\text{cor}}^{\mathcal{H}}(\mathbf{Q}^{-1})^{\mathcal{H}} \\ &= N_{\text{PN}}^2\mathbf{P}_{\text{circ}}^{-1}\mathbf{P}_{\text{cor}}^{-1}\mathbf{P}_{\text{cor}}\mathbf{P}_{\text{cor}}^{\mathcal{H}}(\mathbf{P}_{\text{cor}}^{-1})^{\mathcal{H}}(\mathbf{P}_{\text{circ}}^{-1})^{\mathcal{H}} \\ &= N_{\text{PN}}^2\mathbf{P}_{\text{circ}}^{-1}(\mathbf{P}_{\text{circ}}^{\mathcal{H}})^{-1} \\ &= N_{\text{PN}}^2(\mathbf{P}_{\text{circ}}^{\mathcal{H}}\mathbf{P}_{\text{circ}})^{-1} \\ &= N_{\text{PN}}\mathbf{Q}^{-1}.\end{aligned}\quad (4.33)$$

As \mathbf{Q} is known for a given m-sequence, its inverse is easily obtained:

$$\mathbf{Q}^{-1} = \begin{bmatrix} \frac{2N_{\text{PN}}}{N_{\text{PN}}+1} & \frac{N_{\text{PN}}}{N_{\text{PN}}+1} & \frac{N_{\text{PN}}}{N_{\text{PN}}+1} & \cdots & \frac{N_{\text{PN}}}{N_{\text{PN}}+1} \\ \frac{N_{\text{PN}}}{N_{\text{PN}}+1} & \frac{2N_{\text{PN}}}{N_{\text{PN}}+1} & \frac{N_{\text{PN}}}{N_{\text{PN}}+1} & \cdots & \frac{N_{\text{PN}}}{N_{\text{PN}}+1} \\ \frac{N_{\text{PN}}}{N_{\text{PN}}+1} & \frac{N_{\text{PN}}}{N_{\text{PN}}+1} & \frac{2N_{\text{PN}}}{N_{\text{PN}}+1} & \cdots & \frac{N}{N+1} \\ \vdots & \vdots & \vdots & \ddots & \vdots \\ \frac{N_{\text{PN}}}{N_{\text{PN}}+1} & \frac{N_{\text{PN}}}{N_{\text{PN}}+1} & \frac{N_{\text{PN}}}{N_{\text{PN}}+1} & \cdots & \frac{2N_{\text{PN}}}{N_{\text{PN}}+1} \end{bmatrix}\quad (4.34)$$

Replace (4.33) and (4.34) into (4.32), the MSE can be computed as:

$$\varepsilon_{\hat{h}_1} = \frac{2\sigma_w^2}{N_{\text{PN}}+1}.\quad (4.35)$$

Comparing (4.35) and (4.30), it can be found that the estimation error floor is removed by the \mathbf{Q}^{-1} operation. In the meantime, the MSE in the low SNR region (before the error floor appearing) is approximately twice as much as it is before the operation.

The estimator (4.31) coincides with the LS estimator reported in [154] although they are derived from different perspectives. Moreover, this estimator performs a deconvolution of the received PN sequence in the time domain. Considering the duality of the time domain convolution and frequency domain multiplication, this estimator has the potential similarity with the frequency domain estimator as proposed in Section 4.5. They provide same estimation accuracy. However, this does not mean that the time domain

estimator has no interest. Because for any m-sequence with a given length, the matrix \mathbf{Q}^{-1} is identical and can be pre-computed and stored with quite little storage cost (only two real values have to be saved). This permits to carry out low-complexity channel estimation in the time domain. In addition, the performance of this estimator can be improved with the help of the knowledge of the channel length as it will be presented in the next subsection.

4.6.2.2 Method 1 with the Information of the Channel Length

Suppose the CIR length L is perfectly known, the estimate (4.27) is truncated to L -length. The estimator becomes:

$$\tilde{\mathbf{h}} = \mathbf{I}_{L \times N_{\text{PN}}} \bar{\mathbf{h}} = \bar{\mathbf{Q}} \mathbf{h} + \frac{1}{N_{\text{PN}}} \mathbf{I}_{L \times N_{\text{PN}}} \mathbf{P}_{\text{cor}} \mathbf{w}, \quad (4.36)$$

where \mathbf{h} is the L -length vector of the real CIR, $\bar{\mathbf{Q}}$ is an $L \times L$ matrix that contains the first L rows and columns of matrix \mathbf{Q} and is still full rank. Similar as in (4.31), we can left multiply the inverse matrix $\bar{\mathbf{Q}}^{-1}$ to estimator (4.36):

$$\hat{\mathbf{h}}'_1 = \bar{\mathbf{Q}}^{-1} \tilde{\mathbf{h}} = \mathbf{h} + \frac{1}{N_{\text{PN}}} \bar{\mathbf{Q}}^{-1} \mathbf{I}_{L \times N_{\text{PN}}} \mathbf{P}_{\text{cor}} \mathbf{w}. \quad (4.37)$$

The estimator is still unbiased. The estimation error is $\boldsymbol{\xi}_{\hat{\mathbf{h}}'_1} = \frac{1}{N_{\text{PN}}} \bar{\mathbf{Q}}^{-1} \mathbf{I}_{L \times N_{\text{PN}}} \mathbf{P}_{\text{cor}} \mathbf{w}$. The MSE of the estimation is:

$$\begin{aligned} \varepsilon_{\hat{\mathbf{h}}'_1} &= \frac{1}{L} \text{Tr} \left(\mathbb{E}[\boldsymbol{\xi}_{\hat{\mathbf{h}}'_1} \boldsymbol{\xi}_{\hat{\mathbf{h}}'_1}^{\mathcal{H}}] \right) \\ &= \frac{1}{L} \text{Tr} \left(\mathbb{E} \left[\frac{1}{N_{\text{PN}}^2} \bar{\mathbf{Q}}^{-1} \mathbf{I}_{L \times N_{\text{PN}}} \mathbf{P}_{\text{cor}} \mathbf{w} \mathbf{w}^{\mathcal{H}} \mathbf{P}_{\text{cor}}^{\mathcal{H}} \mathbf{I}_{L \times N_{\text{PN}}}^{\mathcal{H}} (\bar{\mathbf{Q}}^{-1})^{\mathcal{H}} \right] \right) \\ &= \frac{\sigma_w^2}{LN_{\text{PN}}} \text{Tr} \left(\bar{\mathbf{Q}}^{-1} \bar{\mathbf{Q}} (\bar{\mathbf{Q}}^{-1})^{\mathcal{H}} \right) \\ &= \frac{\sigma_w^2}{LN_{\text{PN}}} \text{Tr} \left(\bar{\mathbf{Q}}^{-1} \right). \end{aligned} \quad (4.38)$$

The inverse of the matrix $\bar{\mathbf{Q}}$ has a similar result as (4.34):

$$\bar{\mathbf{Q}}^{-1} = \begin{bmatrix} a & b & b & \cdots & b \\ b & a & b & \cdots & b \\ b & b & a & \cdots & b \\ \vdots & \vdots & \vdots & \ddots & \vdots \\ b & b & b & \cdots & a \end{bmatrix} \quad (4.39)$$

where

$$\begin{aligned} a &= 1 + \frac{L-1}{N_{\text{PN}}^2 + 2N_{\text{PN}} - N_{\text{PN}}L - L + 1}, \\ b &= \frac{N_{\text{PN}}}{N_{\text{PN}}^2 + 2N_{\text{PN}} - N_{\text{PN}}L - L + 1}. \end{aligned}$$

Therefore, the MSE of the estimation is finally:

$$\begin{aligned}\varepsilon_{\hat{h}'_1} &= \frac{N_{\text{PN}} - L + 2}{N_{\text{PN}}^2 + 2N_{\text{PN}} - N_{\text{PN}}L - L + 1} \sigma_w^2 \\ &= \frac{\frac{1}{N_{\text{PN}}}}{1 + \frac{1-L}{N_{\text{PN}}(N_{\text{PN}}-L+2)}} \sigma_w^2.\end{aligned}\quad (4.40)$$

Comparing (4.35) and (4.40), it can be found that the estimation MSE is reduced thanks to the truncation process. If $N_{\text{PN}} \gg L$, the MSE can be approximated by $\frac{\sigma_w^2}{N_{\text{PN}}}$. In the extreme case when $N_{\text{PN}} = L$, the estimator (4.37) turns to (4.31).

4.6.2.3 Method 2: Subtracting Interference

In this section, we propose another improved estimator which *subtracts* the contribution of the interference from the correlation-based estimation. Separate \mathbf{Q} into two parts:

$$\mathbf{Q} = \mathbf{I}_{N_{\text{PN}}} + \mathbf{\Delta}, \quad (4.41)$$

where $\mathbf{I}_{N_{\text{PN}}}$ is the identity matrix according to the elements in the main diagonal. $\mathbf{\Delta}$ contains all the off-diagonal elements of \mathbf{Q} and its main diagonal elements are 0's. The correlation-based estimator turns to:

$$\bar{\mathbf{h}} = \mathbf{h} + \mathbf{\Delta h} + \frac{1}{N_{\text{PN}}} \mathbf{P}_{\text{cor}} \mathbf{w}. \quad (4.42)$$

Suppose that the CIR length L is perfectly known, the estimate is truncated to L -length. The estimator becomes:

$$\tilde{\mathbf{h}} = \mathbf{h} + \bar{\mathbf{\Delta}} \mathbf{h} + \frac{1}{N_{\text{PN}}} \mathbf{I}_{L \times N_{\text{PN}}} \mathbf{P}_{\text{cor}} \mathbf{w}, \quad (4.43)$$

where $\bar{\mathbf{\Delta}}$ is the $L \times L$ matrix that contains the first L rows and columns of matrix $\mathbf{\Delta}$, \mathbf{h} is the L -length vector of the real CIR.

Considering that $\bar{\mathbf{\Delta}}$ is known for a given m-sequence, we propose to use the estimated $\tilde{\mathbf{h}}$ to reduce the interference. An estimator is thus:

$$\begin{aligned}\hat{\mathbf{h}}_2 &= \tilde{\mathbf{h}} - \bar{\mathbf{\Delta}} \tilde{\mathbf{h}} \\ &= \mathbf{h} + \bar{\mathbf{\Delta}} \mathbf{h} + \frac{1}{N_{\text{PN}}} \mathbf{I}_{L \times N_{\text{PN}}} \mathbf{P}_{\text{cor}} \mathbf{w} - \bar{\mathbf{\Delta}} \mathbf{h} - \bar{\mathbf{\Delta}}^2 \mathbf{h} - \frac{1}{N_{\text{PN}}} \bar{\mathbf{\Delta}} \mathbf{I}_{L \times N_{\text{PN}}} \mathbf{P}_{\text{cor}} \mathbf{w} \\ &= \mathbf{h} + \frac{1}{N_{\text{PN}}} \mathbf{I}_{L \times N_{\text{PN}}} \mathbf{P}_{\text{cor}} \mathbf{w} - \bar{\mathbf{\Delta}}^2 \mathbf{h} - \frac{1}{N_{\text{PN}}} \bar{\mathbf{\Delta}} \mathbf{I}_{L \times N_{\text{PN}}} \mathbf{P}_{\text{cor}} \mathbf{w},\end{aligned}\quad (4.44)$$

where $\bar{\mathbf{\Delta}}^2 \triangleq \bar{\mathbf{\Delta}} \bar{\mathbf{\Delta}}$. The estimation error is:

$$\xi_{\hat{h}_2} = -\bar{\mathbf{\Delta}}^2 \mathbf{h} + \frac{1}{N_{\text{PN}}} \mathbf{I}_{L \times N_{\text{PN}}} \mathbf{P}_{\text{cor}} \mathbf{w} - \frac{1}{N_{\text{PN}}} \bar{\mathbf{\Delta}} \mathbf{I}_{L \times N_{\text{PN}}} \mathbf{P}_{\text{cor}} \mathbf{w}.$$

The MSE of the estimate is:

$$\begin{aligned}
\varepsilon_{\hat{h}_2} &= \frac{1}{L} \text{Tr} \left(\mathbb{E}[\boldsymbol{\xi}_{\hat{h}_2} \boldsymbol{\xi}_{\hat{h}_2}^{\mathcal{H}}] \right) \\
&= \frac{1}{L} \text{Tr} \left(\mathbb{E} \left[\bar{\boldsymbol{\Delta}}^2 \mathbf{h} \mathbf{h}^{\mathcal{H}} (\bar{\boldsymbol{\Delta}}^2)^{\mathcal{H}} + \frac{1}{N_{\text{PN}}^2} \mathbf{I}_{L \times N_{\text{PN}}} \mathbf{P}_{\text{cor}} \mathbf{w} \mathbf{w}^{\mathcal{H}} \mathbf{P}_{\text{cor}}^{\mathcal{H}} \mathbf{I}_{L \times N_{\text{PN}}}^{\mathcal{H}} \right. \right. \\
&\quad \left. \left. + \frac{1}{N_{\text{PN}}^2} \bar{\boldsymbol{\Delta}} \mathbf{I}_{L \times N_{\text{PN}}} \mathbf{P}_{\text{cor}} \mathbf{w} \mathbf{w}^{\mathcal{H}} \mathbf{P}_{\text{cor}}^{\mathcal{H}} \mathbf{I}_{L \times N_{\text{PN}}}^{\mathcal{H}} \bar{\boldsymbol{\Delta}}^{\mathcal{H}} - \frac{1}{N_{\text{PN}}^2} \mathbf{I}_{L \times N_{\text{PN}}} \mathbf{P}_{\text{cor}} \mathbf{w} \mathbf{w}^{\mathcal{H}} \mathbf{P}_{\text{cor}}^{\mathcal{H}} \mathbf{I}_{L \times N_{\text{PN}}}^{\mathcal{H}} \bar{\boldsymbol{\Delta}}^{\mathcal{H}} \right. \right. \\
&\quad \left. \left. - \frac{1}{N_{\text{PN}}^2} \bar{\boldsymbol{\Delta}} \mathbf{I}_{L \times N_{\text{PN}}} \mathbf{P}_{\text{cor}} \mathbf{w} \mathbf{w}^{\mathcal{H}} \mathbf{P}_{\text{cor}}^{\mathcal{H}} \mathbf{I}_{L \times N_{\text{PN}}}^{\mathcal{H}} \right] \right) \\
&= \frac{1}{L} \text{Tr} \left(\bar{\boldsymbol{\Delta}}^2 \bar{\boldsymbol{\Lambda}} (\bar{\boldsymbol{\Delta}}^2)^{\mathcal{H}} + \frac{\sigma_w^2}{N_{\text{PN}}^2} \mathbf{I}_{L \times N_{\text{PN}}} \mathbf{P}_{\text{cor}} \mathbf{P}_{\text{cor}}^{\mathcal{H}} \mathbf{I}_{L \times N_{\text{PN}}}^{\mathcal{H}} + \frac{\sigma_w^2}{N_{\text{PN}}^2} \bar{\boldsymbol{\Delta}} \mathbf{I}_{L \times N_{\text{PN}}} \mathbf{P}_{\text{cor}} \mathbf{P}_{\text{cor}}^{\mathcal{H}} \mathbf{I}_{L \times N_{\text{PN}}}^{\mathcal{H}} \bar{\boldsymbol{\Delta}}^{\mathcal{H}} \right. \\
&\quad \left. - \frac{\sigma_w^2}{N_{\text{PN}}^2} \mathbf{I}_{L \times N_{\text{PN}}} \mathbf{P}_{\text{cor}} \mathbf{P}_{\text{cor}}^{\mathcal{H}} \mathbf{I}_{L \times N_{\text{PN}}}^{\mathcal{H}} \bar{\boldsymbol{\Delta}}^{\mathcal{H}} - \frac{\sigma_w^2}{N_{\text{PN}}^2} \bar{\boldsymbol{\Delta}} \mathbf{I}_{L \times N_{\text{PN}}} \mathbf{P}_{\text{cor}} \mathbf{P}_{\text{cor}}^{\mathcal{H}} \mathbf{I}_{L \times N_{\text{PN}}}^{\mathcal{H}} \right), \tag{4.45}
\end{aligned}$$

where $\bar{\boldsymbol{\Lambda}}$ is the $L \times L$ matrix that contains the first L rows and columns of matrix $\boldsymbol{\Lambda}$. The first term of the MSE expression is:

$$\begin{aligned}
&\bar{\boldsymbol{\Delta}}^2 \bar{\boldsymbol{\Lambda}} (\bar{\boldsymbol{\Delta}}^2)^{\mathcal{H}} = \\
&= \begin{bmatrix} \frac{L-1}{N_{\text{PN}}^2} & \frac{L-2}{N_{\text{PN}}^2} & \cdots & \frac{L-2}{N_{\text{PN}}^2} \\ \frac{L-2}{N_{\text{PN}}^2} & \frac{L-1}{N_{\text{PN}}^2} & \cdots & \frac{L-2}{N_{\text{PN}}^2} \\ \vdots & \vdots & \ddots & \vdots \\ \frac{L-2}{N_{\text{PN}}^2} & \frac{L-2}{N_{\text{PN}}^2} & \cdots & \frac{L-1}{N_{\text{PN}}^2} \end{bmatrix} \begin{bmatrix} \alpha_0^2 & 0 & \cdots & 0 \\ 0 & \alpha_1^2 & \cdots & 0 \\ \vdots & \vdots & \ddots & \vdots \\ 0 & 0 & \cdots & \alpha_{L-1}^2 \end{bmatrix} \begin{bmatrix} \frac{L-1}{N_{\text{PN}}^2} & \frac{L-2}{N_{\text{PN}}^2} & \cdots & \frac{L-2}{N_{\text{PN}}^2} \\ \frac{L-2}{N_{\text{PN}}^2} & \frac{L-1}{N_{\text{PN}}^2} & \cdots & \frac{L-2}{N_{\text{PN}}^2} \\ \vdots & \vdots & \ddots & \vdots \\ \frac{L-2}{N_{\text{PN}}^2} & \frac{L-2}{N_{\text{PN}}^2} & \cdots & \frac{L-1}{N_{\text{PN}}^2} \end{bmatrix} \\
&= \begin{bmatrix} \alpha_0^2 \frac{(L-1)^2}{N_{\text{PN}}^4} + \alpha_1^2 \frac{(L-2)^2}{N_{\text{PN}}^4} & & & + \alpha_{L-1}^2 \frac{(L-2)^2}{N_{\text{PN}}^4} \\ & \alpha_0^2 \frac{(L-2)^2}{N_{\text{PN}}^4} + \alpha_1^2 \frac{(L-1)^2}{N_{\text{PN}}^4} & & + \alpha_{L-1}^2 \frac{(L-2)^2}{N_{\text{PN}}^4} \\ & & \ddots & \\ & & & \alpha_0^2 \frac{(L-2)^2}{N_{\text{PN}}^4} + \alpha_1^2 \frac{(L-2)^2}{N_{\text{PN}}^4} & & + \alpha_{L-1}^2 \frac{(L-1)^2}{N_{\text{PN}}^4} \end{bmatrix} \tag{4.46}
\end{aligned}$$

The second term of the MSE is:

$$\begin{aligned}
&\frac{\sigma_w^2}{N_{\text{PN}}^2} \mathbf{I}_{L \times N_{\text{PN}}} \mathbf{P}_{\text{cor}} \mathbf{P}_{\text{cor}}^{\mathcal{H}} \mathbf{I}_{L \times N_{\text{PN}}}^{\mathcal{H}} \\
&= \frac{\sigma_w^2}{N_{\text{PN}}} \mathbf{I}_{L \times N_{\text{PN}}} \mathbf{Q} \mathbf{I}_{L \times N_{\text{PN}}}^{\mathcal{H}} \\
&= \frac{\sigma_w^2}{N_{\text{PN}}} \bar{\mathbf{Q}}, \tag{4.47}
\end{aligned}$$

where $\bar{\mathbf{Q}}$ is the $L \times L$ matrix that contains the first L rows and columns of matrix \mathbf{Q} .

The third term of the MSE,

$$\begin{aligned}
& \frac{\sigma_w^2}{N_{\text{PN}}^2} \bar{\Delta} \mathbf{I}_{L \times N_{\text{PN}}} \mathbf{P}_{\text{cor}} \mathbf{P}_{\text{cor}}^H \mathbf{I}_{L \times N_{\text{PN}}}^H \bar{\Delta}^H \\
&= \frac{\sigma_w^2}{N_{\text{PN}}} \bar{\Delta} \bar{\mathbf{Q}} \bar{\Delta}^H \\
&= \frac{\sigma_w^2}{N_{\text{PN}}} \begin{bmatrix} \frac{(L-1)(N_{\text{PN}}-L+2)}{N_{\text{PN}}^3} & & & \\ & \frac{(L-1)(N_{\text{PN}}-L+2)}{N_{\text{PN}}^3} & & \\ & & \ddots & \\ & & & \frac{(L-1)(N_{\text{PN}}-L+2)}{N_{\text{PN}}^3} \end{bmatrix}. \quad (4.48)
\end{aligned}$$

The fourth term of the MSE,

$$\begin{aligned}
& \frac{\sigma_w^2}{N_{\text{PN}}^2} \mathbf{I}_{L \times N_{\text{PN}}} \mathbf{P}_{\text{cor}} \mathbf{P}_{\text{cor}}^H \mathbf{I}_{L \times N_{\text{PN}}}^H \bar{\Delta}^H \\
&= \frac{\sigma_w^2}{N_{\text{PN}}} \bar{\mathbf{Q}} \bar{\Delta}^H \\
&= \frac{\sigma_w^2}{N_{\text{PN}}} \begin{bmatrix} \frac{L-1}{N_{\text{PN}}^2} & & & \\ & \frac{L-1}{N_{\text{PN}}^2} & & \\ & & \ddots & \\ & & & \frac{L-1}{N_{\text{PN}}^2} \end{bmatrix}. \quad (4.49)
\end{aligned}$$

The fifth term has the same trace as the fourth one. In general, putting (4.46), (4.47), (4.48) and (4.49) into (4.45), it yields:

$$\varepsilon_{\hat{h}_2} = \frac{(L-1)(L^2-3L+3)}{N_{\text{PN}}^4 L} + \frac{1}{N_{\text{PN}}} \sigma_w^2 + \frac{(L-1)(2-L-N_{\text{PN}})}{N_{\text{PN}}^4} \sigma_w^2. \quad (4.50)$$

Comparing (4.50) with (4.30), the estimation error floor is reduced by a ratio of approximately $\left(\frac{L}{N_{\text{PN}}}\right)^2$.

Note that, [138] reported a similar idea of using the estimated CIR to mitigate the interference between different channel taps. Being different from the method proposed in this section, the method of [138] iteratively finds several strongest paths and removes the interference introduced by them from the N_{PN} -length correlation results. In the channel where there are only a few dominant paths, the method of [138] needs less complexity than the method proposed in this section. However, in the channels that have many paths with similar power, the proposed method can achieve better performance than the method of [138] because the proposed method removes the interference of all paths.

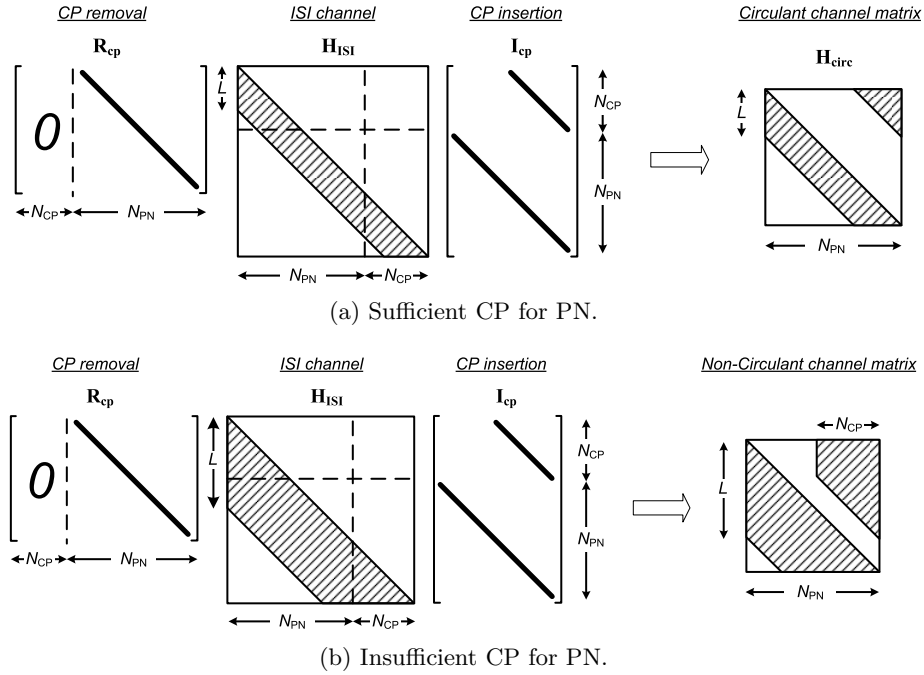


Figure 4.6: The equivalent channel matrices given sufficient and insufficient long CP for PN sequence.

4.7 Estimators in the Insufficient long CP Case

In previous sections, we have studied the channel estimation techniques using PN sequence when the CP of the PN is longer than the channel length. In this section, we investigate the situation when CP is sufficient.

Recall the CP insertion and removal processes as shown in Section 2.2.1. After discarding the CP portion, the received PN sequence of the i^{th} OFDM data symbol becomes:

$$\mathbf{d}^{(i)} = \mathbf{R}_{\text{cp}} \mathbf{H}_{\text{ISI}} \mathbf{I}_{\text{cp}} \mathbf{p}^{(i)} + \mathbf{R}_{\text{cp}} \mathbf{H}_{\text{IBI}} \mathbf{x}^{(i-1)} + \mathbf{w}, \quad (4.51)$$

where \mathbf{H}_{ISI} and \mathbf{H}_{IBI} are $\nu \times \nu$ matrices (c.f. (2.59) and (2.60)) representing the intra- and inter-block interferences, respectively. $\mathbf{x}^{(i-1)}$ is the vector composed of the last ν samples of the previous OFDM data symbol. \mathbf{I}_{cp} is the $\nu \times N_{\text{PN}}$ matrix representing the CP insertion. \mathbf{R}_{cp} is the $N_{\text{PN}} \times \nu$ matrix representing CP removal. The definitions of \mathbf{I}_{cp} and \mathbf{R}_{cp} are similar to (2.55) and (2.61). If $N_{\text{CP}} \geq L$, as depicted in Figure 4.6a, $\mathbf{R}_{\text{cp}} \mathbf{H}_{\text{ISI}} \mathbf{I}_{\text{cp}} = \mathbf{H}_{\text{circ}}$ is a circulant matrix and $\mathbf{R}_{\text{cp}} \mathbf{H}_{\text{IBI}} = \mathbf{0}_{N_{\text{PN}} \times N_{\text{PN}}}$. The PN-based estimators presented in the previous sections can directly be used. However, as shown in

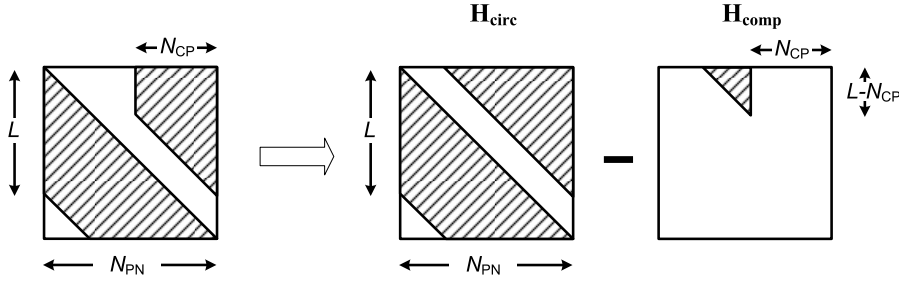
Figure 4.7: Separate $\mathbf{R}_{\text{cp}}\mathbf{H}_{\text{ISI}}\mathbf{I}_{\text{cp}}$.

Figure 4.6b, if the length of the CP is insufficient ($N_{\text{CP}} < L$),

$$\mathbf{R}_{\text{cp}}\mathbf{H}_{\text{ISI}}\mathbf{I}_{\text{cp}} = \begin{bmatrix} h_0 & 0 & \cdots & 0 & h_{N_{\text{CP}}} & \cdots & h_1 \\ \vdots & \ddots & \ddots & 0 & h_{L-1} & \ddots & \vdots \\ \vdots & & & \ddots & \ddots & \ddots & h_{L-1} \\ h_{L-1} & & & h_0 & & \ddots & 0 \\ 0 & \ddots & & & \ddots & \ddots & \vdots \\ \vdots & \ddots & \ddots & & & & 0 \\ 0 & \cdots & 0 & h_{L-1} & \cdots & \cdots & h_0 \end{bmatrix}_{N_{\text{PN}} \times N_{\text{PN}}} \quad (4.52)$$

which is no longer circulant matrix. In addition, the IBI can not be totally eliminated. In this case, the IBI matrix becomes:

$$\mathbf{R}_{\text{cp}}\mathbf{H}_{\text{IBI}} = \begin{bmatrix} 0 & \cdots & 0 & h_{L-1} & \cdots & h_{N_{\text{CP}}+1} \\ \vdots & \ddots & & \ddots & \ddots & \vdots \\ \vdots & & & h_{L-1} & & 0 \\ \vdots & & & \ddots & \ddots & \vdots \\ 0 & \cdots & \cdots & 0 & \cdots & \cdots \end{bmatrix}_{N_{\text{PN}} \times \nu} \quad (4.53)$$

Although the $\mathbf{R}_{\text{cp}}\mathbf{H}_{\text{ISI}}\mathbf{I}_{\text{cp}}$ is not a circulant matrix, it still has a structure close to the circulant one. More specifically, as shown in Figure 4.7, we can separate the matrix $\mathbf{R}_{\text{cp}}\mathbf{H}_{\text{ISI}}\mathbf{I}_{\text{cp}}$ as two parts, namely a circulant part and a compensation one:

$$\mathbf{R}_{\text{cp}}\mathbf{H}_{\text{ISI}}\mathbf{I}_{\text{cp}} = \mathbf{H}_{\text{circ}} - \mathbf{H}_{\text{comp}}, \quad (4.54)$$

system [64, 155]. More precisely, the average power⁽³⁾ of the interference is:

$$\sigma_I^2 = 2 \cdot \frac{1}{N_{\text{PN}}} \sum_{k=N_{\text{CP}}+1}^{L-1} \sum_{l=k}^{L-1} |h_l|^2. \quad (4.59)$$

Based on the analysis above, we can reduce the interference via cyclicity reconstruction and residual IBI cancellation. A first means is to compensate the missing elements in the circulant channel matrix to restore the cyclicity. In practice, it is not possible to perfectly compensate the channel matrix because the CIR is unknown. However, using well estimated CIR can achieve a good approximation. It leads:

$$\tilde{\mathbf{d}}^{(i)} = \mathbf{d}^{(i)} + \hat{\mathbf{H}}_{\text{comp}} \mathbf{p}^{(i)} \approx \mathbf{H}_{\text{circ}} \mathbf{p}^{(i)} + \mathbf{R}_{\text{cp}} \mathbf{H}_{\text{IBI}} \mathbf{x}^{(i-1)} + \mathbf{w}, \quad (4.60)$$

where the elements in $\hat{\mathbf{H}}_{\text{comp}}$ are obtained from the channel estimate of the previous OFDM symbol. The compensated PN sequence (4.60) adapts to the previously proposed estimators but contains more disturbance.

In addition to the cyclicity reconstruction, a second means is to subtract the IBI component from the received PN sequence. With the knowledge of previously detected data symbols $\hat{\mathbf{x}}^{(i-1)}$, IBI can be eliminated:

$$\check{\mathbf{d}}^{(i)} = \tilde{\mathbf{d}}^{(i)} - \mathbf{R}_{\text{cp}} \hat{\mathbf{H}}_{\text{IBI}} \hat{\mathbf{x}}^{(i-1)} \approx \mathbf{H}_{\text{circ}} \mathbf{p}^{(i)} + \mathbf{w}. \quad (4.61)$$

Various detection algorithms such as [110, 156, 142, 14] can be used to determine the data symbols $\hat{\mathbf{x}}^{(i-1)}$ providing many performance-complexity trade-offs.

4.8 Complexity

In order to compare the computational complexity of each estimation method, we investigate the required basic operations, i.e. multiplication, additions and FFT's etc., to obtain the *CIR estimate*. The complexities of these methods are listed in Table 4.3.

For the frequency domain method as shown in (4.15), the perfect and received PN sequences should be first converted to the frequency domain. This requires twice N_{PN} -length FFT. The following frequency domain LS estimation needs N_{PN} complex divisions. The conversion of N_{PN} -length CFR to CIR takes an N_{PN} -length IFFT. In general, the frequency domain estimation method requires three N_{PN} -length (I)FFT's and N_{PN} complex divisions which is $\mathcal{O}(N_{\text{PN}} \cdot \log N_{\text{PN}})$.

Concerning the time domain estimation methods, the basic operation is the N_{PN} -length circular convolution. If the correlator is used, it takes N_{PN} multiplications and $N_{\text{PN}} - 1$ additions for each delay. That is N_{PN}^2 multiplications and $N_{\text{PN}} \times (N_{\text{PN}} - 1)$ additions for an N_{PN} -length CIR estimate. Therefore, the complexity is $\mathcal{O}(N_{\text{PN}}^2)$. Considering that the circular convolution can also be computed by using the FFT [38], the computational complexity can be reduced to $\mathcal{O}(N_{\text{PN}} \cdot \log N_{\text{PN}})$.

(3). Although the contribution of the interference concentrates in the first few samples of the received PN sequence, the estimators will spread the interference to other samples through either the FFT/IFFT operation or the circular convolution process. Therefore, it is still meaningful to investigate the average interference power over the whole length of the PN sequence.

Table 4.3: Complexities of the PN-based channel estimation methods.

Estimator		Complexity
Basic methods	Frequency domain estimator (4.15)	$\mathcal{O}(N_{\text{PN}} \log N_{\text{PN}})$
	Time domain correlation-based estimator (4.25)	$\mathcal{O}(N_{\text{PN}}^2)$ or $\mathcal{O}(N_{\text{PN}} \log N_{\text{PN}})$
Improved time domain estimators	multiplying matrix inverse N_{PN} -length (4.31)	$\mathcal{O}(N_{\text{PN}}^2)$
	multiplying matrix inverse L -length (4.37)	$\mathcal{O}(L^2)$
	subtracting interference (4.44)	$\mathcal{O}(L^2)$
Insufficient CP case	cyclicity compensation	$\mathcal{O}((L - N_{\text{CP}})^2)$
	IBI removal	$\mathcal{O}(N \cdot \log N)$

As far as the improved time domain estimators are concerned, additional complexities are needed by the estimation refinement process. For instance, in the estimator (4.31), the matrix \mathbf{Q}^{-1} depends only on the PN sequence and can thus be pre-computed and stored⁽⁴⁾. The matrix multiplication needs N_{PN}^2 multiplications and $N_{\text{PN}} \times (N_{\text{PN}} - 1)$ additions. Therefore, the additional complexity is $\mathcal{O}(N_{\text{PN}}^2)$. In the meantime, the matrix multiplication can be carried out in a reduced length L as done in estimator (4.37). For the same reason as in the previous situation, the computation of $\bar{\mathbf{Q}}^{-1}$ does not need any additional effort. The corresponding additional complexity is therefore reduced to $\mathcal{O}(L^2)$.

For the estimator (4.44), the refinement of each channel tap needs $(L - 1)$ additions. That is, $L \times (L - 1)$ additions are required for the whole CIR estimate, which corresponds to a computational complexity of $\mathcal{O}(L^2)$.

In the case when the CP of the PN is not sufficient, since the channel estimate is obtained from the previous OFDM symbol and is thus known, the operation for compensating the cyclicity in (4.60) requires $(L - N_{\text{CP}}) \times (L - N_{\text{CP}})/2$ multiplications and $(L - N_{\text{CP}}) \times (L - N_{\text{CP}} + 2)/2$ additions. In other words, the complexity is $\mathcal{O}((L - N_{\text{CP}})^2)$, which depends on how much the channel spreads beyond the CP of the PN sequence. Concerning the IBI removal in (4.61), more operations are needed. The major operations are allocated to acquiring the estimate of the time domain data symbol $\hat{x}^{(i-1)}$. It is obtained from the decision results of the previous OFDM data symbol via an N -point IFFT. After that, the same amount of operations as in the cyclicity compensation case are spent by the convolution and IBI subtraction process. In all, the computational complexity of the IBI removal process is $\mathcal{O}(N \cdot \log N)$.

To conclude, the frequency and time domain estimators have similar computational complexities, namely $\mathcal{O}(N_{\text{PN}} \cdot \log N_{\text{PN}})$. For the time domain estimator, more operations should be carried out to mitigate the estimation error floor. The additional complexity ranges from $\mathcal{O}(L^2)$ to $\mathcal{O}(N_{\text{PN}}^2)$ as given in Table 4.3.

(4). In fact, the matrix \mathbf{Q}^{-1} is quite structured. There are only two values – diagonal and off-diagonal elements. Hence, it is not necessary to store all the elements of the matrix. Instead, it is smarter to record the two values only. The cost of the storage is therefore negligible.

4.9 Performance Evaluation and Analysis

In this section, we evaluate the performance of different estimators through simulations and compare it with the results obtained from the analyses in the previous sections. The TU-6 and HT channel models are employed in the simulations. The power delay profiles of the two channels are given in Table 2.2 and Table 2.3 in Section 2.1.5.2. The maximum delay spreads of TU-6 and HT channels are $5 \mu\text{s}$ and $17.2 \mu\text{s}$, according to $L = 43$ and $L = 135$ samples of the DTMB systems. The channels are assumed to be stationary throughout the experiments of this chapter. The SFN channel which has extremely long time delay spread is used to evaluate the performance of the insufficient CP case. The detailed description of SFN channel is given in Section 2.1.7. Other simulation parameters are chosen according to the specifications of the DTMB system [4]. The power of GI is the same as the data symbols.

4.9.1 Frequency Domain and Time Domain Estimators

The first experiment gives the performance comparison of time domain and frequency domain estimators. Figure 4.8 and Figure 4.9 present the MSE of the N -length CFR estimates in the TU-6 channel and SFN channel, respectively. The performance with different PN sequences is also given in the figures. From the results, we can have following observations and conclusions:

1. *The time domain correlation-based estimator outperforms the frequency domain method.* The advantage comes from the strong noise suppression and useful signal extraction abilities of the correlation of PN sequences. Comparing the MSE expressions of (4.30) and (4.18), it can be found that the MSE of the frequency estimator is η time higher than the time domain estimator in low SNR region. η is a constant value for a given PN sequence. For instance, $\eta \approx 2.0$ given an m-sequence. Therefore, the time domain estimator is about twice better than the frequency estimator in the low SNR region. However, the time domain estimator suffers an estimation error floor in the high SNR region. Such a floor is observed in the Figure 4.8 around 25 dB and 30 dB given 255- and 511-length PN sequences, respectively. This proves with the analysis in Section 4.6.1.

2. *Truncation of the CIR estimate to the real channel length is an effective way to reduce the overall CFR estimation error.* From the analysis, the truncation reduces the MSE of the N -length CFR estimate with a ratio of $\frac{L}{N_{\text{PN}}}$. The improvement comes from the elimination of noise components in the estimate longer than L . This is verified in Figure 4.9 by the fact that the improvement brought by the truncation decreases compared to a shorter CIR case as in Figure 4.8.

3. *Better estimation performance can be achieved when longer PN sequences are used in the time domain correlation based estimator.* From the analysis in (4.30) and also from the simulations, longer PN sequence results in lower estimation error floor. When the truncation process is taken into account, the gain of using longer PN sequence is more obvious because it achieves a higher noise reduction factor $\frac{L}{N_{\text{PN}}}$.

4. *The numerical results coincide with the analytical ones.* It proves that the analyses presented in the previous sections are correct and the assumptions and approximations made in the derivations are reasonable. Therefore, the analytical expressions of the MSE of the estimators are reliable and can be used in further studies.

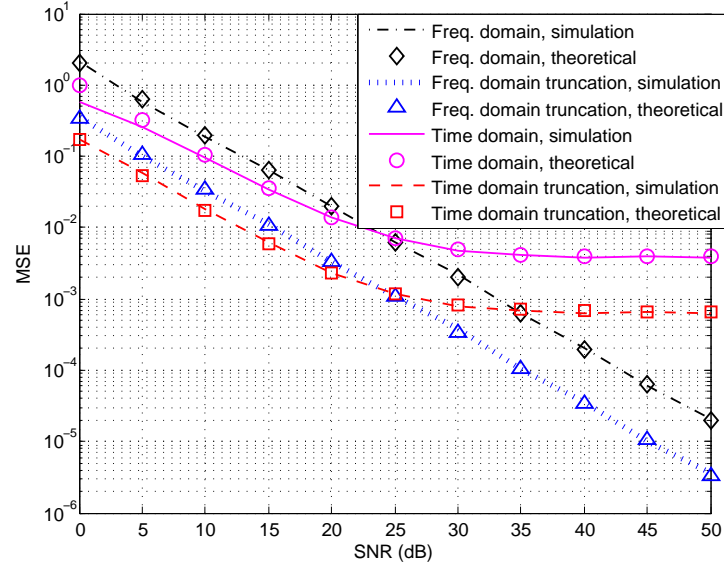
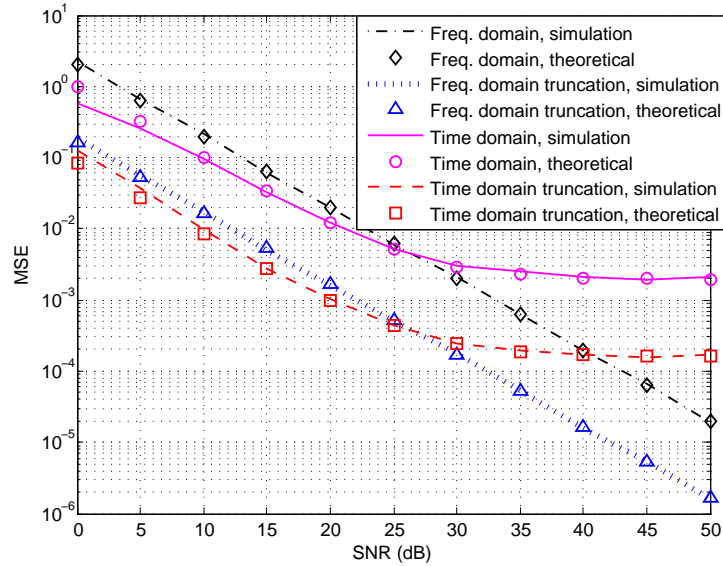
(a) $\nu = 420$, $N_{\text{PN}} = 255$, $N_{\text{CP}} = 165$.(b) $\nu = 945$, $N_{\text{PN}} = 511$, $N_{\text{CP}} = 434$.

Figure 4.8: Performance comparison of time and frequency domain estimators. Results are obtained from 500 realizations of TU-6 channel with a maximum delay of $5 \mu\text{s}$, or $L = 43$ samples of the DTMB system.

4.9.2 Improved Time Domain Estimators

In this experiment, the performance of the proposed improved time domain estimators is investigated with different PN sequences and channels as shown in Figure 4.10 and Figure 4.11. Numerical results are also compared with the analytical ones. The curves labeled by ‘correlation-based’, ‘improved 1’, ‘improved 1 truncation’ and ‘improved 2’ present

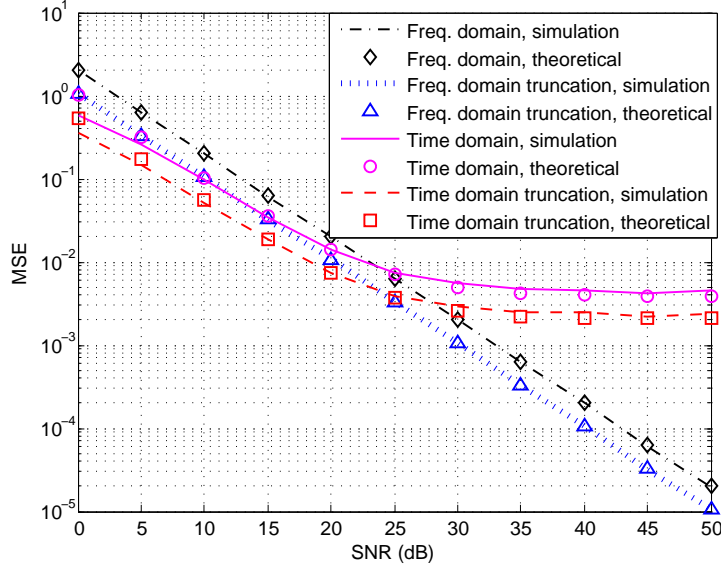
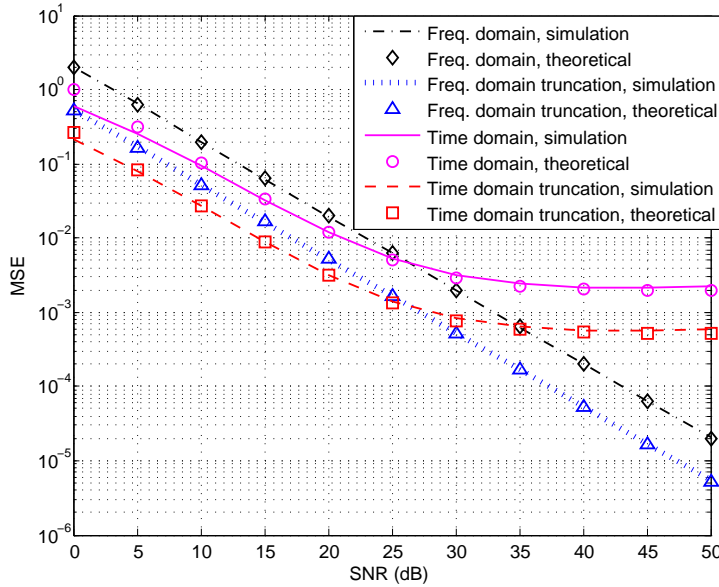
(a) $\nu = 420$, $N_{\text{PN}} = 255$, $N_{\text{CP}} = 165$.(b) $\nu = 945$, $N_{\text{PN}} = 511$, $N_{\text{CP}} = 434$.

Figure 4.9: Performance comparison of time and frequency domain estimators. Results are obtained from 500 realizations of Hilly Terrain (HT) channel with a maximum delay of $17.2 \mu\text{s}$, or $L = 135$ samples of the DTMB system.

the performance of the basic time-domain correlation-based estimator (4.27) and the three improved estimators (4.31), (4.37) and (4.44), respectively.

From the figures, we can have the following observations:

1. *Multiplying the inverse of the correlation matrix ('improved 1') eliminates the estimation error floor but boosts the noise variance as well.* The left multiplying the inverse

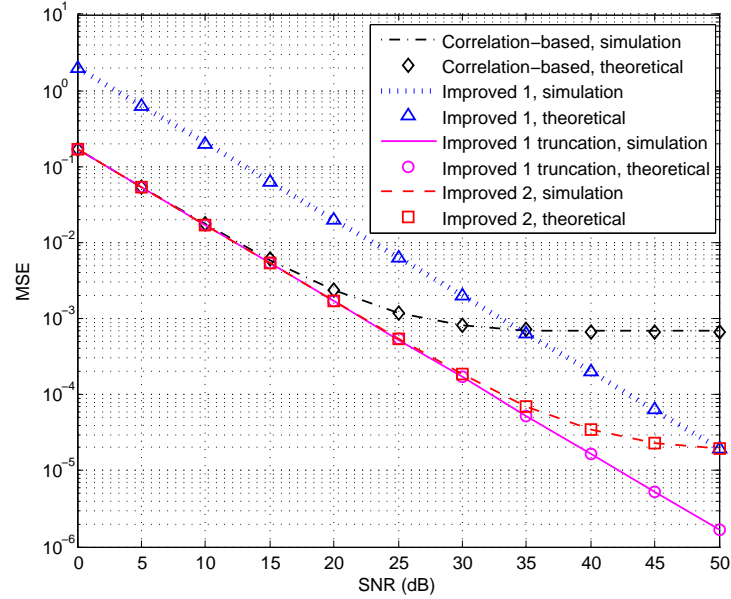
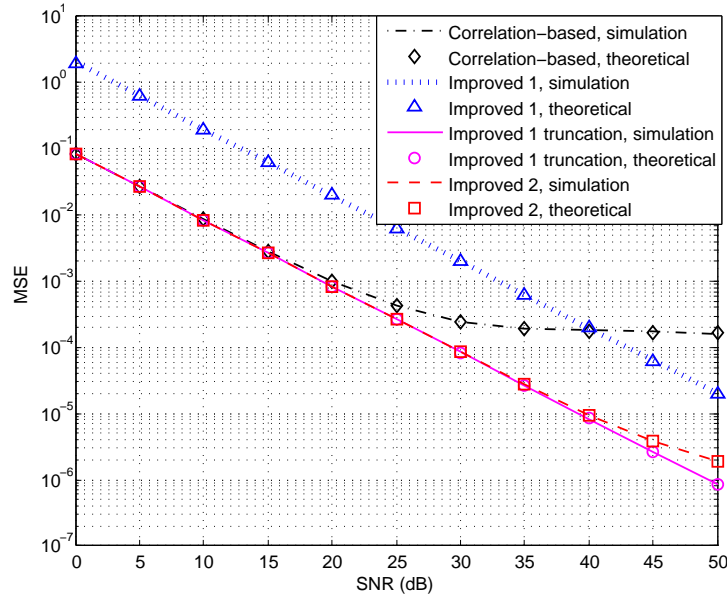
(a) $\nu = 420$, $N_{\text{PN}} = 255$, $N_{\text{CP}} = 165$.(b) $\nu = 945$, $N_{\text{PN}} = 511$, $N_{\text{CP}} = 434$.

Figure 4.10: Performance comparison of several time domain estimators. Results are obtained from 500 realizations of TU-6 channel with a maximum delay of $5 \mu\text{s}$, or $L = 43$ samples of the DTMB system.

of the correlation matrix to the basic time domain estimator in (4.31) can create a perfect identity matrix. This leads to an unbiased estimator. In other words, the estimation error floor is removed as shown by the dashed blue line in Figure 4.10. The side effect of

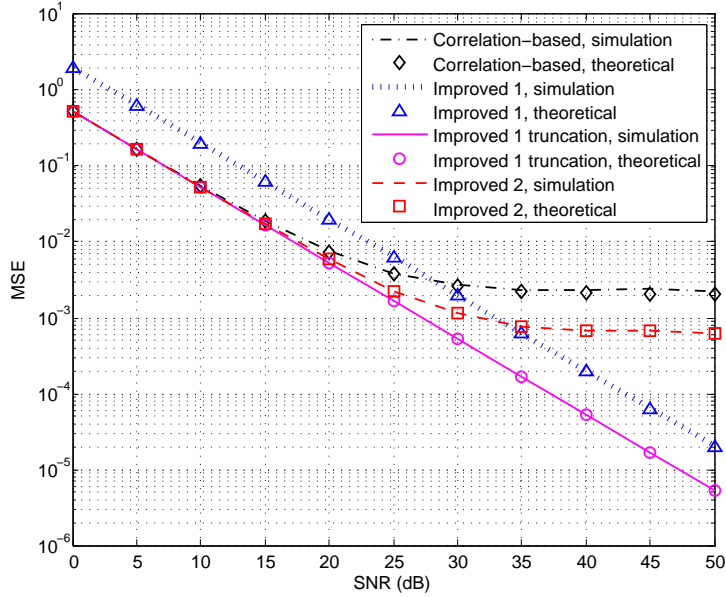
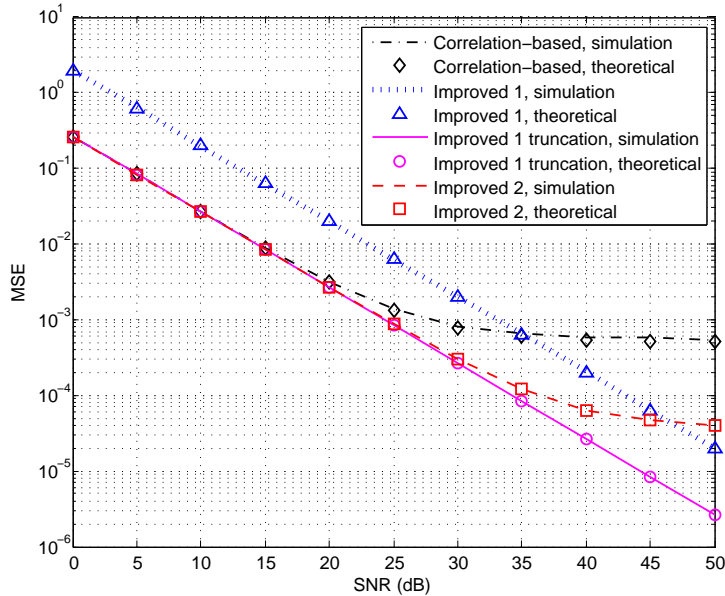
(a) $\nu = 420$, $N_{\text{PN}} = 255$, $N_{\text{CP}} = 165$.(b) $\nu = 945$, $N_{\text{PN}} = 511$, $N_{\text{CP}} = 434$.

Figure 4.11: Performance comparison of several time domain estimators. Results are obtained from 500 realizations of Hilly Terrain (HT) channel with a maximum delay of $17.2 \mu\text{s}$, or $L = 135$ samples of the DTMB system.

this operation is that the noise power is also boosted. It can be seen that the estimation performance is degraded in low SNR region (comparing the curve with \triangle and \diamond).

2. The method multiplying the inverse of correlation matrix with the truncated CIR estimate ('improved 1 truncation') and the one subtracting the estimated CIR ('improved 2')

do not boost the noise while reducing the estimation error floor. The MSE keeps the same level as the basic correlation-based estimator in the low SNR region. In the meantime, the estimation error floor is reduced to a lower level. For instance, the estimation error floor using the ‘improved 2’ estimator is reduced to about 2×10^{-5} when 255-length PN sequence is adopted. The reduction is more significant when a longer PN sequence is used as explained in Section 4.6.2.1.

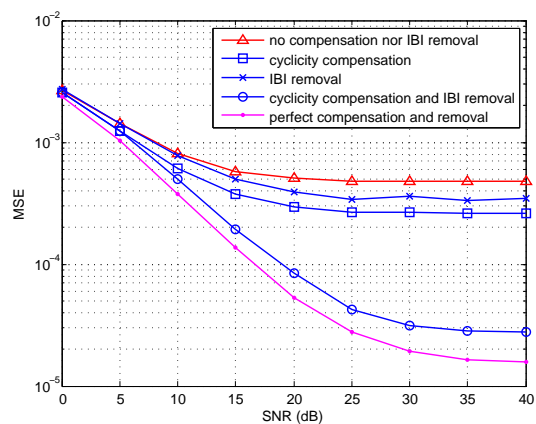
3. *The ‘improved 1 truncation’ method performs better with a longer channel spread.* Comparing Figure 4.10a and Figure 4.11a, it can be found that the performance of the ‘improved 2’ method degrades with the increase of the channel length. The performance achieves an error floor at a high MSE level. The ‘improved 2’ method performs worse than the ‘improved 1’ method in high SNR region. In contrast, the ‘improved 1 truncation’ method outperforms the others. It does not produce estimation error floor until an MSE level of 1×10^{-5} .

4.9.3 Improved Estimators in the Insufficient CP Case

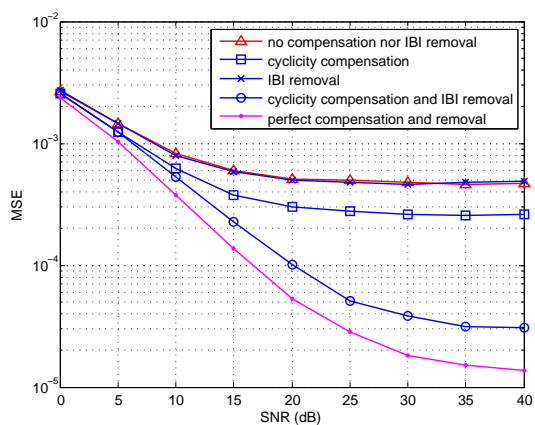
In this section, we investigate the proposed estimator in the insufficient CP case. The method is tested in the SFN channel with 8 km propagation difference which results an overall time delay spread of $31.64 \mu\text{s}$ corresponding to 244 samples of the DTMB system. The channel delay spread is about the same length of the PN sequence while longer than the CP of the PN sequence ($N_{\text{CP}} = 165$). The length of the PN sequence determines the maximum length of the channel that can be estimated using this PN sequence. In other words, the channel estimation method approaches the maximum length that the 255-length PN sequence can support. The power attenuation factor is set to 0.5 which indicates that a large amount of IBI will affect the PN sequence. The performance is obtained from 200 realizations of the channel. The time domain correlation-based estimator is used in this experiment. A hard decision feedback is used in the IBI removal process. The performance of the estimator without cyclicity compensation and IBI removal and with perfect compensation and removal is given as the benchmarks. Simulation results with different constellations are presented in Figure 4.12.

From the results, we find that either cyclicity compensation or the IBI removal can partially improve the performance. The performance of cyclicity compensation operation is robust with different constellations. Whereas, the improvement brought by the IBI removal is affected by the accuracy of the hard decision. It is higher with QPSK and lower with higher order constellations. In the lower order constellation cases, the decision is more reliable and the IBI removal consequently achieves better performance, while more decision errors may occur in the higher order constellation cases, which compromises the performance of the IBI removal. The combination of them will achieve even greater improvements. For example, the MSE of the CIR estimation is reduced from 4.91×10^{-4} to 3.74×10^{-5} with the help of the cyclicity compensation and IBI removal in the QPSK case. The improvements decreases in the higher order constellation cases such as 16QAM and 64QAM. This degradation can be attributed to the worse quality of the IBI removal in the higher order constellation cases.

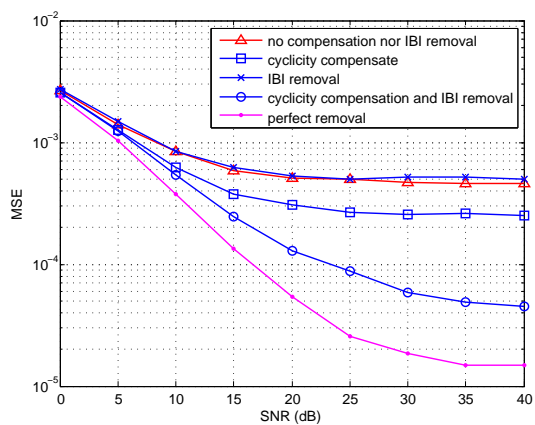
We should note that the performance of the cyclicity compensation and IBI removal processing relies on the quality of the channel estimate and the estimated data symbols (which also depend on the channel estimate) of the previous OFDM symbol. It means that these two techniques should be integrated with robust estimators. Otherwise, it may



(a) QPSK



(b) 16QAM



(c) 64QAM

Figure 4.12: Performance of estimator with IBI removal and cyclic reconstruction. $\nu = 420$, $N_{\text{PN}} = 255$, $N_{\text{CP}} = 165$. Time domain correlation-based estimator is used. 200 realizations of SFN channel with $L = 244$.

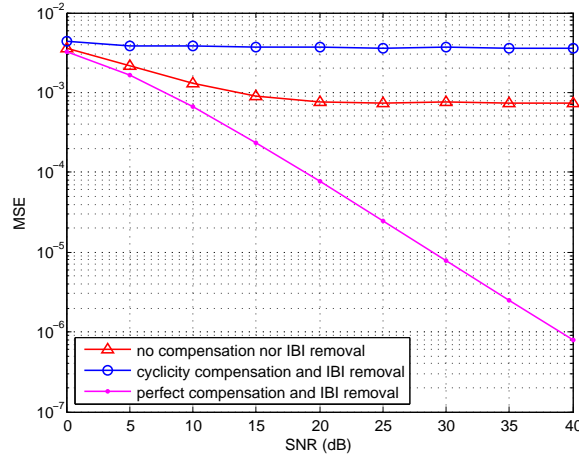


Figure 4.13: Performance of estimator with IBI removal and cyclic reconstruction. $\nu = 420$, $N_{\text{PN}} = 255$, $N_{\text{CP}} = 165$. Frequency domain estimator is used. 200 realizations of SFN channel with $L = 244$.

result in error propagation which seriously degrades the performance of the estimator. An example is shown in Figure 4.13 where the frequency domain estimator is used in the experiment. From the discussion in Section 4.10.1, we know that the frequency domain estimator is sensitive to the excessive IBI and can not provide reliable estimation results. Consequently, the estimated CIR and data symbols are not accurate enough. It is risky to use them to refine the channel estimation. This can be verified in Figure 4.13. The frequency domain estimator with compensation and IBI removal using the estimated CIR performs worse than the one without compensation and IBI removal. It indicates that the “compensation” and “removal” processing in fact introduces more disturbance than it eliminates. Therefore, the cyclicity compensation and IBI removal techniques are not effective for the frequency domain estimator.

4.10 Discussions about the PN-based Channel Estimation Strategies

4.10.1 Time or Frequency Domain Estimator?

Recall that the frequency domain LS estimator can be written as element-wise division:

$$\hat{H}[k] = \frac{D[k]}{P[k]} = H[k] + \frac{W[k]}{P[k]}, \quad (4.62)$$

where $W[k]$ follows the zero mean complex Gaussian distribution. As proved in Appendix B, the variance of the estimation error is affected by the *norm of the frequency response of the PN sequence*. As far as the m-sequence is concerned, the norm of its frequency response is written as:

$$P[k] = \begin{cases} \frac{1}{N_{\text{PN}}} & k = 0 \\ \frac{N_{\text{PN}}+1}{N_{\text{PN}}} & 0 < k < N_{\text{PN}} \end{cases}, \quad (4.63)$$

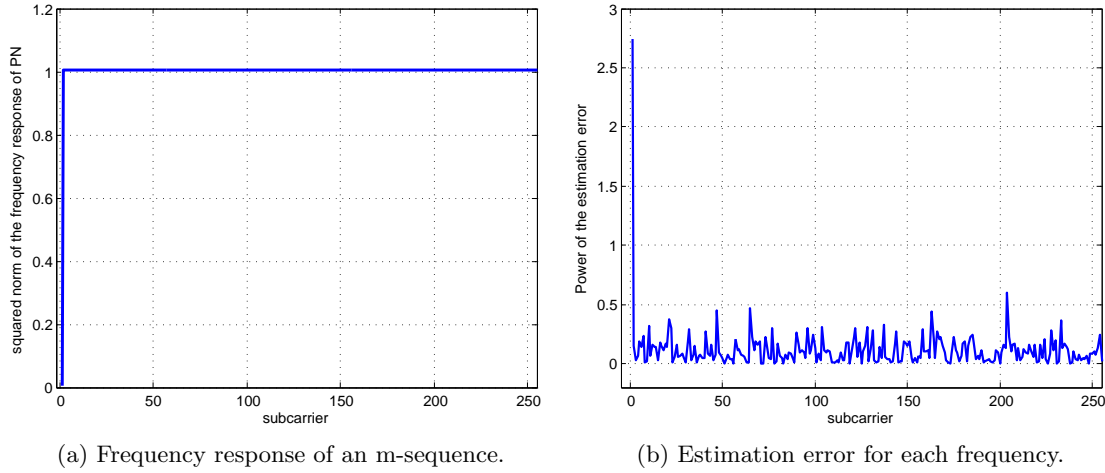


Figure 4.14: Noise boost in the frequency domain estimator.

which is proved in Appendix C. Figure 4.14a depicts the squared norm of a 255-length m-sequence. It can be observed that the frequency response of m-sequence is flat in all frequencies except the direct current (DC) where the value of the frequency response is relatively small. The small value in denominator will introduce a boost in the division (and also the estimation) result. Figure 4.14b gives an example of the estimation error for each frequency. It can be found that the error for the DC component is significantly higher than for any other position. That is to say, the channel estimate for the DC position is sensitive to the noise and is not reliable.

The inaccuracy of the CFR estimate for the DC component may not be dangerous for the frequency domain equalization. Because the subcarrier corresponding to the DC is not used for transmitting data in many OFDM systems such as WLAN and WiMAX to avoid the problem in the digital-to-analog converter (DAC). In the DTMB system, the DC subcarrier carries the TPS information which is protected by the spreading code and is robust to the channel estimation error. However, we should note that the channel estimate is not only used for the equalization but also for the PN removal. The estimation error in the DC component in the frequency domain turns to an universal error for all the channel taps in the time domain. This results in a low-quality PN removal and consequently introduces interference to OFDM data symbols. Furthermore, IBI brings strong disturbance to the PN sequence and in some channel conditions the influence of this IBI is concentrated around the DC [155]. This aggravates the noise boost problem in the frequency domain estimator. Therefore, some algorithms such as [76] force the channel taps with small values to zero to reduce the disturbance from the CFR estimation error in the DC component.

In contrast, the cross-correlation-based time domain estimator does not have the error boost problem. The estimation error due to the imperfect correlation property of the PN sequence is spread in the time domain and can be partially removed by truncating the CIR estimate to L samples. The estimation performance of time domain estimator is better than the frequency domain estimator. However, the side effect of the time domain

estimator is that it produces an estimation error floor in high SNR region. This may result in a decoding error floor for higher order constellations. Therefore, some additional treatments such as those proposed in Section 4.6.2 should be used to mitigate this error floor.

In general, when the m-sequence is used as training sequence for channel estimation, the frequency domain estimator may encounter more difficulties than the time domain estimator. The latter is more effective when the channel is shorter than the CP and is more robust when the channel is long. Therefore, a better PN-based, more precisely m-sequence-based, channel estimation algorithm is *the time domain correlation-based estimator in combination with some error floor reduction processing* as presented in Section 4.6.2.

4.10.2 Linear or Circular Cross-Correlation?

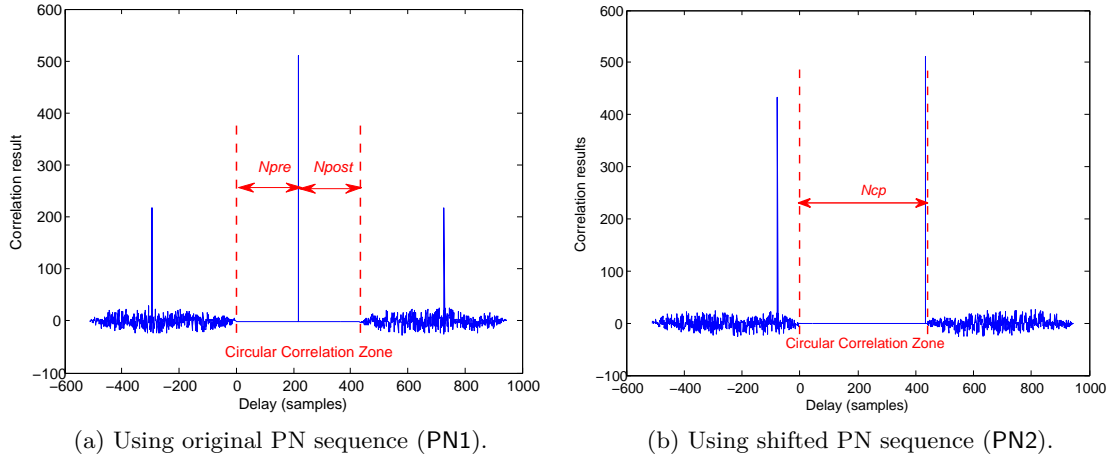


Figure 4.15: Linear cross-correlation between the GI and the PN sequence.

Another interesting question regarding the PN-based channel estimation is whether linear or circular cross-correlation should be used in the time domain estimator. The time domain estimators proposed in Section 4.6.1 are based on the circular cross-correlation of the m-sequence. A premise of these estimators is that the system is already symbol synchronized, i.e. the estimator knows where one OFDM symbol starts. Considering that the TDS-OFDM based system normally adopts a linear cross-correlation for the symbol synchronization, it would be better if the time domain estimator can reuse this linear cross-correlator for channel estimation.

Figure 4.15 presents the linear cross-correlation results of the GI and the PN sequence. In Figure 4.15a, GI is cross correlated with the original PN sequence, i.e. the PN1 (c.f. Figure 4.1). Due to the pre- and post-circular extension, there exists a region where the linear cross-correlation result is equal to the circular one, namely the result equals to N_{PN} for the in-phase correlation and equals to -1 for others. This is because the linear cross-correlation is equivalent to the circular one for some specific shifts thanks to the prefix and postfix. The length of the region that correlation result is equal to -1 is N_{pre} and N_{post}

samples before and after the main correlation peak. This provides a possible solution of using linear cross-correlation to make the channel estimation. When the channel spread is shorter than both prefix and postfix, the linear cross-correlation results after the position of main peak gives the same CIR estimate as it can be obtained using a circular cross-correlation. Note that, this solution is a trade-off between the tolerable channel spread length and the computational complexity.

However, if the shifted PN sequence, i.e. the PN2 as shown in Figure 4.1, is used in the linear cross-correlation, the main peak (in-phase correlation) appears at the end of the circular correlation zone. That is to say we can not obtain the CIR estimate via linear cross-correlation using the shift PN sequence.

4.11 Conclusion

In this chapter, we have investigated the channel estimation methods exploring the PN sequence in the GI of TDS-OFDM based systems. More specifically, we first analyzed the structure of the GI specified in DTMB which is, up to now, the only system adopting TDS-OFDM. Based on the structure, we studied the channel estimation methods in either frequency or time domains using the PN sequence, instead of the whole GI, as the training sequence. The frequency domain estimator is easy to implement with least complexity while the time domain estimator provides better performance but suffers from an estimation error floor. In order to mitigate the error floor in the time domain estimator, we proposed novel improved estimators which either turn the convolution matrix of PN sequence into a perfect identity matrix, or subtract the interference using the estimated CIR. Through the analyses and simulations, we have found that the proposed estimator ‘improved 1 truncation’ is the preferred estimation method, because it achieves the best performance in all PN-based estimators which are considered in our study. Furthermore, we analyzed the performance loss due to long CIR. Based on the analysis, we proposed improved methods including the cyclicity compensation and the IBI removal process.

Data-aided Channel Estimation for TDS-OFDM

As the accurate channel estimate plays a very important role in the reception of the TDS-OFDM signal and the PN-sequence-based estimation is not effective in the channel with extremely long delay spread, it is necessary to propose some techniques to enhance the performance of the channel estimation for TDS-OFDM. In this chapter, we propose a novel data-aided channel estimation algorithm with reduced computational complexity for TDS-OFDM.

5.1 Introduction

Several PN sequence based channel estimation algorithms have been discussed in the previous chapter. The main idea is to use a CP to protect the training sequence from ISI. However, in some cases with long channel delays such as in the SFN case of broadcasting, ISI could spread beyond the GI and affect the training sequence. The performance of the PN based channel estimation is degraded with the increase of channel length. Hence it is necessary to propose an effective channel estimation method that is applicable in worse channel situations.

In some literatures [140, 146], CP is designed the same length as the training sequence. That means the overall length of the GI (CP + training sequence) is twice as long as the maximum channel length. The expense is the same as the overhead (CP + frequency domain pilots for channel estimation) in a well-designed CP-OFDM system. TDS-OFDM does not enjoy the advantage of high-efficiency any more. It is meaningful to limit the GI length from the system efficiency perspective.

A possible solution of improving the training based channel estimation is to use the semiblind channel estimation approaches [119, 114, 118, 120]. It exploits the *a priori* information from the received data to enhance the estimation performance. Several interesting semiblind channel estimation methods are overviewed in Section 4.1. Their main disadvantage lies in the mass storage and intense computation. Besides, the performance loss may also result from the mismatch of the data model adopted by the semiblind methods.

The iterative receiver structure is another promising means to refine the training based channel estimation. This leads to the decision-directed channel estimation [110, 157, 158]. The principle of the decision-directed algorithms is to determine the transmitted data symbols using a previous channel estimate and then to estimate the current channel

based on the decided data symbols with the assumption that all the decisions are correct. In fact, this assumption puts the algorithm in a dilemma: if all the decisions are correct, there is no benefit from refining the channel estimation; otherwise, if the decisions are not correct, the resulting channel estimation is not reliable, either. If the iterative approach is used, it is inevitable to cause error propagation problem. Besides, it is not robust in higher order constellations as the decision is more risky when the Euclidean distance between constellation points reduces.

To overcome this problem, some literatures proposed to use the so-called soft decision [156, 159, 160] which makes hard decision only to the reliable symbols while keeping the uncertainty in the unreliable ones. This method can reduce the possibility of error decisions and improve the estimation compared to the hard decision [159, 160].

Meanwhile, some researches were carried out to find a better decision boundary or decision region [161, 140, 141, 142]. Only the symbols falling into decision regions are hard decided and selected as the “virtual pilots”. The difficulty of this method is that it is not easy to adaptively adjust the decision boundary and a predetermined decision threshold may not suitable to all channel conditions. Besides, since virtual pilots may appear in arbitrary subcarrier positions, it can hardly guarantee the construction of the channel estimation over all subcarriers through interpolation.

Some works, such as [110, 162, 163, 164], proposed to exploit the error correction capability of the channel coding in the decision-directed approaches. These methods use the decoded data output from decoder to regenerate the transmitted data symbols. As the involved channel coding can correct some errors, the quality of virtual pilots is much higher than those obtained from the previous decision-directed methods. The decision-directed channel estimation is accordingly improved. Whereas, the implicit hard decision embedded in these approaches substantially destroys the information pertaining to how likely each of the possible symbols might be [165].

The Turbo equalization is believed to be a good solution to recover transmitted data where soft information on the code bits is exchanged between the equalizer and decoder in an iterative fashion [166, 167, 168, 169]. Both equalizer and decoder are soft-in soft-output (SISO) to prevent the loss of information in the iterative process. Using a similar philosophy, the turbo channel estimation adopts the soft information feedback from the decoder as input reference signal [170, 171, 172, 173, 174, 14]. The Turbo channel estimation techniques, on one hand, adopt error correcting channel codings to provide reliable virtual reference sequence, on the other hand, keep the reliability of the reference sequence to direct the channel estimation. Therefore, it provides a superior performance than the hard decision-directed ones [172]. The turbo channel estimation often suffers from the high computational load for the decoding process and for the computing of soft information. This disadvantage is further aggravated in the iterative process. Another obvious drawback of the turbo channel estimation is the extremely high complexity and long time delay, especially in the systems which equip sophisticated channel decoder and deep interleaver. **For example, the DTMB system adopts LDPC code and convolutional interleaver with a time delay of 170 (or 510) OFDM blocks. Turbo channel estimation seems to be cumbersome in such systems.**

Among the existing channel estimation methods, some have the merit to be low complex but are not enough robust in face of severe channel conditions, and others are more efficient but remain very complex to use in practical systems. Therefore, it is interesting

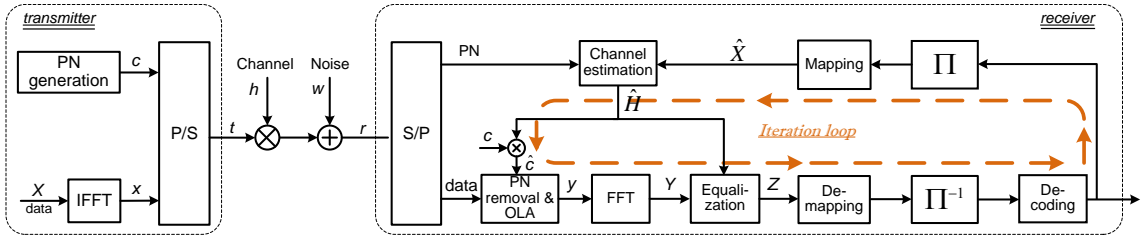


Figure 5.1: Block diagram of TDS-OFDM system using classical Turbo channel estimation.

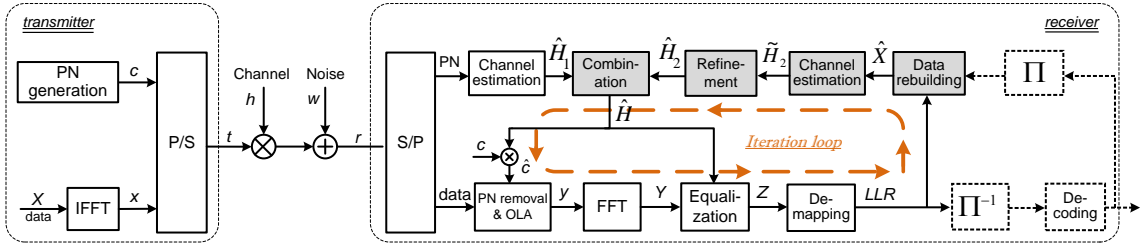


Figure 5.2: Block diagram of TDS-OFDM system using proposed data-aided channel estimation. The shaded blocks are the processings used for the proposed method. The dashed blocks are the additional processings needed for the turbo channel estimation.

to propose some new data-aided channel estimation techniques with practical time delay and computational complexity, which is the main concern of this chapter.

5.2 General Presentation of the Proposed Method

The block diagram of the classical iterative turbo channel estimation algorithm [14] is shown in Figure 5.1. The decoded information output from the decoder is used to rebuild the data symbols which consequently serve as the virtual training sequence for the data-aided channel estimation. We notice that the iteration loop contains de-interleaver, decoder and interleaver which introduce intensive computation and long time delay. Iterative process aggravates this burden with respect to the iteration times.

In this chapter, we propose a low-complex but efficient channel estimation algorithm which makes use of the advantages of training-based channel estimation method as well as those of the data-aided approach. In contrast to the classical turbo channel estimation algorithm, the proposed method excludes the deinterleaving, channel decoding and interleaving processings from the feedback loop as shown in Figure 5.2. In other words, the estimated data symbols used for data-aided channel estimation are rebuilt directly using the output information of the demapper. Hence, we go in for avoiding these cumbersome processes in the iteration loop.

The main idea is (a) *excluding the channel decoder, interleaver and de-interleaver from the iterative process*, and (b) *exploiting the correlation property of the CFR to obtain improved estimation results*. More concretely, the proposed method is performed in three steps:

1. An initial channel estimation is made using the PN-sequence-based channel estimation. It is then used to equalize the received signal.
2. A data-aided channel estimation is carried out using the rebuilt *soft data symbols*. More concretely, we propose to rebuild data symbols using the likelihood information output from the *demapper*, and then make a coarse channel estimation based on these rebuilt symbols. Being different from the traditional decision feedback methods, no decision is made on the rebuilt symbols. Hence, the proposed method does not cause error propagation due to imprudent hard decisions. The uncertainty (noise) is kept in the rebuilt soft data symbols. Consequently, several techniques including one-dimensional (1-D)/two-dimensional (2-D) moving average and Wiener filtering (as demonstrated in the “Refinement” block in Figure 5.2) are proposed to mitigate the noise effect. Since the data-aided channel estimation does not include the interleaving and channel decoding processes, the computational complexity is obviously reduced compared to the traditional turbo channel estimation.
3. The channel estimates obtained in the previous two steps are combined according to their mean square error (MSE) in order to achieve an optimal combination.

The proposed methods operate in an iterative manner to progressively refine the channel estimation results.

Excluding decoder from the iteration loop can significantly reduce the computational complexity. However, if no extrinsic information is introduced in each iteration, the rebuilt data symbols converge to the hard decision results even though the soft demapping is used. In fact, a better combined channel estimation is obtained after each iteration, which means better PN sequence removal, namely less interference caused by the residual PN sequence in the next iteration. This can be recognized as some additional information being introduced in the iteration loop. Moreover, as refining the quality of the channel estimate can improve the quality of the symbol decoding, the channel refinement process can therefore be seen as virtual error correction process in the iterative process as well. Consequently, rebuilt data symbols with improved quality will lead to more reliable data-aided channel estimate in the next iteration. This is how the propose method progressively improve the channel estimation quality. In general, the channel estimate refinement and combination provide a channel estimate with better quality and virtually play the role of the error correction block in the conventional turbo schemes. It is the source where the benefit of the iterative process comes from.

5.3 Data-aided Instantaneous Channel Estimation

5.3.1 Received Signal

Suppose that the length of the GI exceeds the delay spread of the channel, there is no ISI between two adjacent OFDM symbols. After PN removal and OLA processes, the received time domain signal becomes a circular of the CIR and data:

$$r^{(i)}[n] = \sum_{l=0}^{L-1} h_l^{(i)} x^{(i)}[n-l]_N + w'[n] + \xi[n], 0 \leq n < N, \quad (5.1)$$

where $w'(n)$ is the noise after OLA with an equivalent noise power $\sigma_{w'}^2 = \frac{N+\nu}{N}\sigma_w^2$, $\xi[n]$ is the contribution of the residual PN sequence due to the imperfect PN removal. After the FFT operation, the received frequency domain TDS-OFDM signal has a similar representation as CP-OFDM:

$$Y[i, k] = \frac{1}{\sqrt{N}} \sum_{n=0}^{N-1} y^{(i)}[n] e^{-j\frac{2\pi}{N}nk} = H[i, k]X[i, k] + W''[i, k] \quad (5.2)$$

where W'' is the combination of AWGN and the interference with a variance $\sigma_{W''}^2 = \sigma_{W'}^2 + \sigma_I^2$. Using the initial channel estimate $\hat{H}[i, k]$, the TDS-OFDM signal can thus be easily equalized by a one-tap equalizer:

$$Z[i, k] = \frac{Y[i, k]}{\hat{H}[i, k]}. \quad (5.3)$$

5.3.2 Soft Data Symbol Rebuilding

The soft-output demapper demodulates the complex data symbols into Log-likelihood ratio (LLR) of bits [175]. The LLR $\lambda_l[i, k]$ corresponding to the l^{th} bit of the $(i, k)^{\text{th}}$ equalized data symbol $Z[i, k]$ is defined as:

$$\lambda_l[i, k] \triangleq \log \frac{P(b[i, k, l] = 1 | Z[i, k])}{P(b[i, k, l] = 0 | Z[i, k])}, \quad (5.4)$$

where the $P(b[i, k, l] = 1 | Z[i, k])$ is the conditional probability of the l^{th} bit equal to 1 given $Z[i, k]$. The sign of the LLR decides the corresponding bit equal to 1 or 0, and its absolute value gives the reliability of the decision. Based on the LLR, the probabilities of a bit equal to 1 and 0 are:

$$P(b[i, k, l] = 1 | Z[i, k]) = \frac{e^{\lambda_l[i, k]}}{1 + e^{\lambda_l[i, k]}}, \quad (5.5)$$

and

$$P(b[i, k, l] = 0 | Z[i, k]) = 1 - P(b[i, k, l] = 1 | Z[i, k]) = \frac{1}{1 + e^{\lambda_l[i, k]}}. \quad (5.6)$$

They are then used as *a priori* probabilities to estimate the data symbol. First, the probability that the transmitted symbol $X[i, k]$ is equal to a specific constellation point α_j is computed as the product of the probabilities of all the bits belonging to this constellation:

$$P(X[i, k] = \alpha_j | Z[i, k]) = \prod_{l=1}^{\log_2 \mu} P(b[i, k, l] = \kappa_l(\alpha_j) | Z[i, k]), \quad (5.7)$$

where μ is the modulation order and $\kappa_l(\alpha_j) \in \{0, 1\}$ is the value of the l^{th} bit of the constellation point α_j . The soft data symbol is an expected value taking the *a priori* probabilities (5.7) into account:

$$\hat{X}[i, k] = \mathbb{E}[X[i, k] | Z[i, k]] = \sum_{\alpha_j \in \Psi} \alpha_j \cdot P(X[i, k] = \alpha_j | Z[i, k]), \quad (5.8)$$

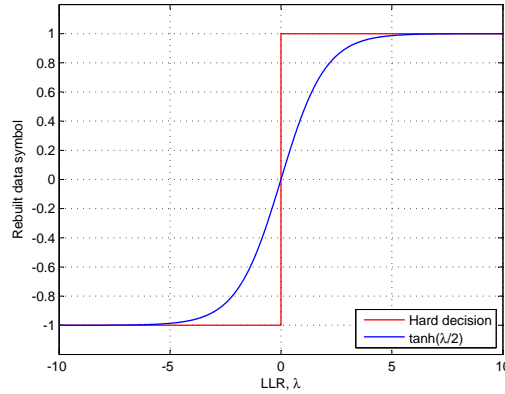


Figure 5.3: Hard decision vs soft decision using $\tanh(\frac{\lambda}{2})$ function.

where Ψ is the set of the constellation points of a given modulation scheme. Accordingly, the second moment of $X[i, k]$ is computed by:

$$\mathbb{E} \left[|X[i, k]|^2 | Z[i, k] \right] = \sum_{\alpha_j \in \Psi} |\alpha_j|^2 \cdot P(X[i, k] = \alpha_j | Z[i, k]). \quad (5.9)$$

More specifically, in the case of BPSK and Gray-coded QPSK, the rebuilt soft data symbol is simply:

$$\hat{X}[i, k] = \tanh\left(\frac{\lambda_1[i, k]}{2}\right), \text{ for BPSK}, \quad (5.10)$$

$$\hat{X}[i, k] = \frac{1}{\sqrt{2}} \left[\tanh\left(\frac{\lambda_1[i, k]}{2}\right) + j \tanh\left(\frac{\lambda_2[i, k]}{2}\right) \right], \text{ for QPSK}. \quad (5.11)$$

Both (5.10) and (5.11) can be easily realized by a look-up table in the hardware implementation.

Note that, in the classical decision feedback channel estimation methods such as [142] and [98], hard decision is made here in order to get a rebuilt data symbol with exact value corresponding to a given constellation point. This imprudent decision is sometimes jeopardous and may affect the following channel estimation [159]. By contrast, the symbol rebuilding process in (5.10) and (5.11) avoids the hard decision. Indeed, it can be recognized as *soft decision* [159, 160]. The input-output relations of the hard and soft decision are presented in Figure 5.3.

The difference between the two decision mechanisms lies in the region where the absolute value of LLR is small, i.e. around the decision threshold 0. Recall the definition of the LLR, small absolute value means the probabilities of a bit equal to 0 or 1 are comparative. It is not certain that the bit should be decided as 0 or 1. This is the situation that the error decision most easily occurs in the hard decision mechanism. Whereas, the soft decision mechanism does not hastily make its decision. Instead, it indicates the reliability (or, equivalently, uncertainty) of the decision by the amplitude of the soft-decided symbol. For example, given an uncertain BPSK-modulated symbol X_u with probability $P(X_u = 1|Z) = 0.55$, the soft decision result is 0.1. While, when the value of LLR is high, e.g. greater than ± 5 , the output of the soft decision approaches that of the hard decision. The difference between them becomes imperceptible. That is to say, the soft decision device makes hard decision to the relatively reliable symbols. An example of

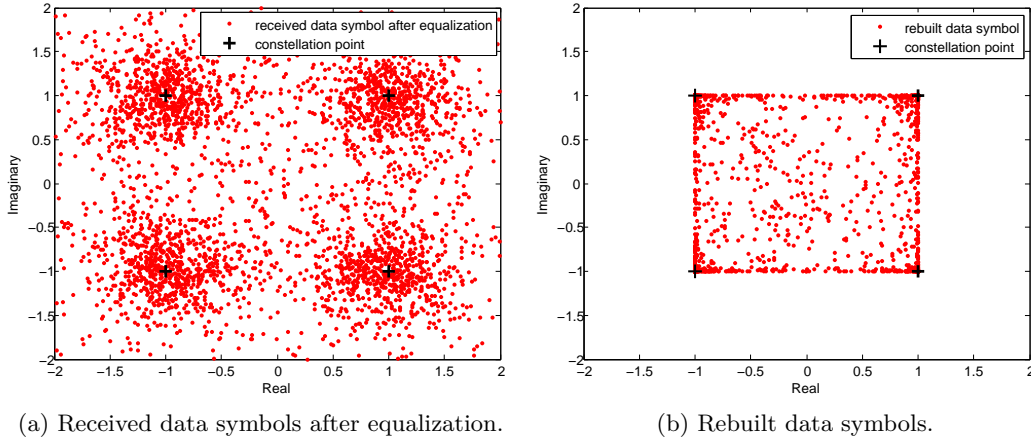


Figure 5.4: Example of QPSK-modulated data symbols after equalization and rebuilt data symbols when the SNR is 10 dB.

the soft data symbol rebuilding is illustrated in Figure 5.4. The soft decision mechanism keeps risky uncertainty in the soft-decided data symbol and avoids the error propagation commonly happened in hard decision case, which makes it significantly better than the hard decision [159, 160].

5.3.3 Instantaneous Channel Estimation

Using the rebuilt soft data symbols as virtual training sequence, a data-aided channel estimation can be carried out. In the quasi-static channel, there is almost no ICI among subcarriers introduced by Doppler effect. The received frequency-domain data symbols are:

$$\mathbf{Y} = \mathbf{X}\mathbf{H} + \mathbf{W}, \quad (5.12)$$

where $\mathbf{Y} = [Y[i, 0], Y[i, 1], \dots, Y[i, N-1]]^T$, $\mathbf{H} = [H[i, 0], H[i, 1], \dots, H[i, N-1]]^T$, $\mathbf{W} = [W[i, 0], W[i, 1], \dots, W[i, N-1]]^T$ are the vector forms of Y , H and W belonging to the i^{th} OFDM symbol. $\mathbf{X} = \text{diag}([X[i, 0], X[i, 1], \dots, X[i, N-1]])$ is a diagonal matrix whose principal diagonal elements are X 's. An LS channel estimator is found by minimizing the following cost function [159]:

$$\tilde{\mathbf{H}}^{\text{LS}} = \arg \min_H \underbrace{\mathbb{E}[\|\mathbf{Y} - \mathbf{X}\mathbf{H}\|^2 | \mathbf{Z}]}_{\text{cost function}}. \quad (5.13)$$

Setting the derivative of the cost function to 0, it yields:

$$\begin{aligned}
& \frac{\partial}{\partial \mathbf{H}} \mathbb{E}[\|\mathbf{Y} - \mathbf{X}\mathbf{H}\|^2 | \mathbf{Z}] = 0 \\
\Rightarrow & \frac{\partial}{\partial \mathbf{H}} \mathbb{E}[(\mathbf{Y} - \mathbf{X}\mathbf{H})^{\mathcal{H}}(\mathbf{Y} - \mathbf{X}\mathbf{H}) | \mathbf{Z}] = 0 \\
\Rightarrow & \frac{\partial}{\partial \mathbf{H}} \mathbb{E}[\mathbf{Y}^{\mathcal{H}}\mathbf{Y} - 2\mathbf{Y}^{\mathcal{H}}\mathbf{X}\mathbf{H} + \mathbf{H}^{\mathcal{H}}\mathbf{X}^{\mathcal{H}}\mathbf{X}\mathbf{H} | \mathbf{Z}] = 0 \\
\Rightarrow & \frac{\partial}{\partial \mathbf{H}} \left(\mathbf{Y}^{\mathcal{H}}\mathbf{Y} - 2\mathbf{Y}^{\mathcal{H}}\mathbb{E}[\mathbf{X} | \mathbf{Z}]\mathbf{H} + \mathbf{H}^{\mathcal{H}}\mathbb{E}[\mathbf{X}^{\mathcal{H}}\mathbf{X} | \mathbf{Z}]\mathbf{H} \right) = 0 \\
\Rightarrow & -2\mathbb{E}[\mathbf{X}^{\mathcal{H}} | \mathbf{Z}]\mathbf{Y} + 2\mathbb{E}[\mathbf{X}^{\mathcal{H}}\mathbf{X} | \mathbf{Z}]\mathbf{H} = 0 \\
\Rightarrow & \tilde{\mathbf{H}}^{\text{LS}} = \mathbb{E}[\mathbf{X}^{\mathcal{H}}\mathbf{X} | \mathbf{Z}]^{-1} \mathbb{E}[\mathbf{X}^{\mathcal{H}} | \mathbf{Z}]\mathbf{Y}
\end{aligned} \tag{5.14}$$

Considering that \mathbf{X} is diagonal, the above equation yields a LS channel estimate:

$$\begin{bmatrix} \tilde{H}^{\text{LS}}[i, 0] \\ \tilde{H}^{\text{LS}}[i, 1] \\ \vdots \\ \tilde{H}^{\text{LS}}[i, N-1] \end{bmatrix} = \begin{bmatrix} \frac{\mathbb{E}[X[i,0]|Z[i,0]]^*}{\mathbb{E}[|X[i,0]|^2|Z[i,0]]} & \cdots & \cdots & 0 \\ \vdots & \frac{\mathbb{E}[X[i,1]|Z[i,1]]^*}{\mathbb{E}[|X[i,1]|^2|Z[i,1]]} & & \vdots \\ \vdots & & \ddots & \vdots \\ 0 & \cdots & \cdots & \frac{\mathbb{E}[X[i,N-1]|Z[i,N-1]]^*}{\mathbb{E}[|X[i,N-1]|^2|Z[i,N-1]]} \end{bmatrix} \begin{bmatrix} Y[i, 0] \\ Y[i, 1] \\ \vdots \\ Y[i, N-1] \end{bmatrix}.$$

That is, the expectation and the second moment of $X[i, k]$ given the equalized data $Z[i, N-1]$ (obtained by (5.8) and (5.9), respectively) can be used to carry out a data-aided channel estimation. More specifically, for each subcarrier, the instantaneous estimator is:

$$\tilde{H}_2^{\text{LS}}[i, k] = \frac{\hat{X}[i, k]}{\mathbb{E}[|X[i, k]|^2 | Z[i, k]]} Y[i, k]. \tag{5.15}$$

The MSE of the estimator (5.15) under the condition of the equalized data $Z[i, N-1]$ is:

$$\begin{aligned}
& \mathbb{E}[\|\mathbf{Y} - \mathbf{X}\tilde{\mathbf{H}}^{\text{LS}}\|^2 | \mathbf{Z}] = \mathbb{E}[(\mathbf{Y} - \mathbf{X}\hat{\mathbf{H}})^{\mathcal{H}}(\mathbf{Y} - \mathbf{X}\hat{\mathbf{H}}) | \mathbf{Z}] \\
& = \mathbb{E}[\mathbf{Y}^{\mathcal{H}}(\mathbf{I} - \mathbf{X}\mathbb{E}[\mathbf{X}^{\mathcal{H}}\mathbf{X} | \mathbf{Z}]^{-1}\mathbb{E}[\mathbf{X}^{\mathcal{H}} | \mathbf{Z}])^{\mathcal{H}}(\mathbf{I} - \mathbf{X}\mathbb{E}[\mathbf{X}^{\mathcal{H}}\mathbf{X} | \mathbf{Z}]^{-1}\mathbb{E}[\mathbf{X}^{\mathcal{H}} | \mathbf{Z}])\mathbf{Y} | \mathbf{Z}] \\
& = \mathbf{Y}^{\mathcal{H}}(\mathbf{I} - \mathbb{E}[\mathbf{X} | \mathbf{Z}]\mathbb{E}[\mathbf{X}^{\mathcal{H}}\mathbf{X} | \mathbf{Z}]^{-1}\mathbb{E}[\mathbf{X}^{\mathcal{H}} | \mathbf{Z}])\mathbf{Y}.
\end{aligned} \tag{5.16}$$

5.3.3.1 Simplified Estimator

As the computation of the second moment of $X[i, k]$ needs a weighted combination of $\log_2 \mu$ elements to be performed, more computational complexity is required especially when the constellation order is high. We thus propose to use the power of the soft data symbol, i.e. $E_{\hat{X}}[i, k] = |\hat{X}[i, k]|^2$, to replace the second moment in (5.15) for the purpose of reducing complexity. The estimator turns to:

$$\begin{aligned}
\tilde{H}_2[i, k] & = \frac{1}{E_{\hat{X}}[i, k]} \hat{X}[i, k]^* Y[i, k] \\
& = \frac{\hat{X}[i, k]^* X[i, k]}{E_{\hat{X}}[i, k]} H[i, k] + \frac{1}{E_{\hat{X}}[i, k]} \hat{X}[i, k]^* W''[i, k].
\end{aligned} \tag{5.17}$$

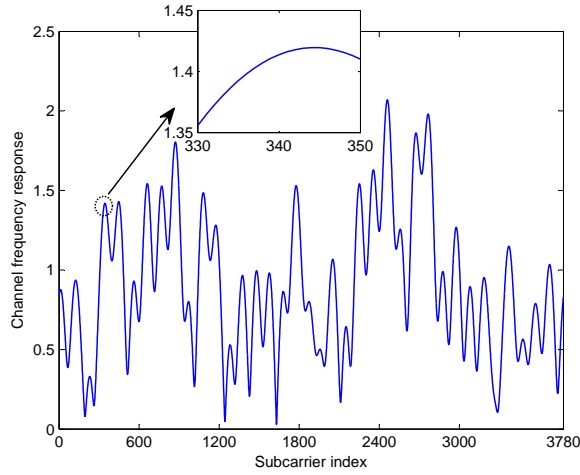


Figure 5.5: CFR of a TU-6 channel.

Note that $E_{\hat{X}}[i, k]$ is approximated to the second moment when the soft data symbol is close to a specific constellation point. Intuitively, when SNR goes high, data symbols are well rebuilt, i.e. $\hat{X}[i, k] = X[i, k]$, (5.17) turns to:

$$\tilde{H}_2[i, k] = \frac{X[i, k]^*}{X[i, k]^* X[i, k]} Y[i, k] = H[i, k] + \frac{W''[i, k]}{\sqrt{E_X[i, k]}}, \quad (5.18)$$

which coincides with the LS estimator in the pilot assisted channel estimation case [93]. In other words, the simplified estimator in (5.17) leads to an asymptotical LS estimator. We will verify this simplification by simulation in Section 5.7.2.6.

A special case of the simplified estimator can be obtained when using the uniform power constellations such as BPSK or QPSK, where the power of the constellation is a known, constant value. Hence, $E_{\hat{X}}[i, k]$ is replaced by the power of the constellation E_α :

$$\tilde{H}_2[i, k] = \frac{1}{E_\alpha} \hat{X}[i, k]^* Y[i, k]. \quad (5.19)$$

5.4 Channel Estimation Refinements

In contrast to a fully iterative turbo channel estimation as [14, 160], the proposed method does not include any error correction in the feedback loop. The rebuilt soft data symbols are affected by the noise and the channel fades. It is quite possible that the instantaneous channel estimates are inaccurate and even erroneous for some subcarriers. Fortunately, as both the time delay spread and the Doppler spectrum of the channel are limited, the CFR is highly correlated, i.e. almost identical within the coherence bandwidth and coherence time [9]. Moreover, the coherence bandwidth spreads over several adjacent subcarriers in the OFDM system with large FFT size. Figure 5.5 shows the CFR of TU-6 channel with an FFT size of 3780. Meanwhile, the coherence time is longer than several OFDM symbol durations in low and medium velocity cases. This enables us to refine the data-aided channel estimation using the correlation property of CFR. Several channel estimation refinements are proposed in the following sections. According to the

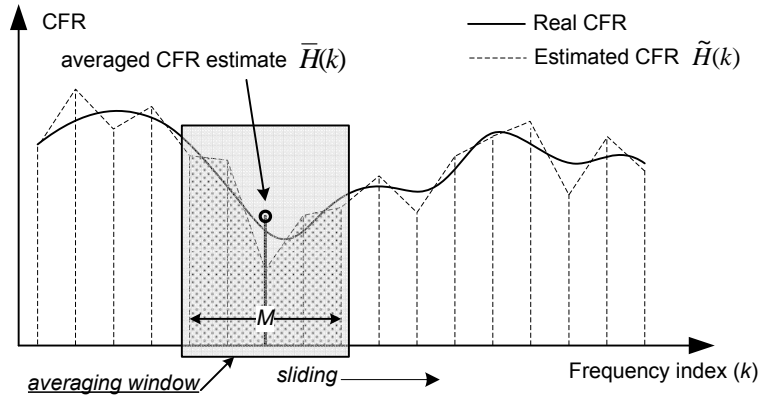


Figure 5.6: 1-D moving average.

used time-frequency range, they are catalogued into 1-D (frequency domain) and 2-D (time-frequency domain) ones.

5.4.1 1-D Approaches

The 1-D refinement approaches process the instantaneous data-aided channel estimates within one OFDM symbol to get an improved estimation result. Only the frequency domain correlation property of the channel is exploited. As the 1-D refinement approaches are carried out in a (OFDM) symbol-by-symbol fashion, they can track a fast variation of the channel and require minimum storage capacity. The OFDM symbol index i is omitted in this section for the sake of notation simplicity.

5.4.1.1 1-D Moving Average

Since the CFR is almost identical within coherence bandwidth, the most straightforward way to improve the estimation quality is to perform a moving average [15] with a length less or equal to the coherence bandwidth. More precisely, M consecutive instantaneous channel estimates within a “window” are averaged to get a more precise estimate for the central position of the window. As the CFR is constant while the noise is independently random process, the variance of the noise is reduced to $\frac{1}{M}$ after averaging. When the window slides over all active subcarriers, a refined channel estimate is obtained. The moving average process is depicted in Figure 5.6. Specifically, the moving-averaged CFR estimate (5.17) for the k^{th} subcarrier is expressed as:

$$\begin{aligned}
 \bar{H}_2[k] &= \frac{1}{M} \sum_{m \in \Theta_k} \tilde{H}_2[m] \\
 &= \frac{H[k]}{M} \sum_{m \in \Theta_k} \frac{\hat{X}[m]^* X[m]}{E_{\hat{X}}[m]} + \frac{1}{M} \sum_{m \in \Theta_k} \frac{\hat{X}[m]^* W''[m]}{E_{\hat{X}}[m]} \\
 &\approx H[k] + \frac{1}{M} \sum_{m \in \Theta_k} \frac{\hat{X}[m]^* W''[m]}{E_{\hat{X}}[m]}, 0 \leq k \leq N-1,
 \end{aligned} \tag{5.20}$$

where $\Theta_k = \{k - \lfloor \frac{M-1}{2} \rfloor, k - \lfloor \frac{M-1}{2} \rfloor + 1, \dots, k + \lfloor \frac{M-1}{2} \rfloor\}$ is the set of subcarrier indices within the moving average window with the k^{th} subcarrier the central frequency, M is the

length of the moving average window and W'' is the noise and interference component. The moving average length M is chosen less than or equal to the coherence bandwidth. It can be either empirically pre-selected according to the “worst case” of the application scenario or be adaptively chosen by computing the coherence bandwidth using the estimated CIR from initial PN based channel estimation. The impact of the average length on the estimation is investigated via simulation in Section 5.7.2.2. The variance of the averaged CFR estimate for the k^{th} subcarrier is:

$$\begin{aligned}
\sigma_{\bar{H}_2}^2[k] &= \mathbb{E} \left\{ |H[k] - \bar{H}_2[k]|^2 \right\} \\
&= \mathbb{E} \left\{ \left| \frac{1}{M} \sum_{m \in \Theta_k} \frac{\hat{X}[m]W''[m]}{E_{\hat{X}}[m]} \right|^2 \right\} \\
&= \frac{1}{M^2} \sum_{m \in \Theta_k} \frac{|\hat{X}[m]|^2 \sigma_{W''}^2}{E_{\hat{X}}[m]^2} \\
&= \frac{\sigma_{W''}^2}{M^2} \sum_{m \in \Theta_k} \frac{1}{E_{\hat{X}}[m]}. \tag{5.21}
\end{aligned}$$

It suggests that when the data symbols are well rebuilt, the variance of the estimation error is reduced M times. The MSE of the data-aided CFR estimate for the i^{th} OFDM symbol can be estimated by averaging (5.21) over N subcarriers:

$$\varepsilon_{\bar{H}_2,1D} = \frac{1}{N} \sum_{k=0}^{N-1} \mathbb{E} \left\{ |H[k] - \bar{H}_2[k]|^2 \right\} = \frac{\sigma_{W''}^2}{M^2 N} \sum_{k=0}^{N-1} \sum_{m \in \Theta_k} \frac{1}{E_{\hat{X}}[m]}. \tag{5.22}$$

Specifically, given the uniform power constellation with a power of E_α ,

$$\varepsilon_{\bar{H}_2,1D} = \frac{\sigma_{W''}^2}{(ME_\alpha)^2 N} \sum_{k=0}^{N-1} \sum_{m \in \Theta_k} |\hat{X}[k]|^2 = \frac{\sigma_{W''}^2}{ME_\alpha^2} \bar{E}_{\hat{X}}, \tag{5.23}$$

where $\bar{E}_{\hat{X}} = \frac{1}{N} \sum_{k=0}^{N-1} |\hat{X}[k]|^2$ is the mean power of the rebuilt data symbols.

5.4.1.2 1-D Wiener filtering

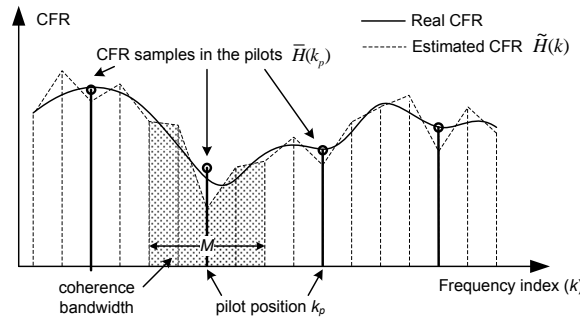


Figure 5.7: 1-D averaging and interpolation.

The proposed Wiener filtering based refinement is depicted in Figure 5.7. It consists of two steps: *averaging* and *interpolation*.

A bunch of subcarriers are first selected as “virtual pilots”. The virtual pilots locate uniformly in the frequency domain. The spacing between two adjacent virtual pilots is L_f (in terms of subcarriers). Detailed discussions on pilot arrangement is presented in section 5.4.3. Denote Ξ the set of virtual pilots indices, i.e. $\Xi = \{k_p | k_p = pL_f, 0 \leq p \leq \lfloor \frac{N}{L_f} \rfloor - 1\}$. The cardinality of Ξ (the quantity of virtual pilots) is K_f .

The instantaneous channel estimates within the averaging window around each virtual pilot $k_p \in \Xi$ are averaged to get a more accurate channel estimate $\bar{H}_2[k_p]$. Its expression can be obtained by setting $k = k_p$ in (5.20). Repeating the averaging process in all virtual pilots, we can get K_f accurate CFR estimate samples $\bar{H}_2[k_p], \forall k_p \in \Xi$.

To obtain the CFR estimate \hat{H}_2 for all subcarriers, several interpolation techniques such as linear, FFT based and Wiener filtering based interpolations could be performed. Among all these techniques, the Wiener filtering based one provides the best interpolation results [104].

The interpolated CFR can be expressed as a weighted linear combination of the CFR estimate samples in pilot positions:

$$\hat{H}_2[k] = \sum_{k_p \in \Xi} \omega_f[k, k_p] \bar{H}_2[k_p], \quad 0 \leq k \leq N - 1, \quad (5.24)$$

where $\omega_f[k, k_p]$'s are the weighting coefficients. Rearrange the samples in vector form $\bar{\mathbf{H}}_2 = [\bar{H}_2[k_0], \bar{H}_2[k_1], \dots, \bar{H}_2[k_{K_f-1}]]^T$. Accordingly, the output vector is $\hat{\mathbf{H}}_2 = [\hat{H}_2[0], \hat{H}_2[1], \dots, \hat{H}_2[N-1]]^T$ and the vector form of CFR is $\mathbf{H} = [H[0], H[1], \dots, H[N-1]]^T$. (5.24) is thus rewritten as:

$$\hat{\mathbf{H}}_2 = \boldsymbol{\omega}_f^{\mathcal{H}} \bar{\mathbf{H}}_2. \quad (5.25)$$

where $\boldsymbol{\omega}_f$ is the $K_f \times N$ coefficient matrix with the (m, n) th element $\omega_f[m, n]$. The optimal coefficients is obtained to minimize the MSE of the interpolation:

$$\boldsymbol{\omega}_f^{opt} = \arg \min_{\boldsymbol{\omega}_f} \mathbb{E}\{\|\mathbf{H} - \boldsymbol{\omega}_f^{\mathcal{H}} \bar{\mathbf{H}}_2\|^2\}. \quad (5.26)$$

The solution of the above problem yields the coefficients of the Wiener filter [95]:

$$\boldsymbol{\omega}_f = \boldsymbol{\Phi}_f^{-1} \boldsymbol{\theta}_f, \quad (5.27)$$

where $\boldsymbol{\Phi}_f = \mathbb{E}\{\bar{\mathbf{H}}_2 \bar{\mathbf{H}}_2^{\mathcal{H}}\} = (\mathbf{R}_f^{(1)} + \sigma_{\bar{\mathbf{H}}_2}^2 \mathbf{I})$ is the $K_f \times K_f$ autocorrelation matrix of CFR estimation samples on pilot positions obtained in (5.20), $\sigma_{\bar{\mathbf{H}}_2}^2$ is the variance of the estimation error $\bar{\mathbf{H}}_2$ derived in (5.22), \mathbf{I} is the identity matrix. $\boldsymbol{\theta}_f = \mathbb{E}\{\bar{\mathbf{H}}_2 \mathbf{H}^{\mathcal{H}}\} = \mathbf{R}_f^{(2)}$ is the $K_f \times N$ cross-correlation matrix of CFR estimates $\bar{\mathbf{H}}_2$ and the real CFR \mathbf{H} . $\mathbf{R}_f^{(1)}$ and $\mathbf{R}_f^{(2)}$ are the autocorrelation matrix of the real CFR, and its components can be computed by (2.31). Note that the coefficients of the Wiener filter can be computed in either non-adaptive [95, 96] or adaptive manners [176]. The MSE of the CFR estimate after frequency domain filtering is:

$$\varepsilon_{\hat{H}_2, 1D} = \frac{1}{N} \text{Tr} \left(\mathbf{R}_f^{(3)} - \mathbf{R}_f^{(2)T} \boldsymbol{\Phi}_f^{-1} \mathbf{R}_f^{(2)*} \right), \quad (5.28)$$

where $\text{Tr}(\cdot)$ is the trace operation, $\mathbf{R}_f^{(3)}$ is the $N \times N$ autocorrelation matrix of the CFR.

For given positions of the virtual pilots, the autocorrelation matrices $\mathbf{R}_f^{(1)}$, $\mathbf{R}_f^{(2)}$ and $\mathbf{R}_f^{(3)}$ can be pre-computed with specific assumption of the channel delay power spectrum to simplify the computational complexity. For instance, the channel delay power spectrum can be assumed to be uniformly distributed as in [95], which yields the coefficients that adapt to the worst channel situation.

5.4.2 2-D Approaches

As presented above, 1-D refinement approaches only exploit the frequency domain correlation property of the channel. More processing gain can be acquired if the time domain correlation property is also taken into account. This leads to the 2-D moving average and Wiener filtering methods.

5.4.2.1 2-D Moving Average

Expanding the average range in (5.20) to 2-D, namely to several consecutive OFDM symbols, more instantaneous channel estimates can be involved in the moving average process. Given enough similarities among the CFR for different subcarriers and OFDM symbols, the 2-D moving average results are expected to be better than the 1-D counterpart. More specifically, the subcarrier indices within the 2-D averaging region with the k^{th} subcarrier of the i^{th} OFDM symbol its central position is given by the set $\Theta_{i,k} = \{(p, q) | i - \lfloor \frac{M_t-1}{2} \rfloor \leq p \leq i + \lfloor \frac{M_t-1}{2} \rfloor, k - \lfloor \frac{M_f-1}{2} \rfloor \leq q \leq k + \lfloor \frac{M_f-1}{2} \rfloor\}$. The 2-D moving-averaged CFR estimates are written as:

$$\begin{aligned} \bar{H}_2[i, k] &= \frac{1}{M_t M_f} \sum_{p, q \in \Theta_{i, k}} \tilde{H}_2[p, q] \\ &\approx H[i, k] + \frac{1}{M_t M_f} \sum_{p, q \in \Theta_{i, k}} \frac{\hat{X}[p, q] W''[p, q]}{E_{\hat{X}}[p, q]}. \end{aligned} \quad (5.29)$$

The variance of the estimation error in (5.29) is then:

$$\begin{aligned} \sigma_{\bar{H}_2}^2[i, k] &= \mathbb{E}\{|H[i, k] - \bar{H}_2[i, k]|^2\} \\ &= \mathbb{E}\left\{\left|\frac{1}{M_t M_f} \sum_{p, q \in \Theta_{i, k}} \frac{\hat{X}[p, q] W''[p, q]}{E_{\hat{X}}[p, q]}\right|^2\right\} \\ &= \frac{\sigma_{W''}^2}{(M_t M_f)^2} \sum_{p, q \in \Theta_{i, k}} \left|\frac{\hat{X}[p, q]}{E_{\hat{X}}[p, q]}\right|^2 \\ &= \frac{\sigma_{W''}^2}{(M_t M_f)^2} \sum_{p, q \in \Theta_{i, k}} \frac{1}{E_{\hat{X}}[p, q]}. \end{aligned} \quad (5.30)$$

Comparing the above equation and (5.21), it can be seen that the estimation error is further reduced M_t times thanks to the additional time domain averaging. The MSE of

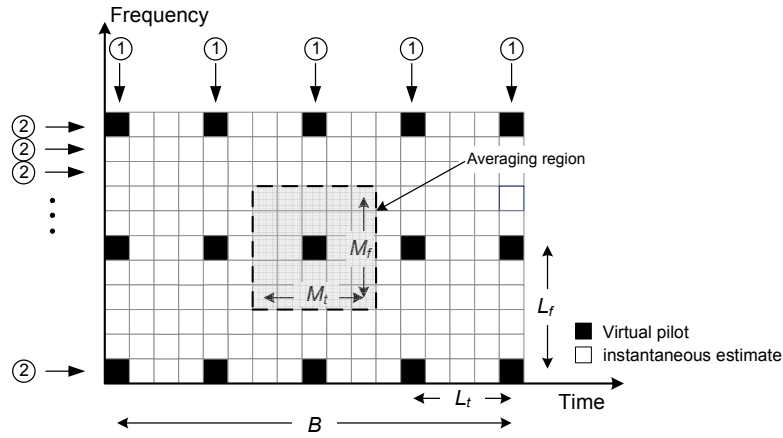


Figure 5.8: 2-D averaging and interpolating. The averaging is performed in the 2-D averaging region (shaded area). The interpolation is first carried out in frequency domain (①) and secondly in time domain (②).

the 2-D moving averaged CFR is:

$$\begin{aligned} \varepsilon_{\bar{H}_2, 2D} &= \frac{1}{N} \sum_{k=0}^{N-1} \mathbb{E} \left\{ |H[i, k] - \bar{H}_2[i, k]|^2 \right\} \\ &= \frac{\sigma_{W''}^2}{(M_t M_f)^2 N} \sum_{k=0}^{N-1} \sum_{p, q \in \Theta_{i, k}} \frac{1}{E_{\hat{X}}[p, q]}. \end{aligned} \quad (5.31)$$

5.4.2.2 2-D Wiener Filtering

The 2-D estimate refinement and interpolation are carried out over a number of OFDM symbols within an interpolation block as shown in Figure 5.8. The block size B , i.e. the number of OFDM symbols in the block, is chosen according to the latency, storage and complexity considerations.

For low-complexity consideration, some time-frequency indices $(i_p, k_q) \in \Omega$ are pre-selected as virtual pilots. L_f and L_t are the virtual pilot spacings in frequency and time domains, while $K_f = \lfloor \frac{N}{L_f} \rfloor$ and $K_t = \lfloor \frac{B}{L_t} \rfloor$ are the number of virtual pilots within one OFDM symbol and the number of OFDM symbols including virtual pilots, respectively. The selection of L_f and L_t will be discussed in Section 5.4.3. The set of indices of virtual pilots is $\Omega = \{(i_p, k_q) | i_p = pL_t, 0 \leq p \leq K_t - 1; k_q = qL_f, 0 \leq q \leq K_f - 1\}$.

Then, a refined CFR estimate for the virtual pilot located at (i_p, k_p) is computed by averaging all the instantaneous CFR estimates within the coherence region Θ_{i_p, k_p} . The averaged estimate can be obtained from (5.29) by setting $i = i_p$ and $k = k_p$. Repeating this process over all virtual pilots in the interpolation block, $K_t \cdot K_f$ refined CFR estimates are obtained. With these reliable estimates, the CFR estimate for all subcarriers can thus be obtained via a 2-D interpolation.

The 2-D Wiener filtering outperforms other interpolation techniques, e.g. linear interpolation, FFT-based interpolation etc. in terms of interpolation quality. However its computational complexity is considerably high. An alternative is to use two concatenated 1-D Wiener filters which significantly reduces the computational complexity with negli-

gible performance degradation compared to the optimum 2-D Wiener filter [95, 96]. As shown in Figure 5.8, the Wiener filtering is first performed in frequency domain in each OFDM symbol that carries the virtual pilots. Consequently, another Wiener filtering is carried out for all subcarriers in time domain. The 2×1-D Wiener filtering is represented as:

$$\hat{H}_2[i, k] = \underbrace{\sum_{i_p} \omega_t[i, k, i_p]}_{\text{time domain}} \underbrace{\sum_{k_p} \omega_f[k, i_p, k_p]}_{\text{frequency domain}} \bar{H}_2[i_p, k_p], \quad (5.32)$$

where ω_t 's and ω_f 's are the coefficients of the 1-D Wiener filters in time and frequency domains, respectively. The coefficients of frequency domain Wiener filter is the same as those given in (5.27). Arrange the filtered channel estimates in a $K_f \times K_t$ matrix $\bar{\mathbf{H}}_2$ whose (m, n) th element is $\bar{H}_2[m, n]$. The 2-D Wiener filtering result can be written in vector form:

$$\hat{\mathbf{H}}_2 = (\boldsymbol{\omega}_t^{\mathcal{H}} (\boldsymbol{\omega}_f^{\mathcal{H}} \bar{\mathbf{H}}_2)^T)^T = (\boldsymbol{\omega}_t^{\mathcal{H}} (\hat{\mathbf{H}}_2^f)^T)^T, \quad (5.33)$$

where the $N \times K_t$ matrix $\hat{\mathbf{H}}_2^f = \boldsymbol{\omega}_f^{\mathcal{H}} \bar{\mathbf{H}}_2$ denotes the output of the frequency domain 1-D Wiener filter. The coefficients matrix of the frequency domain Wiener filtering $\boldsymbol{\omega}_f$ is given in (5.27), while the coefficients of the time domain Wiener filter can be computed as:

$$\boldsymbol{\omega}_t = \boldsymbol{\Phi}_t^{-1} \boldsymbol{\theta}_t, \quad (5.34)$$

where $\boldsymbol{\Phi}_t = \mathbb{E}\{\bar{\mathbf{H}}_2^{fT} \bar{\mathbf{H}}_2^f\} = (\mathbf{R}_t^{(1)} + \sigma_{\bar{\mathbf{H}}_2^f}^2 \mathbf{I})$ is the $K_t \times K_t$ autocorrelation matrix of the filtered CFR estimates, $\sigma_{\bar{\mathbf{H}}_2^f}^2$ is the variance of the estimation error derived in (5.28).

$\boldsymbol{\theta}_t = \mathbb{E}\{\bar{\mathbf{H}}_{2,k}^{fT} \mathbf{H}_t^*\} = \mathbf{R}_t^{(2)}$ is the $K_t \times B$ cross-correlation matrix of CFR estimates $\bar{\mathbf{H}}_{2,k}^f$ for the k^{th} subcarrier with different time and the real CFR for a particular subcarrier with different time \mathbf{H}_t . $\mathbf{R}_t^{(1)}$ and $\mathbf{R}_t^{(2)}$ are the autocorrelation matrix of the real CFR in time domain, and its components is computed by (2.34).

The MSE of the CFR estimate after time domain filtering is:

$$\varepsilon_{\hat{H}_2, 2D} = \frac{1}{B} \text{Tr} \left(\mathbf{R}_t^{(3)} - \mathbf{R}_t^{(2)T} \boldsymbol{\Phi}_t^{-1} \mathbf{R}_t^{(2)*} \right). \quad (5.35)$$

5.4.3 Pilot Pattern Selection

5.4.3.1 Pilot Spacing

In the OFDM system, the channel estimation can be viewed as a 2-D sampling and reconstruction process. A trade-off should be made: adjacent pilots should be close enough to guarantee reliable reconstruction, in the mean time, the amount of pilots should be kept as small as possible to avoid unnecessary cost of spectrum efficiency. A reasonable requirement is that the pilot spacing should substantially fulfil the sampling theorem in both frequency and time domains [95, 96, 104].

Frequency domain Considering a channel with maximum delay spread τ_{max} (L samples), the frequency-domain sampling rate $f_{s,f}$ should be:

$$f_{s,f} \geq 2\tau_{max} \quad \Rightarrow \quad \frac{1}{L_f \Delta f} \geq 2LT_s, \quad (5.36)$$

where Δf and T_s are the subcarrier spacing and the sampling interval, respectively, and recall that we have $\Delta f = 1/NT_s$ in the OFDM system. The sampling is carried out with a certain oversampling ratio to achieve better performance [104, 95]. For instance, with a $2\times$ oversampling ratio, L_f is determined so that:

$$L_f \leq \frac{N}{4L}. \quad (5.37)$$

Time domain Since the time varying channel is (one-sided) bandlimited to the maximum Doppler frequency f_d , according to the sampling theorem, the time-domain sampling rate $f_{s,t}$ should fulfil:

$$f_{s,t} \geq 2f_d \Rightarrow \frac{1}{L_t T_b} \geq 2f_d, \quad (5.38)$$

where T_b is the duration of one OFDM block including OFDM data symbol and GI. Taking the $2\times$ oversampling ratio into account, the spacing between virtual symbols L_t (in terms of OFDM symbols) is selected so that:

$$L_t \leq \frac{1}{4T_b f_d}. \quad (5.39)$$

The inequalities (5.37) and (5.39) suggest the general requirements of the pilot spacings. If the computational complexity is acceptable, increasing the density of pilots can further improve the channel estimation performance. The selection of the pilot spacing is investigated through simulation in Section 5.7.2.3 and Section 5.7.3.1

5.4.3.2 Pilot Shape

Figure 5.9 depicts several commonly used pilot patterns, namely block-type, comb-type, rectangular-shape and diamond-shape. In the block-type arrangement, some OFDM symbols are reserved for channel estimation, in which *all* subcarriers are used to transmit pilot sequence. The channel estimation is carried out periodically. In each estimation time, a complete estimation of CFR is obtained for all subcarriers. Thus there is no error introduced by the interpolation operation in the frequency domain. This scheme assumes that the channel does not vary between two successive estimations. It is suitable for the static channel case. In the comb-type arrangement, the pilot symbols are allocated to some specific subcarriers for *all* OFDM symbols. In each OFDM symbol, the CFR is first estimated for the subcarriers containing pilot symbols. Then some interpolation techniques are used to obtain CFR estimation for all subcarriers. As there are pilot symbols for all OFDM symbols, this kind of pilot arrangement is suitable to track the channel variation in time. It was shown in [107] that the comb-type pilot pattern with some proper interpolation techniques outperforms the block-type one in terms of estimation accuracy. Moreover, it was proved that the best pilot arrangement in frequency domain is the equi-spaced and equi-powered pattern [105, 177, 178]. The pilot pattern used in the 1-D Wiener filtering based method is the comb-type. As the CFR's for adjacent OFDM symbols have strong correlation, it is more convenient to allocate pilots in every a few OFDM symbols rather than in all of them. It yields the rectangular-shape pilot pattern. Every L_t th OFDM symbol contains virtual pilots. For each OFDM symbol carrying virtual pilots, the pilot positions are fixed with a spacing of L_f subcarriers. A

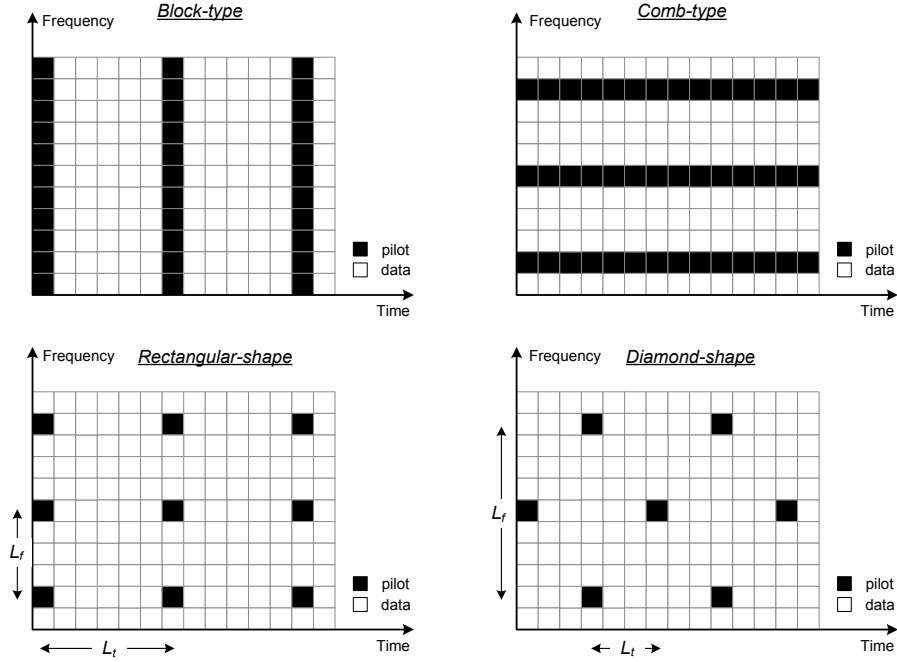


Figure 5.9: Several commonly used pilot patterns.

modified rectangular-shape pattern is to linearly increase the frequency indices from one OFDM symbol to the next. This linearly increasing rectangular-shape pattern is adopted in the DVB-T standard. A special case of linearly increasing rectangular-shape is the diamond-shape, in which the pilot positions circularly shift $\frac{L_f}{2}$ from one OFDM symbol containing pilots to the next. It was proved in [109] that the diamond-shape pattern is the optimum in the sense of minimum channel estimation error. Some simulation results are shown in Section 5.7.3.1 to show the influence of the pilot pattern.

5.5 MMSE Combination

When both PN-based and data-aided channel estimates are obtained, a linear combination is proposed to get a final CFR estimate:

$$\hat{H} = \beta \hat{H}_1 + (1 - \beta) \hat{H}_2, \quad (5.40)$$

where \hat{H}_2 is a generic expression of the data-aided channel estimations which can be obtained from (5.20), (5.24), (5.29) or (5.32) using different techniques. The combination is carried out only for the active subcarriers and the CFR estimates for null subcarriers are kept as the results obtained from the PN-based one. The optimum weight values β_{opt} can be obtained using the MMSE criteria:

$$\begin{aligned} \beta_{opt} &= \arg \min_{\beta} \left\{ E\{|H - \hat{H}|^2\} \right\} \\ &= \arg \min_{\beta} \left\{ \beta^2 \varepsilon_{\hat{H}_1} + (1 - \beta)^2 \varepsilon_{\hat{H}_2} \right\}. \end{aligned} \quad (5.41)$$

The above equation uses the fact that \hat{H}_1 and \hat{H}_2 are obtained from different sources and thus uncorrelated. Since the MSE function is convex, the β_{opt} is obtained by setting the derivative with respect to β equal to zero and the solution is:

$$\beta_{opt} = \frac{\varepsilon_{\hat{H}_2}}{\varepsilon_{\hat{H}_1} + \varepsilon_{\hat{H}_2}}, \quad (5.42)$$

where $\varepsilon_{\hat{H}_1}$ is the MSE of the PN-based estimation, while $\varepsilon_{\hat{H}_2}$ is the MSE of the data-aided channel estimation and is computed from (5.22), (5.28), (5.30) or (5.35) depending on different methods. After a given maximum number of iterations, the combined CFR (5.40) estimate is output as the final CFR estimate. Otherwise it is used as the initial channel estimate for the next iteration for PN subtraction and equalization.

5.6 Complexity Analysis

Since both CIR and CFR are needed in the equalization of TDS-OFDM signal, the use of N -length FFT (IFFT) is inevitable by all channel estimation methods. Hence, we only analyze the additional computational complexity introduced by the different methods. The complexity is evaluated in terms of required real multiplications and real additions for each OFDM symbol per iteration. One complex multiplication is counted as 2 real additions and 4 real multiplications although there exist some smarter ways requiring fewer multiplication times [179]. It is also assumed that arithmetic with individual elements has complexity $\mathcal{O}(1)$, as it is the case with fixed-precision floating-point arithmetic [180].

The computational complexity of the PN-based methods depends on the length of PN sequence N_{PN} . The major operation in the frequency domain method is the N_{PN} -length FFT/IFFT conversions of PN sequences. The complexity is $\mathcal{O}(N_{PN} \log N_{PN})$. On the other hand, the channel estimation of time domain method is carried out via an N_{PN} -length cyclic correlator such as the one given in [181]. Its complexity is hence $\mathcal{O}(N_{PN}^2)$. As the length of the PN sequence is much smaller than the number of subcarriers, the complexity of PN-based methods is generally trivial compared to other operations in the receiver such as equalization and decoding.

The data rebuilding process including (5.4), (5.7) and (5.8) needs $(N \cdot \mu \log_2 \mu + N \cdot 2 \log_2 \mu)$ multiplications and $N \cdot 2 \log_2 \mu$ additions. The instantaneous data-aided estimation (5.17) needs $8N$ multiplications and $3N$ additions.

The computational complexities required by the estimate refinement vary with respect to different strategies. For the 1-D moving average method, the averaging for each subcarrier with an averaging length M requires $2(M - 1)$ additions and 2 multiplications, neglecting the edge effect. Hence, the moving averaging over N subcarriers requires $2(M - 1)N$ additions and $2N$ multiplications. The combination of the two channel estimates requires $2N$ additions and $4N$ multiplications. The overall basic operations are $((\mu + 2) \log_2 \mu + 14)N$ multiplications and $(2 \log_2 \mu + 2M + 3)N$ additions for each iteration. Given $M \ll N$, the additional complexity of the 1-D moving average based channel estimation is $\mathcal{O}(N)$.

The 2-D moving average method, on the other hand, has generally the same computational complexity except that the averaging process for each subcarrier requires $2(M_t M_f - 1)N$ additions and $2N$ multiplications and the overall required additions turns

Table 5.1: Complexity Comparison

Method		Complexity
PN-based estimations	Frequency domain method	$\mathcal{O}(N_{\text{PN}} \log N_{\text{PN}})$
	Time domain method	$\mathcal{O}(N_{\text{PN}}^2)$
Proposed estimate refinements	Moving Average based	$\mathcal{O}(N)$
	Wiener filtering based	$\mathcal{O}(N)$ to $\mathcal{O}(N^2)$
MUCK03 [12]		$\mathcal{O}(\nu \cdot \log \nu)$ when $B \ll \nu$, $\mathcal{O}(\nu^2)$ otherwise
SONG05 [138]		$\mathcal{O}(N_{\text{PN}}^2)$ for short L , $\mathcal{O}(N_{\text{PN}} \cdot (2N + \nu))$ for long L
YANG08 [140]		$\mathcal{O}(N)$
WANG05 [137]		$\mathcal{O}(N \cdot \log N)$
TANG07 [76]		$\mathcal{O}((N + \nu) \cdot \log(N + \nu))$
TANG08 [142]		$\mathcal{O}(N \cdot \log N)$
STEENDAM07 [61]		$\mathcal{O}(N^3)$
ZHAO08 [14]		$(\mathcal{O}(N) + \text{complexity of decoding})$ for iteration, $\mathcal{O}(N^2)$ or $\mathcal{O}(N^3)$ for final stage

to $(2 \log_2 \mu + 2M_t M_f + 3)N$. Given the condition $M_t M_f \ll N$ fulfilled, the complexity is still $\mathcal{O}(N)$.

As far as the Wiener filtering based approaches are concerned, for the K virtual pilots in each OFDM symbol, the averaging of the instantaneous estimates in the coherence bandwidth requires $2(M - 1)K$ real additions and $2K$ real multiplications. As the coefficients of the Wiener filter is real [95], the Wiener filtering needs $2KN$ multiplications and $2KN$ additions. Taking the symbol rebuilding and combination into account, the overall operations for 1-D Wiener filtering based method is $(2 \log_2 \mu + 5 + 2K)N + 2(M - 1)K$ additions and $((\mu + 2) \log_2 \mu + 12 + 2K)N + 2K$ multiplications, which is between $\mathcal{O}(N)$ and $\mathcal{O}(N^2)$.

While for the 2-D Wiener filtering case, in each block consisting of B OFDM symbols, the averaging and 1-D frequency domain Wiener filtering is repeated K_t times which counts $2(N + M_t M_f - 1)K_f K_t$ additions and $2(N + 1)K_f K_t$ multiplications. Then, the time domain Wiener filtering needs $2K_t B N$ multiplications and additions. Therefore, the overall operations per OFDM symbol per iteration for 2-D Wiener filtering based method is $((\mu + 2) \log_2 \mu + 12 + 2 \frac{K_f}{L_t} + 2K_t)N + \frac{2K_f}{L_t}$ multiplications and $(2 \log_2 \mu + 5 + 2 \frac{K_f}{L_t} + 2K_t)N + 2 \frac{(M_t M_f - 1)K_t K_f}{B}$ additions, which is, similar to 1-D Wiener filtering case, between $\mathcal{O}(N)$ and $\mathcal{O}(N^2)$. Even lower complexity can be achieved by reducing the size of Wiener filter as in [104].

The computational complexities of several typical existing methods [12, 61, 137, 138, 76, 142, 140, 14] are shown in Table 5.1. In this table, we compare the complexity of the different algorithms without considering the processes shared by all the methods, e.g. the CIR-CFR conversion and PN removal. In [12], the channel estimation (MUCK03) is carried out via an averaging of training sequence over B OFDM blocks followed by a frequency domain LS estimation. The averaging process requires $2(\nu \cdot B - 1)$ real additions and

negligible divisions. Given B is significantly smaller than ν , the complexity is dominated by the ν -length FFT and IFFT operations, which is $\mathcal{O}(\nu \cdot \log \nu)$. Otherwise, if B is equivalent or greater than ν , the complexity is $\mathcal{O}(\nu^2)$. As in the method proposed by [140], the dominant process is symbol-by-symbol partial decision, the complexity is thus $\mathcal{O}(N)$. For the methods proposed in [137, 76, 142] (WANG05, TANG07, TANG08), the dominant process is time domain data rebuilding by FFT/IFFT conversions. The complexity is thus $\mathcal{O}(N \cdot \log N)$. Concerning the methods proposed in [138] (SONG05), the CIR is estimated by autocorrelation of PN sequences. The corresponding complexity is $\mathcal{O}(N_{\text{PN}}^2)$. When the CIR is long, it needs additional complexity $\mathcal{O}(N_{\text{PN}} \cdot (2N + \nu))$ which is caused by time domain ISI removal. For the maximum-likelihood (ML) estimator proposed in [61] (STEENDAM07), the dominant process is the matrix inversion which requires complexity of $\mathcal{O}(N^3)$. For the turbo channel estimation method proposed in [14] (ZHAO08), the complexity needed by each iteration is ($\mathcal{O}(N)$ + complexity of MAP decoding), and that needed by the final estimation stage is $\mathcal{O}(N^2)$ or $\mathcal{O}(N^3)$ for ML and MMSE estimators, respectively. Through this comparison, it can be concluded that the proposed method needs the minimum computational complexity among the typical existing methods.

5.7 Simulation Results

5.7.1 Experiment Setups

Simulation parameters are chosen from the DTMB standard [4]. The length of GI is set to $\nu = 420$ samples. For a BER simulation, both the convolutional interleaver and LDPC code are included in the simulation in order to perform a system level evaluation. The convolutional interleaver is set to (52, 240) which corresponds to a time delay of 170 OFDM symbols. The TU-6 channel model is employed in the simulation. Following the computation in [9], when the frequency correlation function is 0.9, the coherence bandwidth of TU-6 channel is 18.8 kHz, which is equivalent to 9 subcarrier spacings of the DTMB system. The frequency domain averaging length M is therefore selected as 9 subcarriers which automatically fulfils the sampling theorem as discussed in Section 5.4.3. The experiments in Section 5.7.2.2 will verify the feasibility of this selection.

Proposed algorithm is also assessed in the single frequency network (SFN) scenario. SFN is considered as the most severe channel conditions due to the presence of strong echoes with long time delay. For instance, when the distance difference is 7 km, the corresponding propagation time difference is 23.33 μs . Therefore, the overall time delay spread of the SFN channel is 28.33 μs which is longer than the duration of the CP of the PN. In addition, the SFN channel is very frequency selective. Given the frequency correlation function of 0.9, the coherence bandwidth of this SFN channel is 2.94 kHz. The power attenuation (as shown in Figure 2.13) is set to 10 dB in our simulation.

5.7.2 1-D Methods

5.7.2.1 MSE

Figure 5.10a presents the MSE performance of the proposed data-aided channel estimation algorithm with QPSK in TU-6 channel, using 1-D moving average and 1-D Wiener filtering methods, respectively. It can be seen that the quality of the channel estimate

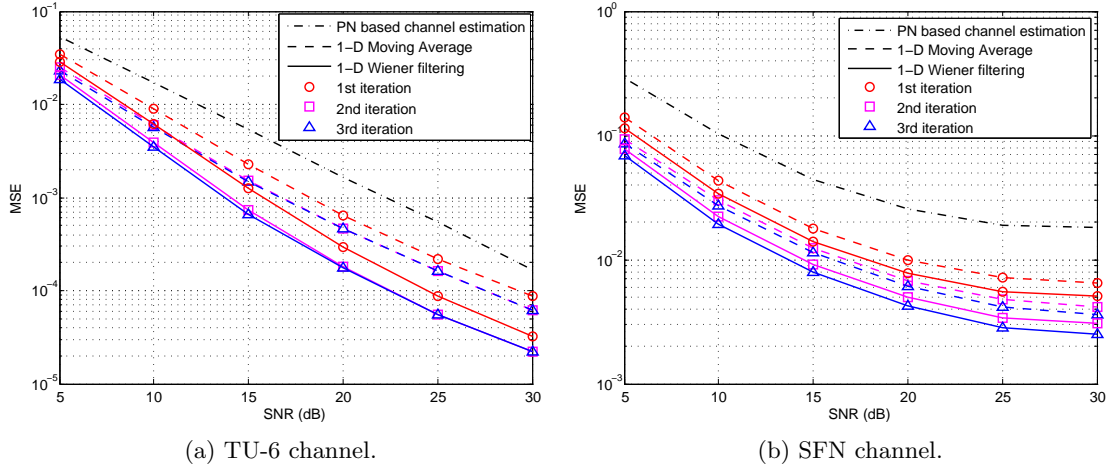


Figure 5.10: MSE comparison of 1-D Moving Average method and 1-D Wiener filtering method, *frequency domain method* as initial estimation. For both moving average and Wiener filtering, $M = 9$ for TU-6 and $M = 3$ for SFN channel. $L_f = 9$ and $L_f = 3$ for TU-6 and SFN channel, respectively.

is progressively improved. A significant improvement can be obtained after only two iterations. More specifically, when the 1-D moving average is used, the proposed method acquires about 4.1 dB gain in terms of required SNR to achieve an MSE level of 1×10^{-2} compared with the PN sequence based one. If the more powerful 1-D Wiener filtering technique is adopted, the gain increases to 5.1 dB. The higher the SNR, the more efficient the Wiener filtering.

On the other hand, in the SFN channel, since the channel time spreading is much longer than the CP of the PN sequence, there is strong IBI on the PN sequence. This can be seen from Figure 5.10b that the performance of the PN based channel estimation is seriously degraded and appears an estimation error floor at high SNR. Furthermore, as the coherence bandwidth of SFN channel is quite narrow, a much shorter averaging length is used in the SFN cases, which limits the noise mitigation ability in the data-aided channel estimation. Even in such harsh channels, the data-aided method offers 6.9 dB and 8.1 dB gains in terms of required SNR to achieve an MSE of 5×10^{-2} compared to the PN based method, when using the 1-D moving average and Wiener filtering, respectively. Moreover, the estimation performance is improved about ten times at high SNR.

Figure 5.11 presents the proposed data-aided channel estimation method using time domain approach as the initial estimation with QPSK. As the time domain method provides more accurate channel estimation results than the frequency domain method, the overall data-aided channel estimation results are better when combining with the time domain method. For instance, we examine the required SNR to achieve an MSE level of 1×10^{-2} in the TU-6 channel. Compared with the case of using frequency domain method, using the time domain method as initial estimation can bring 1.8 dB and 1.5 dB gains when combining with 1-D moving average and Wiener filtering, respectively.

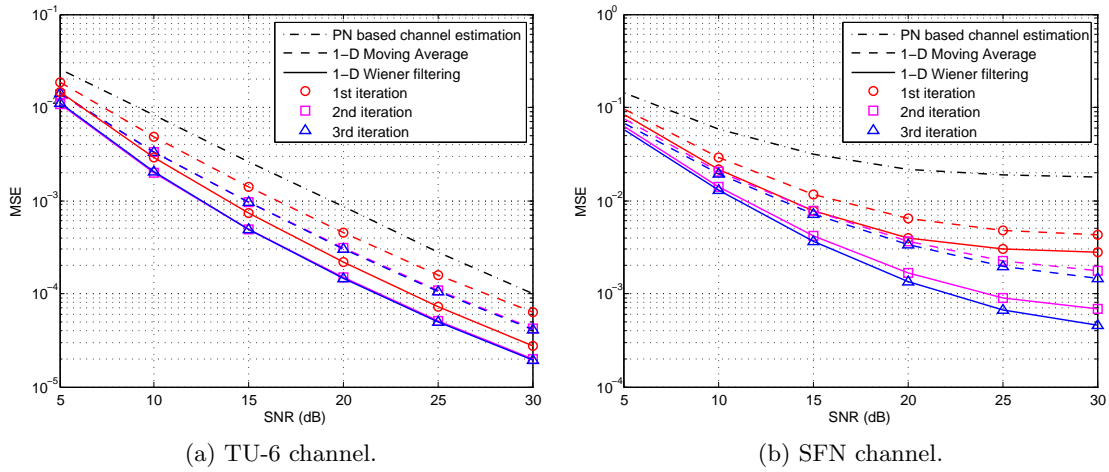


Figure 5.11: MSE comparison of 1-D Moving Average method and 1-D Wiener filtering method, *time domain method* as initial estimation. For both moving average and Wiener filtering, $M = 9$ for TU-6 and $M = 3$ for SFN channel. $L_f = 9$ and $L_f = 3$ for TU-6 and SFN channel, respectively.

Similar interpretations can be drawn in the case of SFN channel. From Figure 5.11b, the proposed method brings 5 dB and 5.8 dB gains (with respect to the MSE level of 5×10^{-2}) over the PN based method when combining with 1-D moving average and Wiener filtering, respectively. In the mean time, compared to the performance presented in Figure 5.10b, using time domain method as the initial estimation improves the estimation results by 1.2 dB and 0.8 dB in the case of moving average and Wiener filtering, respectively. In high SNR region, the improvement of using time domain method is even more obvious.

Form Figure 5.10 and Figure 5.11, some general conclusions can be made. First of all, the Wiener filtering technique is more efficient than moving average due to its powerful noise mitigation capability. This is more obvious in the TU-6 channel in which the dominant factor that determines the accuracy of the channel estimation is the noise. Moreover, adopting Wiener filtering in the proposed method does not necessarily mean that the algorithm becomes cumbersome. An interesting observation is that the performance of using Wiener filtering after only one iteration is as good as the best performance that moving average can achieve. This provides a less processing delay (less iteration) trade-off with higher computational complexity in each iteration. In SFN channel, on the other hand, the inaccuracy of the initial estimation affects the quality of the rebuilt data symbols and consequently compromises the data-aided channel estimation. It can be verified by the fact that the performance of moving average and Wiener filtering is quite close in Figure 5.10b. Therefore, using a more sophisticated initial estimation brings significant improvement to the overall channel estimation results. Finally, it can be found that the performance of the algorithm after three iterations converges. Therefore, the iteration time is set to two iterations in the BER evaluations.

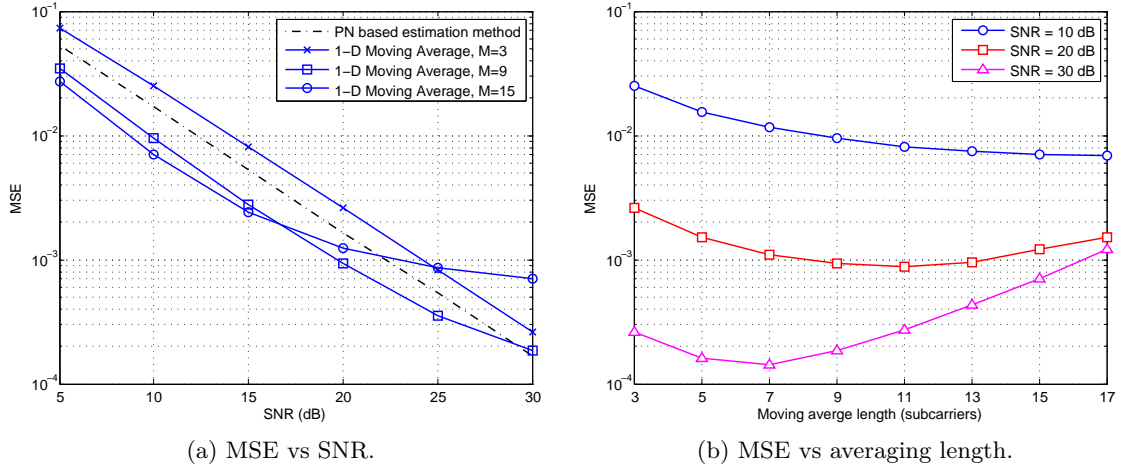


Figure 5.12: MSE of 1-D Moving Average method *before* combination with different averaging lengths, frequency domain method as initial estimation.

5.7.2.2 Impact of the Averaging Length

As the soft data symbols are rebuilt from the uncorrected information, the instantaneous data-aided channel estimates are not reliable. The main means to improve the accuracy of the estimation results is to average the instantaneous estimates within the coherence bandwidth. The averaging can be seen as lower-pass filtering. When the assumption that the channel response does not vary within the averaging length is held, the filtering selects the components very near to the direct current (mainly the constant channel response) and suppresses other frequency components (noise components). Intuitively, the greater the averaging length is, the better the noise mitigation capability can be obtained in the averaging. However, we should pay attention here that the channel varies more significantly in a larger averaging length. The lower-pass filtering will also destroy the channel varying effect in the estimation. Therefore, the averaging length should be carefully selected.

Figure 5.12 presents the MSE of data-aided channel estimate (before combination) using different averaging lengths in the TU-6 channel. In low SNR region, e.g. less than 15 dB, where the noise is the dominant source of the inaccuracy, larger averaging length brings higher estimation accuracy. The loss of channel varying detail after averaging is covered by the contribution of the noise mitigation at low SNR. Whereas, this drawback appears in high SNR region. For instance, an estimation error floor is found at high SNR in the $M = 15$ case. In fact, when the SNR is high, the rebuilt data symbols are accurate and the data-aided estimation is more reliable. Hence, a shorter averaging length is sufficient to suppress the noise. Therefore, it is necessary to find a trade-off between the noise suppression and channel variations.

In the ideal case, the averaging length should be selected adaptively according to the real channel situation and noise level in order to suit different application situations. However, a less complex solution is to choose a fixed value for the typical channel in which

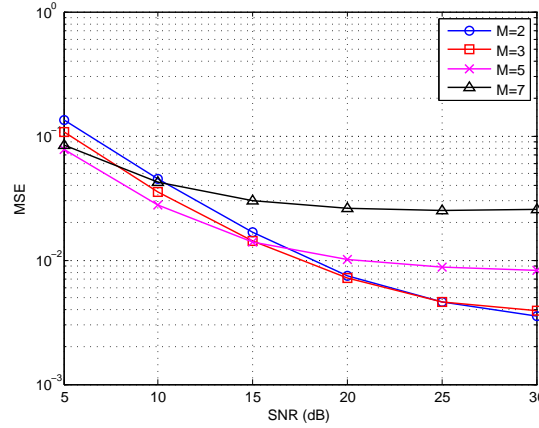


Figure 5.13: Impact of the averaging length on the data-aided estimation results in the SFN channel with a propagation difference of 7km.

the system will be used. For instance, the impact of the averaging length on the MSE of the estimation in the TU-6 channel is studied in detail in Figure 5.12b. At a low SNR, e.g. 10 dB, the MSE is monotonically decreasing with the increase of the averaging length. However, at a higher SNR, especially at 30 dB, the MSE of the averaged estimation results is degraded with a long averaging length. Hence, a moderate averaging length, say $M = 7 \sim 9$, is a proper choice. Considering that the data-aided channel estimation is more crucial in lower SNR region, it is better to bias our selection to a greater length. Therefore, $M = 9$ is a good trade-off that suits all noise levels for the TU-6 channel.

Similar conclusions can be drawn in the SFN channel. As shown in Figure 5.13, longer averaging lengths (e.g. $M = 5$) bring more gain in low SNR region while encounter an estimation error in high SNR region. Among the four candidates shown in the figure, $M = 3$ is the best trade-off of the averaging length in the SFN channel.

5.7.2.3 Pilot spacing in Wiener filtering

As the Wiener filtering based data-aided channel estimation consists of two steps – averaging and interpolation, both the averaging length and the pilot spacing affect the accuracy of the interpolation results. Intuitively, greater averaging length and more pilots will provide more accurate estimation results. In the mean time, they also mean higher computational complexity. Therefore, we study the impacts of the averaging and interpolation separately to find appropriate trade-offs for each of them in this section.

Impact of the Averaging Length Figure 5.14 presents the MSE of the interpolation results using the 1-D Wiener filtering method, with fixed pilot spacing ($L_f = 9$) and different averaging lengths. Recall that the coherence bandwidth of TU-6 channel is about 9 subcarriers. When the averaging length is much shorter than the coherence bandwidth, e.g. $M = 3$, the performance bottleneck of the data-aided estimation method is the insufficient noise suppression capability. The estimation performance with inadequate averaging length is always inferior to the case with an averaging length equal to the coherence bandwidth within the observation range. At the same time, since the averaging process diminishes the channel variation within the averaging length as well, excessive

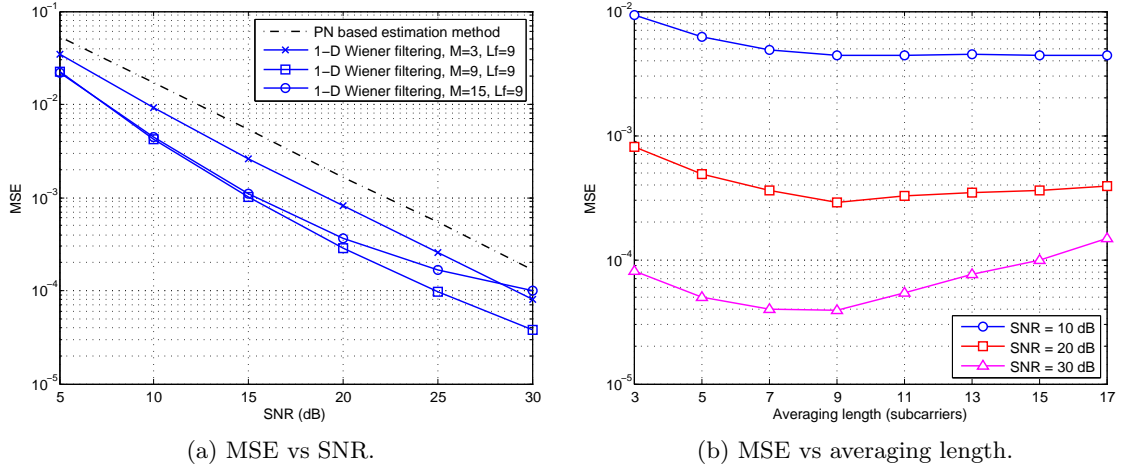


Figure 5.14: MSE of 1-D Wiener filtering method *before* combination with different averaging lengths, frequency domain method as initial estimation. Pilot spacing $L_f = 9$ for all cases.

averaging length is not definitely a good choice. For example, in the case of $M = 15$, the estimation performance is compromised in higher SNR region (greater than 15 dB). The precise relationship between the averaging length and estimation MSE is presented in Figure 5.14b. It can be concluded that an averaging length equal to the coherence bandwidth, as defined previously, is a good trade-off for both low and high SNR cases.

Impact of the Pilot Spacing Figure 5.15 depicts the estimation performance of the 1-D Wiener filtering method with fixed averaging length $M = 9$ and different pilot spacings. The number of pilots is insufficient if we choose the pilot spacing according to the sampling theorem [96]. While when the pilot spacing is selected according to a $2\times$ oversampling ratio, the performance is dramatically improved. If we continue decreasing the pilot spacing, even better estimation performance can be achieved. It comes from the stronger noise suppression capability of the Wiener filter when more pilots are adopted. However, the performance can not be constantly improved by decreasing the pilot spacing. From Figure 5.15b, it is clear that there is almost no improvement when the pilot spacing decreases to less than 9 subcarriers. It suggests that the quality of the averaged estimates for the pilot positions is a more significant factor to determine the accuracy of the estimation results. There is no need to select the pilot spacing smaller than the averaging length since more pilots can not bring more gains. Therefore, we select the pilot spacing equal to 9 subcarriers—as long as averaging length—for the TU-6 channel.

As far as the SFN channel is concerned, some similar conclusions can be made as in the moving average case. From Figure 5.16, the proposed method achieves its best performance when both the averaging length and the pilot spacing are selected the same as the coherence bandwidth, i.e. $M = L_f = 3$.

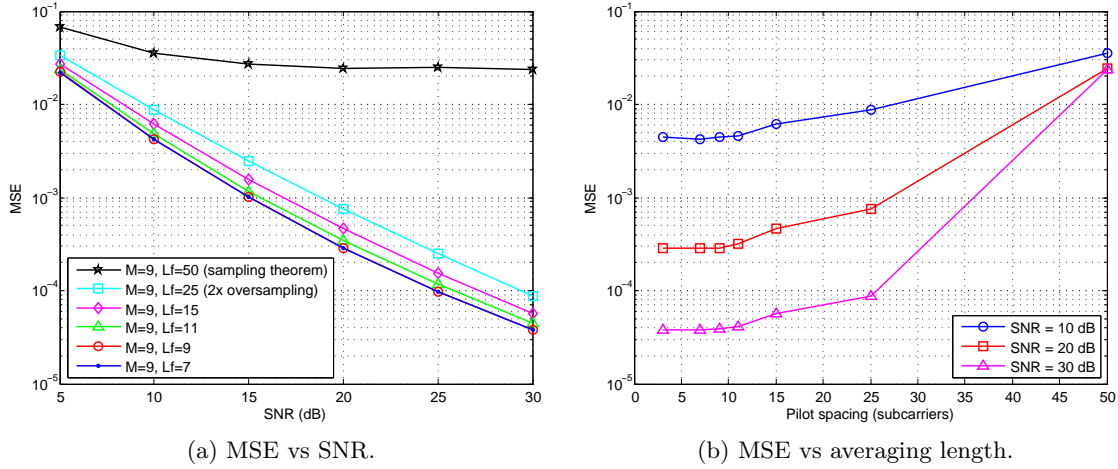


Figure 5.15: MSE of 1-D Wiener filtering method *before* combination with different pilot spacings, frequency domain method as initial estimation. Averaging length $M = 9$ for all cases.

5.7.2.4 BER

Figure 5.17, Figure 5.18, Figure 5.19 and Figure 5.20 present the bit error rate (BER) performance of the DTMB system using the proposed data-aided channel estimation method. In order to thoroughly evaluate the proposed method, we present the performance of all the combinations of the two initial estimation methods (time domain/frequency domain, TD/FD) and two data-aided estimation methods (moving average/Wiener filtering, MA/WF). That is, TD-MA, TD-WF, FD-MA and FD-WF. The modulation is QPSK. The LDPC code with a rate of $R = 0.8$ specified in [4] is used. The mobile speed is set to 30 km/h which introduces a maximum Doppler frequency of 13.89 Hz, given the carrier frequency 500 MHz. In the SFN channel case, we selected two propagation differences, namely 7 km and 8 km, in our simulation to show the variation of the performance in different channel conditions. ⁽¹⁾

The performance is compared with the PN-based time-domain and frequency-domain estimation methods as well as some representative methods proposed in the literatures [76](TANG07), [142](TANG08) and [12](MUCK03). The velocity is set to 30 km/h for the PN-based methods as well as methods TANG07 and TANG08. While the performance of method MUCK03 is obtained with a velocity of 6 km/h, because it is only valid for static or slowly-varying channels. The averaging window is selected to 50 OFDM symbols for method MUCK03.

To quantify the improvement brought by the proposed method, we observe the required SNR to achieve a BER level of 5×10^{-5} . To avoid wordy explanations to the simulation

(1). The 8 km propagation difference corresponds to $26.67 \mu s$ time delay equivalent to 244 samples of the DTMB system. It approaches to the longest CIR that the 255-length PN sequence can estimate. The corresponding coherence bandwidth is 2.58 kHz given the frequency correlation function of 0.9.

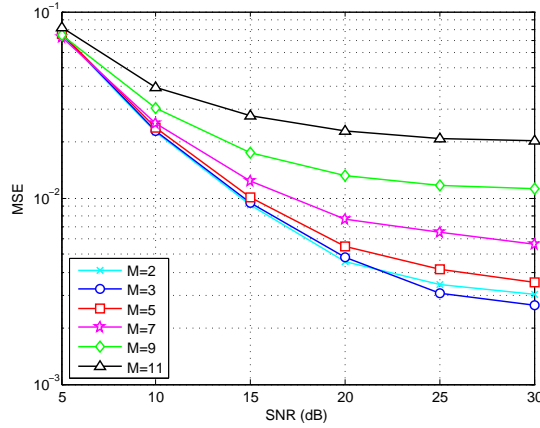


Figure 5.16: Impact of the averaging length on the data-aided estimation results in the SFN channel. Pilot spacing $L_f = 3$.

Table 5.2: Summary of the gains obtained using the data-aided channel estimation methods with QPSK.

Channel	method	Gain over PN-base method (dB) ^a	Gain over method TANG07 (dB)	Gain over method TANG08 (dB)	Gain over method MUCK03 (dB)	Gap away from perfect estimation (dB) ^a
TU-6	FD-MA	0.5	1.1	1.4	0.3	0.5
	FD-WF	0.6	1.2	1.5	0.4	0.4
	TD-MA	0.2	1.2	1.5	0.4	0.4
	TD-WF	0.4	1.4	1.7	0.6	0.2
SFN	FD-MA	1.7 [4.2]	-	-	-0.1 [-1.4]	1.3 [3.0]
	FD-WF	1.8 [4.4]	-	-	0.04 [-1.2]	1.2 [2.8]
	TD-MA	1.0 [1.5]	-	-	0.1 [0.5]	0.8 [1.1]
	TD-WF	1.1 [1.6]	-	-	0.5 [0.6]	0.8 [1.0]

^a The first value is obtained in SFN channel with 7 km propagation difference, while the value in the square brackets is obtained in SFN channel with 8 km propagation difference.

results and give a clear view, we present the gains over the reference methods as well as the gaps between the proposed method and the perfect estimation in Table 5.2.

Here we draw some remarks on these results.

1. *The proposed methods provide significant improvements over the reference methods.* For instance, the proposed estimation methods bring 1.4 to 1.7 dB gains over the method in [142] in the TU-6 channel. The first source of the improvement is the better strategy to use the PN sequence. Recall that the method [142] uses the whole PN sequence in GI for the channel estimation and iteratively removes ISI from the sequence to refine the estimation. However, the residual ISI compromises the estimation performance. On the other hand, the PN based methods proposed in Chapter 4 use the ISI-free part of the PN sequence for the channel estimation and thus avoids the influence of ISI. We get 0.9 dB gain when using the frequency domain PN based estimation method and 1.3 dB gain when using the time domain one. Moreover, the data-aided estimation methods provide further improvements ranging from 0.2 dB to 0.6 dB. For the same reason, the proposed method

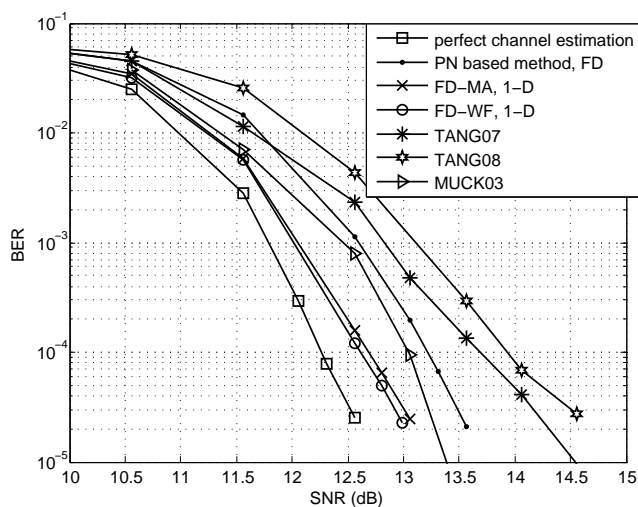


Figure 5.17: BER of the DTMB system using the data-aided channel estimation methods with TU-6 channel. QPSK, $R=0.8$. *Frequency domain* PN based method is used as initial channel estimation.

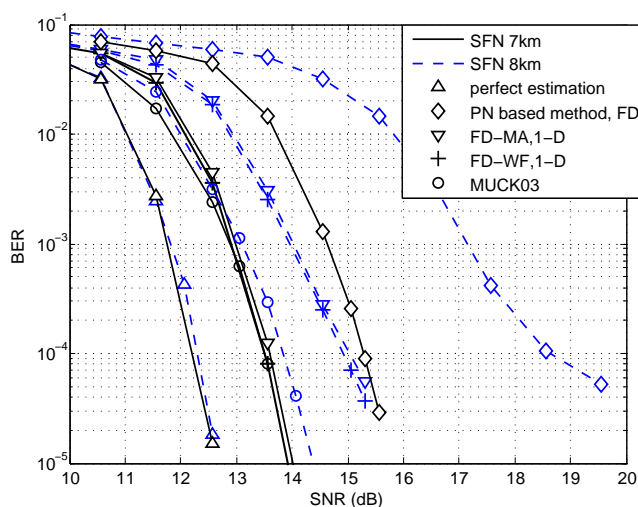


Figure 5.18: BER of the DTMB system using the data-aided channel estimation methods with SFN channel. QPSK, $R=0.8$. *Frequency domain* PN based method is used as initial channel estimation.

acquires more than 1.1 dB gain over the method in [76]. As far as the SFN channel is concerned, the PN based method becomes less efficient due to the existence of ISI. The improvements provided by the data-aided channel estimation are more significant and important. More precisely, the proposed methods acquire 1.0 dB to 1.8 dB gain compared to the PN-based ones. The improvements are more notable when the frequency domain method is used as the initial estimation. When the propagation difference is increased to 8 km, the channel conditions become even harsher, namely stronger ISI and higher frequency selectivity. In this case, the gain brought by the proposed method is even greater, i.e. ranging from 1.5 dB to 4.4 dB.

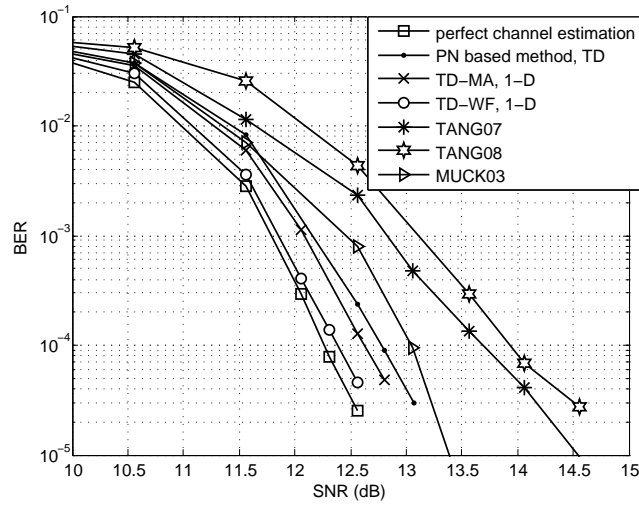


Figure 5.19: BER of the DTMB system using the data-aided channel estimation methods with TU-6 channel. QPSK, $R=0.8$. *Time domain* PN based method is used as initial channel estimation.

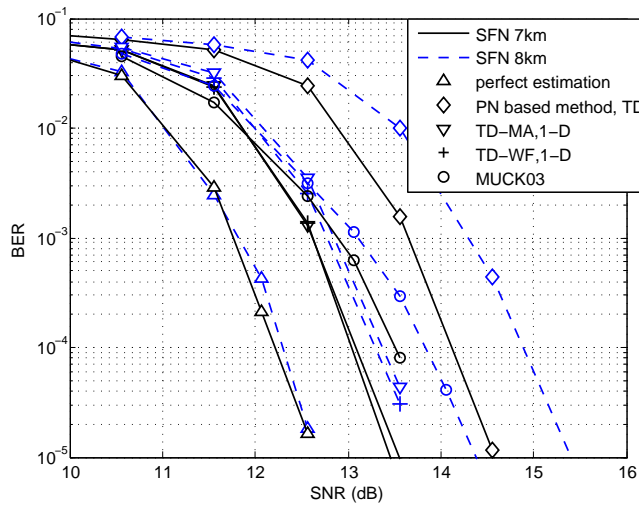


Figure 5.20: BER of the DTMB system using the data-aided channel estimation methods with SFN channel. QPSK, $R=0.8$. *Time domain* PN based method is used as initial channel estimation.

The performance of method MUCK03 mainly depends on the length of averaging window. As we select a greater window width⁽²⁾, method MUCK03 achieves good performance in the slowly-varying channel. The proposed methods (with velocity of 30 km/h) are 0.3 dB to 0.6 dB better than method MUCK03 (with velocity of 6 km/h) in TU-6 channel. In SFN cases, the method MUCK03 does not show significant performance degradation, while the PN-based estimation is affected by the ISI. Hence, the method MUCK03 performs bet-

(2). The typical length of averaging window is 20 to 40 OFDM symbols for BPSK and QPSK modulations in [12].

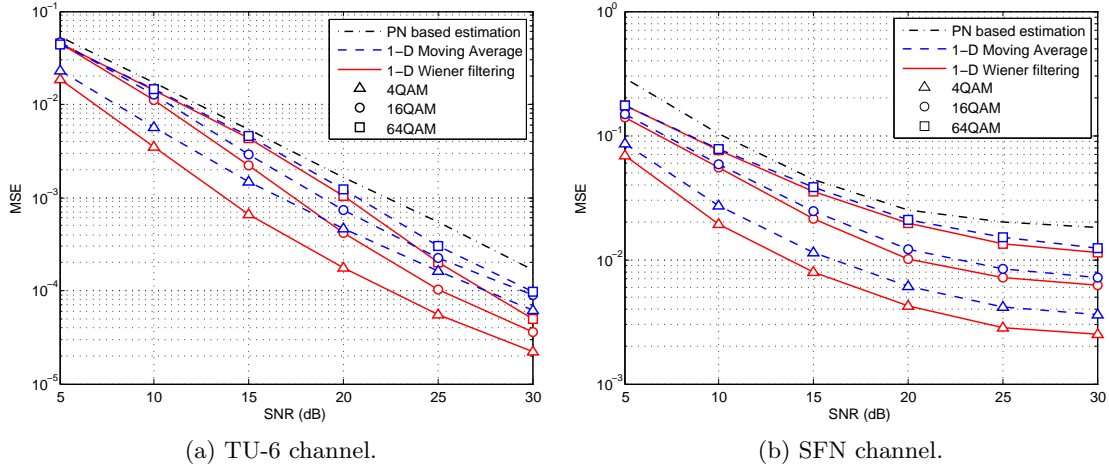


Figure 5.21: MSE of 1-D data-aided approaches with higher order constellations.

ter than proposed methods with frequency domain initial estimation. However, when time domain method is adopted, the proposed method performs better than method MUCK03. Moreover, in a scenario with higher mobility, the method MUCK03 suffers several dB performance loss.

2. *The performance gap between the proposed method and the perfect channel estimation case is small.* The proposed methods provide a performance that is only 0.2 to 0.5 dB away from the case with perfect channel information in the TU-6 channel. The performance is also inspiring in the SFN channels. When the frequency domain method is used as the initial estimation, the gap ranges from 1.2 dB to 3.0 dB. While when the time domain method is adopted, the gap is merely 0.8 dB to 1.1 dB, which is a very encouraging result.

3. *The proposed method provides satisfactory performance when the CP of training sequence is insufficient.* In the SFN channel case, the CIR is such long that a part of ISI will affect the training sequence⁽³⁾. The proposed methods, especially the TD-MA and TD-WF, show reliable performance with disturbance of ISI. This indicates that the system which adopts the proposed methods can work with shorter GI, which means improvements of system efficiency.

4. *The Wiener filtering and moving average have similar performance given the same channel conditions.* However, it does not mean that there is no interest to use the Wiener filtering technique. As mentioned in previous discussion, the performance using Wiener filtering with only one iteration is as good as the one using moving average with several iterations. This offers flexibility in the trade-off between computational complexity and processing delay.

5. *The time-domain initial estimation is crucial to the overall estimation results.* This is because a high-quality initial channel estimate leads to accurate rebuilt data symbols and consequently produces better data-aided channel estimation.

(3). The lengths of CIR are 219 and 244 samples when the propagation difference is 7 km and 8 km, respectively. The length of CP is 165 samples given 420-length GI in the DTMB system.

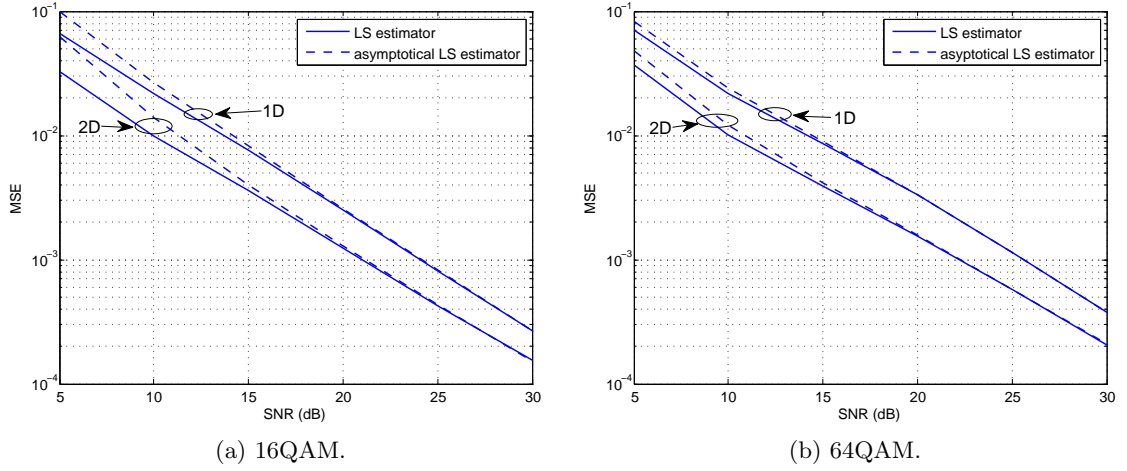


Figure 5.22: Comparison of the MSE of moving-averaged channel estimation using LS and asymptotical LS estimators in TU-6 channel with velocity of 6 km/h.

6. Among all combinations, the TD-WF performs best: 0.2 dB gap in the TU-6 channel and less than or equal to 1 dB gap in the SFN channel. On the other hand, the FD-MA, the one with the least computational complexity, provides satisfactory results. Except for the SFN channel with 8 km propagation difference, the gap between the performance of FD-MA and that with perfect knowledge of channel is limited to less than 1.3 dB. Even in the case of SFN channel with 8 km difference, FD-MA acquires 4.2 dB gain over the PN based estimation and decreases the gap to 3 dB.

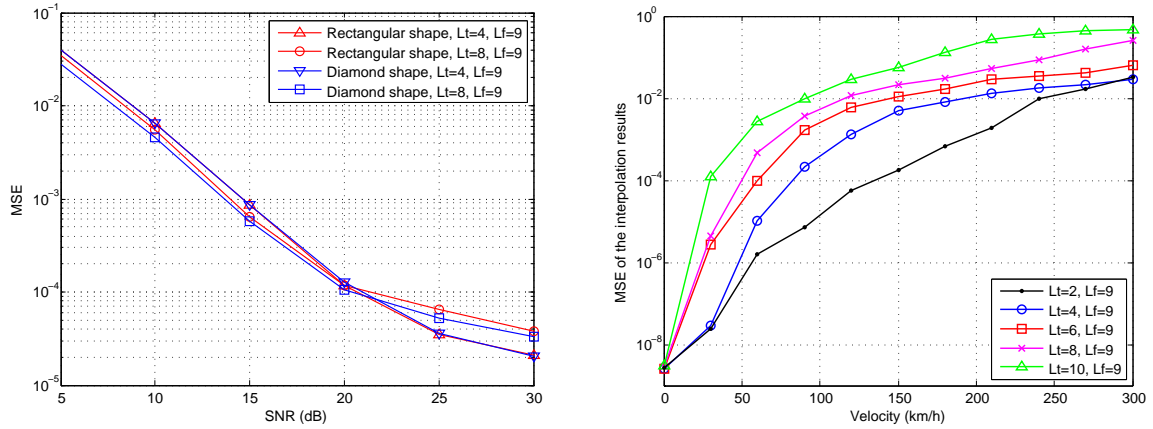
7. Finally, it should be noted that all the gains discussed above are obtained *after* decoding process of the LDPC code which is so powerful that it can provide satisfactory BER performance even with a poor channel estimation. Therefore, more gains can be expected when less powerful (and less complex in the same time) channel coding scheme is adopted.

5.7.2.5 1-D Methods with higher order constellations

Figure 5.21 depicts the MSE of the proposed data-aided channel estimation methods with higher order constellations, namely 16QAM and 64QAM. It can be found that the gain brought by the proposed method decreases with higher order constellations. This can be explained by the fact that the higher order constellations are more sensitive to the noise as well as to the channel fading. Therefore, the rebuilt data symbols are less reliable and the performance of the data-aided channel estimation is consequently degraded.

5.7.2.6 Approximate Normalization

Figure 5.22 illustrates the MSE of the data-aided channel estimation using the LS and the asymptotical LS estimators presented in (5.15) and (5.17), respectively. The estimation error introduced by the approximation is generally tolerable. More precisely, the approximation error is more visible in the low SNR region (e.g. less than 10 dB), while



(a) MSE of the 2-D Wiener filtering based method with 16QAM using different pilot patterns. Velocity is 6 km/h for all cases.

(b) Interpolation error of the 2-D Wiener filter interpolator in the TU-6 channel, interpolation block size $B = 21$. Carrier frequency is 500 MHz

Figure 5.23: Influence of pilot pattern on the MSE of the estimation.

the performance difference between two estimators is negligible in high SNR region (e.g. greater than 15 dB). Meanwhile, the approximation error is not evident with 64QAM for all SNR's. We will therefore use the asymptotical LS estimator throughout the simulations in the following sections.

5.7.3 2-D Methods

5.7.3.1 Pilot Pattern Selection

Since the performance of the 2-D methods relies on the virtual pilot pattern, it is necessary to find out the suitable pilot arrangement first. Since the impact of the frequency domain pilot spacing on the interpolation results has been investigated in Section 5.7.2.3, we hereby fix the frequency domain pilot spacing as $L_f = 9$ and focus on the impact of time domain pilot spacing.

Figure 5.23a presents the MSE performance of proposed method adopting rectangular shape and diamond shape pilot patterns as illustrated in Figure 5.8. The averaging lengths in time and frequency domains are set to be equal to the pilot spacings. It can be observed that the difference of the performance provided by the two pilot patterns is imperceptible given the same time and frequency domain pilot spacings. Hence the rectangular shape pattern is used in the following simulations for the convenience of implementation. In contrast, the density of the pilots has more significant influence on the estimation results. More concretely, the estimation error floor in the high SNR region which mainly comes from the interpolation error is lower in $L_t = 4$ case than in $L_t = 8$ case.

In the next experiment, we will investigate the selection of the time domain pilot with respect to different velocities. In order to exclude the influence of the averaging length, the samples for the interpolation are directly picked from the real CFR. The interpolated CFR is then compared to the real one to evaluate the accuracy of the interpolation. The

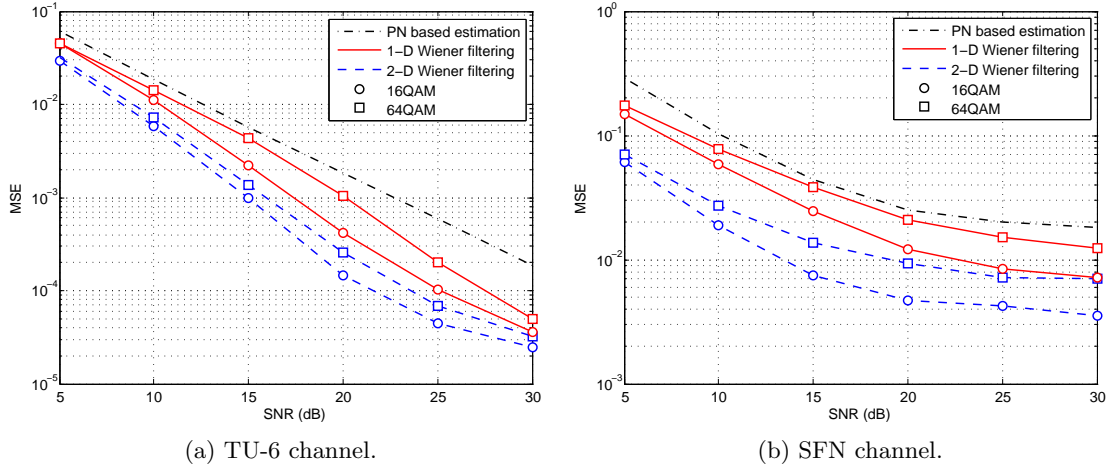


Figure 5.24: MSE of 1-D and 2-D Wiener filtering based estimation methods, after 3 iterations. $L_t = M_t = 2$, $L_f = M_f = 9$ for the TU-6 channel, $L_t = M_t = 2$, $L_f = M_f = 3$ for the SFN channel. Frequency domain method is used as the initial estimation. Velocity is set to 30 km/h for both TU-6 and SFN channels.

MSE of the interpolation is presented in Figure 5.23b. Smaller pilot spacing brings better interpolation results given the same velocity. In addition, higher pilot density provides a better adaptation to the fast channel variation. We should choose the time-domain pilot spacing so that the error introduced by the interpolation is a less significant factor in the overall estimation results. For example, in order to limit the interpolation error to less than 10^{-4} , we have to choose the spacing $L_t = 8$ when the velocity is 30 km/h and $L_t = 2$ when the velocity is 120 km/h. On the other hand, recall that the sampling theorem claiming $L_t T_b f_d \leq 1/2$, that is, $L_t \leq 64$ and $L_t \leq 16$ with velocity of 30 km/h and 120 km/h, respectively.⁽⁴⁾ It indicates that in practice the pilot spacing should be significant (e.g. four times) smaller than the limit imposed by the sampling theorem in order to keep the interpolation error in an imperceptible level.

5.7.3.2 MSE

1-D method vs 2-D method Figure 5.24 shows the comparison of the MSE of the proposed method using 1-D and 2-D Wiener filtering techniques in high-order-constellation cases. Obviously, the 2-D Wiener filtering provides a notable improvement over its 1-D counterpart. For instance, the required SNR to achieve an MSE level of 1×10^{-3} using 2-D method is 4.2 dB less than that using 1-D method with 64QAM in the TU-6 channel. Similar effects can be found with 16QAM as well. The data-aided approach is more meaningful in the SFN channel. The MSE of the estimation using 2-D method is reduced several times compared to the 1-D method. Take the 64QAM case as an example, the

(4). The maximum Doppler frequencies (f_d) corresponding to velocities of 30 km/h and 120 km/h are 13.89 Hz and 55.56 Hz given a carrier frequency of 500 MHz. T_b is equal to $555.6 \mu\text{s}$ when the GI is 420 samples in the DTMB system.

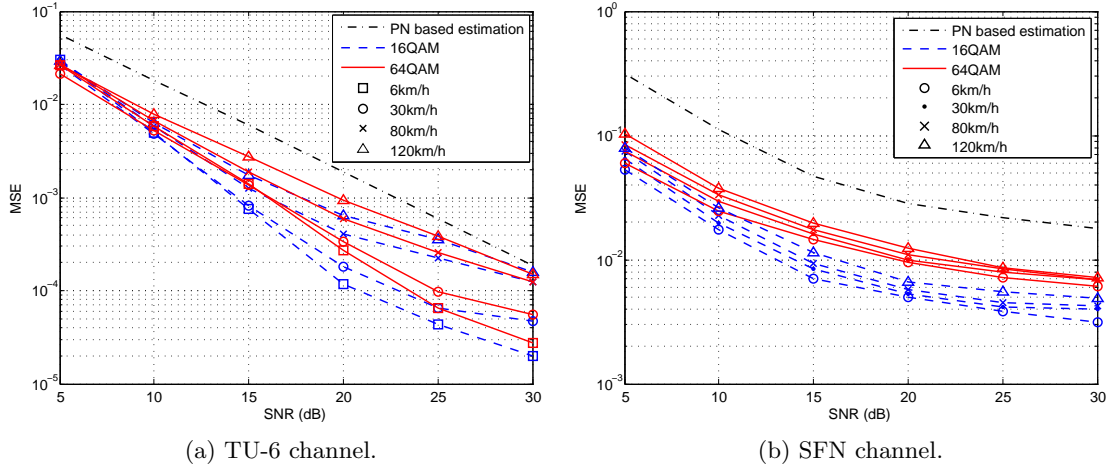
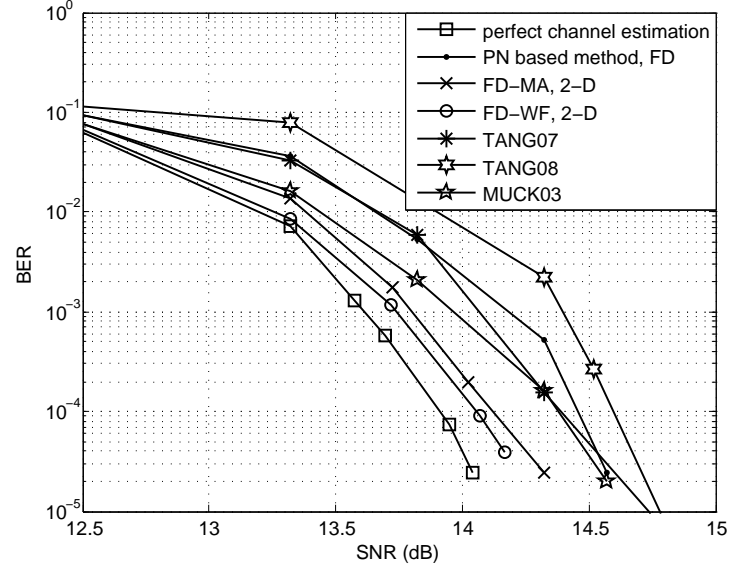


Figure 5.25: MSE of 2-D Wiener filtering with different speed. $L_t = M_t = 2$, $L_f = M_f = 9$ for the TU-6 channel, $L_t = M_t = 2$, $L_f = M_f = 3$ for the SFN channel.

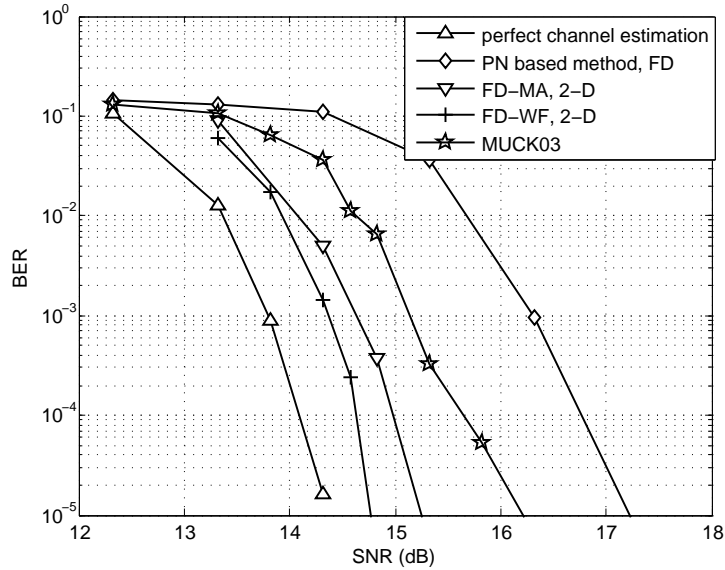
MSE given SNR equal to 20 dB is reduced from 2×10^{-2} to less than 10^{-2} . As shown in Section 5.7.3.3, this reduction of estimation error will bring significant improvement in terms of BER. This improvement owes to the stronger noise suppression capability coming from the expanded averaging range as well as the additional time-domain Wiener filtering in the 2-D approach. Considering that the time domain averaging length M_t is set to only 2 in this experiment, more benefit will be acquired when greater M_t is used in a static channel. In general, this experiment shows that the proposed method is efficient with higher order modulations such as 16QAM and 64QAM in both TU-6 and SFN channels.

MSE Performance with Different Velocities In this experiment, we examine the performance variation of the proposed method with respect to different velocities of the receiver. Figure 5.25a and 5.25b present the MSE of the estimation in the TU-6 channel and the SFN channel, respectively. The time domain spacing of the virtual pilots is set to $M_t = 2$ in order to adapt to the high channel variations. With the increase of the velocity, the variation of the channel among consecutive OFDM symbols becomes more notable, which limits the accuracy in the averaging results in (5.29). In low SNR region (e.g. SNR less than 10 dB), the channel variation is a less significant influence that affects the performance of estimation compared to the noise. While in high SNR region where the noise is no longer the dominant influence, the channel variation compromises the performance of the proposed method. However, it should be noted that the proposed method can still provide adequate improvement. For instance, in TU-6 channel with velocity of 30 km/h, the proposed method obtains 8.3 dB gain with 16QAM in terms of required SNR to achieve MSE of 1×10^{-3} . Whereas in the SFN channel, as ISI is so strong that the effect of the channel variation is not a significant factor. Therefore, the degradation of performance due to the channel variation is not obvious in the SFN channel.

5.7.3.3 BER



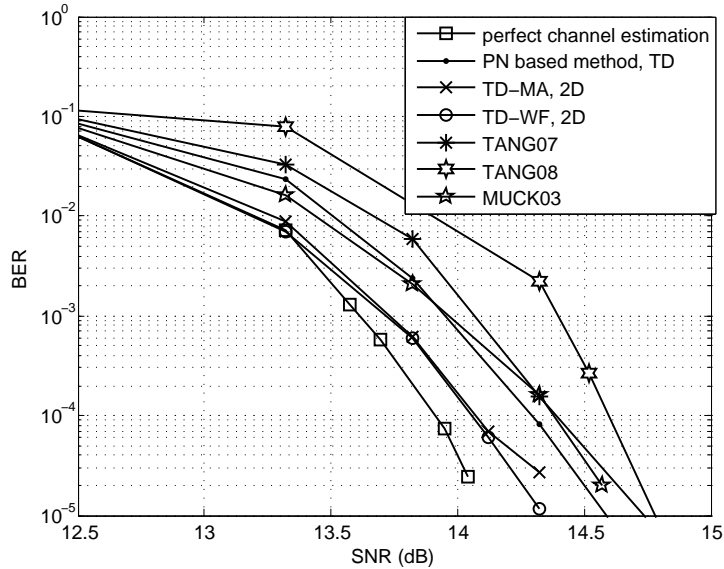
(a) TU-6 channel.



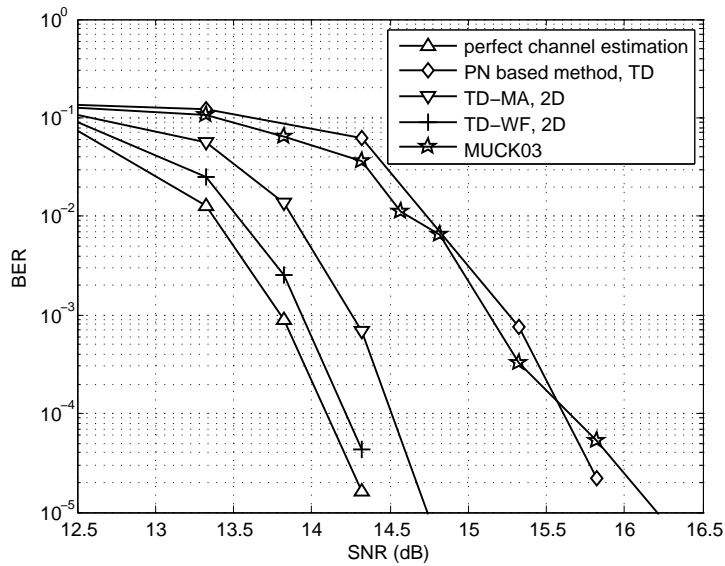
(b) SFN channel.

Figure 5.26: BER of DTMB system using the 2-D approaches. 16QAM $R=0.6$. $M_t = 2$, $M_f = 9$ for the TU-6 channel, $M_t = 2$, $M_f = 3$ for the SFN channel.

Comprehensive simulations are carried out to evaluate the proposed data-aided channel estimation with 2-D refinement approaches. The PN-based time-domain and frequency-domain estimation methods as well as the methods proposed in [76](TANG07), [142](TANG08) and [12](MUCK03) are still chosen as reference methods for comparison. The BER performance are shown in Figure 5.26, 5.27, 5.28 and 5.29. To quantify the improvements



(a) TU-6 channel.



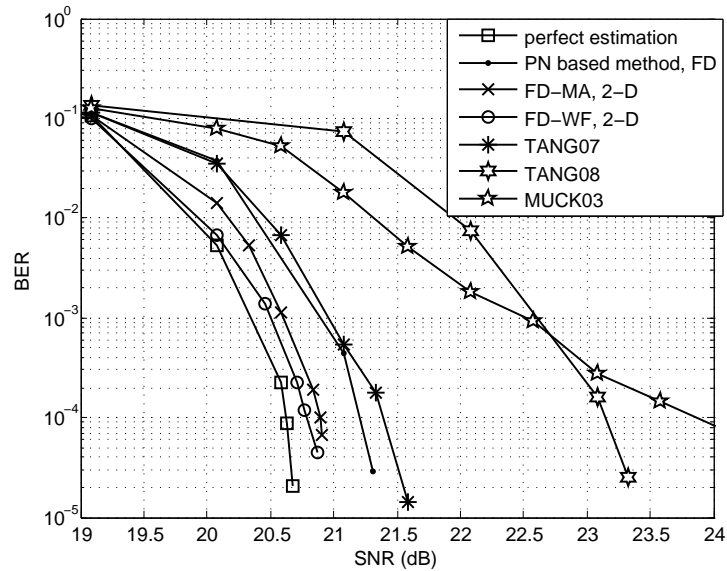
(b) SFN channel.

Figure 5.27: BER of DTMB system using the 2-D approaches. 16QAM $R=0.6$. $M_t = 2$, $M_f = 9$ for the TU-6 channel, $M_t = 2$, $M_f = 3$ for the SFN channel.

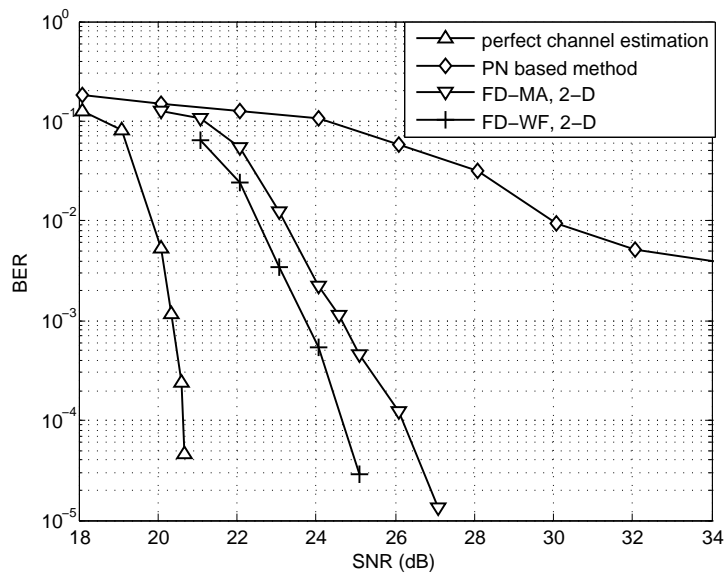
brought by the proposed method, we observe the required SNR to achieve a BER level of 5×10^{-5} . Similar as in Section 5.7.2.4, the performance differences among these methods are concluded in Table 5.3 and 5.4.

Besides the remarks drawn in the 1-D case (c.f. Section 5.7.2.4), some interesting observations are found from the simulation results:

1. *The proposed data-aided methods perform the best among all the reference methods in the comparison.* More precisely, compared with method TANG07, the proposed methods



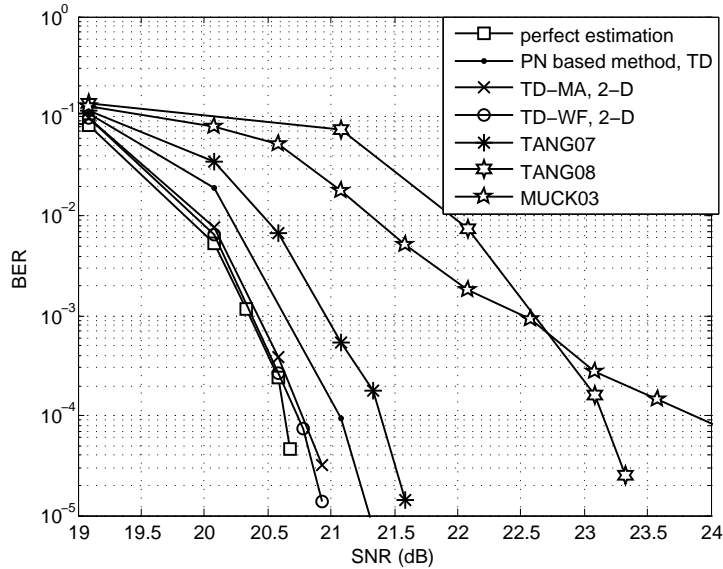
(a) TU-6 channel.



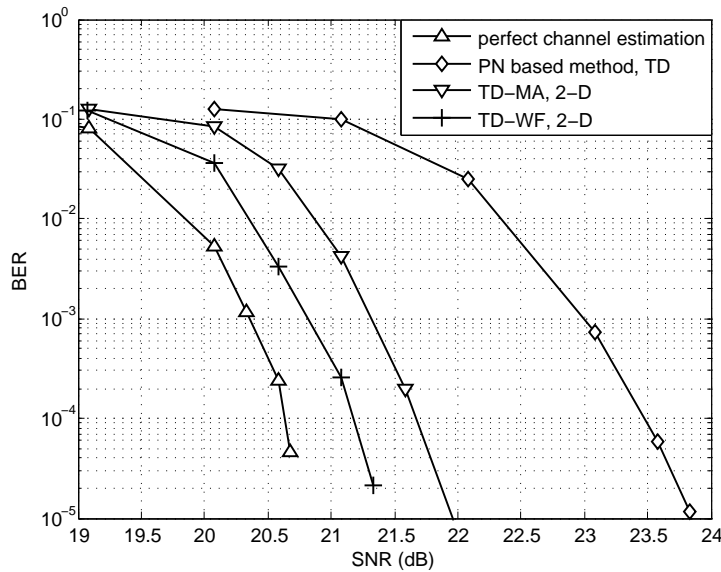
(b) SFN channel.

Figure 5.28: BER of DTMB system using the 2-D approaches. 64QAM $R=0.6$. $M_t = 2$, $M_f = 9$ for the TU-6 channel, $M_t = 2$, $M_f = 3$ for the SFN channel.

provide more than 0.3 dB gain with 16QAM and more than 0.5 dB gain with 64QAM in the TU-6 channel. These improvements mainly come from the fact that the reference method suffers from ISI while the proposed method uses the ISI-free part of the PN sequence for the initial estimation. When ISI becomes stronger, for instance in the SFN channel, the performance of the reference method is severely degraded. As far as the method TANG08 is concerned, the partial-decision based ISI cancellation is not very effective in the



(a) TU-6 channel.



(b) SFN channel.

Figure 5.29: BER of DTMB system using the 2-D approaches. 64QAM $R=0.6$. $M_t = 2$, $M_f = 9$ for the TU-6 channel, $M_t = 2$, $M_f = 3$ for the SFN channel.

channels containing deep fades such as TU-6 and SFN channels. Therefore, the proposed method outperforms the method TANG08 more than 0.4 dB and 2.3 dB with 16QAM and 64QAM, respectively. Concerning method MUCK03, it provides a similar performance as frequency domain PN-based method with 16QAM. However, method MUCK03 seems not effective with 64QAM. The BER slope declines slower than other methods, which indicates a channel estimation error floor at a high MSE level. It suggests that method

Table 5.3: Summary of the gains obtained using the data-aided channel estimation methods with 16QAM.

Channel	method	Gain over PN-base method (dB)	Gain over method TANG07 (dB)	Gain over method TANG08 (dB)	Gain over method MUCK03 (dB)	Gap away from perfect estimation (dB)
TU-6	FD-MA	0.3	0.3	0.4	0.2	0.2
	FD-WF	0.4	0.4	0.5	0.3	0.2
	TD-MA	0.2	0.3	0.5	0.3	0.2
	TD-WF	0.2	0.4	0.5	0.3	0.2
SFN	FD-MA	1.9	-	-	0.8	0.9
	FD-WF	2.2	-	-	1.2	0.5
	TD-MA	1.1	-	-	1.3	0.4
	TD-WF	1.3	-	-	1.5	0.2

Table 5.4: Summary of the gains obtained using the data-aided channel estimation methods with 64QAM.

Channel	method	Gain over PN-base method (dB)	Gain over method TANG07 (dB)	Gain over method TANG08 (dB)	Gain over method MUCK03 (dB)	Gap away from perfect estimation (dB)
TU-6	FD-MA	0.3	0.5	2.3	>3	0.3
	FD-WF	0.4	0.6	2.4	>3.1	0.2
	TD-MA	0.3	0.6	2.4	>3.1	0.2
	TD-WF	0.3	0.6	2.4	>3.1	0.2
SFN	FD-MA	>7	-	-	-	5.8
	FD-WF	>8	-	-	-	4.2
	TD-MA	1.8	-	-	-	1.1
	TD-WF	2.3	-	-	-	0.6

MUCK03 should combine some additional treatments such as frequency domain pilots or ISI cancellation when used in 64QAM case. This coincides with the conclusion in [12].

Moreover, the proposed methods achieve near optimal performance in the TU-6 channel. The degradations compared with the perfect channel estimation case are only 0.2 dB to 0.3 dB. While in the SFN channel, these gaps are limited to less than 1 dB in the 16QAM case. When the 64QAM is used in the SFN channel, the frequency-domain PN based method is not efficient and yields an error floor. The 2-D FD-MA/FD-WF methods can eliminate this error floor in the observed BER range (with an inferior boundary of as low as 3×10^{-5}). The performance of 2-D TD-MA/TD-WF methods is more close to the perfect channel estimation case. Only 1.1 dB and 0.6 dB gaps can be found between them.

2. *The 2-D moving average and 2-D Wiener filtering techniques provide approximately the same BER performance in the TU-6 channel.* The efficiency of the Wiener filtering is more obvious in the SFN channel. For instance, the Wiener filtering approach brings 1.6 dB additional gains over the moving average one when the frequency domain method is used as initial estimation in the 64QAM case.

5.8 Conclusion

In this chapter, we have proposed novel iterative data-aided channel estimation algorithms. In contrast to the classical turbo channel estimation, the proposed algorithms do not include the decoding and interleaving processing when rebuilding the data symbols. By doing so, we can exclude the extremely deep interleaver and de-interleaver specified in DTMB from the feedback loop in order to reduce the computational complexity and processing time. Instantaneous data-aided channel estimates are obtained using the soft data symbols rebuilt from the output of the demapper. Several techniques including moving average and Wiener filtering in both 1-D and 2-D have been studied to refine the data-aided channel estimation. Comprehensive simulation results show that the proposed data-aided channel estimation algorithms provide superior performance over the PN-based methods as well as the methods in the literatures for all constellations in different channel conditions.

Conclusions and Prospects

Conclusions

IN THIS THESIS, we have focused on the newly issued Chinese DTTB standard – DTMB. Our research works have concentrated on three aspects:

- **First, we performed analyses and comparisons between two important DTTB standards–DTMB and DVB-T from system specifications, power efficiency, BER and spectral efficiency perspectives.** It has been shown that the two systems achieve similar performance and can provide equivalent working modes for different application scenarios. The analyses and comparisons presented a clear view of these two systems and provide good bases for the further studies on each system.
- **Then, we investigated the PN-sequence-based channel estimation algorithms which are the key techniques in the reception of the TDS-OFDM signal.** Concretely, we proposed several channel estimation methods that exploit the PN sequence either in the time domain or in the frequency domain. Through the theoretical and numerical analyses, we showed that the time domain correlation based channel estimation method is more effective solution for TDS-OFDM. Consequently, we proposed several improved time domain estimation methods that significantly reduce the estimation error floor resulting from the correlation of PN sequences.
- **Finally, we studied novel data-aided channel estimation algorithms with low computational complexity.** Specifically, we proposed to use the rebuilt soft data symbols as the virtual training sequence for the channel estimation. The cumbersome LDPC decoder and the convolutional interleaver were excluded from the feedback loop when rebuilding the data symbols in order to reduce the computational complexity as well as the processing delay of the DTMB system. Several techniques including 1-D/2-D moving average and Wiener filtering were used to mitigate the noise in the channel estimate obtained using the virtual training sequence. Simulation results showed that the new data-aided channel estimation methods can

significantly improve the accuracy of the channel estimate obtained from the PN sequence, and, more importantly, provide effective channel estimation in the severe SFN channels.

Prospects

Many directions can be pursued to carry out some further researches. In our opinion, the interesting research topics include, but not limited to, the following three general aspects:

1. **The extension of the TDS-OFDM signal waveform in the Multiple-Input Multiple-Output (MIMO) case.** It is well known that the use of multiple antennas at both the transmitter and receiver sides can effectively improve the throughput of communication systems [182, 183, 184]. Many latest communication standards have taken the MIMO transmission scheme into account in their new proposals. For instance, the IEEE 802.11n WLAN standard, released in October 2009, recommends MIMO-OFDM solution. In addition, the proposals for the next generation cellular phone system, i.e. High-Speed Packet Access plus (HSPA+) and Long Term Evolution (LTE), also take MIMO scheme into account. The MIMO implementation is also considered in the new development of the DTTB standards. The Multiple-Input Single-Output (MISO) with the Alamouti scheme [185] can be used in DVB-T2. The latest proposal to DVB-T2 also points out the possibility to use multiple receiving antennas [186]. Some proposals of MIMO extension for the DTMB system are also reported in the recent literatures [187, 188, 189, 190]. In our opinion, the MIMO extension of the DTMB system should be considered in the following two aspects:

- (a) *Combination of the MIMO transmission and the TDS-OFDM signal waveform.* Although there exist some proposals in the literatures, more research works should be carried out to find an optimal combination of the MIMO transmission and the TDS-OFDM signal waveform. The general requirements are: the new MIMO-TDS-OFDM scheme should be robust to different channel conditions, should have simple but efficient equalization methods, and should have good backwards compatibility to the traditional Single-Input Single-Output (SISO) TDS-OFDM scheme.
- (b) *Effective channel estimation algorithms adapted to the MIMO scheme.* To achieve this goal, we should find out an optimal GI structure that can efficiently prevent ISI and, more importantly, is suitable for estimating the MIMO channels. Besides the m-sequence, some other PN sequence such as Golay complementary sequences may be considered to serve as the training sequence.

2. **Enhanced reception algorithms for the DTMB system that adapt to mobile reception cases.** Being different from the DVB-T and ATSC standards which are designed primarily for the fixed reception using rooftop aerials, the support of the mobile reception was a fundamental requirement in the initial call for proposals of the DTMB standard. Specifically, the mobile reception contains two typical application scenarios:

- (a) *Mobile reception in the urban area.* Nowadays, the people in the metropolitans have to spend several hours each day to go to and come back from their works. If DTV broadcast covers the main city transportations such as motor roads, metro, bus, taxis, etc., it will not only provide good leisure and entertainment for the public, but also create huge opportunities for the business. In this application scenario, as the velocity is not very high, the influence of the Doppler frequency shift is not significant. The main challenge is the multipath propagation environment in the urban area. In addition, SFN should be implemented in order to achieve a good DTV coverage over every corner of the city including tunnels, underground metro lines and so on. However, it leads to serious multipath channel conditions which make the channel estimation very difficult. We have already noticed and studied this interesting but challenging application, and proposed an effective data-aided channel estimation algorithms in Chapter 5. Further studies can be carried out pursuing this direction to develop more reception schemes that can handle the complicated channel conditions in the urban area.
 - (b) *The reception in extremely high speed scenarios.* More than four billion passengers take the railways each year in China. However, there are hardly any on-board entertainments. The railway operators hope to provide multimedia services, especially live DTV broadcasting, in the train. Consider that the maximum operating speed of the high speed railway is as high as 350 km/h and is expected to exceed 500 km/h in a short future, the DTV broadcast system should support extremely high speed reception. In this case, the channel can significantly vary within an OFDM symbol duration. It is necessary to design more efficient reception schemes that adapt the high dynamic channel conditions.
3. **Global performance comparisons between pilot-assisted CP-OFDM based systems and TDS-OFDM based systems.** In Chapter 3, we have compared the CP-OFDM based DVB-T system and the TDS-OFDM based DTMB system from a system perspective. In addition, [191] presented the performance comparisons of the WLAN systems using CP-OFDM and PRP-OFDM waveforms, respectively. However, these comparisons are associated to the system specifications and the unique structures of the known sequences in the GI. Therefore, it will be interesting to carry out comparative studies between CP-OFDM based and TDS-OFDM based systems taking into account the accuracies of different channel estimation and synchronization algorithms for each OFDM waveforms. All the factors that affect the efficiency of the transmission, including the amount of the transmission overhead, power boost, channel estimation and synchronization methods etc., should be involved in the studies. The studies could be carried out in terms of theoretically analyses and comprehensive numerical simulations. These studies would provide directive knowledge for the system designers and engineers who work on the CP- or TDS-OFDM systems.

Derivation of (2.82)

Substitute $H_{m,k} = \frac{1}{N} \sum_{n=0}^{N-1} H[k, n] e^{-j\frac{2\pi}{N}n(m-k)}$ into (2.82), it leads:

$$\begin{aligned}
 \mathbb{E}[|H_{m,k}|^2] &= \frac{1}{N^2} \sum_{n_1=0}^{N-1} \sum_{n_2=0}^{N-1} \mathbb{E}[H^*[k, n_1]H[k, n_2]] e^{-j\frac{2\pi}{N}(n_2-n_1)(m-k)} \\
 &= \frac{1}{N^2} \sum_{n_1=0}^{N-1} \sum_{n_2=0}^{N-1} \phi_H(0, (n_2 - n_1)T_s) e^{-j\frac{2\pi}{N}(n_2-n_1)(m-k)} \\
 &= \frac{1}{N^2} \sum_{n_1=0}^{N-1} \sum_{n_2=0}^{N-1} \phi_t((n_2 - n_1)T_s) \sum_l \sigma_l^2 e^{-j\frac{2\pi}{N}(n_2-n_1)(m-k)} \\
 &= \frac{1}{N^2} \sum_{n_1=0}^{N-1} \sum_{n_2=0}^{N-1} J_0(2\pi f_m(n_2 - n_1)T_s) e^{-j\frac{2\pi}{N}(n_2-n_1)(m-k)}. \quad (\text{A.1})
 \end{aligned}$$

where $\phi_H(\Delta f, \Delta t)$ and $\phi_t(\Delta t)$ are the spaced-frequency spaced-time autocorrelation function and spaced-time correlation function defined in Section 2.1.3.2, respectively. σ_l^2 is the average power of the l th path. Normally we have a channel with normalized power i.e. $\sum_l \sigma_l^2 = 1$. $J_0(\cdot)$ zeroth-order *Bessel* function of the first kind, f_m is the maximum Doppler frequency shift and T_s is the baseband symbol duration.

		$\xrightarrow{n_1}$				
		0	1	2	...	N-1
$\downarrow n_2$	0	0	-1	-2	...	-(N-1)
	1	1	0	-1	...	-(N-2)
	2	2	1	0	...	-(N-3)
	\vdots	\vdots	\vdots	\vdots	\ddots	\vdots
	N-1	N-1	N-2	N-3	...	0

Figure A.1: Substituting $d = n_2 - n_1$, the resulting value of d .

Substituting $d = n_2 - n_1$ in above equation, the resulting the number of each value of d is given in Figure A.1. Considering that $J_0(\cdot)$ is an even function, we can get:

$$\mathbb{E}[|H_{m,k}|^2] = N + 2 \sum_{d=1}^{N-1} \left[(N-d) J_0(2\pi f_m d T_s) \cos\left(\frac{2\pi}{N} d(m-k)\right) \right]. \quad (\text{A.2})$$

Therefore, the power of ICI for the m^{th} subcarrier is:

$$\begin{aligned} P_{\text{ICI}}(m) &= \sum_{\substack{k=0 \\ k \neq m}}^{N-1} \mathbb{E}[|X[k]H_{m,k}|^2] \\ &= \frac{N-1}{N} + \frac{2}{N^2} \sum_{\substack{k=0 \\ k \neq m}}^{N-1} \sum_{d=1}^{N-1} \left[(N-d) J_0(2\pi f_m d T_s) \cos\left(\frac{2\pi}{N} d(m-k)\right) \right]. \square \end{aligned}$$

Analysis of the Estimation Error of the Frequency Estimator

From (4.62), the estimation error of the frequency domain estimator is given by a complex-value division:

$$\xi[k] = \frac{W[k]}{P[k]} = \frac{W[k]P[k]^*}{|P[k]|^2}, \quad (\text{B.1})$$

where $P[k]$ is a deterministic complex value and $W[k]$ is the complex Gaussian random variable, i.e. $W[k] \sim \mathcal{CN}(0, \sigma_W^2)$. Moreover, the real and imaginary parts of the $W[k]$ are uncorrelated Gaussian random variables. Considering that the $P[k]$ is deterministic, it can be easily verified that the estimation error $\xi[k]$ is still a complex Gaussian random variable with zero-mean. Its real and imaginary parts are also uncorrelated. Therefore, the variance of the estimation error is:

$$\mathbb{E}[\xi[k]^* \xi[k]] = \frac{\mathbb{E}[W[k]^* W[k]] |P[k]|^2}{|P[k]|^4} = \frac{\sigma_W^2}{|P[k]|^2}. \quad (\text{B.2})$$

That is to say, the estimation error is affected by the norm of the frequency response of the PN sequence. \square



Norm of the Frequency Response of m-sequence

According to the property of the cross-correlation [150, p.450], the norm of frequency of the m-sequence can be computed by the Fourier transform of its circular cross-correlation:

$$\begin{aligned} |P[k]|^2 &= \frac{1}{\sqrt{N_{\text{PN}}}} \sum_{n=0}^{N_{\text{PN}}-1} p^*[n] e^{j\frac{2\pi}{N_{\text{PN}}}nk} \cdot \frac{1}{\sqrt{N_{\text{PN}}}} \sum_{n'=0}^{N_{\text{PN}}-1} p[n'] e^{-j\frac{2\pi}{N_{\text{PN}}}n'k} \quad (\text{C.1}) \\ &= \sum_{m=0}^{N_{\text{PN}}-1} \underbrace{\left(\frac{1}{N_{\text{PN}}} \sum_{n'=0}^{N_{\text{PN}}-1} p^*[n] p[n+m] \right)}_{C_p[m]} e^{-j\frac{2\pi}{N_{\text{PN}}}mk} \end{aligned}$$

Recall that the correlation property of the m-sequence:

$$C_p[m] = \frac{1}{N_{\text{PN}}} p[n] \otimes p[n+m] = \begin{cases} 1 & m = 0 \\ -\frac{1}{N_{\text{PN}}} & 0 < m < N_{\text{PN}} \end{cases} \quad (\text{C.2})$$

The squared norm of the frequency response of the PN sequence can easily computed as:

$$\begin{aligned} |P[k]|^2 &= \sum_{m=0}^{N_{\text{PN}}-1} C_p[m] e^{-j\frac{2\pi}{N_{\text{PN}}}mk} \\ &= 1 - \frac{1}{N_{\text{PN}}} \sum_{m=1}^{N_{\text{PN}}-1} e^{-j\frac{2\pi}{N_{\text{PN}}}mk} \\ &= 1 + \frac{1}{N_{\text{PN}}} - \frac{1}{N_{\text{PN}}} \sum_{m=0}^{N_{\text{PN}}-1} e^{-j\frac{2\pi}{N_{\text{PN}}}mk} \\ &= \begin{cases} \frac{1}{N_{\text{PN}}} & k = 0 \\ \frac{N_{\text{PN}}+1}{N_{\text{PN}}} & 0 < k < N_{\text{PN}} \end{cases} \quad (\text{C.3}) \end{aligned}$$

□

List of Figures

1	DTTB normes dans le monde [7].	viii
2	Différents types d'intervalle de garde	xi
3	Schéma de modulation/démodulation OFDM.	xi
4	Schéma du système DVB-T.	xvi
5	Schéma du système DTMB.	xvi
6	Comparaison des performances TEB dans le canal P1, avec différentes modulations, taux de codage et méthodes d'estimation de canal.	xix
7	Comparaison de l'efficacité spectrale dans le canal P1.	xix
8	Comparaison des performances des estimateurs dans les domaines temporel et fréquentiel. Les résultats sont obtenus avec 500 réalisations du canal TU-6.	xxiii
9	Comparaison des performances des différents estimateurs dans le domaine temporel. Les résultats sont obtenus avec 500 réalisations de TU-6 canal.	xxiv
10	Schéma fonctionnel du système TDS-OFDM. Les cases ombrées correspondent aux traitements utilisés pour la méthode proposée. Les blocs en pointillés correspondent aux traitements complémentaires nécessaires à l'estimation de canal Turbo.	xxv
11	Moving average en 1-D.	xxvii
12	Filtage de Wiener en 1-D.	xxvii
13	Filtage de Wiener en 2-D.	xxviii
14	TEB du système DTMB avec estimation de canal 1-D basée sur les données. 4QAM, $R = 0,8$. L'estimation basée sur la séquence PN est faite dans le domaine fréquentiel.	xxix
15	TEB du système DTMB avec estimation de canal 2-D. 64QAM $R=0,6$. $M_t = 2$, $M_f = 9$ pour canal TU-6, $M_t = 2$, $M_f = 3$ pour canal SFN. . . .	xxx
16	Research scope of the project "Mobile TV World".	3
1.1	Worldwide TV market revenue 2006-2013 [18].	8
1.2	DTV transition progress in the world [19].	9
1.3	Coverage improvement after DTV transition in Philadelphia U.S. [22]. . .	10
1.4	Worldwide TV reception modes 2006-2013 [18].	11

1.5	DTTB standards in the world (source from [7]).	12
2.1	Large- and small-scale fading.	20
2.2	Multipath propagation.	21
2.3	Responses of the TU-6 channel.	22
2.4	Channel frequency response of TU-6 channel with different velocities. Carrier frequency is 500 MHz. Channel bandwidth is 7.56 MHz. Each time slot represents $50\mu s$	24
2.5	Quadrature amplitude modulation.	25
2.6	Symbol-spaced tapped delay line channel model.	27
2.7	OFDM signal waveform.	31
2.8	Relationship among the channel correlation functions and power density functions.	33
2.9	Flat fading and frequency-selective fading.	35
2.10	Relationship of signal frequency/time selectivity and coherence bandwidth/time.	35
2.11	Sample spaced CIR generation by interpolation.	38
2.12	SFN broadcasting.	38
2.13	Equivalent CIR of the SFN channel.	39
2.14	OFDM signal waveform.	41
2.15	Block diagram of OFDM modulation and demodulation.	43
2.16	Ideal OFDM transmission model.	45
2.17	Different types of GI.	46
2.18	Overlap-and-add process to equalize ZP-OFDM signal.	47
2.19	Some variants of the GI formation.	49
2.20	Intercarrier interference when there is a frequency shift.	50
2.21	ICI resulting from the Doppler frequency in DTMB with $T_s = 1/7.56\mu s$, $N = 3780$	53
3.1	Block diagram of the DVB-T system.	56
3.2	Block diagram of the DTMB system.	57
3.3	Block diagram of the encoder of channel coding in DTMB.	60
3.4	Structure of the convolutional interleaver.	61
3.5	Frequency signal structures of DVB-T and DTMB in a 8 MHz channel.	62
3.6	BER comparison of DVB-T and DTMB without outer codes in AWGN channel, $GI = 1/4$	66
3.7	BER comparison of DVB-T and DTMB with outer codes in AWGN channel, $GI = 1/4$	67
3.8	BER comparison of DVB-T and DTMB in F1 channel with outer codes, $GI = 1/4$	68
3.9	BER comparison of DVB-T and DTMB in P1 channel with outer codes, $GI = 1/4$	68
3.10	BER performance comparison in F1 channel, with different modulations, code rates and channel estimation methods.	69
3.11	BER performance comparison in P1 channel, with different modulations, code rates and channel estimation methods.	70
3.12	BER performance comparison in TU-6 channel with a velocity of 30km/h, with different modulations, code rates and channel estimation methods.	71

3.13	Spectral efficiency comparison in F1 (Ricean) channel, $GI = 1/4$	72
3.14	Spectral efficiency comparison in P1 (Rayleigh) channel, $GI = 1/4$	72
3.15	Spectral efficiency comparison in TU-6 channel, $GI = 1/4$	73
3.16	Spectral efficiency comparison in F1 (Ricean) channel with $GI = 1/8$ in DVB-T and $GI = 1/9$ in DTMB.	73
3.17	Spectral efficiency comparison in P1 (Rayleigh) channel with $GI = 1/8$ in DVB-T and $GI = 1/9$ in DTMB.	74
3.18	Spectral efficiency comparison in TU-6 channel with a velocity of 30km/h. $GI = 1/8$ in DVB-T and $GI = 1/9$ in DTMB.	74
4.1	Structure of the GI.	81
4.2	PN removal of the TDS-OFDM signal.	82
4.3	OLA.	83
4.4	Distribution of the interference resulted from the residual PN sequence when $SNR = 10$ dB in the TU-6 channel.	85
4.5	Circular correlation result of the m-sequence.	89
4.6	The equivalent channel matrices given sufficient and insufficient long CP for PN sequence.	97
4.7	Separate $\mathbf{R}_{cp}\mathbf{H}_{ISI}\mathbf{I}_{cp}$	98
4.8	Performance comparison of time and frequency domain estimators. Results are obtained from 500 realizations of TU-6 channel with a maximum delay of $5 \mu s$, or $L = 43$ samples of the DTMB system.	103
4.9	Performance comparison of time and frequency domain estimators. Results are obtained from 500 realizations of Hilly Terrain (HT) channel with a maximum delay of $17.2 \mu s$, or $L = 135$ samples of the DTMB system.	104
4.10	Performance comparison of several time domain estimators. Results are obtained from 500 realizations of TU-6 channel with a maximum delay of $5 \mu s$, or $L = 43$ samples of the DTMB system.	105
4.11	Performance comparison of several time domain estimators. Results are obtained from 500 realizations of Hilly Terrain (HT) channel with a maximum delay of $17.2 \mu s$, or $L = 135$ samples of the DTMB system.	106
4.12	Performance of estimator with IBI removal and cyclic reconstruction. $\nu = 420$, $N_{PN} = 255$, $N_{CP} = 165$. Time domain correlation-based estimator is used. 200 realizations of SFN channel with $L = 244$	108
4.13	Performance of estimator with IBI removal and cyclic reconstruction. $\nu = 420$, $N_{PN} = 255$, $N_{CP} = 165$. Frequency domain estimator is used. 200 realizations of SFN channel with $L = 244$	109
4.14	Noise boost in the frequency domain estimator.	110
4.15	Linear cross-correlation between the GI and the PN sequence.	111
5.1	Block diagram of TDS-OFDM system using classical Turbo channel estimation.	115
5.2	Block diagram of TDS-OFDM system using proposed data-aided channel estimation. The shaded blocks are the processings used for the proposed method. The dashed blocks are the additional processings needed for the turbo channel estimation.	115
5.3	Hard decision vs soft decision using $\tanh(\frac{\lambda}{2})$ function.	118

5.4	Example of QPSK-modulated data symbols after equalization and rebuilt data symbols when the SNR is 10 dB.	119
5.5	CFR of a TU-6 channel.	121
5.6	1-D moving average.	122
5.7	1-D averaging and interpolation.	123
5.8	2-D averaging and interpolating. The averaging is performed in the 2-D averaging region (shaded area). The interpolation is first carried out in frequency domain (①) and secondly in time domain (②).	126
5.9	Several commonly used pilot patterns.	129
5.10	MSE comparison of 1-D Moving Average method and 1-D Wiener filtering method, <i>frequency domain method</i> as initial estimation. For both moving average and Wiener filtering, $M = 9$ for TU-6 and $M = 3$ for SFN channel. $L_f = 9$ and $L_f = 3$ for TU-6 and SFN channel, respectively.	133
5.11	MSE comparison of 1-D Moving Average method and 1-D Wiener filtering method, <i>time domain method</i> as initial estimation. For both moving average and Wiener filtering, $M = 9$ for TU-6 and $M = 3$ for SFN channel. $L_f = 9$ and $L_f = 3$ for TU-6 and SFN channel, respectively.	134
5.12	MSE of 1-D Moving Average method <i>before</i> combination with different averaging lengths, frequency domain method as initial estimation.	135
5.13	Impact of the averaging length on the data-aided estimation results in the SFN channel with a propagation difference of 7km.	136
5.14	MSE of 1-D Wiener filtering method <i>before</i> combination with different averaging lengths, frequency domain method as initial estimation. Pilot spacing $L_f = 9$ for all cases.	137
5.15	MSE of 1-D Wiener filtering method <i>before</i> combination with different pilot spacings, frequency domain method as initial estimation. Averaging length $M = 9$ for all cases.	138
5.16	Impact of the averaging length on the data-aided estimation results in the SFN channel. Pilot spacing $L_f = 3$	139
5.17	BER of the DTMB system using the data-aided channel estimation methods with TU-6 channel. QPSK, R=0.8. <i>Frequency domain</i> PN based method is used as initial channel estimation.	140
5.18	BER of the DTMB system using the data-aided channel estimation methods with SFN channel. QPSK, R=0.8. <i>Frequency domain</i> PN based method is used as initial channel estimation.	140
5.19	BER of the DTMB system using the data-aided channel estimation methods with TU-6 channel. QPSK, R=0.8. <i>Time domain</i> PN based method is used as initial channel estimation.	141
5.20	BER of the DTMB system using the data-aided channel estimation methods with SFN channel. QPSK, R=0.8. <i>Time domain</i> PN based method is used as initial channel estimation.	141
5.21	MSE of 1-D data-aided approaches with higher order constellations.	142
5.22	Comparison of the MSE of moving-averaged channel estimation using LS and asymptotical LS estimators in TU-6 channel with velocity of 6 km/h.	143
5.23	Influence of pilot pattern on the MSE of the estimation.	144

5.24	MSE of 1-D and 2-D Wiener filtering based estimation methods, after 3 iterations. $L_t = M_t = 2$, $L_f = M_f = 9$ for the TU-6 channel, $L_t = M_t = 2$, $L_f = M_f = 3$ for the SFN channel. Frequency domain method is used as the initial estimation. Velocity is set to 30 km/h for both TU-6 and SFN channels.	145
5.25	MSE of 2-D Wiener filtering with different speed. $L_t = M_t = 2$, $L_f = M_f = 9$ for the TU-6 channel, $L_t = M_t = 2$, $L_f = M_f = 3$ for the SFN channel.	146
5.26	BER of DTMB system using the 2-D approaches. 16QAM R=0.6. $M_t = 2$, $M_f = 9$ for the TU-6 channel, $M_t = 2$, $M_f = 3$ for the SFN channel. . . .	147
5.27	BER of DTMB system using the 2-D approaches. 16QAM R=0.6. $M_t = 2$, $M_f = 9$ for the TU-6 channel, $M_t = 2$, $M_f = 3$ for the SFN channel. . . .	148
5.28	BER of DTMB system using the 2-D approaches. 64QAM R=0.6. $M_t = 2$, $M_f = 9$ for the TU-6 channel, $M_t = 2$, $M_f = 3$ for the SFN channel. . . .	149
5.29	BER of DTMB system using the 2-D approaches. 64QAM R=0.6. $M_t = 2$, $M_f = 9$ for the TU-6 channel, $M_t = 2$, $M_f = 3$ for the SFN channel. . . .	150
A.1	Substituting $d = n_2 - n_1$, the resulting value of d	157

List of Tables

1	Principaux paramètres de DVB-T et DTMB.	xvii
2	Comparaison de l'efficacité d'exploitation de la puissance émise.	xviii
1.1	Main Parameters of DTTB standards	14
2.1	Parameters of the P1 and F1 channels	36
2.2	Power Delay Profile of the TU-6 Channel Model	37
2.3	Power Delay Profile of the Hilly Terrain (HT) Channel Model	37
3.1	Main Parameters of the DVB-T and DTMB Systems.	58
3.2	Comparison of the Net Bit Rates in 6 MHz and 8 MHz Channels [84].	59
3.3	LDPC Codes Performance [89].	60
3.4	Power Efficiency Comparison.	63
3.5	Simulation Parameters and useful bitrates with $GI = 1/4$	64
4.1	Composition of the GI specified in DTMB.	81
4.2	Kurtosis values of the interference caused by the imperfect PN removal.	85
4.3	Complexities of the PN-based channel estimation methods.	101
5.1	Complexity Comparison	131
5.2	Summary of the gains obtained using the data-aided channel estimation methods with QPSK.	139
5.3	Summary of the gains obtained using the data-aided channel estimation methods with 16QAM.	151
5.4	Summary of the gains obtained using the data-aided channel estimation methods with 64QAM.	151

Bibliography

- [1] European Telecommunications Standards Institute (ETSI). Digital Video Broadcasting (DVB); Framing Structure, Channel Coding and Modulation for Terrestrial Television. ETSI EN 300 744 V1.5.1, November 2004.
- [2] Association of Radio Industries and Businesses (ARIB). Terrestrial Integrated Services Digital Broadcasting (ISDB-T) – Specifications of Channel Coding, Framing Structure, and Modulation, September 1998.
- [3] Advanced Television Systems Committee. ATSC Digital Television Standard. Document A/53, September 1995.
- [4] Framing Structure, Channel Coding and Modulation for Digital Television Terrestrial Broadcasting System. Chinese National Standard, Aug. 2006.
- [5] L. Yang, K. Gong, and Z.X. Yang. Pseudo-random sequence padding in an OFDM modulation system, July 2006. US Patent 7,072,289.
- [6] Tous Au Numérique. Calendrier général du passage à la Télé Tout Numérique. http://www.tousaunumerique.fr/tele_numerique.php, 2010.
- [7] Digital Video Broadcasting Project. <http://www.dvb.org/>.
- [8] W. C. Jakes. *Microwave Mobile Communications*. Wiley, 1974.
- [9] T. Rappaport. *Wireless Communications: Principles and Practice*. Prentice Hall, 2001.
- [10] B. Muquet, Z. Wang, G.B. Giannakis, M. de Courville, and P. Duhamel. Cyclic prefixing or zero padding for wireless multicarrier transmissions? *IEEE Transactions on Communications*, 50(12):2136–2148, 2002.
- [11] Z. Yang, L. Tong, and L. Yang. Outage probability comparison of CP-OFDM and TDS-OFDM for broadcast channels. In *Proceedings of the IEEE Global Telecommunications Conference (GLOBECOM'02)*, pages 594–598, November 2002.
- [12] M. Muck, M. de Courville, M. Debbah, and P. Duhamel. A pseudo random postfix OFDM modulator and inherent channel estimation techniques. In *Proceedings of the IEEE Global Telecommunications Conference (GLOBECOM'03)*, pages 2380–2384, December 2003.

- [13] O. Rousseaux, G. Leus, and M. Moonen. Estimation and equalization of doubly selective channels using known symbol padding. *IEEE Transactions on Signal Processing*, 54(3):979–990, 2006.
- [14] M. Zhao, Z. Shi, and M. Reed. Iterative turbo channel estimation for OFDM system over rapid dispersive fading channel. *IEEE Transactions on Wireless Communications*, 7(8):3174–3184, August 2008.
- [15] S.W. Smith et al. *The scientist and engineer's guide to digital signal processing*. California Technical Pub., 1997.
- [16] J. Braun. Worldwide TV unaffected by the crisis! http://www.international-television.org/archive/2010-03-21_global-tv-euro-data-worldwide_2009.pdf, March 2010.
- [17] Nielsen. The Final Tally – 4.7 Billion Tunes in to Beijing 2008 – More Than Two in Three People Worldwide. http://en-us.nielsen.com/main/news/news_releases/2008/september/the_final_tally_-, September 2008.
- [18] IDATE. World Television Market. http://www.idate-research.com/en/News/TV-2010_631.html, January 2010.
- [19] Wikipedia. Digital television transition. http://en.wikipedia.org/w/index.php?title=Digital_television_transition&oldid=369918036, 2010. [Online; accessed 25-June-2010].
- [20] Digital UK. When do I switch? http://www.digitaluk.co.uk/when_do_i_switch, 2010.
- [21] Wikipedia. Digital television. http://en.wikipedia.org/w/index.php?title=Digital_television&oldid=367616467, 2010. [Online; accessed 24-June-2010].
- [22] FCC. DTV Reception Maps. <http://www.fcc.gov/mb/engineering/maps/>.
- [23] European Broadcasting Union (EBU). How should we use the digital dividend? Long-term public interest versus short-term profit. http://www.ebu.ch/CMSimages/fr/___A5_digital-dividend_EN_tcm7-65144.pdf, April 2009.
- [24] Z. X. Yang. The Development of Digital Terrestrial Television Standards and Technologies. Presentation in CCBN2010 China Digital Television Summit (CDTS), March 2010.
- [25] DVB Mobile TV: Services, Trials & Pilots. <http://www.dvb-h.org/services.htm>.
- [26] Advanced Television Systems Committee. ATSC-Mobile DTV Standard . Document A/153, October 2009.
- [27] M. R. Chari, F. Ling, A. Mantravadi, R. Krishnamoorthi, R. Vijayan, G. K. Walker, and R. Chandhok. FLO physical layer: an overview. *IEEE Transactions on Broadcasting*, 53(1 Part 2):145–160, 2007.
- [28] G. Lee, S. Cho, K. T. Yang, Y. K. Hahm, and S. I. Lee. Development of terrestrial DMB transmission system based on Eureka-147 DAB system. *IEEE Transactions on Consumer Electronics*, 51(1):63–68, 2005.
- [29] State Administration of Radio, Film, and Television (SARFT). Mobile Multimedia Broadcasting Part 1: Framing Structure, Channel Coding and Modulation for Broadcasting Channel. Industry standards, GY/T 220.1-2006, October 2006.

- [30] European Telecommunications Standards Institute (ETSI). Frame structure channel coding and modulation for a second generation digital terrestrial television broadcasting system (DVB-T2). EN 302 755 V1.1.1, September 2009.
- [31] Digital Terrestrial Television Action Group (DigiTAG). Understanding DVB-T2 – Key technical, business, & regulatory implications. http://www.digitag.org/DTTResources/DVB-T2_Handbook.pdf, 2009.
- [32] P. Kelley and C. Rigal. DVB-SH – mobile digital TV in S-Band. *EBU Technical Review*, July 2007.
- [33] DVB Project. DVB-NGH, Next Generation Handheld. <http://www.dvb.org/technology/dvb-ngh/>, November 2009.
- [34] Z. X. Yang, Z. Wang, J. Wang, J. Wang, K. Peng, F. Yang, and J. Song. Technical Review for Chinese Future DTTB System. In *Proceedings of the 72nd IEEE Vehicular Technology Conference Fall (VTC 2010-Fall)*, pages 1–6, September 2010.
- [35] B. Sklar. Rayleigh fading channels in mobile digital communication systems. I. Characterization. *IEEE Communications Magazine*, 35(7):90–100, July 1997.
- [36] J. G. Proakis. *Digital Communications*. McGraw-Hill, 2001.
- [37] D. Tse and P. Viswanath. *Fundamentals of Wireless Communication*. Cambridge University Press, 2005.
- [38] A. V. Oppenheim, R. W. Schaffer, and J. R. Buck. *Discrete-Time Signal Processing (2nd ed.)*. Prentice-Hall, 1999.
- [39] Y. Li. Simplified channel estimation for OFDM systems with multiple transmit antennas. *IEEE Transactions on Wireless Communications*, 1(1):67–75, January 2002.
- [40] C. Gutiérrez-Díaz de León, M. Cabrera-Bean, and M. Pätzold. On the problem of symbol-spaced tapped-delay-line models for WSSUS channels. In *Proceedings of the 66th IEEE Vehicular Technology Conference (VTC 2007 Fall)*, 2007.
- [41] Olivier Rousseaux. *Block Transmission Techniques for Wireless Communications*. PhD thesis, Katholieke Universiteit Leuven, <ftp://ftp.esat.kuleuven.be/pub/SISTA/ida/reports/05-18.pdf>, Dec. 2004.
- [42] A. V. Oppenheim and A. S. Willsky. *Signals and Systems*. Prentice-Hall, 1997.
- [43] P. Bello. Characterization of randomly time-variant linear channels. *IEEE Transactions on Communications Systems*, 11(4):360–393, 1963.
- [44] M. Failli. COST 207 Digital Land Mobile Radio Communications. *Commission of the European Communities*, page 137, 1988.
- [45] Y. Li, L.J. Cimini Jr., and N.R. Sollenberger. Robust channel estimation for OFDM systems with rapid dispersive fading channels. *IEEE Transactions on Communications*, 46(7):902–915, July 1998.
- [46] M. Pätzold. *Mobile Fading Channels*. John Wiley & Sons, 2003.
- [47] IEEE P802.15 Wireless Personal Area Networks. Suggested Requirements for a Consumer PAN High Rate Video/MM Link. www.ieee802.org/.../00050r1P802-15_HRSG-Suggested-Requirements.doc, March 2000.
- [48] W. C. Y. Lee. *Mobile Cellular Communications*. McGraw-Hill, 1989.

- [49] R. Steele and L. Hanzo. *Mobile Radio Communications*. Pentech Press Plymouth, 1992.
- [50] S. Weinstein and P. Ebert. Data transmission by frequency-division multiplexing using the discrete Fourier transform. *IEEE Transactions on Communication Technology*, 19(5):628–634, October 1971.
- [51] L. Cimini Jr. Analysis and Simulation of a Digital Mobile Channel Using Orthogonal Frequency Division Multiplexing. *IEEE Transactions on Communications*, 33(7):665–675, July 1985.
- [52] ITU-T Recommendation. Asymmetric digital subscriber line (ADSL) transceivers. G.992.1, June 1999.
- [53] European Telecommunications Standards Institute (ETSI). Radio Broadcasting Systems; Digital Audio Broadcasting (DAB) to mobile, portable and fixed receivers. Final draft ETSI EN 300 401 V1.4.1, January 2006.
- [54] IEEE Standard for Local and metropolitan area networks. Part 11: Wireless LAN Medium Access Control (MAC) and Physical Layer (PHY) specifications High-speed Physical Layer in the 5 GHz Band. 802.11a-1999, February 1999.
- [55] IEEE Standard for Local and metropolitan area networks. Part 16: Air Interface for Broadband Wireless Access Systems. 802.16-2009, May 2009.
- [56] 3GPP. LTE. <http://www.3gpp.org/LTE>, 2010.
- [57] IEEE 802.15 Working Group for WPAN. <http://www.ieee802.org/15/>.
- [58] IEEE 802.20 Mobile Broadband Wireless Access (MBWA). <http://grouper.ieee.org/groups/802/20/>.
- [59] Matthieu Crussière. *Étude et optimisation de communications à haut-débit sur lignes d'énergie : exploitation de la combinaison OFDM/CDMA*. PhD thesis, Institut National des Sciences Appliquées de Rennes (INSA-Rennes), 2005.
- [60] S. Haykin. *Adaptive Filter Theory (4th Edition)*. Prentice-Hall, 2001.
- [61] H. Steendam and M. Moeneclaey. Different guard interval techniques for OFDM: performance comparison. In *Proceedings of the 6th International Workshop on Multicarrier Spread Spectrum (MC-SS'07)*, pages 11–24, Herrsching, Germany, May 2007.
- [62] A. Batra, J. Balakrishnan, G.R. Aiello, J.R. Foerster, and A. Dabak. Design of a multiband OFDM system for realistic UWB channel environments. *IEEE transactions on Microwave Theory and Techniques*, 52(9):2123–2138, 2004.
- [63] M. Toeltsch and A.F. Molisch. Efficient OFDM transmission without cyclic prefix overfrequency-selective channels. In *Proceedings of the 11th IEEE International Symposium on Personal, Indoor and Mobile Radio Communications (PIMRC 2000)*, 2000.
- [64] D. Kim and G.L. Stüber. Residual ISI cancellation for OFDM with applications to HDTV broadcasting. *IEEE Journal on Selected Areas in Communications*, 16(8):1590–1599, 1998.
- [65] X. G. Xia. Precoded and vector OFDM robust to channel spectral nulls and with reduced cyclic prefix length in single transmit antenna systems. *IEEE Transactions on communications*, 49(8):1363–1374, 2001.

- [66] X. Wang, Y. Wu, and J.Y. Chouinard. On the comparison between conventional OFDM and MSE-OFDM systems. In *Proceedings of the IEEE Global Telecommunications Conference (GLOBECOM'03)*, pages 35–39, December 2003.
- [67] V. J. Rhodes. Adaptive guard intervals in OFDM systems, October 2009. US Patent 7,602,696.
- [68] N. Wang and S. D. Blostein. Adaptive Zero-Padding OFDM over Frequency-Selective Multipath Channels. *EURASIP Journal on Applied Signal Processing*, 2004(10):478–1488, 2004.
- [69] L. Deneire, B. Gyselinckx, and M. Engels. Training sequence vs. cyclic prefix a new look on single carrier communication. In *Proceedings of the IEEE Global Telecommunications Conference (GLOBECOM'00)*, pages 1056–1060, 2000.
- [70] L. Deneire, B. Gyselinckx, and M. Engels. Training sequence versus cyclic prefix—a new look on single carrier communication. *IEEE Communication Letters*, 5(7):292–294, July 2001.
- [71] R. Cendrillon and M. Moonen. Efficient equalizers for single and multi-carrier environments with known symbol padding. In *Proceedings of the 6th International Symposium on Signal Processing and its Applications (ISSPA'01)*, pages 607–610, 2002.
- [72] H. Witschnig, T. Mayer, A. Springer, A. Koppler, L. Maurer, M. Huemer, and R. Weigel. A different look on cyclic prefix for SC/FDE. In *Proceedings of the 13th IEEE International Symposium on Personal, Indoor and Mobile Radio Communications (PIMRC2002)*, pages 824–828, September 2002.
- [73] D. Falconer, S.L. Ariyavisitakul, A. Benyamin-Seeyar, and B. Eidson. Frequency domain equalization for single-carrier broadband wireless systems. *IEEE Communications Magazine*, 40(4):58–66, 2002.
- [74] N. Benvenuto and S. Tomasin. On the comparison between OFDM and single carrier modulation with a DFE using a frequency-domain feedforward filter. *IEEE Transactions on Communications*, 50(6):947–955, 2002.
- [75] Y. Zeng and T.S. Ng. Pilot cyclic prefixed single carrier communication: channel estimation and equalization. *IEEE Signal Processing Letters*, 12(1):56–59, 2005.
- [76] S. Tang, F. Yang, K. Peng, C. Pan, K. Gong, and Z. Yang. Iterative channel estimation for block transmission with known symbol padding—a new look at TDS-OFDM. In *Proceedings of the IEEE Global Telecommunications Conference (GLOBECOM'07)*, pages 4269–4273, 2007.
- [77] C.-S. Yeh, Y. Lin, and Y. Wu. OFDM system channel estimation using time-domain training sequence for mobile reception of digital terrestrial broadcasting. *IEEE Transactions on Broadcasting*, 46(3):215–220, September 2000.
- [78] Y.-C. Chen, W.-J. Lin, and J.-S. Lin. Channel estimation technique with assistance of PN-coded training sequences for wireless OFDM communications. In *Proceedings of the 2007 International Conference on Wireless Communications and Mobile Computing (IWCMC'07)*, pages 109–114, 2007.
- [79] J.-C. Lin. Channel estimation assisted by postfixed pseudo-noise sequences padded with null samples for mobile OFDM communications. *Proceedings of the IEEE*

- Wireless Communications and Networking Conference (WCNC 2008)*, pages 846–851, March 2008.
- [80] J. S. Lin, H. Y. Chen, and J. C. Lin. Channel estimation technique assisted by postfixed PN sequences with zero padding for wireless OFDM communications. *IEICE Transactions on Communications*, 91(4):1095, 2008.
- [81] M. Al-Gharabally and P. Das. On the Performance of OFDM Systems in Time Varying Channels with Channel Estimation Error. In *Proceedings of the IEEE International Conference on Communications (ICC'06)*, pages 5180–5185, June 2006.
- [82] W. Zhang, Y. Guan, W. Liang, D. He, F. Ju, and J. Sun. An Introduction of the Chinese DTTB Standard and Analysis of the PN595 Working Modes. *IEEE Transactions on Broadcasting*, 53:8–13, Mar. 2007.
- [83] J. Song, Z. Yang, L. Yang, K. Gong, C. Pan, J. Wang, and Y. Wu. Technical Review on Chinese Digital Terrestrial Television Broadcasting Standard and Measurements on Some Working Modes. *IEEE Transactions on Broadcasting*, 53(1):1–7, March 2007.
- [84] C. Pan. Chinese Terrestrial DTV standard DTMB. presentation, available online www.cntv.org.co/cntv_bop/tdt/...agosto_13/estandar_chino2.pdf, August 2008.
- [85] P. Duhamel and M. Vetterli. Fast fourier transforms: A tutorial review and a state of the art. *Signal Processing*, 19(4):259–299, 1990.
- [86] T.Y. Sung and Y.S. Shieh. Split-radix FFT/IFFT processor, May 2006. US Patent App. 11/432,355.
- [87] Z. X. Yang, Y. Hu, C. Pan, and L. Yang. Design of a 3780-point IFFT processor for TDS-OFDM. *IEEE Transactions on Broadcasting*, 48(1):57–61, March 2002.
- [88] J.G. Nash. A High Performance Scalable FFT. In *Proceedings of the IEEE Wireless Communications and Networking Conference (WCNC 2007)*, pages 2367–2372, March 2007.
- [89] W. Liang, W. Zhang, D. He, Y. Guan, Y. Wang, and J. Sun. Digital Terrestrial Television Broadcasting in China. *IEEE Multimedia*, 14:92–97, 2007.
- [90] D. J. MacKay, S. T. Wilson, and M.C. Davey. Comparison of constructions of irregular gallager codes. *IEEE Transactions on Communications*, 47(no. 10.):1449–1454, October 1998.
- [91] K. Liu, Z. Fei, J. Kuang, and X. Li. A novel algorithm for removing cycles in quasi-cyclic LDPC codes. In *Proceedings of the 20th IEEE International Symposium on Personal, Indoor and Mobile Radio Communications (PIMRC)*, 2009.
- [92] A. Morello and V. Mignone. DVB-S2– ready for lift off. *EBU technical review*, pages 1–10, October 2004.
- [93] J.J. Van de Beek, O. Edfors, M. Sandell, S.K. Wilson, and P.O. Borjesson. On channel estimation in OFDM systems. In *Proceedings of the 45th IEEE Vehicular Technology Conference (VTC'95)*, pages 815–819, 1995.
- [94] O. Edfors, M. Sandell, J.J. van de Beek, S.K. Wilson, and P.O. Börjesson. OFDM Channel Estimation by Singular Value Decomposition. *IEEE Transactions on Communications*, 46(7), 1998.

- [95] P. Hoeher, S. Kaiser, and P. Robertson. Pilot-symbol-aided channel estimation in time and frequency. In *Proceedings of the IEEE Global Telecommunications Conference (GLOBECOM'97)*, pages 90–96, 1997.
- [96] P. Hoeher, S. Kaiser, P. Robertson, et al. Two-dimensional pilot-symbol-aided channel estimation by Wiener filtering. In *Proceedings of the IEEE International Conference on Acoustics Speech and Signal Processing (ICASSP'97)*, pages 1845–1848, 1997.
- [97] Y. Li, N. Seshadri, and S. Ariyavisitakul. Channel estimation for OFDM systems with transmitter diversity in mobile wireless channels. *IEEE Journal on Selected Areas in Communications*, 17(3):461–471, March 1999.
- [98] Y. Li. Pilot-symbol-aided channel estimation for OFDM in wireless systems. *IEEE Transactions on Vehicular Technology*, 49(4):1207–1215, July 2000.
- [99] J.K. Cavers. An analysis of pilot symbol assisted modulation for Rayleigh fading channels. *IEEE Transactions on Vehicular Technology*, 40(4):686–693, 1991.
- [100] R. Nilsson, O. Edfors, M. Sandell, and P.O. Borjesson. An analysis of two-dimensional pilot-symbol assisted modulation for OFDM. In *Proceedings of the IEEE International Conference on Personal Wireless Communications*, pages 71–74, 1997.
- [101] C.R.N. Athaudage and A.D.S. Jayalath. Low-complexity channel estimation for wireless OFDM systems. In *Proceedings of the 14th IEEE International Symposium on Personal, Indoor and Mobile Radio Communications (PIMRC 2003)*, pages 521–525, 2003.
- [102] O. Edfors, M. Sandell, J.J. Van De Beek, S.K. Wilson, and P.O. Börjesson. Analysis of DFT-based channel estimators for OFDM. *Wireless Personal Communications*, 12(1):55–70, 2000.
- [103] F.G. Garcia, JM Paez-Borrillo, and S. Zazo. DFT-based channel estimation in 2D-pilot-symbol-aided OFDM wireless systems. In *Proceedings of the 53rd IEEE Vehicular Technology Conference (VTC 2001 Spring)*, pages 810–814, 2001.
- [104] X. Dong, W.S. Lu, and A.C.K. Soong. Linear interpolation in pilot symbol assisted channel estimation for OFDM. *IEEE Transactions on Wireless Communications*, 6(5):1910–1920, 2007.
- [105] R. Negi and J. Cioffi. Pilot tone selection for channel estimation in a mobile OFDM system. *IEEE Transactions on Consumer Electronics*, 44(3):1122–1128, August 1998.
- [106] M.J.F.G. Garcia, S. Zazo, and JM Paez-Borrillo. Pilot patterns for channel estimation in OFDM. *Electronics Letters*, 36(12):1049–1050, 2002.
- [107] S. Coleri, M. Ergen, A. Puri, and A. Bahai. Channel estimation techniques based on pilot arrangement in OFDM systems. *IEEE Transactions on Broadcasting*, 48(3):223–229, 2002.
- [108] A. Stamoulis, S.N. Diggavi, and N. Al-Dhahir. Intercarrier interference in MIMO OFDM. *IEEE Transactions on Signal Processing*, 50(10):2451–2464, October 2002.
- [109] J.W. Choi and Y.H. Lee. Optimum pilot pattern for channel estimation in OFDM systems. *IEEE Transactions on Wireless Communications*, 4(5):2083–2088, 2005.

- [110] V. Mignone and A. Morello. CD3-OFDM: A novel demodulation scheme for fixed and mobile receivers. *IEEE Transactions on Communications*, 44(9):1144–1151, September 1996.
- [111] P. Schniter. Low-complexity estimation of doubly-selective channels. In *Proceedings of the 4th IEEE Workshop on Signal Processing Advances in Wireless Communications (SPAWC)*, pages 200–204, 2003.
- [112] L. Tong and S. Perreau. Multichannel blind identification: From subspace to maximum likelihood methods. *Proceedings of the IEEE*, 86(10):1951–1968, 1998.
- [113] R.W. Heath Jr and G.B. Giannakis. Exploiting input cyclostationarity for blind channel identification in OFDM systems. *IEEE Transactions on Signal Processing*, 47(3):848–856, 2002.
- [114] B. Muquet, M. De Courville, and P. Duhamel. Subspace-based blind and semi-blind channel estimation for OFDM systems. *IEEE Transactions on Signal Processing*, 50(7):1699–1712, 2002.
- [115] B. Muquet and M. de Courville. Blind and semi-blind channel identification methods using second order statistics for OFDM systems. In *Proceedings of the IEEE International Conference on Acoustics, Speech, and Signal Processing (ICASSP'99)*, pages 2745–2748, 2002.
- [116] L. Tong, G. Xu, and T. Kailath. Blind identification and equalization based on second-order statistics: A time domain approach. *IEEE Transactions on Information Theory*, 40(2):340–349, March 1994.
- [117] C. Li and S. Roy. Subspace-based blind channel estimation for OFDM by exploiting virtual carriers. *IEEE Transactions on Wireless Communications*, 2(1):141–150, 2003.
- [118] E. de Carvalho and D.T.M. Slock. Blind and semi-blind FIR multichannel estimation: (global) identifiability conditions. *IEEE Transactions on Signal Processing*, 52(4):1053 – 1064, apr. 2004.
- [119] E. De Carvalho and D.T.M. Slock. Cramer-Rao bounds for semi-blind, blind and training sequence based channel estimation. In *Proceedings of the 1st IEEE Signal Processing Workshop on Signal Processing Advances in Wireless Communications*, pages 129–132, 1997.
- [120] T. Cui and C. Tellambura. Semiblind Channel Estimation and Data Detection for OFDM Systems With Optimal Pilot Design. *IEEE Transactions on Communications*, 55(5):1053 –1062, May 2007.
- [121] M. Muck, M. De Courville, and P. Duhamel. Postfix design for pseudo random postfix OFDM modulators. In *Proceedings of the 9th International OFDM Workshop*, Dresden, Germany, September 2004.
- [122] Y. Ma, N. Yi, and R. Tafazolli. Channel estimation for PRP-OFDM in slowly time-varying channel: first-order or second-order statistics? *IEEE Signal Processing Letters*, 13(3):129–132, 2006.
- [123] K.U. Schmidt, M. Muck, J. Schoentier, and M. de Courville. Time or Frequency Domain Pilots for Channel Tracking in Wireless OFDM Systems. In *International OFDM Workshop*, Dresden, Germany, September 2004.

- [124] M. Muck, A.R. Dias, M. de Courville, and P. Duhamel. A Pseudo Random Postfix OFDM based modulator for multiple antennae systems. In *Proceedings of the IEEE International Conference on Communications (ICC'04)*, pages 2392–2396, 2004.
- [125] M. Muck, L. Mazet, M. de Courville, and P. Duhamel. Pseudo Random Postfix OFDM based channel estimation in a Doppler scenario. In *Proceedings of the Mobile IST Summit*, Dresden, Germany, June 2005.
- [126] M. Muck, M. de Courville, and P. Duhamel. A pseudorandom postfix OFDM modulator – semi-blind channel estimation and equalization. *IEEE Transactions on Signal Processing*, 54(3):1005, 2006.
- [127] M. Muck, M. de Courville, X. Miet, and P. Duhamel. Iterative interference suppression for pseudo random postfix OFDM based channel estimation. In *Proceedings of the IEEE International Conference on Acoustics, Speech, and Signal Processing (ICASSP'05)*, 2005.
- [128] H. Steendam, M. Moeneclaey, and H. Bruneel. The Cramer-Rao bound and ML estimate for data-aided channel estimation in KSP-OFDM. In *Proceedings of the 18th IEEE International Symposium on Personal, Indoor and Mobile Radio Communications (PIMRC 2007)*, pages 1–5, 2007.
- [129] H. Steendam, M. Moeneclaey, and H. Bruneel. An ML-Based Estimate and the Cramer-Rao Bound for Data-Aided Channel Estimation in KSP-OFDM. *EURASIP Journal on Wireless Communications and Networking*, 2008, 2008.
- [130] D. Van Welden, H. Steendam, and M. Moeneclaey. Frequency-domain data-aided channel estimation for KSP-OFDM. In *Proceedings of the 10th International Symposium on Spread Spectrum Techniques and Applications (ISSSTA'08)*, 2008.
- [131] D. Van Welden, H. Steendam, and M. Moeneclaey. Iterative DA/DD Channel Estimation for KSP-OFDM. In *Proceedings of the IEEE International Conference on Communications (ICC'08)*, pages 693–697, 2008.
- [132] D. Van Welden and H. Steendam. Near optimal iterative channel estimation for KSP-OFDM. *IEEE Transactions on Signal Processing*, 58(9):4948–4954, 2010.
- [133] Z. X. Yang, J. Wang, C. Pan, and Y. Lin. Channel estimation method of digital television terrestrial broadcasting. *Chinese Journal of Electronics*, 30:1298–1301, 2002.
- [134] Z. X. Yang, J. Wang, M. Han, C. Pan, L. Yang, and Z. Han. Channel estimation of DMB-T. In *Proceedings of the IEEE 2002 International Conference on Communications, Circuits and Systems and West Sino Expositions*, pages 1069–1072, 2003.
- [135] Z.W. Zheng, Z.X. Yang, C.Y. Pan, and Y.S. Zhu. Synchronization and channel estimation for TDS-OFDM systems. In *Proceedings of the 58th IEEE Vehicular Technology Conference (VTC 2003 Fall)*, pages 1229–1233, 2004.
- [136] J. Fu, C.Y. Pan, Z.X. Yang, and L. Yang. Low-complexity equalization for TDS-OFDM systems over doubly selective channels. *IEEE Transactions on Broadcasting*, 51(3):401–407, 2005.
- [137] J. Wang, Z.X. Yang, C.Y. Pan, J. Song, and L. Yang. Iterative padding subtraction of the PN sequence for the TDS-OFDM over broadcast channels. *IEEE Transactions on Consumer Electronics*, 51(4):1148, 2005.

- [138] B. Song, L. Gui, Y. Guan, and W. Zhang. On channel estimation and equalization in TDS-OFDM based terrestrial HDTV broadcasting system. *IEEE Transactions on Consumer Electronics*, 51(3):790–797, 2005.
- [139] G. Liu and J. Zhang. ITD-DFE based channel estimation and equalization in TDS-OFDM receivers. *IEEE Transactions on Consumer Electronics*, 53(2):304–309, May 2007.
- [140] F. Yang, K. Peng, J. Song, C. Pan, and Z. Yang. Novel decision-directed channel estimation method for TDS-OFDM system. In *Proceedings of the 11th IEEE Singapore International Conference on Communication Systems (ICCS 2008)*, pages 1096–1100, 2008.
- [141] F. Yang, J. Wang, J. Wang, J. Song, and Z. Yang. Novel channel estimation method based on PN sequence reconstruction for Chinese DTTB system. *IEEE Transactions on Consumer Electronics*, 54(4):1583–1589, 2008.
- [142] S. Tang, K. Peng, K. Gong, J. Song, C. Pan, and Z. Yang. Novel decision-aided channel estimation for TDS-OFDM systems. In *Proceedings of the IEEE International Conference on Communications (ICC'08)*, pages 946–950, 2008.
- [143] L. Gui, Q. Li, B. Liu, W. Zhang, and C. Zheng. Low complexity channel estimation method for TDS-OFDM based Chinese DTTB system. *IEEE Transactions on Consumer Electronics*, 55(3):1135–1140, August 2009.
- [144] Q. Xie, K. Peng, F. Yang, and Z. Yang. Iterative NR decoding and channel estimation for TDS-OFDM system. In *Proceedings of the IEEE Global Telecommunications Conference (GLOBECOM'09)*, pages 1–6, 2010.
- [145] G. Liu. Channel estimation method and system using linear correlation based interference cancellation (LCIC) with decision-feedback-equalization (DFE), May 2007. US Patent App. 11/744,627.
- [146] F. Yang, K. Peng, J. Wang, J. Song, and Z. Yang. Simplified decision-directed channel estimation method for OFDM system with transmit diversity. In *Proceedings of the 69th IEEE Vehicular Technology Conference (VTC 2009 Spring)*, pages 1–5, 2009.
- [147] J. Fu, J. Wang, J. Song, C. Pan, and Z.-X. Yang. A simplified equalization method for dual PN-sequence padding TDS-OFDM systems. *IEEE Transactions on Broadcasting*, 54(4):825–830, December 2008.
- [148] Z. X. Yang, X. Wang, Z. Wang, J. Wang, and J. Wang. Improved channel estimation for TDS-OFDM based on flexible frequency-binary padding. *IEEE Transactions on Broadcasting*, 56(3):418–424, September 2010.
- [149] D.V. Sarwate and M.B. Pursley. Crosscorrelation properties of pseudorandom and related sequences. *Proceedings of the IEEE*, 68(5):593–619, May 1980.
- [150] K.F. Riley, M.P. Hobson, and S.J. Bence. *Mathematical Methods for Physics and Engineering: A Comprehensive Guide 3rd edition*. Cambridge University Press, 2006.
- [151] Youssef Nasser. *Sensibilité des Systéme OFDM-CDMA aux Erreurs de Synchronisation en Réception Radio Mobile*. PhD thesis, Institut National Polytechnique de Grenoble, France, Oct. 2006.

- [152] S.M. Kay. *Fundamentals of statistical signal processing: estimation theory*. Prentice-Hall, 1993.
- [153] V. D. Nguyen, H.-P. Kuchenbecker, and M. Patzold. Estimation of the channel impulse response length and the noise variance for OFDM systems. In *Proceedings of the 61st IEEE Vehicular Technology Conference (VTC 2005 Spring)*, pages 429–433, Stockholm, Sweden, May 2005.
- [154] S. Xi and H.-C. Wu. Fast channel estimation using maximum-length shift-register sequences. In *Proceedings of the 62nd IEEE Vehicular Technology Conference (VTC 2005 Fall)*, September 2005.
- [155] W. Henkel, G. Taubock, P. Odling, P.O. Borjesson, and N. Petersson. The cyclic prefix of OFDM/DMT-an analysis. In *Proceedings of the 2002 International Zurich Seminar on Broadband Communications, Access, Transmission, Networking*, 2002.
- [156] G.A. Al-Rawi, T.Y. Al-Naffouri, A. Bahai, and J. Cioffi. An iterative receiver for coded OFDM systems over time-varying wireless channels. In *Proceedings of the IEEE International Conference on Communications (ICC'03)*, pages 3371–3376, 2003.
- [157] P.K. Frenger, N. Arne, and B. Svensson. Decision-directed coherent detection in multicarrier systems on Rayleigh fading channels. *IEEE Transactions on Vehicular Technology*, 48(2):490–498, March 1999.
- [158] J. Akhtman and L. Hanzo. Decision directed channel estimation aided OFDM employing sample-spaced and fractionally-spaced CIR estimators. *IEEE Transactions on Wireless Communications*, 6(4):1171–1175, 2007.
- [159] M. Sandell, C. Luschi, P. Strauch, and R. Yan. Iterative channel estimation using soft decision feedback. In *Proceedings of the IEEE Global Telecommunications Conference (GLOBECOM'98)*, pages 3728–3733, 1998.
- [160] M.C. Valenti and B.D. Woerner. Iterative channel estimation and decoding of pilot symbol assisted turbo codes over flat-fading channels. *IEEE Journal on Selected Areas in Communications*, 19(9):1697–1705, 2001.
- [161] J. Zhu and W. Lee. Channel estimation with power-controlled pilot symbols and decision-directed reference symbols. In *Proceedings of the 58th IEEE Vehicular Technology Conference (VTC 2003 Fall)*, pages 1268–1272, October 2003.
- [162] L. Jarbot. Combined decoding and channel estimation of OFDM systems in mobile radio networks. In *Proceedings of the 47th IEEE Vehicular Technology Conference (VTC'97)*, pages 1601–1604, May 1997.
- [163] J.W. Jwa and H.S. Lee. Interleaved TC 8DPSK/OFDM with decision-directed channel estimation on frequency-selective Rayleigh fading channels. *IEEE Communications Letters*, 6(10):413–415, 2002.
- [164] Y.H. Kim, K.S. Kim, and J.Y. Ahn. Iterative estimation and decoding for an LDPC-coded OFDMA system in uplink environments. In *Proceedings of the IEEE International Conference on Communications (ICC'04)*, pages 2478–2482, 2004.
- [165] R. Koetter, A.C. Singer, and M. Tüchler. Turbo equalization. *IEEE Signal Processing Magazine*, 21(1):67–80, 2004.

- [166] C. Douillard, M. Jézéquel, C. Berrou, et al. Iterative correction of intersymbol interference: Turbo-equalization. *European Transactions on Telecommunications*, 6(5):507–511, 1995.
- [167] J. Hagenauer. The turbo principle: Tutorial introduction and state of the art. In *Proceedings of the International Symposium on Turbo Codes and Related Topics*, pages 1–11, 1997.
- [168] M. Tüchler, R. Koetter, and A.C. Singer. Turbo equalization: principles and new results. *IEEE Transactions on Communications*, 50(5):754–767, 2002.
- [169] K. R. Narayanan. Turbo equalization. *Wiley Encyclopedia of Telecommunications*, pages 2716–2727, January 2003.
- [170] S. Song, A.C. Singer, and K.M. Sung. Turbo equalization with an unknown channel. In *Proceedings of the IEEE International Conference on Acoustics, Speech, and Signal Processing (ICASSP'02)*, 2002.
- [171] M. Tüchler, R. Otnes, and A. Schmidbauer. Performance of soft iterative channel estimation in turbo equalization. In *Proceedings of the IEEE International Conference on Communications (ICC'02)*, pages 1858–1862, 2002.
- [172] R. Otnes and M. Tüchler. Iterative channel estimation for turbo equalization of time-varying frequency-selective channels. *IEEE Transactions on Wireless Communications*, 3(6):1918–1923, 2004.
- [173] M. Zhao, Z. Shi, and M.C. Reed. An iterative receiver with channel estimation for MIMO-OFDM over a time and frequency dispersive fading channel. In *Proceedings of the IEEE Global Telecommunications Conference (GLOBECOM'07)*, pages 4155–4159, November 2007.
- [174] M. Zhao, Z. Shi, and M.C. Reed. Iterative Turbo Channel Estimation for OFDM System over Rapid Dispersive Fading Channel. In *Proceedings of the IEEE International Conference on Communications (ICC '07)*, pages 4849–4854, June 2007.
- [175] F. Tosato and P. Bisaglia. Simplified soft-output demapper for binary interleaved COFDM with application to HIPERLAN/2. In *Proceedings of the IEEE International Conference on Communications (ICC'02)*, pages 664–668, 2002.
- [176] C. Sgraja and J. Lindner. Estimation of rapid time-variant channels for OFDM using Wiener filtering. In *Proceedings of IEEE International Conference on Communications (ICC'03)*, pages 2390–2395, 2003.
- [177] M. Dong, L. Tong, and B.M. Sadler. Training placement for tracking fading channels. In *Proceedings of IEEE International Conference on Acoustics, Speech, and Signal Processing (ICASSP'02)*, 2002.
- [178] M. Dong, L. Tong, and B.M. Sadler. Optimal pilot placement for channel tracking in OFDM. In *Proceedings of the Military Communications Conference (MILCOM)*, pages 602–606, 2002.
- [179] Eric W. Weisstein. Complex multiplication. <http://mathworld.wolfram.com/ComplexMultiplication.html>.
- [180] Wikipedia. Computational complexity of mathematical operations, 2010.
- [181] Y. Chen and Y. Chen. Design of Cyclic Correlator for Channel Estimation in DTMB System. In *Proceedings of the 7th International Conference on ASIC (ASICON'07)*, pages 954–957, 2007.

- [182] G.J. Foschini and M.J. Gans. On limits of wireless communications in a fading environment when using multiple antennas. *Wireless personal communications*, 6(3):311–335, 1998.
- [183] G.G. Raleigh and J.M. Cioffi. Spatio-temporal coding for wireless communication. *IEEE Transactions on Communications*, 46(3):357–366, 1998.
- [184] G.J. Foschini. Layered space-time architecture for wireless communication in a fading environment when using multi-element antennas. *Bell labs technical journal*, 1(2):41–59, 1996.
- [185] S.M. Alamouti. A simple transmit diversity technique for wireless communications. *IEEE Journal on Selected Areas in Communications*, 16(8):1451–1458, 1998.
- [186] C. Gomez-Calero, L.C. Navarrete, L. de Haro, and R. Martinez. A 2x2 MIMO DVB-T2 System: Design, New Channel Estimation Scheme and Measurements With Polarization Diversity. *IEEE Transactions on Broadcasting*, 56(2):184–192, June 2010.
- [187] J. Wang, C. Y. Pan, and Z. X. Yang. A simple space-frequency transmitter diversity scheme for TDS-OFDM in SFN. In *Proceedings of the 2005 International Conference on Communications, Circuits and Systems*, pages 260–264, 2005.
- [188] J.T. Wang, J. Song, J. Wang, C.Y. Pan, Z.X. Yang, and L. Yang. A general SFN structure with transmit diversity for TDS-OFDM system. *IEEE Transactions on Broadcasting*, 52(2):245–251, 2006.
- [189] F. Yang, K. Peng, J. Wang, J. Song, and Z. Yang. Transmit diversity scheme and flexible channel estimation for TDS-OFDM system. In *Proceedings of the 69th IEEE Vehicular Technology Conference (VTC 2009 Spring)*, pages 1–5, 2009.
- [190] W. Chang, J. Wang, J. Song, and C. Pan. Transmit diversity scheme for TDS-OFDM system over the time selective fading channel. In *Proceedings of the 6th International Wireless Communications and Mobile Computing Conference*, pages 251–255, 2010.
- [191] Markus Muck. *Pseudo Random Postfix Orthogonal Frequency Division Multiplexing*. PhD thesis, Ecole Nationale Supérieure des Télécommunications (ENST) de Paris, <http://markus.muck.free.fr/data/these.pdf>, May 2006.

AVIS DU JURY SUR LA REPRODUCTION DE LA THESE SOUTENUE

Titre de la thèse : Analysis and optimization of the Asian Mobile and Terrestrial Digital Television Systems

Nom Prénom de l'auteur : LIU Ming

Membres du jury : Monsieur BROSSIER
Madame DOUILLARD
Monsieur HELARD
Monsieur DUHAMEL
Monsieur GELLE
Monsieur UNTERSEE
Monsieur CRUSSIÈRE



Président du jury : *Pierre DUTAILLE*

Date de la soutenance : 30/03/2011

Reproduction de la thèse soutenue :

- Thèse pouvant être reproduite en l'état
- Thèse ne pouvant être reproduite
- Thèse pouvant être reproduite après corrections suggérées

Le Directeur,

M'Hamed DRISSI

Rennes, le 30/03/2011

Signature du Président du jury

